University of Cincinnati

Date: 5/27/2015

I, Mohammed Mahmoud Zaki Mohammed Shaheen , hereby submit this original work as part of the requirements for the degree of Doctor of Philosophy in Aerospace Engineering.

It is entitled:

Design and Assessment of Vertical Axis Wind Turbine Farms

Student's name: **Mohammed Mahmoud Zaki Mohammed Shaheen**

This work and its defense approved by:

Committee chair: Shaaban Abdallah, Ph.D.

Committee member: Milind Jog, Ph.D.

Committee member: Mark Turner, Sc.D.

14019

Design and Assessment of Vertical Axis Wind Turbine Farms

A dissertation submitted to the
Graduate School
of the University of Cincinnati
in partial fulfillment of the
requirements for the degree of

Doctor of Philosophy

in the Department of Aerospace Engineering and Engineering Mechanics
of the College of Engineering
by

Mohammed Mahmoud Zaki Shaheen

May, 2015

B.S. Military Technical College, Egypt 2001
M.S. Military Technical College, Egypt 2008

Committee Chair: Shaaban Abdallah, Ph.D.

Abstract

Wind energy is the fastest growing of all renewable energy resources. Most of the existing wind turbine farms consist of Horizontal Axis Wind Turbines because the efficiency of an isolated Horizontal Axis Wind Turbines is the highest of all other wind turbines. This thesis is interested in Vertical Axis Wind Turbines farms, we developed Savonius and Darrieus Vertical Axis Wind Turbine efficient and patterned farms for energy generation. The developed farms consist of multiples of triangular three Vertical Axis Wind Turbine clusters. The three turbines in the cluster are arranged in a close proximity in order to enhance their average power output and power density. The geometry of the cluster is optimized using numerical solutions of two co-rotating and counter-rotating turbines in parallel and oblique configurations. The gap distances and oblique angles between upstream and downstream turbines of the cluster are carefully chosen to achieve a maximum average power coefficient by the clusters. The numerical method is validated by simulation of the flow field around a single Savonius and Darrieus turbines, the numerical results for the power coefficients of the single turbines are compared with the available experimental data at different tip speed ratios. The unsteady Reynolds averaged Navier-Stokes equations are solved using Fluent 14.5 solver. The results for the single turbines show a good agreement with the experimental data. The numerical solutions of two parallel and oblique co-rotating and counter-rotating Savonius and Darrieus turbines show a mutual enhancement in the power coefficient of individual turbines in particular configurations. Efficient triangular three turbine clusters are developed based on the results of the two parallel and oblique co-rotating and counter-rotating turbines. The efficiencies of the developed three Savonius and Darrieus turbine clusters are 26% and 30% higher than their isolated counterparts

respectively. We used these findings in developing patterned efficient farms with the triangular cluster as a building unit and having the same geometric topology of the cluster, for example, a triangular nine turbine farm consists of a three turbine cluster at each vertex and a triangular twenty-seven turbine farm consists of a nine turbine farm at each vertex, etc. The developed farms performance parameters are assessed numerically in terms of moment and power coefficients against Vertical Axis Wind Turbine farms having the same number, type and size of isolated turbines. The pattern of the developed farms and power coefficient enhancement are confirmed by numerical solutions of Savonius nine and twenty-seven turbine farms, and a Darrieus nine turbine farm. The results show that the developed Vertical Axis Wind Turbine farms have the same power ratios achieved by the three turbine clusters. Also, the power densities of the Savonius nine and twenty-seven turbine farms are seven and four times that of the isolated turbine farms respectively. On the other hand, the power density of the Darrieus nine turbine farm is about thirteen times that of the isolated counterpart. These patterned efficient farm designs make the Vertical Axis Wind Turbine farms more efficient than the Horizontal Axis Wind Turbines farms.

Acknowledgment

In the name of God, most Gracious, most Merciful.

I wish to express my sincere appreciation to those who have contributed to this thesis and supported me in one way or the other during this amazing journey.

First, I am extremely grateful to my advisor, Professor Shaaban Abdallah, for his guidance and all the useful discussions and brainstorming sessions, especially during the difficult conceptual development stage. His deep insights helped me at various stages of my research. I also remain indebted for his understanding and support during the times when I was really down and depressed due to personal problems.

My sincere gratitude is reserved for my committee members: Professor Mark Turner and Professor Milind Jog for their precious insights and suggestions and for their friendly meetings and encouraging.

Special thanks to the Department of Aerospace Engineering and Engineering Mechanics for giving me the opportunity to carry out my doctoral research.

I would also like to take this opportunity to thank the Egyptian Armed Forces, and the Military Technical College in Cairo. It would have been impossible for me to even start my study had they not given me the opportunity and the financial support for traveling to the United States.

PhD students often talk about loneliness during the course of their study but this is something which I have never experienced at the University of Cincinnati. A heartfelt thanks to the really supportive friends who made the experience something special.

I am also indebted to my Family, my father Mahmoud Shaheen who gave me the dream since I was a little child, my mother who always supported me and encouraged me for always being the first in my classes.

Words cannot express the feelings I have for my kids Nourhan, Youssef and Kareem for their constant unconditional emotional support.

Finally, I would like to acknowledge the most important person in my life – my wife Walaa Mazhar. She has been a constant source of strength and inspiration. There were times during the past three years when everything seemed hopeless, I can honestly say that it was only her determination and encouragement that ultimately made it possible for me to see this project through to the end. Thanks for your patience.

Table of Contents

List of Figures

List of Tables

Nomenclature

A_S	Turbine swept area As= DH, m2	S_l	Cluster height, m
C_m	Torque coefficient, $T/(0.5\ \rho V_\infty^2 RAS)$	T	Torque, N/m
C_{ms}	Static torque coefficient, $Ts / (0.5\ \rho V_\infty^2 RAS)$	T_s	Static torque, N/m
C_p	Power coefficient, $T\Omega/(\rho V_\infty^3 RH)$	V_∞	Free stream velocity, m/sec
D	Rotor diameter, m	ρ	Density, kg/m3
d	Bucket diameter, m	Ω	Rotation speed, rad/sec
e	Overlap ratio of the rotor buckets, e = S/d	λ	Tip speed ratio, $\Omega R/V_\infty$
H	Rotor height, m	θ	Azimuth angle of the turbine
R	Rotor radius, m	α	Oblique angle between rotors
S	Gap distance between turbines, m	Γ	Circulation

Chapter 1

Introduction

1.1. Motivation

Non-renewable energy resources, coal, petroleum and natural gas, need thousands of years to reform, they cannot be replaced as fast as they are being consumed. In the next few decades, harvesting fossil based resources will become too costly and environmentally damaging. The humanity will need to shift its reliance to other sources of energy. The solar, wind, wave, biomass and geothermal energies are based on renewable resources. Renewable energy contributed by 19% to the global energy consumption and 22% to electricity generation in 2014 [1]. The global steady expansion of the renewable energy sector is creating a clean energy revolution which is expected to continue to grow rapidly in the coming years. Consequently, there are substantial economic opportunities for the countries that will invest in inventing, manufacturing and exporting clean energy technologies. Developing innovative ideas and tailored market driven solutions drives investment in sustainable energy to meet the challenge of global energy demand in addition to environmental requirements.

"Of all the forces of nature, I should think the wind contains the largest amount of motive power", Abraham Lincoln (1860). Among the renewable energy sources wind power is the fastest growing (13.5% by mid-2014 on an annual basis) [2]. The global wind energy capacity was 360 GW at the end of 2014, this provided the world by 4% of its electric energy demands.

The development of the wind energy market is attributed to the economic advantages of wind power, and the urgent need for emission free technologies [3].

The United States currently relies heavily on coal, oil, and natural gas for its energy by more than 70%. Energy prices, supply uncertainties, and environmental concerns are driving the United States to rethink its energy mix and develop diverse sources of clean, renewable energy without contributing to climate change or major adverse environmental impacts. The United States investment in the wind energy market has been growing since 1980. The United States possesses more than 8,000 GW of available land-based wind resources. This led to a collaborative effort in 2006 in order to explore a modeled energy scenario through which wind will provide 20% of the U.S. electricity demands by 2030 [4]. In the end of 2012, the cumulative installed wind capacity in the U.S. reached 60 GW across all fifty states, representing about 20% of the global installed wind capacity.

Electricity must be transmitted from where it is generated to areas of high electricity demand using the existing transmission system or new transmission lines. The delivery cost of wind power increases when costs associated with connecting the electric grid are included. Energy costs for wind vary by type of location and by class of wind power density. Recent wind prices are hard to beat and is competitive with expected future cost of burning fuel. Wind resources could be available for $20 per megawatt-hour (MWh), including production tax credit provided by governments to encourage the development in the wind energy production sector [5].

A wind turbine is a device that extracts kinetic energy from the wind and converts it into electrical power. The power characteristics of a wind turbine includes cut-in and cut-out speeds,

rated power, efficiency and power coefficient. The value known as the power coefficient (Cp) is the ratio of the mechanical power output by the turbine to the power of the free-stream air through the turbine cross-sectional area. Betz was able to show that the maximum coefficient of power of a wind turbine is 0.59 [6]. Engineering development over the years resulted in two types of wind turbines: Horizontal Axis Wind Turbines (HAWT) and Vertical Axis Wind Turbine (VAWT). Horizontal axis wind turbines (HAWTs) dominate the majority of the wind industry for the last 30 years. 74% of the small wind turbines manufacturers invested in the HAWT, however 18% adopted VAWTs [3]. Mostly wind turbine farms consist of HAWTs because of the higher efficiency of an isolated HAWT compared to a VAWT of the same size. Land-based HAWT farms have successfully been implemented, a modern HAWT farm consists of an array of 30 to 150 turbines [5]. The available power extracted from a HAWT farm is limited by the requirement of separating each turbine from adjacent turbines wakes. To maintain 90% of the performance of isolated HAWTs, the turbines in a HAWT farm must be spaced 3–5 turbine diameters apart in the cross-wind direction and 6–10 diameters apart in the downwind direction. A Typical HAWT farm has a power densities, defined as the power extracted divided by the area of its foot print, between 2 to 3 W/m^2 [7]. The low power density of a HAWT farm can be compensated by using larger turbine diameters to increase the farm power output. However larger diameter means larger swept area and larger turbine footprint and consequently lower power density. A taller tower base allows access to higher wind speeds to capture more energy, but actually this increases the energy cost and causes negative impacts on the environment and radar signals.

In the contrary to HAWTs, close arrangement of VAWTs improves their performance relative to the isolated turbines. VAWT farms have potential to be more cost effective than

HAWT farms since they can have higher power densities by minimizing the separation distances between array members to benefit from their positive aerodynamic interference and reduce land usage costs. This encouraged many scientists to perform research work to investigate the optimum layout of multiple VAWTs in a wind farm. Experimental researches at CalTech found that the power density of VAWT farms can be increased up to 30 watt/m^2 by optimizing the placement of the turbines that enables them to extract energy from adjacent turbines wakes [8]. A geometric arrangement based on the configuration of shed vortices in the wake of schooling fish showed a significantly increase in performance coefficient of an array of 16×16 VAWTs. The results suggest increases in power output of over one order of magnitude for a given area of land as compared to HAWTs [9]. The performance of two counter rotating VAWTs set at a center distance of 1.5-2.0 of the rotor diameter was tested experimentally, an increase of 11% over the efficiency obtained by their stand-alone counterpart was achieved [10]. Numerical analysis on two dimensional clusters of VAWTs showed that the performance of turbines operating completely in the wake of other turbines can be improved by choosing their angular position such that they see a higher flow velocity due to the presence of other turbines and associated stream-tube contraction [11]. A Study on of the effect of the relative angular position on aerodynamic interference between two curved blade Darrieus VAWTs showed a power reduction for the downstream turbine at small oblique angular positions, as the tip speed ratio of the upwind turbine increases, the blade circulation increases accompanied by an increase in the strength of the shed vortices, resulting in higher induced velocities, and consequently lower angles of attack at the downstream turbines, and correspondingly lower torque and power output [12]. Combining multiple Savonius VAWTs in the horizontal plane enhances their performance in particular configurations. Power improvement interactions occur due to the Magnus effect that

bends the main stream behind the upstream turbine providing additional rotation to the downstream turbine, and the periodic coupling of local flow between the two turbines associated with vortex shedding and cyclic pressure fluctuations [13]. A Study on closely arranged Savonius rotors showed that the power enhancement in their power coefficients is a function of the gap distance, relative direction of rotation and relative phase angle between the rotors [14].

All the previous studies didn't extended their results for efficient VAWT layouts to develop larger VAWT farms that generate the highest possible power output and possesses a high power density at the same time. The goal of this study is to investigate the performance of closely oriented VAWT layouts in order to develop an efficient VAWT cluster. The efficient turbine cluster benefits from the performance enhancement that occurs between closely oriented VAWTs, in addition to the high power density achieved. The efficient cluster is used as a building unit for the development of VAWT by using multiples of the cluster to construct the farm keeping the same topology of the cluster. This results in the development of patterned VAWT farms having the same performance enhancement of the cluster. The idea of the patterned VAWT farms introduces the capability of designing wind turbine farms efficient from the point of view of maintenance, construction, cost and time of design, power management and performance. Numerical solutions are obtained for a single VAWTs turbine of Savonius and Darrieus types, clusters of two co-rotating and counter-rotating turbines in parallel and oblique positions, and triangular clusters of three turbines are studied. The numerical solution of the single turbine is used for numerical model validation by comparing the computed results with the available experimental data. The results of the two turbines in parallel and oblique layouts are used to determine the optimum gap distances and oblique angles between adjacent turbines that generate the maximum power output and keeps high values of power density. Base on the results

of the two turbine layouts, efficient triangular three VAWT clusters are developed. The developed three turbine clusters are used as building units for the construction of efficient VAWT farms. The developed farms consist of multiple clusters with scaled geometrical ratios of the three turbine cluster keeping the same topology of the cluster. This resulted in patterned farms that have the same power enhancement ratio of the three turbine cluster. Numerical simulation of farms are performed to confirm the enhancement and the pattern progression.

1.2. Horizontal Axis Wind Turbines

A horizontal axis wind turbine (HAWT) is a lift device composed of one, two or three rotating blades. The blades are connected to a hub assembly, the hub is connected to a low speed shaft. A gearbox transmits the rotation from the low speed shaft to a high speed shaft attached to a generator as shown in figure 1.1. The generator converts the rotation of the high speed shaft into electrical energy. The wind speed data is transmitted to a controller, which turns on the machine by releasing its backing system when wind speeds are within the desired range for power production. A HAWT contains a yaw system that directs the rotor towards the wind direction and a pitch system to adjust the blades angles in order to maximize power output. A pitch system is also used to feather the blades away of the wind direction at extremely high wind speed conditions [15]. A typically HAWT (70 m dia. mounted to a 60 m tall tower) starts to operate in winds of about 5.36 m/s and produces approximately 1.6 MW, the maximum power output is generated at about 12.52 m/s–13.41 m/s. The turbine blades are feathered to stop its rotation when wind speed reaches 22.35 m/s. Figure 1.2 illustrates the separation distance in cross- and

downwind directions for HAWTs in a farm. A Typical HAWT farm has a power densities, defined as the power extracted divided by the area of its foot print, between 2 to 3 W/m^2 [7].

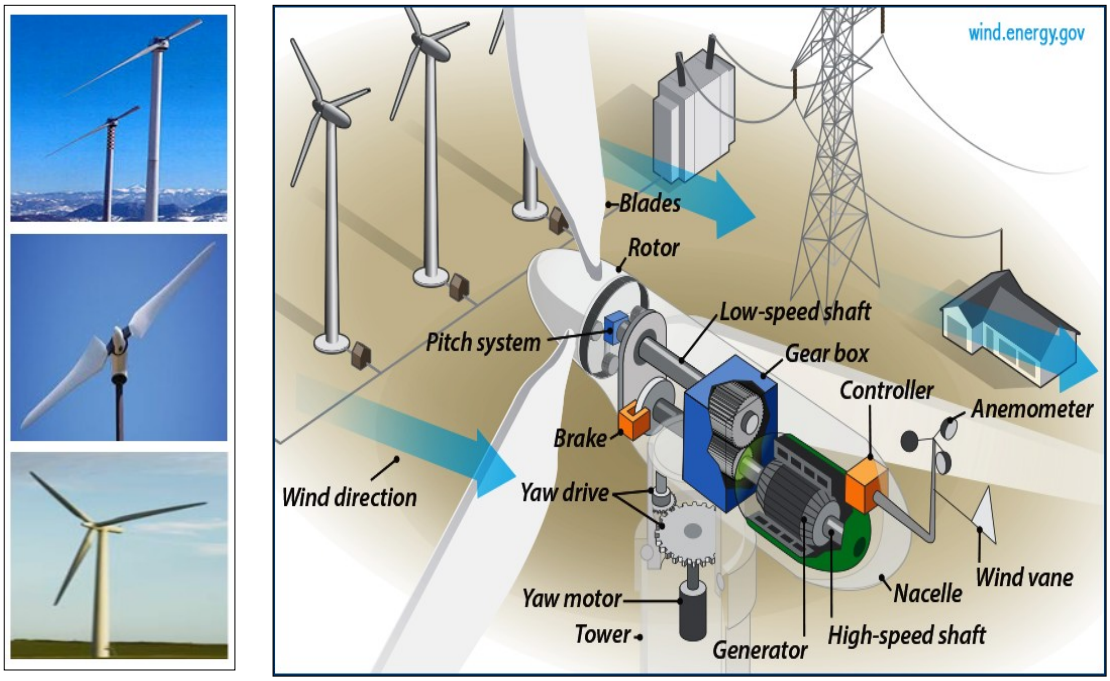

Figure 1.1: Types, Construction and Control System of HAWTs

Figure 1.2: HAWT Separation Distance in Cross and Down-Wind Directions

1.3. Vertical Axis Wind Turbines

A vertical-axis wind turbines (VAWT) is a type of wind turbine where the rotating shaft is set vertically and the main components are located at the base of the turbine. This arrangement allows the generator and gearbox to be located close to the ground, facilitating maintenance and repair. VAWTs do not need to be pointed into the wind which eliminates the need for wind sensing and orientation mechanisms. Three types of VAWTs exist, H-rotor, Darrieus and Savonius shown in figure 1.3. Lift type VAWTs constructed of vertical airfoil blades (H-rotor and Darrieus) gain the interest of most manufacturers. However, drag type VAWTs (Savonius turbines) have the potential to offer significant advantages in high turbulence areas. Table 1.1 shows a comparison between the characteristics of different types of wind turbines [16].

a **b** **c**

Figure 1.3: Different Types of VAWTs (a) H-Rotor, (b) Darrieus, and (c) Savonius

Table 1.1: Characteristics of Different Types of Wind Turbines [16]

	Savonius	Darrieus	HAWT
Power Coefficient	0.15 - 0.2	0.35-0.4	0.45
Blade profile	Simple	Complicated	Complicated
Yaw mechanism needed	No	No	Yes
Pitch mechanism possible	No	Can be Used	Yes
Tower	No	No	Yes
Tip Speed Ratio	Low	Moderate	High
Noise	Low	Moderate	High
Generator position	On ground	On ground	On top of tower
Self starting	Yes	Yes if Curved	Yes
Foundation	Simple	Simple	Extensive
Overall structure	Simple	Simple	Complicated

The main advantages of VAWTs over HAWTs are:

- Lower cut-in wind speed: VAWTs can start producing electricity at lower wind speeds compared to HAWTs which allows VAWTs to be placed closer to the ground.
- Omni-directional rotor: VAWTs do not need a pitch and yaw system to orient the blades into the wind [17].
- Lower noise level operation: VAWTs operate at lower tip speed ratios compared to HAWTs, they do not generate as much noise, and have lower vibration levels.
- Lower construction, installation, and maintenance costs: Construction and installation costs are lower for VAWTs than HAWTs since VAWTs have fewer moving parts. The inverter and generator are located near the ground and a gearbox may not be required (direct generation systems) making a VAWT easier to maintain [17].

1.3.1. Savonius VAWTs

The Savonius wind turbine was invented 1929, it is the simplest of all wind turbines. Aerodynamically, it is a drag-type device, consisting of two, three or more buckets as shown in figure 1.4. Because of the curvature, the buckets experience less drag when they move against the wind (Retarding Bucket) than when moving with the wind (Advancing Bucket). The differential drag causes the Savonius rotor to spin even at low wind speeds. In the symmetric drag position the flow attachment to the convex surface of the advancing bucket produces a low-pressure region that pulls the blade into torque-adding direction [18]. Savonius turbines are not widely used because of their low efficiencies compared to other lift type VAWTs (Savonius turbine efficiency is 15-20%, Darrieus turbine efficiency is 35%) [19, 20], however Savonius turbines have the advantages of simple construction and low noise levels [20].

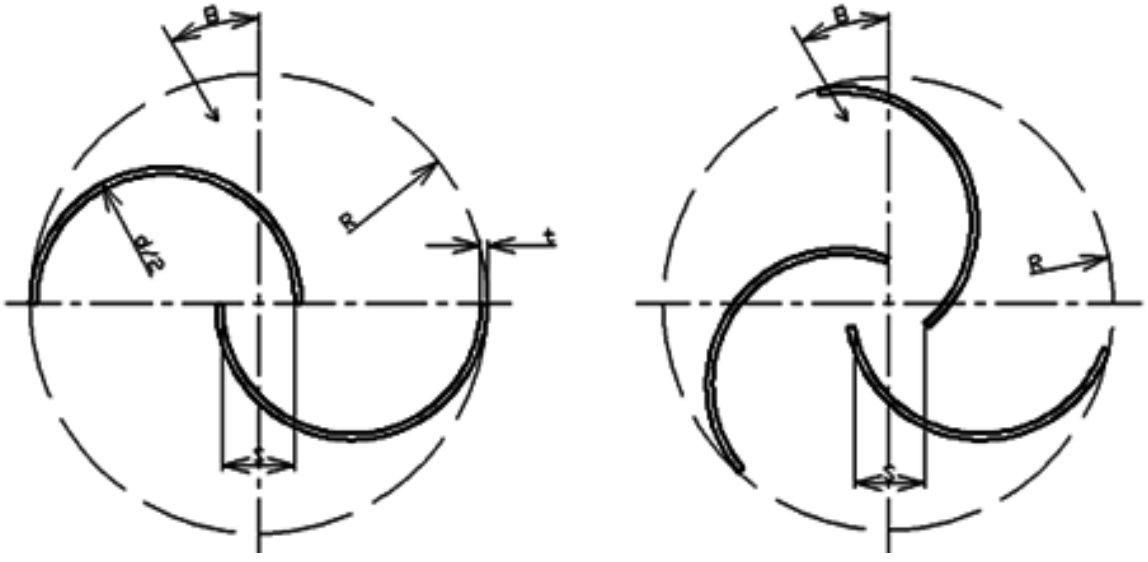

Figure 1.4: Two and Three Buckets Savonius VAWT

Experimental studies have been carried out to improve the performance of Savonius wind turbine rotor by changing the number of blades. The two bucket configuration is found to have better aerodynamic performance than the three bucket configurations, and the three bucket configuration has higher minimum static torque than the two bucket configuration [21]. Setting two Savonius rotors in a vertical arrangement on the same shaft with a relative phase angle 90 degrees as shown in figure 1.5, provides higher power output, higher stability of the auto start-up characteristics, and lower cyclic torsion during rotation [21]. Performance improvement was also done by investigating bucket overlap, gap width, shape of the bucket and reduction of the anti-rotation torque of the rotor shaft using curtains or ducts [21, 22, 23] as shown in figures 1.6, 1.7 and 1.8. The static torque performance is improved by increasing the overlap ratio. The torque and the power coefficients of the Savonius rotor reaches maximum values at an overlap ratio of 0.1-0.15 [24].

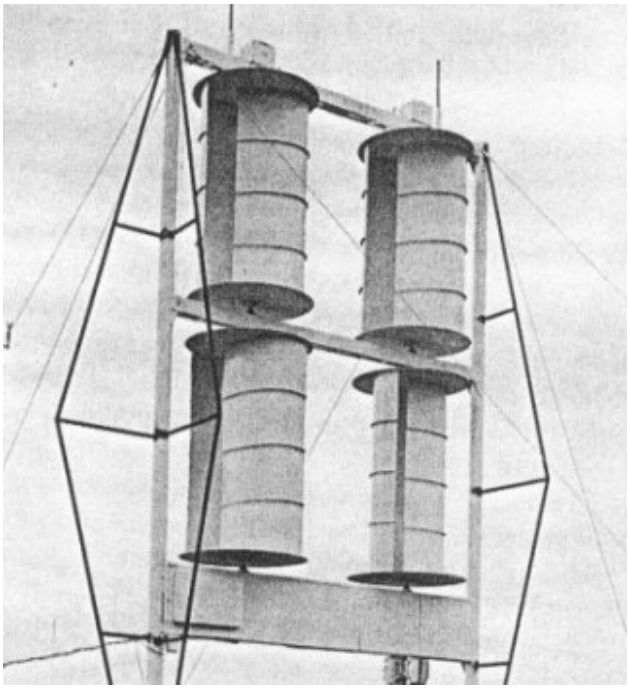

Figure 1.5: Two Vertical Arrangement of Two Sets of Savonius Rotors (Two Buckets), One above the other on the Same Shaft, with a Relative Phase Angle 90 Degrees [21]

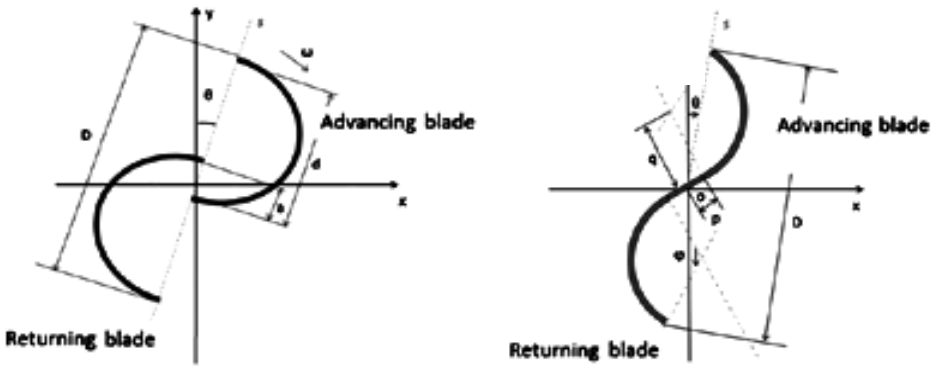

Figure 1.6: Two Buckets Savonius VAWT with Different Shapes [22]

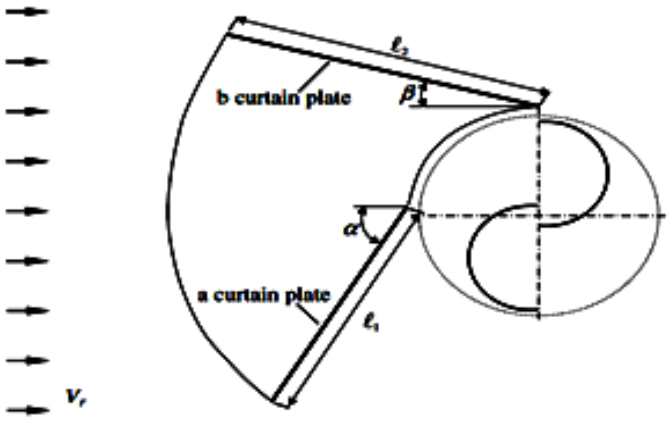

Figure 1.7: Two Buckets Savonius VAWT with Curtains [23]

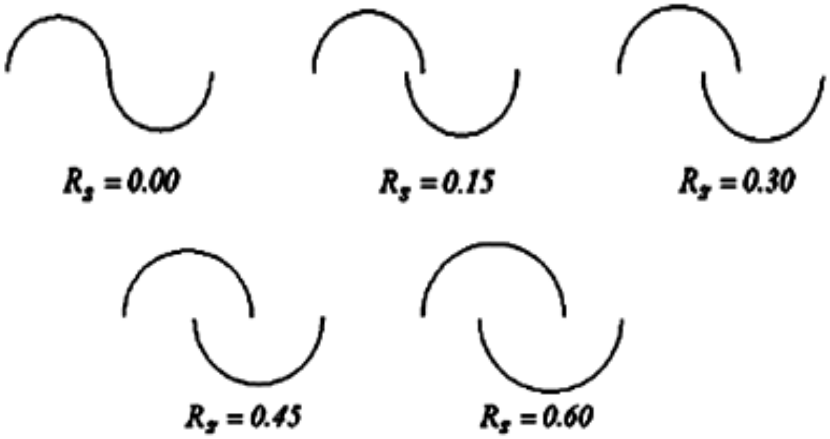

Figure 1.8: Two Buckets Savonius VAWT with Different Overlap Ratios [24]

1.3.2. Darrieus VAWTs

The Darrieus wind turbine was patented in 1931 by a French aeronautical engineer Georges Jean Marie Darrieus, There are two types of Darrieus turbines [25]: the straight blade designs (Giromill or H-rotor) shown in figure 1.3 (a), the curved or spiral blade named as the "eggbeater" shown in figure 1.3 (b). The Darrieus VAWT is a lift-device that operates at tip speed ratios greater than one. It contains of a rotor with two or more airfoil-shaped blades [26]. When the Darrieus turbine blade cuts through the air with an angle of attack, a pressure difference occurs between the opposite surfaces of the blades. Figure 1.9 shows force analysis on Darrieus turbine blades at different azimuth angles [27], the pressure difference results in lift and drag forces, both forces generate torque on the blade. In order to drive the turbine, the net torque caused by the lift forces in the direction of rotation must be greater than the net torque caused the drag forces opposite to it.

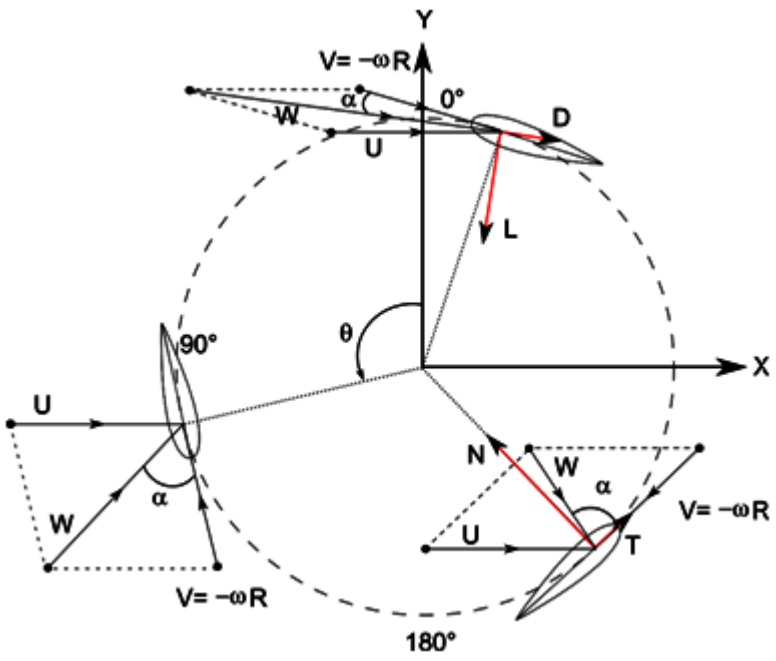

Figure 1.9: Force Analysis on Darrieus Turbine Blades at Different Azimuth Angles [27]

A drawback with lift type VAWTs is that the angle of attack changes as the turbine spins causing a fluctuation in the generated torque values. Each blade experiences maximum lift (torque) twice per revolution, resulting in sinusoidal torque and power output that cause vibration during operation [28]. Another problem of Darrieus type VAWT is that the majority of the mass of the rotating mechanism (Blades mass) is at the periphery rather than at the hub, this results in high centrifugal stresses on the turbine structure. Also the lift based VAWT devices (except for curved blade types) have a low self starting capability, the average torque is zero or sometimes negative at low tip speed ratios. This problem is solved by using starting motors to initiate the rotation [29, 30].

1.4. Small Scale Wind Energy

Large wind energy systems has been forced away from high energy demand population centers and toward remote locations including offshore sites with the requirement of long transmission lines and large installation cost. Small turbines shown in figure 1.10 can offer advantages by saving transmission lines, reducing installation costs, and reducing land farm areas required, in addition to reducing noise levels [31]. At the level of 10 KW output power, constant wind is an ideal condition for HAWT. On the other hand small VAWTs have their advantages on small HAWTs as the later do not operate well when located in urban areas of high turbulence and low wind speed [32]. The tip speed ratio of the HAWT defined as the ratio between the tangential velocity to the free stream velocity is generally about 5 to 7 as shown in figure 1.11, and at such high speed, the blades cut the air flow producing loud aerodynamic noise, also many birds can difficultly escape through such high-speed blade. The tip speed ratio of the VAWT is usually 1.5

to 2, low tip speed ratio operation produces very low aerodynamic noise. This solved the difficulty to erect the wind turbine in urban public facilities and residential areas [19].

Figure 1.10: Small Scale HAWT and VAWT Installed at Residential Areas

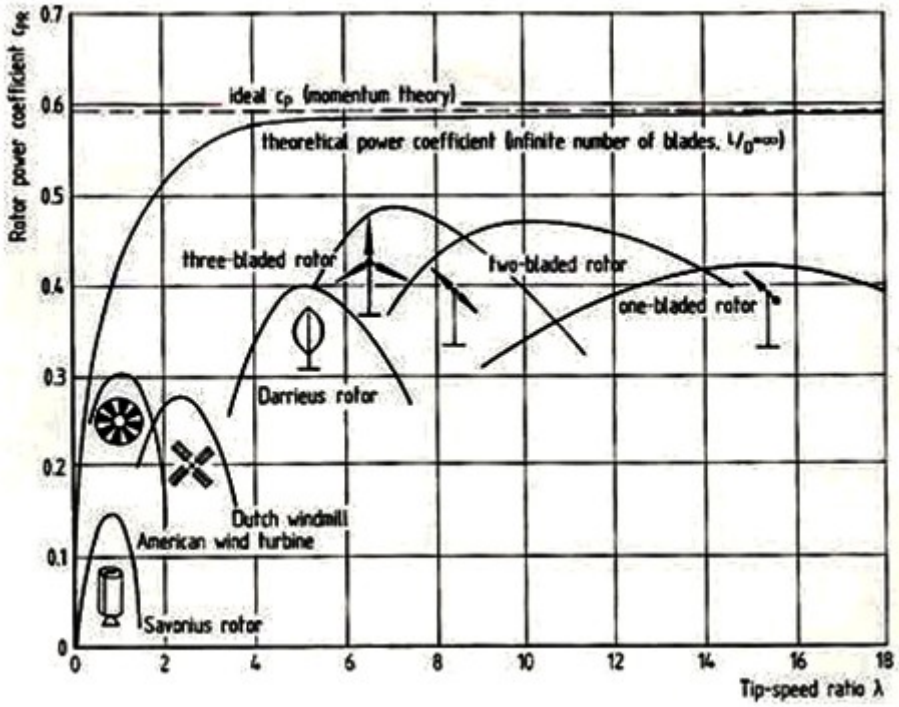

Figure 1.11: Power Coefficient of Different Types of Wind Turbine VS Tip Speed Ratio

1.5. Dissertation Overview

Development of wind technology related areas (material science, aerodynamic, analytical methods, experiment and testing) contributed in the generation of new wind turbines to improve the global wind market [33]. This thesis focuses on the aerodynamic performance and power generation analysis of VAWT clusters and farms. The study of VAWTs aerodynamic performance is classifies into: analytical solution, wind tunnel testing, wind field testing and numerical simulation. Although wind tunnel and wind field testing are the most reliable techniques, however they need high costs and long work cycles. With the development of the computational techniques, computational fluid dynamics (CFD) technology is becoming a significant tool for aerodynamic performance analysis for wind turbines. In this study, clusters of VAWTs are simulated in order to develop efficient VAWT farms, two types of VAWTs are studied: Savonius and Darrieus turbines. The thesis is composed of ten chapters, their contents are described below:

- Chapter 1 provides the motivation of this study, an overview of wind energy and an explanation of the goals and progress of wind energy in the United States. The concept of small-scale wind energy is addressed and a description of the advantages of VAWTs is provided. Also it includes information on research studies relevant to VAWT performance improvement and optimum layouts.
- Chapter 2 presents the validation of the numerical model used for the simulation of Savonius turbine clusters. The performance of a single Savonius turbine is studied with two dimensional and three dimensional numerical solutions and the computed results are compared with the available experimental data.

- Chapter 3 introduces the study of multi- co-rotating Savonius turbine clusters. Numerical solutions are performed for clusters of two turbines in parallel and oblique positions, and triangular clusters of three turbines. An efficient three turbine cluster having a triangular shape is developed.
- Chapter 4 introduces the study of multi- counter-rotating Savonius turbine clusters. Numerical solutions are performed for clusters of two turbines in parallel and oblique positions, and triangular clusters of three turbines. An efficient three turbine cluster having a triangular shape is developed. The numerical results are compared to the results of co-rotating clusters introduced in chapter 3.
- Chapter 5 presents the development of efficient patterned Savonius (VAWT) farms that consists of multiples of the efficient triangular three turbine cluster developed in chapter 4. The pattern is confirmed for the following geometric progressions of common ratio three by numerical simulation solutions of nine and twenty seven turbines farms.
- Chapter 6 presents the validation of the numerical model used for the simulation of Darrieus turbine clusters. The performance of a single Savonius turbine is studied with two dimensional and three dimensional numerical solutions and the computed results are compared with the available experimental data. Physical insights and a comparison between the turbine and a Rankine vortex flow fields is introduced.
- Chapter 7 introduces the study of multi- co-rotating Darrieus turbine clusters. Numerical solutions are performed for clusters of two turbines in parallel and oblique positions, and triangular clusters of three turbines. A triangular three co-rotating turbine cluster is developed.

- Chapter 8 introduces the study of multi- counter-rotating Darrieus turbine clusters. Numerical solutions are performed for clusters of two turbines in parallel and oblique positions, and triangular clusters of three turbines. The numerical results are compared to the results of the co-rotating clusters introduced in chapter 7. Based on the comparison a triangular efficient hybrid three turbine cluster is developed and compared to the three co-rotating turbine cluster introduced in chapter 7.
- Chapter 9 presents the development of efficient patterned Darrieus (VAWT) farms that consists of multiples of the efficient triangular hybrid three turbine cluster developed in chapter 8. The pattern is confirmed for the following geometric progressions of common ratio three by numerical simulation solutions of a nine turbine farm.
- Finally conclusion of this study and recommendations for future work is introduced.

Chapter 2

Numerical Model Validation for Single Savonius Wind Turbine

In this chapter, the performance of a single Savonius VAWT is numerically studied and the different flow patterns around the turbine buckets are identified. Two and three dimensional simulation models are solved, The static and dynamic torque coefficient are calculated at different tip speed ratios, the numerical results are compared with the available experimental data in reference [21] in order to validate the numerical model.

2.1. Two Dimensional Numerical Simulation

The unsteady flow around the Savonius rotor requires a great care in building the CFD model. In order to obtain accurate aerodynamic coefficients, a numerical solution independent of the domain, time-step, grid, and other pertinent modeling conditions is developed. The two types of Vertical axis wind turbines, Savonius and straight blade Darrieus wind turbines, under investigation in this study have constant cross sections all-over their blade heights. A two dimensional CFD simulation model is adopted since this study is aiming to construct wind farms consisting of high aspect ratio VAWTS [10, 11]. The two dimensional CFD model is built using ANSYS 14.5 workbench multi-physics platform, a workflow starting from CAD generation to post-processing of the results is developed. Fluent code is used to solve the unsteady Reynolds averaged Navier-Stokes Eq. (1) using finite volume method [11, 34, 35].

$$\rho \bar{u}_j \frac{\partial \bar{u}_i}{\partial x_j} = \rho \bar{f}_i + \frac{\partial}{\partial x_j}\left[-\bar{p}\delta_{ij} + 2\mu \bar{S}_{ij} - \rho \overline{u_i' u_j'}\right] \qquad \text{Eq. (1)}$$

Where:

$u, \bar{u}, \text{ and } u'$	Instantaneous, mean, and fluctuating velocities, respectively
$\bar{f}_i$	External forces
$\bar{S}_{ij} = \frac{1}{2}\left(\frac{\partial \bar{u}_i}{\partial x_j} + \frac{\partial \bar{u}_j}{\partial x_i}\right)$	Mean rate of strain tensor
ρ	Density
μ	Dynamic viscosity

The procedures of the model creation is done in the following steps:

- 2D CAD model generation and computational domain building.
- Generating a high quality mesh for the domain that satisfies the requirements of the turbulence models and achieves the solutions grid independency.
- Setting the Fluent solver scheme and turbulence model.
- Post-processing of the results.

2.1.1. Features of the Geometry

The Savonius turbine used in this study shown in figure 2.1 is found in the experimental scientific literature [21]. The geometry features of the turbine are listed in table 2.1. An overlap ratio of 0.15 is adopted since the torque and the power coefficients of the rotor are maximum at this ratio [24].

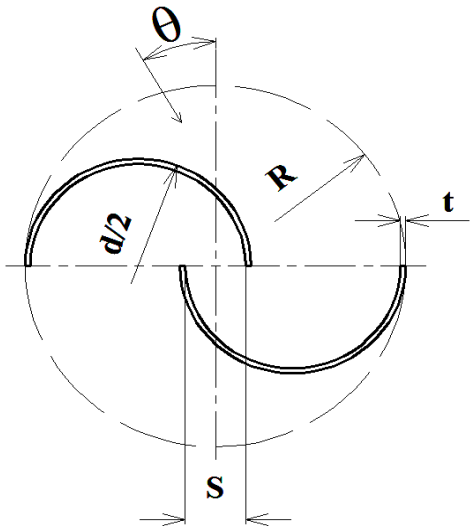

Figure 2.1: Two Bucket Savonius Vertical Axis Wind Turbine

Table 2.1: Savonius Turbine Geometry

Turbine Category	Vertical Axis Wind Turbine
Turbine Type	Savonius Turbine
Number of Buckets	2.0
Blade Diameter (D) [m]	1.0
Blade Height (H) [m]	1.0
Buckets Diameter (d) [m]	0.525
Blade Thickness (t) [mm]	1.0
Overlap ratio (e=S/d)	0.15

2.1.2. Computational Domain Generation

The computational domain is built using the CAD interface ANSYS "Design Modeler". The computational domain is sufficiently large so that the boundaries are far from the turbine vicinity. Several tests are performed to obtain a solution independent on the domain size, the domain shown in figure 2.2 (a) meets the requirements of independence, accuracy and avoid an increase in cell numbers and computational time. The upstream boundary (semi circle) together with the upper and lower boundaries are chosen to be at a distance of 15D (D is the rotor diameter) from the rotor, velocity inlet boundary condition is used with x-velocity component equal to 7 m/sec. The downstream boundary is set at 30D from the rotor with a pressure outlet boundary condition. The unsteady flow is solved using the sliding mesh method, the computational domain consists of two sub-domains: a rotating region (1) that contains the rotor, and a fixed region (2) which extends from the interface of the rotating region (1) to the boundaries of the domain. The surface between the two sub-domains is defined as an interface.

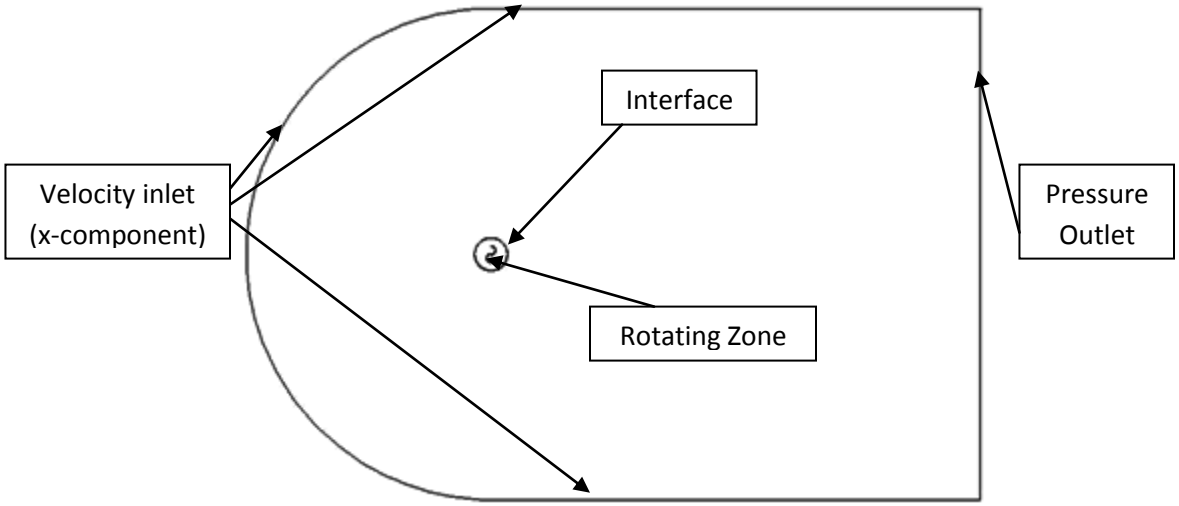

(a)

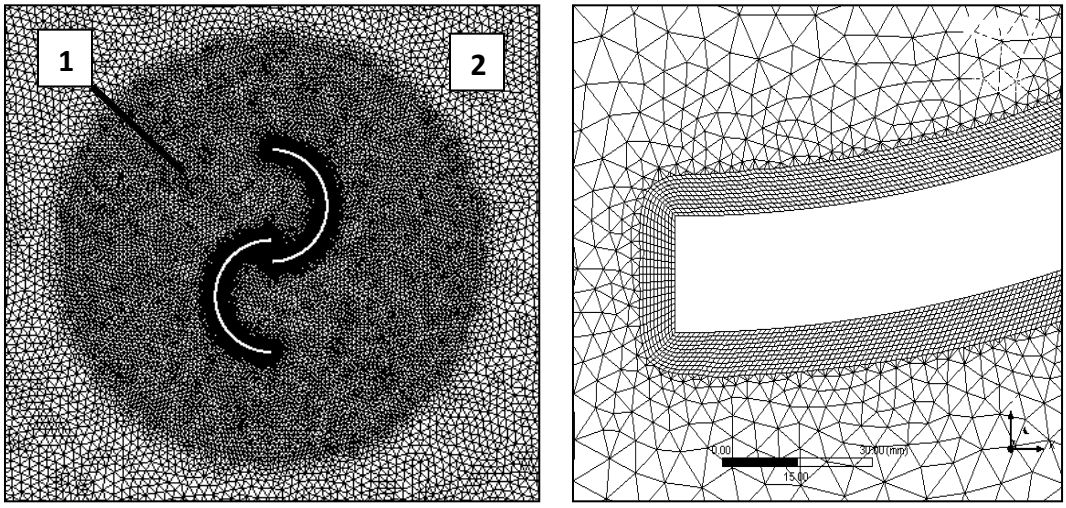

(b) **(c)**

Figure 2.2: Computational Domain and Grid Structure near the Rotor

2.1.3. Grid Generation

High quality non conformal mesh is generated using ANSYS Meshing advanced sizing functions. The computational domain is discretized using unstructured triangular elements and is created from a rotating region (1) and a fixed region (2). The grid structure is shown in figure 2.2 (b) and a magnified view of the grid near the rotor bucket is shown in figure 2.2 (c). A refined

grid with inflation is imposed to the boundary layer of the buckets with 10 levels of quadrilateral cells, so that y+ < 1 as required by turbulence models [36,37], followed by unstructured triangular elements inside and outside the rotating region in order to avoid directionality effects as the circular domain rotates. A grid independence study is carried out by refining the mesh six times until there is no significant change is observed in the result of the torque coefficient as shown in figure 2.4. The levels of mesh refinement adopted are shown in table (2.2). The study showed that level 4, with 100,860 nodes, is enough for the single turbine simulation as the value of the torque coefficient started to differ by $1x10^{-4}$ for the k-omega SST model and by $1x10^{-3}$ for the transition SST model solutions.

Table 2.2: Grid Refinement Levels for Single Savonius Turbine 2D Simulation

Grid Level	No. of Cells	Cm K-omega SST	Cm Transition SST
1	23,714	0.160	0.374
2	38,090	0.165	0.351
3	59,212	0.172	0.254
4	100,860	0.189	0.233
5	180,272	0.190	0.232
6	286,928	0.191	0.231

2.1.4. Solver Settings and Turbulence Model

A parallel processing is performed using 8 logic processors with a maximum speed of 2.4 GHz, this reduces Fluent computational time by 60-70% [38]. The solver is set as pressure based with absolute velocity formulation. The validation process is based on static and dynamic experimental data [21]. The static tests are performed using steady simulation, while the dynamic tests are done using the transient solver to account for the unsteady effects and interactions between blades motion and wake. In the transient solution the cell zone conditions are set for the

rotating region in order to activate the Sliding Mesh Model (SMM). The unsteady Reynolds averaged Navier-Stokes equations are solved using SIMPLE (Semi-Implicit Method for Pressure Linked Equations) algorithm with a second order upwind spatial discretization algorithm for all the pressure, momentum, and turbulence equations and a Least Squares Cell Based algorithm is used for gradients [13].

Turbulence equations are solved through the use of a turbulent-viscosity model. The most widely used two-equation models known for improvement in accuracy are the K-ε model of Jones and Launder (1972) and the K-ω model developed by Wilcox (1993). The K-ω shear stress transport (SST) model accounts for the sub-layer of the boundary layer, this leads to major improvements in the prediction of adverse pressure gradient flows [39]. Similar studies [35, 36] have employed this model, as high boundary layer accuracy is required in investigating the flow field around Savonius rotors. At high tip speed ratios a noticeable increase can be observed in the laminar fraction inside the boundary layer leading to low in-flow velocities. The transition phenomenon becomes significant, this influences a discrepancy between the simulation results and experiment data in the case of the fully turbulent flow assumption used by RANS turbulence models. VAWTs work at low Reynolds numbers, so the use of a transition model should give more accurate prediction of the performance [36]. In this study, the transition SST turbulence model given in details by Menter [40] is used. It is based on SST k-omega transport equations coupled with two additional transport equations (2) and (3), one for intermittency (γ), and the other for the momentum-thickness Reynolds number $Re_{\theta t}$ as follows:

$$\frac{\partial(\rho\gamma)}{\partial t}+\frac{\partial\left(\rho U_j\gamma\right)}{\partial x_j}=P_{\gamma 1}-E_{\gamma 1}+P_{\gamma 2}-E_{\gamma 2}+\frac{\partial}{\partial x_j}\left[\left(\mu+\frac{\mu_t}{\sigma_\gamma}\right)\frac{\partial\gamma}{\partial x_j}\right] \qquad \text{Eq. (2)}$$

$$\frac{\partial(\rho R\tilde{e}_{\theta t})}{\partial t}+\frac{\partial\left(\rho U_j R\tilde{e}_{\theta t}\right)}{\partial x_j}=P_{\theta t}+\frac{\partial}{\partial x_j}\left[\sigma_{\theta t}\left(\mu+\mu_t\right)\frac{\partial R\tilde{e}_{\theta t}}{\partial x_j}\right] \quad \text{Eq. (3)}$$

The transition model interacts with the SST turbulence model by modification of the K-equation (4), the details and definition of all terms are defined in reference [40].

$$\frac{\partial}{\partial t}(\rho k)+\frac{\partial}{\partial x_i}(\rho k u_i)=\frac{\partial}{\partial x_j}\left(\Gamma_k\frac{\partial k}{\partial x_j}\right)+\tilde{G}_k-Y_k+S_k \quad \text{Eq. (4)}$$

2.1.5. Results for Single Savonius Turbine Static and Dynamic Simulation

Both static and dynamic numerical simulations are performed to a single Savonius rotor for the validation of the numerical model. The flow field around a static rotor is solved by a steady flow at different azimuth angle (θ). Cases are solved starting by θ = 0^o to θ =180^o with an increment of 20^o between each case. The convergence of the numerical solution is checked as follows: 1- The residuals of the iteration process for the momentum, continuity and turbulence equations are monitored, convergence criteria are set to satisfy a maximum RMS residual of $1x10^{-6}$ for the static simulation and a drop of at least 3 orders of magnitude in each time step for the time dependent dynamic simulation as well as a minimum of 20 iterations per time step. 2- The momentum coefficient of the rotor is monitored [21]. 3- The mass flow balance between inlet and outlet is also checked. The static torque (Ts) is calculated about the turbine center by summing the cross products of the pressure and viscous forces vectors for each face of the two buckets with the moment vector, which is the vector from the specified moment center to the force origin. Then the static torque coefficient (Cm) is calculated using equation (5):

$$C_{ms}=\frac{T_s}{0.5\rho V_\infty^2 R A_s} \quad \text{Eq. (5)}$$

Figure 2.3 shows a turbulence model sensitivity study using three turbulence models (k-ε, K-ω SST and Transition SST models) on a static rotor, the numerical results are compared with experimental data [21]. Values of Turbulent Intensity (Tu) and Turbulent Viscosity Ratio (TVR) are set to be Tu = 0.1 % and TVR = 10 both in inlet and outlet [38]. The figure shows the static torque coefficient calculated at different azimuth angles , the results calculated by K-ω SST and Transition SST models are closer to the experiments data than the results by k-ε.

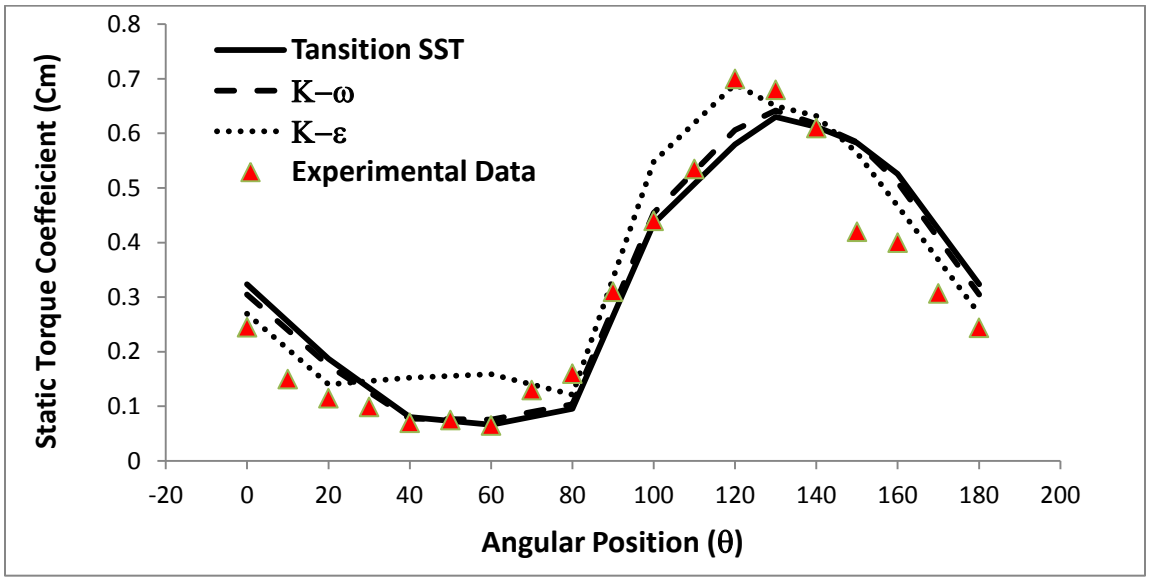

Figure 2.3: C_{ms} at Different Azimuth Angles θ for Two Bucket Savonius Turbine, Re= 4.32×10^5, Comparison between Numerical Results using Different Turbulence Models and Experimental Data [21]

A dynamic simulation is also performed at different tip speed ratios (λ), a steady flow simulation is run initially to set up the flow domain to reasonable parametric values then a fully implicit time advancement scheme is applied using a sliding mesh model (SMM) [36]. Different time step sizes has been tested and a time step size corresponding to a turbine rotation of 1.0 degree has been found to be adequate [10, 41, 42]. Figure 2.4 is a monitoring of the momentum coefficient of the rotor, this value shows a periodic behavior along the azimuth angle of the rotor,

the mean value of the moment coefficient is calculated after periodic convergence for more than ten complete rotor revolutions and compared to experimental data. The torque coefficient is calculated at each time step and averaged from the last two revolutions [18], then the power coefficient (Cp) is calculated using equation (6):

$$C_p = C_m * \lambda \qquad \text{Eq. (6)}$$

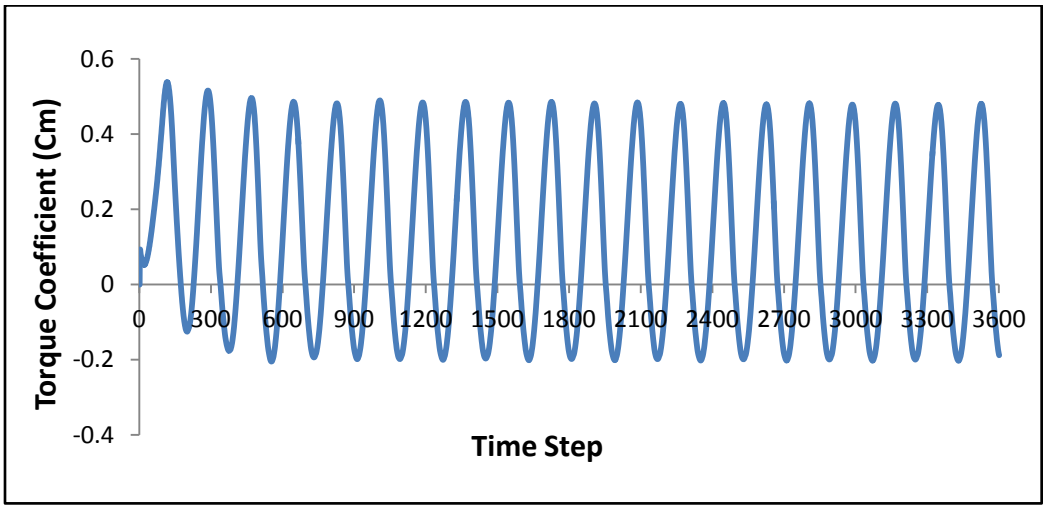

Fig. 2.4: Dynamic Torque Coefficient at Different Time Steps, λ=1

The experimental data [21] are measured in a wind tunnel with a test section (4.1x6.1 m) the tunnel blockage causes the local wind velocity in the test section to increase. This increase is accounted for by applying a tunnel blockage factor (ε). The model frontal area was calculated from the turbine-swept area adding the frontal area of the stand and related hardware. This gave a value for ε= 0.0125:

$$\varepsilon = \frac{1}{4}\frac{Model\ Frontal\ Area}{Test\ Section\ Area}$$

The value of the blockage factor is used to correct the free-stream velocity and dynamic pressure as shown, where the subscript u refers to uncorrected values:

$$V_{\infty} = V_{\infty_u}(1 + \varepsilon)$$

Figure 2.5 shows the power coefficient at different tip speed ratios (λ), the fully turbulent k-omega SST model under predicts the generated power and the Transition SST turbulence model has the closest results to the experimental data at different tip speed ratios, similar findings are reported in ref. [38]. The figure shows that the maximum average power coefficient for a single rotor is found to be 0.23 corresponding to λ equal 1 as shown in figure 2.5.

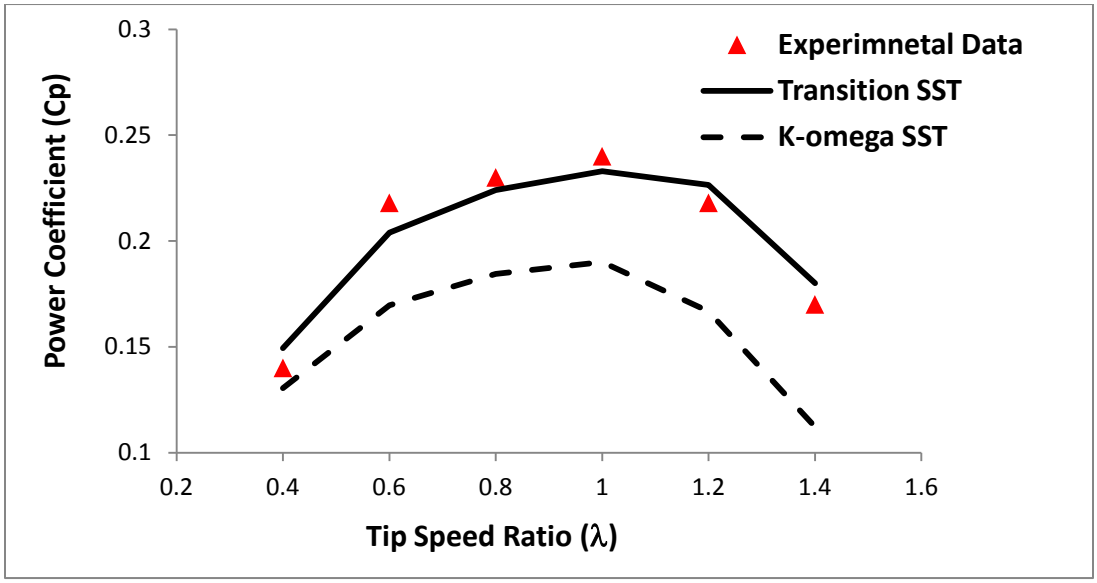

Figure 2.5: Power Coefficient at Different Tip Speed Ratios, Comparison between Numerical Results using Different Turbulence Models and Experimental Data [21]

Intermittency (γ) is the alternation between turbulent and non-turbulent motion that characterizes certain types of flow, it is defined as the ratio of time turbulent to total time at any point, so that it measures the probability of finding turbulent flow at any instant at the point considered. For laminar flow γ=0, for turbulent flow γ=1 and the transition is at $0 < \gamma < 1$.

$$\gamma = \frac{t_{turb}}{t_{lam} + t_{turb}}$$

The average intermittency (γ) on the buckets surface (the value is interpolated from all the mesh nodes of the cells containing the point) is compared for the static and the dynamic solutions as shown in figures 2.6 (a) and figure 2.6 (b) respectively. The results show that the average intermittency (γ) for the static solution is about 0.9 and for the dynamic solution is about 0.4. This explains the close results between the Transition SST model and the K-ω SST fully turbulent model in the static solution case (γ=0.9) and the discrepancy of the k-w SST model from the experimental data (γ=0.4). Figure 2.7 shows how the turbulent intensity contours generated by the two turbulence models. The fully turbulent K-ω SST model shows a fully turbulent flow around the buckets in figure 2.7 (a), however the Transition SST model shows that transition from laminar flow into turbulent flow at some positions as shown in figure 2.7 (b).

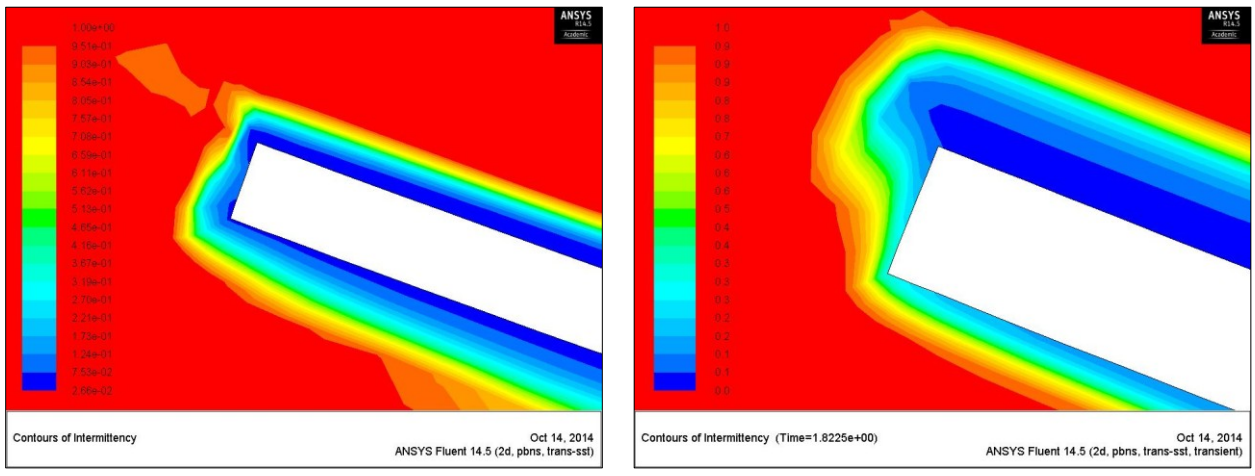

(a) **(b)**

Figure 2.6: Contours of Intermittency in the Vicinity of the Savonius Buckets for Static and Dynamic Solutions

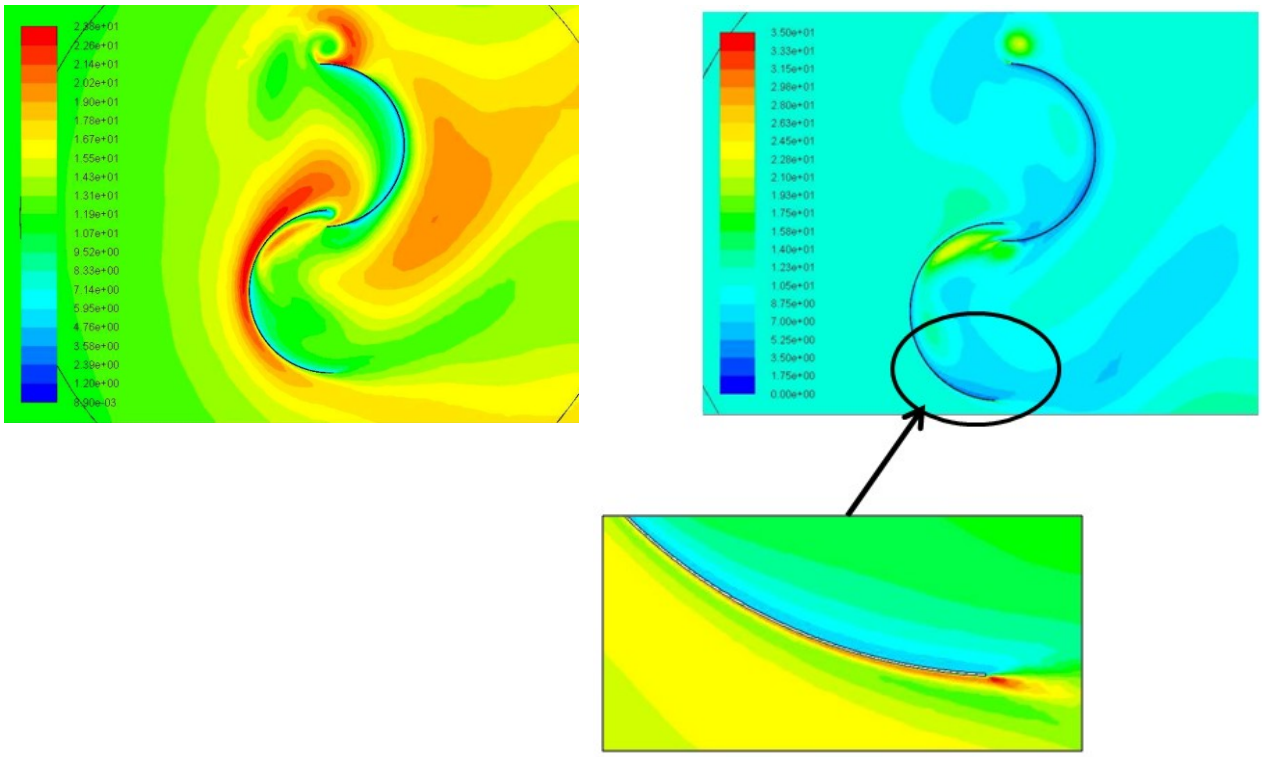

(a) **(b)**

Figure 2.7: Contours of Turbulent Intensity around the Savonius Buckets (a) K-ω SST model. (b) Transition SST model

2.1.6. Flow Pattern around a Single Savonius Rotor

The flow patterns are identified from the velocity vectors around the single Savonius rotor as shown in figure 2.8 (c), the flow pattern is found to be comparable to the experimentally extracted data [43] shown in figures 2.8 (a) and figures 2.8 (b). Flow (I): Coanda like flow (Attached flow along the advancing blade convex side), Flow (II): Dragging flow (from advancing blade convex side to returning blade concave side). Flow (III): Overlap flow though the overlapping area. Flow (IV): Stagnation flow from upstream to the returning blade convex side. Flow (V): Shedding vortex at the advancing blade tip. Flow (VI): Shedding vortex from the returning blade tip.

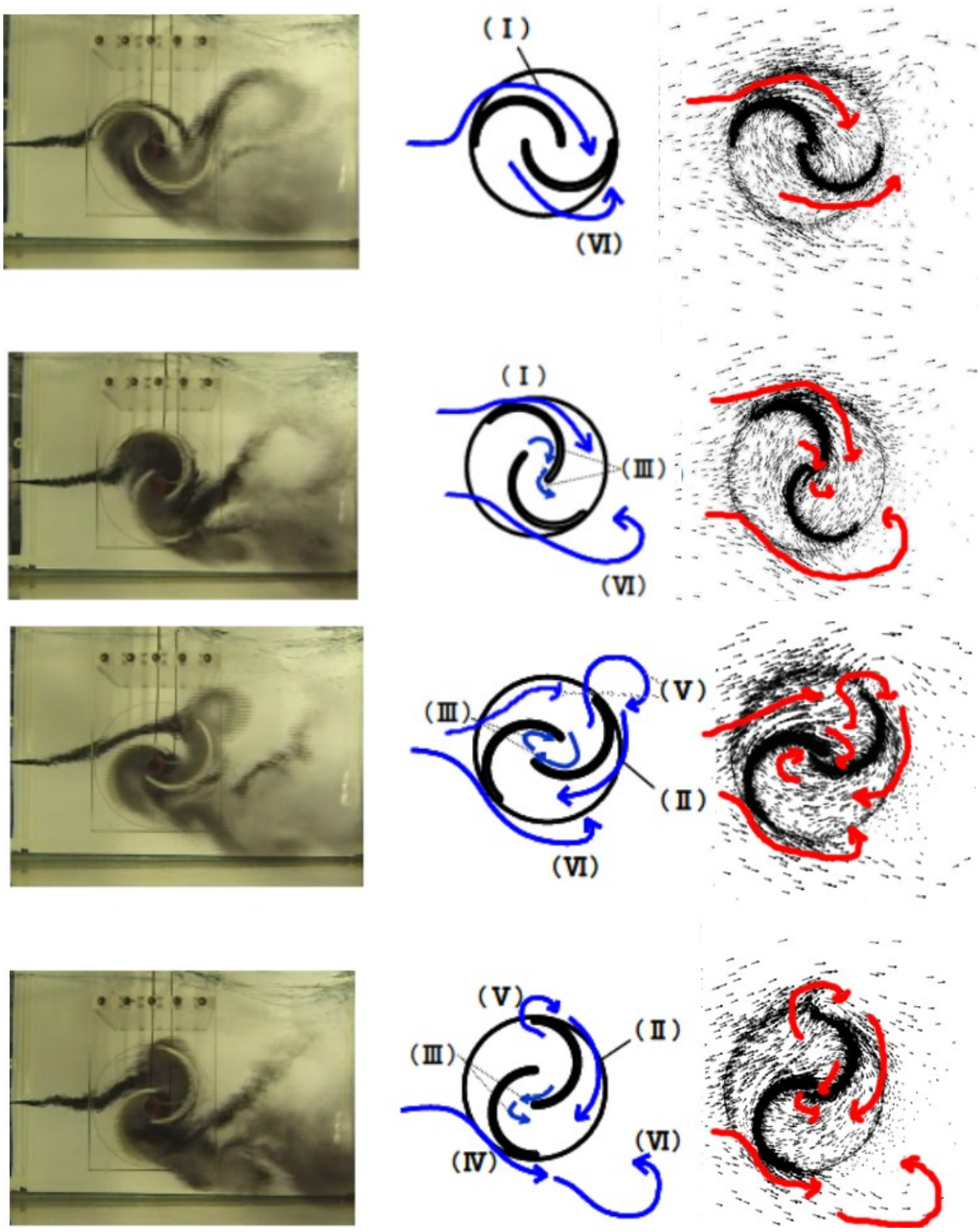

(a) **(b)** **(c)**

Figure 2.8: Flow Pattern around Single Savonius Rotor, Comparison between Numerical Results and Experimental Data [20], (a) Experimental Figures [21]. (b) Flow Patterns Extracted from Experimental Data [21]. (c) Flow Patterns Calculated Numerically

The velocity contours around the single rotor in figure 2.9 show that the flow pattern (I) is observed from 0^o to 45^o and produces lift when attached to the convex side of the advancing bucket. The attached flow (I) becomes a dragging flow (II) towards the concave side of the returning bucket, contributing to the enhancement of the power together with the overlap flow (III). The vortex shedding from the tip of advancing bucket (V) as well as that from the tip of the returning bucket (VI) occur at an angle equal to 90◦. At an angle greater than 90◦, the shedding vortex (V) is separated from the tip of the advancing bucket and grow as it flows to the downstream of the rotor. The flow pattern (IV) contribute to reduce the power of the rotor. Accurate knowledge of the wake structure is important because the vortices within the wake are responsible for creating induced drag on the structure generating them. The flow on the Savonius rotor separates around both sides of the rotor and that the width of the wake agrees closely with the rotor projected width which varies with the rotor angles [44]. Also it was observed that the wake of a single rotor is asymmetric, this is because the flow behind the advancing blade is different from that behind the retarding one as shown in the velocity contours in figure 2.9.

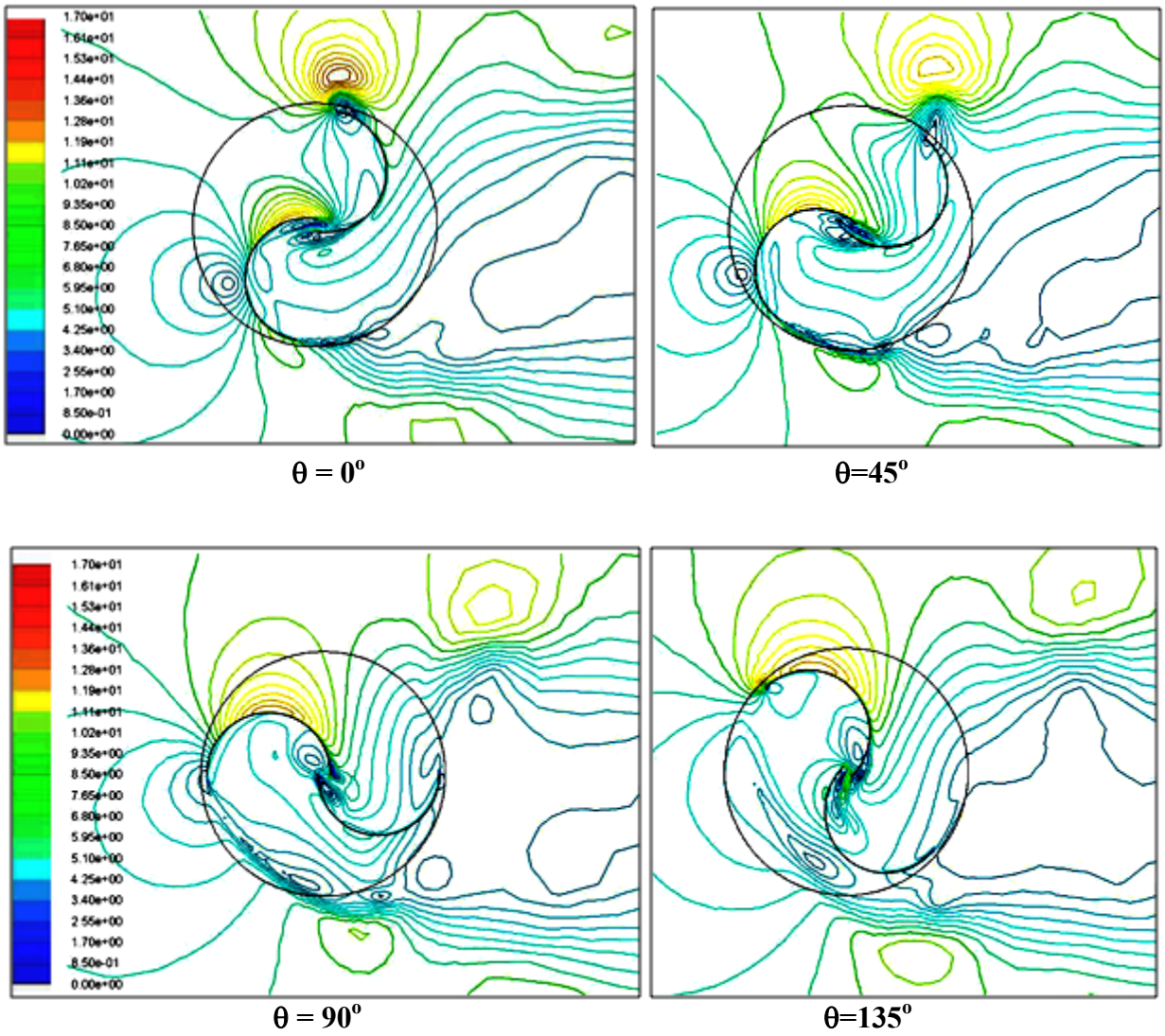

Figure 2.9: Velocity Contours around Single Savonius Rotor at Different Azimuth Angles

2.2. Three Dimensional Numerical Simulation

Previous researches showed that Savonius rotors with high aspect ratios have low losses due to the effect of the tips of the buckets [45], [19], [46], [47] and [48]. The aspect ratio growth of a Savonius turbine has an effect similar to adding end plates. The two end plates in the three dimensional model plays an important role in separating the suction and pressure surfaces of the blades reducing flow leakages [49]. The Savonius turbine under study has an aspect ratio AR=2,

and two end plates at its upper and lower ends. In this section, a 3D simulation of the single rotor is performed at different tip speed ratios, the results are compared to 2D simulation results and to the experimental data [21]. The 3D CAD model of the Savonius rotor shown in figure 2.10 is built using SOLIDWORKS CAD modeler, the upper and lower cap sizes are not mentioned in the experimental data, so they are assumed to have a diameter of 1.2 of the turbine diameter with a thickness of 2 mm.

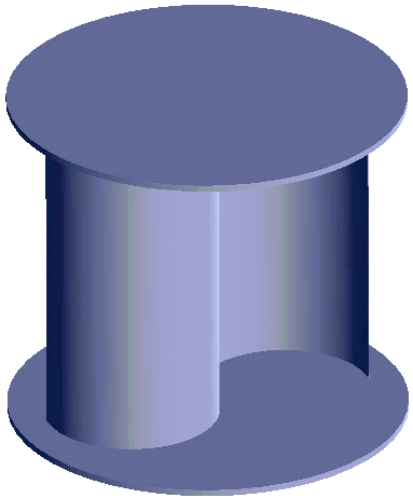

Figure 2.10 Two Bucket Savonius Wind Turbine 3D CAD Model

2.2.1. 3D Computational Domain

The 3D computational domain shown in figure 2.11 is built the same as the 2D domain with the upstream boundary together with the upper and lower boundaries at a distance of 15D from the rotor and a velocity inlet boundary condition of 7 m/sec for the x-velocity component. The downstream boundary is set at 30D from the rotor with a pressure outlet boundary condition. The sliding mesh model and the computational domain consists a rotating and stationary sub-domains. The surface between the two sub-domains is defined as an interface.

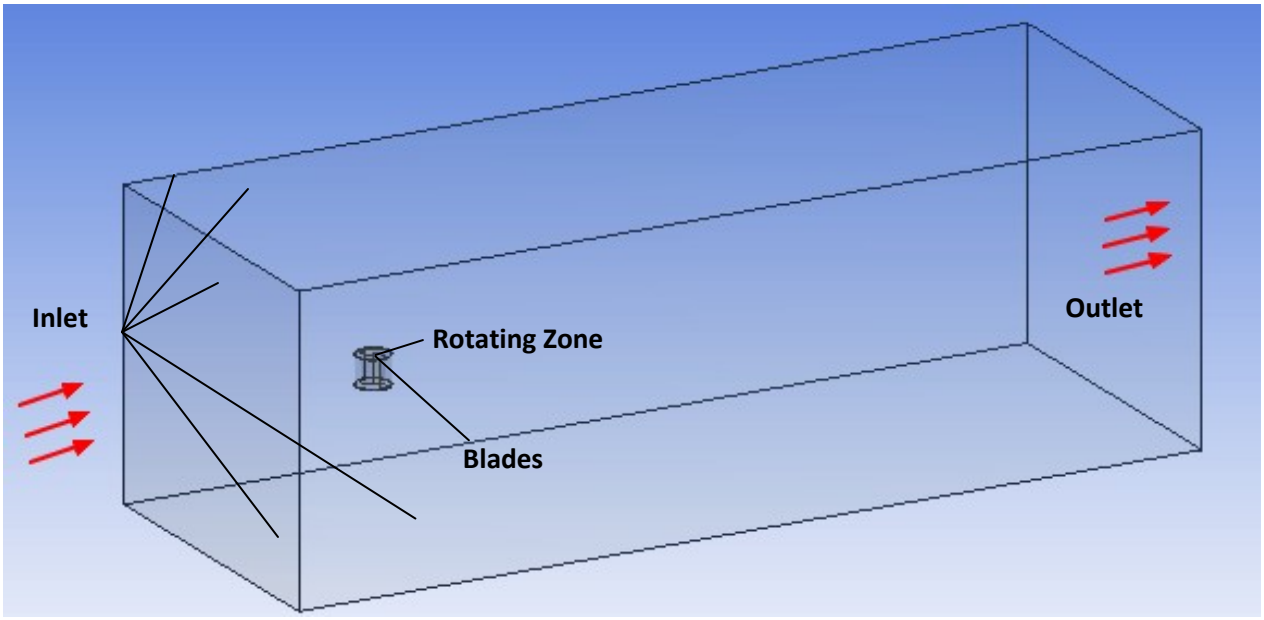

Figure 2.11: Three dimensional Computational Domain

2.2.2. Three Dimensional Grid Generation

The unsteady three dimensional flow is solved using the sliding mesh model, the computational domain is discretized using tetrahedral elements and is created from a rotating zone around the blade and a fixed zones. The experimental data are corrected to account for the tunnel blockage, the boundaries of the computational domain are taken at the same distances of the two dimensional solution so that the computational results can be compared with the corrected experimental data. The grid structure is shown in figure 2.12 (a) and a magnified view of the grid near the rotor is shown in figure 2.12 (b), a refined grid with inflation is imposed in the boundary layer of the buckets with 10 levels of hexahedral cells so that $y+ < 1$ as required by turbulence models [13,14]. A grid independence study is performed using three grid levels shown in table 2.3. Figure 2.13 shows the periodic change in the value of the torque coefficient of the Savonius

rotor calculated at different azimuth angles using the three grid levels, close values are observed for levels 2 and 3 so Level 2 with 1,999,508 cells was found to be adequate for the simulation.

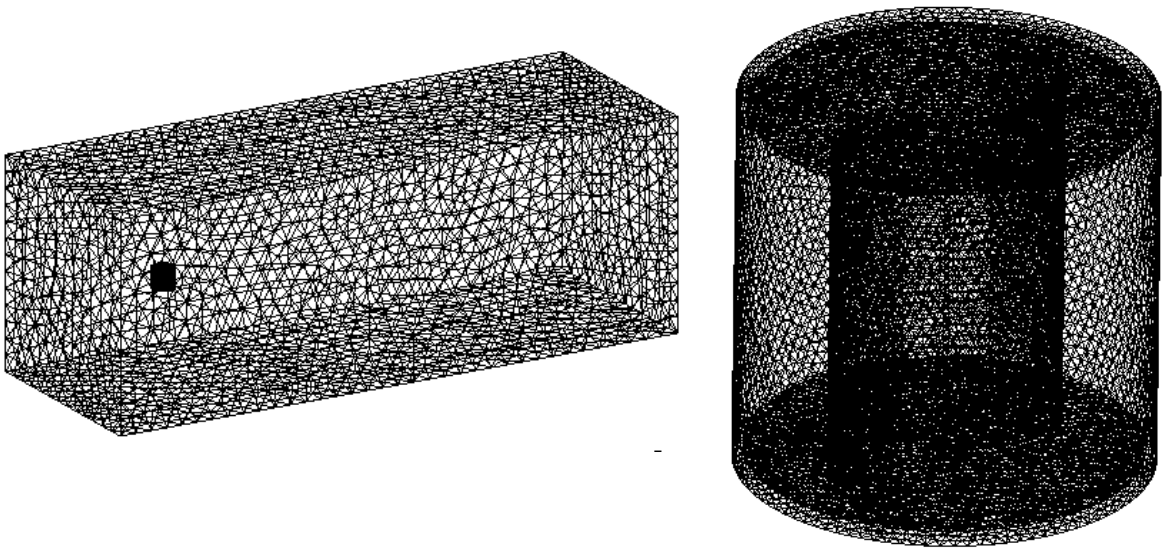

(a) **(b)**

Figure 2.12: Three Dimensional Grid Structure

Table 2.3: Grid Refinement Levels for Single Savonius Turbine 3D Simulation

Grid Level	No. of Cells	Cm Transition SST	Cm DES
1	752,361	0.1461	0.1806
2	1,999,508	0.1561	0.1909
3	4,204,210	0.1557	0.1901

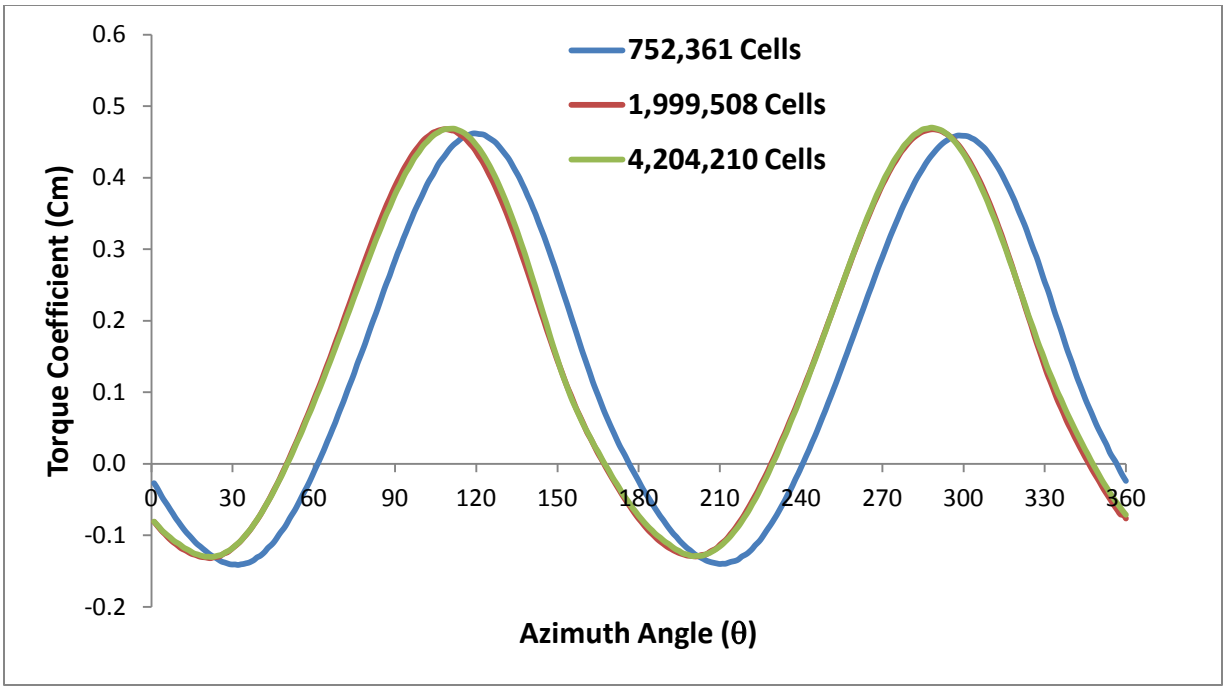

Figure 2.13: Torque Coefficient at Different Azimuth Angles for Three Grid Levels using DES

2.2.3. Three Dimensional Solver Settings, Turbulence Model and Results

The same boundary conditions and turbulence parameters used in the 2D solution are used in the 3D solution. Figure 2.14 shows the static torque coefficient calculated at different azimuth angles using three turbulence models k-ε, K-ω SST and Transition SST, a closer agreement to the experiments data is achieved by the numerical results of the transition models than the results by the other models which is the same as trend achieved by the two dimensional simulation and explained before as the capability of the Transition SST model to capture transition positions rather than dealing with the flow as fully turbulent.

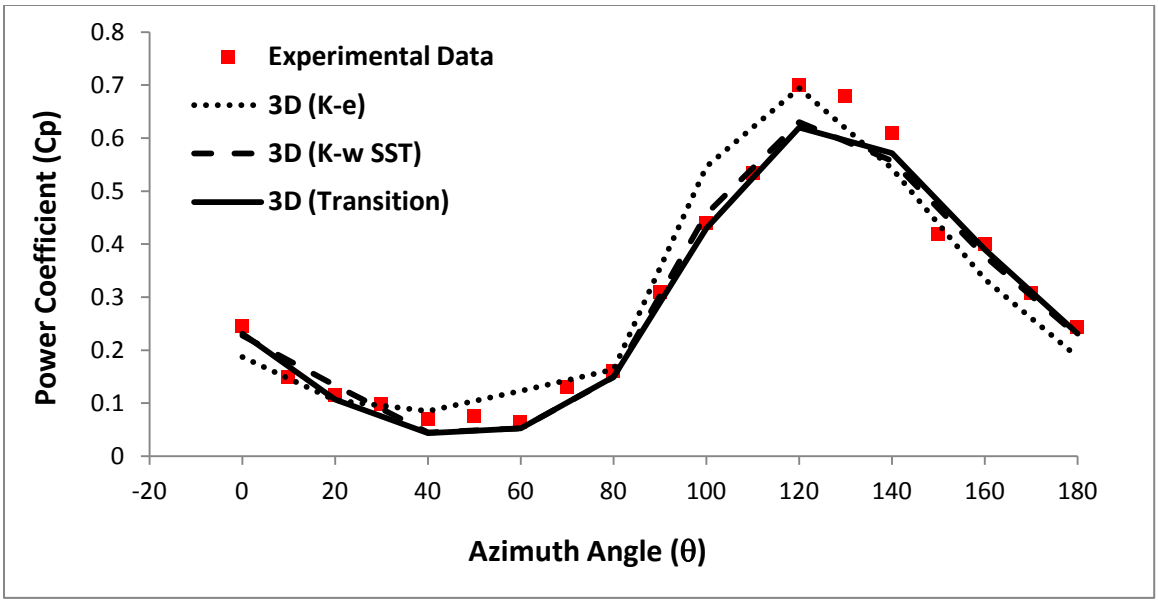

Figure 2.14: C_{ms} at Different Azimuth Angles θ for 3D Savonius Turbine, Re= 4.32×10^5, Comparison between Numerical Results using Different Turbulence Models and Experimental Data [21]

A dynamic simulation is also performed, the unsteady three-dimensional RANS equations are solved using ANSYS Fluent 14.5 solver. A time step corresponding to one degree rotation of the rotor is used and the average power coefficient is calculated at different tip speed ratios (λ). Figure 2.15 shows that the numerical results obtained using the Transition SST turbulence model are lower than experimental data. A similar behavior of RANS models was observed in references [19] and [45] for low aspect ratio VAWTs. The discrepancy obtained between the numerical results and the experimental data is caused by the difficulties to reproduce detached vortex structures by RANS turbulence models. To enhance the simulation, detached eddy simulation (DES) model is used for flow simulation with a near-wall treatment, the obtained numerical results by the DES model are closer to the experimental data for all tip speed ratios as shown in figure 2.15. Comparing the three dimensional simulation results with the two dimensional simulation shows that 2D simulation using transition SST model is the closest to

experimental data. The under prediction of the turbine performance by the 3D solution is accounted for the cap dimensions which are not available in the experimental data [21] and assumed as mentioned above. The velocity contours around the three dimensional Savonius rotor in Figure 2.16 shows a blockage effect by the upper and lower caps, consequently the reduction of the incoming velocity affect the performance results, this gives another reason for the lower power coefficients results in the three dimensional solution compared to the two dimensional.

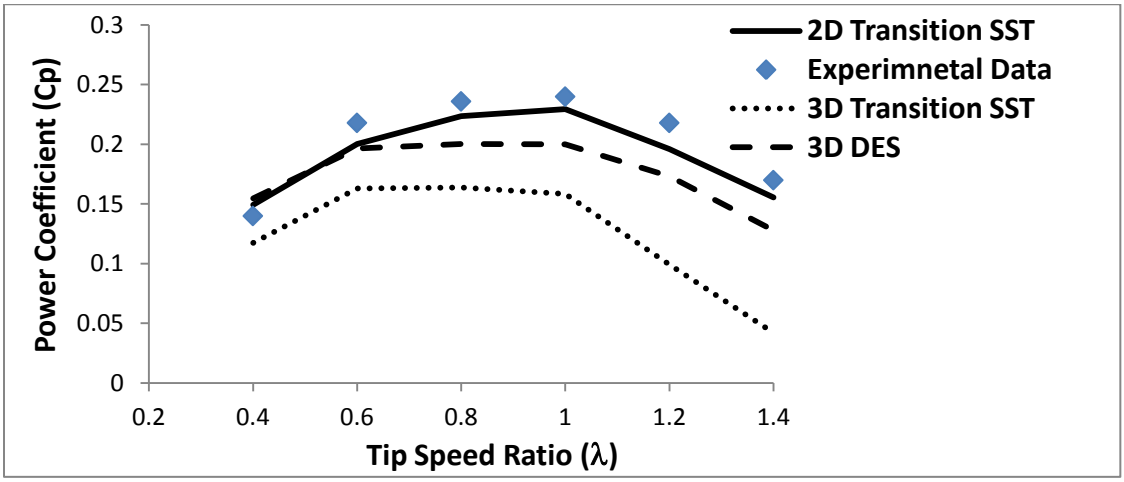

Figure 2.15: Power Coefficient Results for 3D Single Savonius Rotor

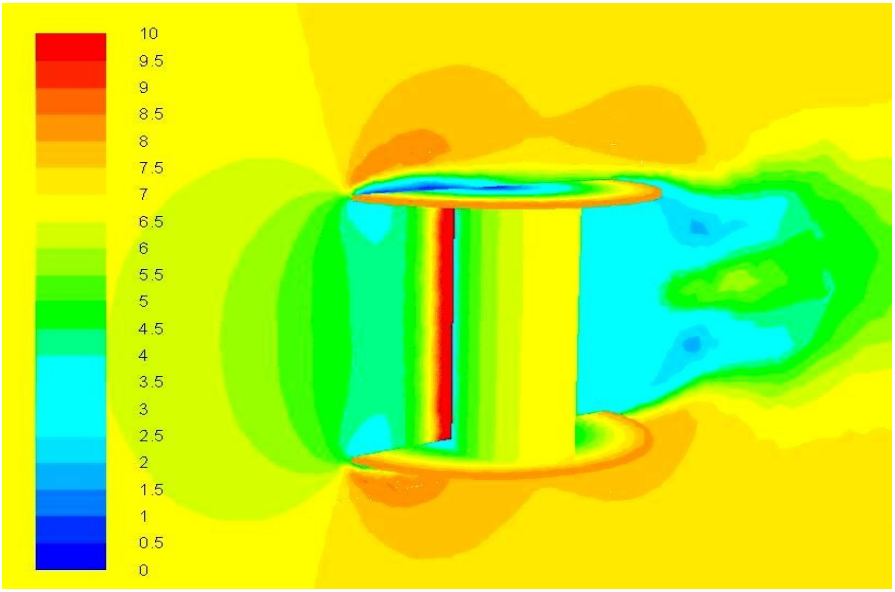

Figure 2.16: Velocity Contours around Three Dimensional Savonius Rotor

2.3. Summery

Numerical solution is performed for a single Savonius turbine in order to validate the numerical simulation model. Two dimensional and three dimensional simulations are performed. The static torque coefficient and dynamic torque coefficient at different tip speed ratios are computed. The different flow patterns around the turbine buckets are identified. The two dimensional computational results shows that the transition SST turbulence model has the closest results to the experimental data, the maximum average power coefficient for a single rotor is found to be 0.23 corresponding to λ equal to 1. For the three dimensional simulation, a discrepancy is obtained between the numerical results and the experimental data due to difficulties to reproduce detached vortex structures by RANS turbulence models. To enhance the simulation, detached eddy simulation (DES) model is used for flow simulation with a near-wall treatment using k-omega SST turbulence model, the obtained numerical results are closer to the experimental data for all tip speed ratios. For further simulations in this study, the two dimensional numerical model with the transition SST turbulence model will be used.

Chapter 3

Numerical Study of Co-Rotating Savonius Wind Turbine Clusters

For a wind farm to produce the highest possible power output, the number of turbines that can be installed in the available plot of land has to be maximized, this requires that the gap distance between turbines has to be reduced in addition to increasing the efficiency of individual turbines. Recent studies show that interactions between closely placed Savonius turbines enhance the output power of these turbines compared to their isolated counter-parts. The purpose of this chapter is to study the mutual performance enhancement which occurs between two co-rotating turbines in parallel and oblique configurations. Parametric studies are performed to determine the gap distance and oblique angle that achieves the maximum power coefficient enhancement. The results are used to develop an efficient triangular three turbine cluster. The numerical simulation of a single Savonius turbine show that the maximum power coefficient is achieved at tip speed ratio λ equal to one. For capturing the maximum performance achieved by Savonius two-turbine clusters, the simulation of the clusters is performed at the tip speed ratio λ equal to one.

3.1. Numerical Simulation of Two Co-Rotating Turbines

Solution of two co-rotating Savonius turbines in parallel and oblique clusters are performed. The enhancement in the power coefficients of the two turbines is studied at different gap distances (S) between the rotors' blade tips. In ref. [14] the performance co-rotating Savonius turbines were found to be independent on the relative phase angles (φ) between the turbines. All cases of co-rotating turbines in this study neglects the change in the relative phase angle.

3.1.1. Two Parallel Co-Rotating Savonius Turbines

Two parallel co-rotating Savonius turbines (1) and (2) are numerically simulated at a tip speed ratio equal to one corresponding to the maximum power output for a single turbine. The two turbines rotate in the clockwise direction. Figure 3.1 shows the contraction of the stream lines from the velocity contours downstream the two turbines, it also shows the strengthening in the tip vortex of turbine in the advancing blades of both turbines. The simulation is performed at different gap distances between the rotors' blade tips and the average power coefficient of each rotor is calculated. A mutual interaction between the two rotors occurs and the performances of both Savonius rotors are enhanced. Figure (3.2) shows the power coefficients of the two rotors at different gap distances compared to the isolated turbine, the maximum performance for both rotors is found at a gap distance equals to 0.2D (where D is the rotor diameter). The power coefficient of rotors (1) and (2) decreases until they reach the value of a single rotor at gap distances 6D and 4D respectively as shown in figure 3.2. Figure 3.3 shows the average power coefficient of the two rotors at different gap distances compared to a single turbine, the

maximum average power coefficient is found to be 0.3 at 0.2D gap distance, this represents an enhancement of 30% higher than isolated turbines placed at approximately 5D gap distance.

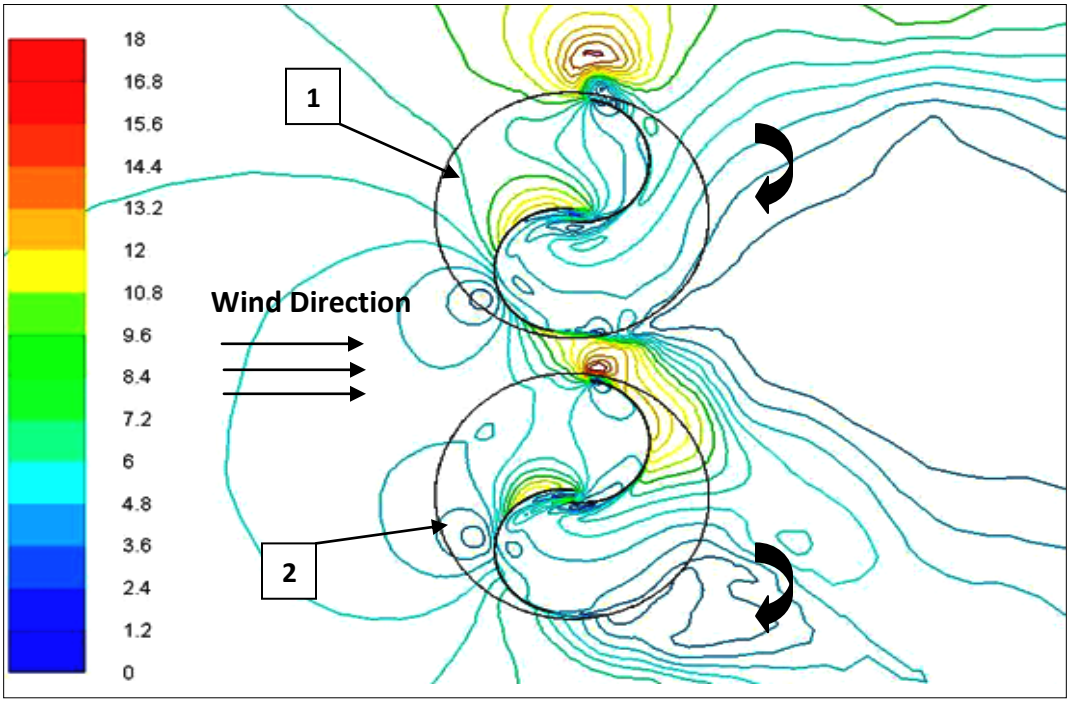

Figure 3.1: Velocity Contours around Two Parallel Co-Rotating Savonius Turbines

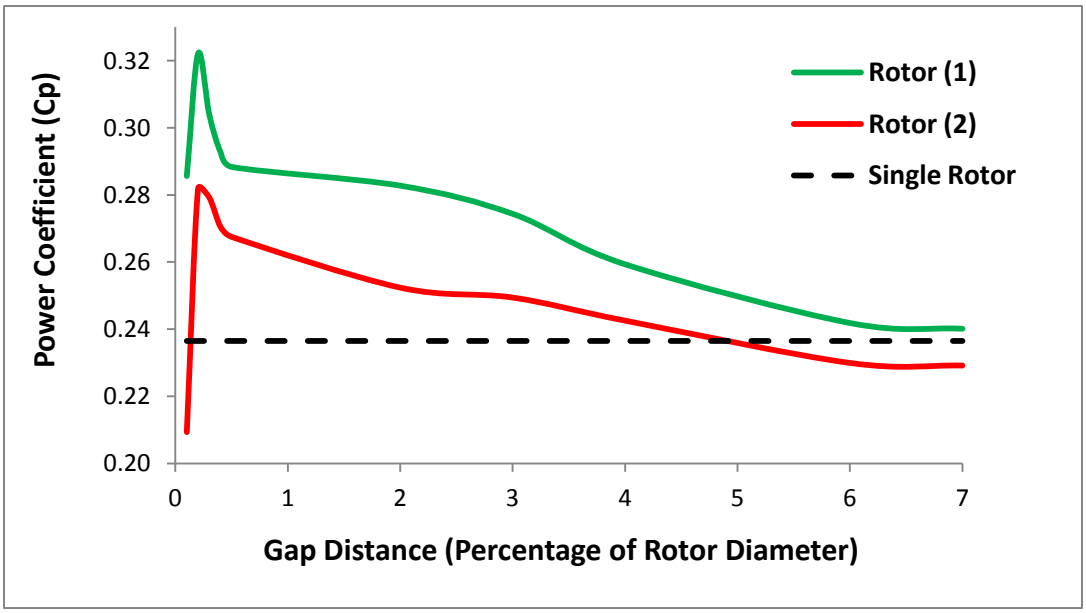

Figure 3.2: C_p of Two Parallel Co-Rotating Savonius Turbines at Different Gap Distances Vs Single Rotor

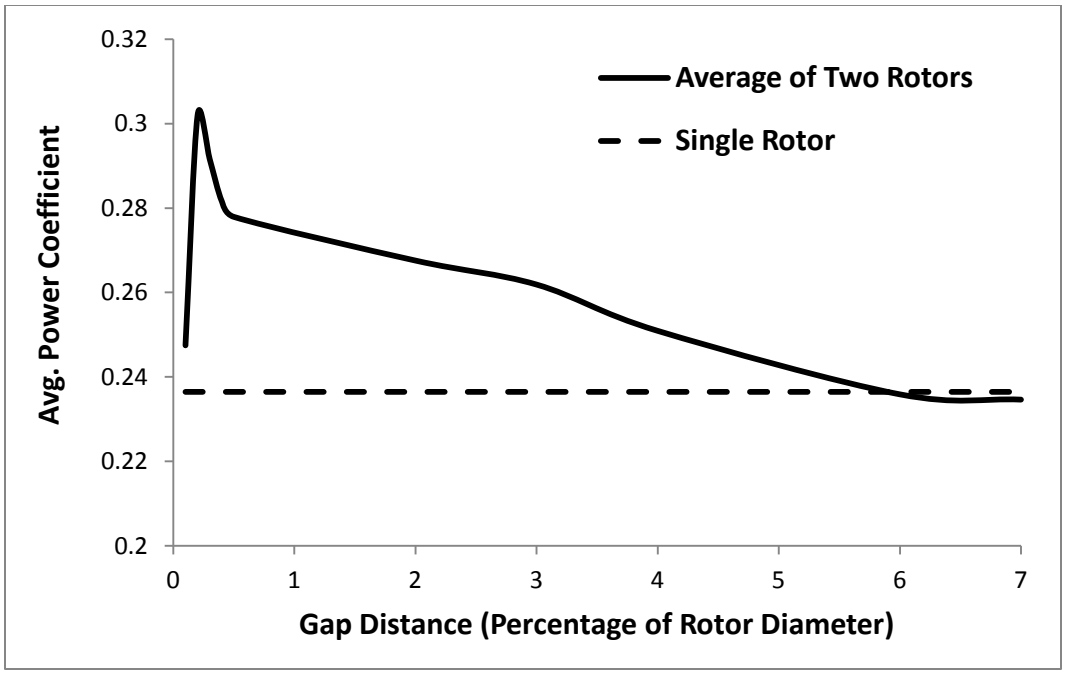

Figure 3.3: Avg. Power Coefficient of Two Parallel Co-Rotating Savonius Turbines at Different Gap Distances Vs Single Rotor

The power coefficient of rotor (1) is higher than that of rotor (2), this can be explained as a result of the higher negative pressure generated on the convex side of its advancing blade compared to rotor (2) as shown in the pressure contours in figure 3.4. This contributes in adding positive torque to rotor (1), especially at the positions between angles 20^o and 120^o as shown in figure 3.5. The strength of the vortex at the tip of the advancing blade of rotor (1) is higher than that of rotor (2). The vortex is strengthened due to the Magnus effect of rotor (2) on rotor (1). The power enhancement of rotor (2) can be explained as the result of the combination of the vortex generated at the tip of the retarding blade of rotor (1) with that generated at the advancing blade of rotor (2). This results in reducing pressure on the concave surface of the advancing blade of rotor (2). Each isolated turbine of one meter diameter and one meter height generates about 48 watt, two isolated turbines have a power density of 13 watt/m^2. The two co-rotating

parallel turbines placed at 0.2D gap distance produce an average power of 63 watt each, this is equivalent to a power density of 57 watt/m^2.

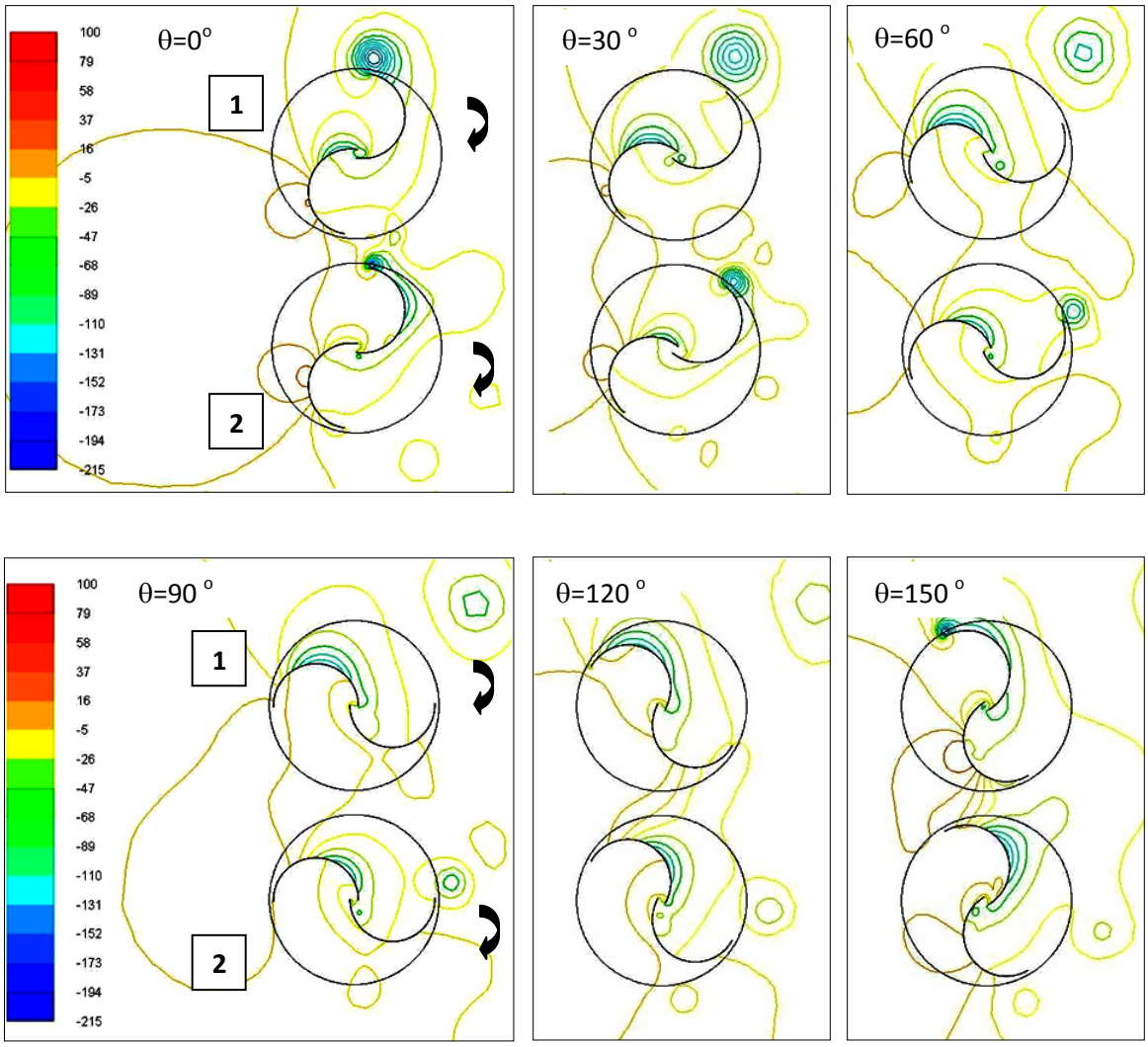

Figure 3.4: Pressure Contours around Two Parallel Co-Rotating Savonius Turbines

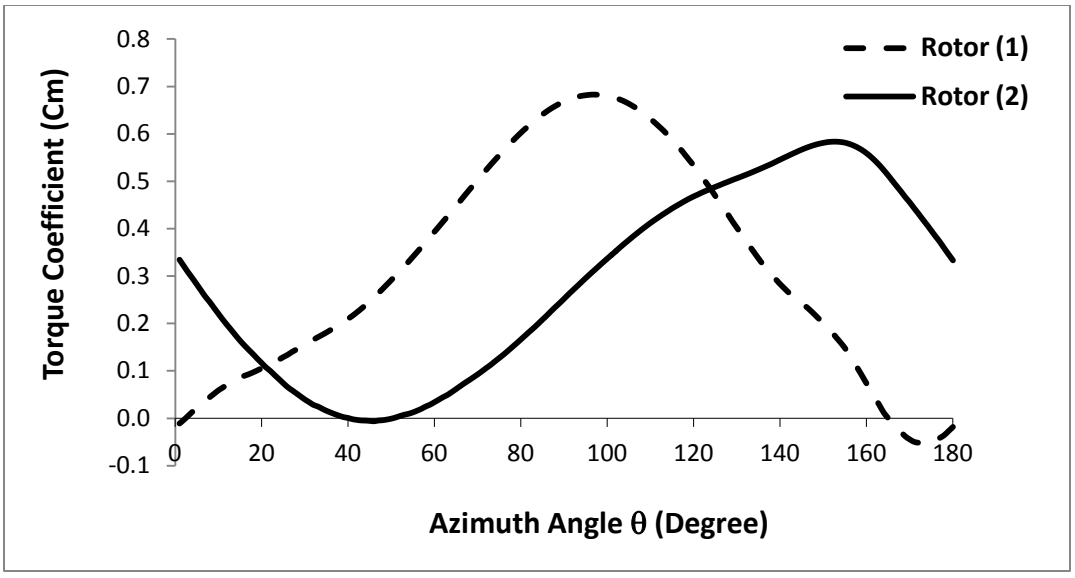

Figure 3.5: C_m for Two Parallel Co-Rotating Savonius Turbines

3.1.2. Two Oblique Co-Rotating Savonius Turbines

Two oblique co-rotating Savonius rotors are simulated using the same numerical model used for the single rotor simulation and a tip speed ratio equal to one. Two cases (A) and (B) of oblique configurations are studied. In case (A): The oblique angle is positive, the inward blade of rotor (1) is the advancing blade (moving with the wind direction) and the inward blade of rotor (2) is the returning blade (moving opposite to the wind direction) as shown in figure 3.6. In case (B): The oblique angle is negative, the inward blade of rotor (1) is the returning blade (moving opposite to the wind direction) and the inward blade of rotor (3) is the advancing blade (moving with the wind direction) as shown figure 3.7. The figures also show the velocity vectors around the two rotors for the oblique co-rotating turbine cases. All turbines rotate in the clockwise direction and the power coefficients of the two rotors are calculated at different gap distances (S) and oblique angles (α) (Angle between inflow and center distance).

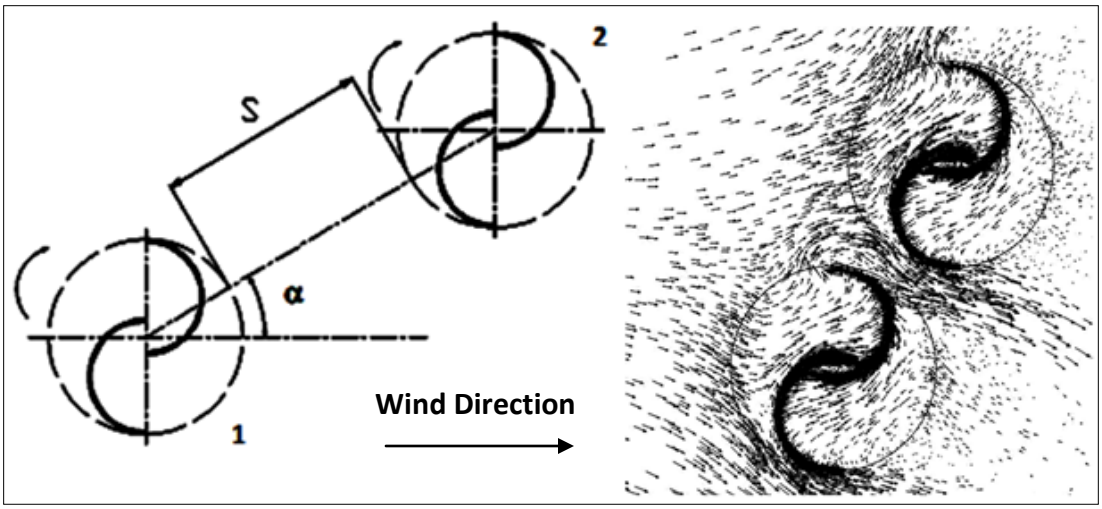

Figure 3.6: Velocity Vectors for Case (A) of Two Co-Rotating Oblique Savonius Rotors

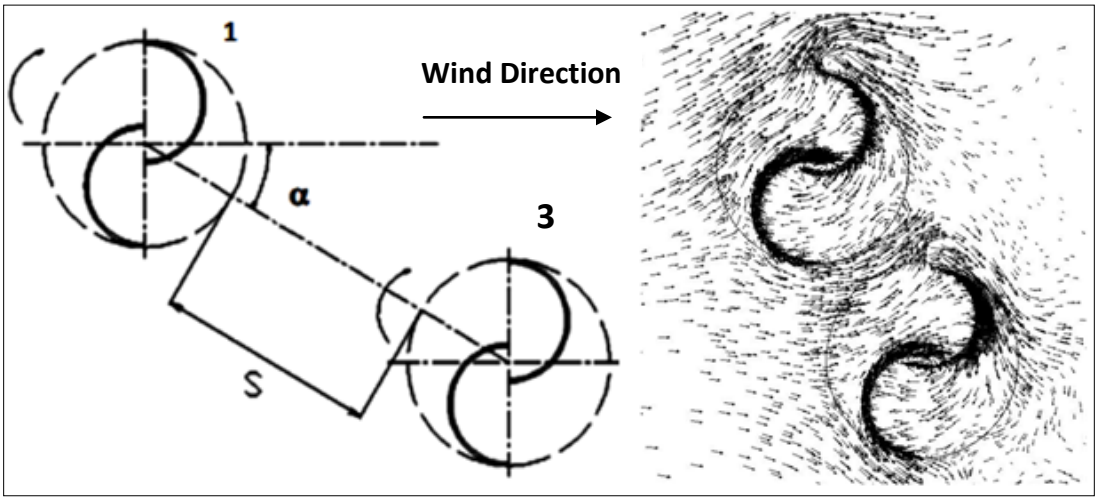

Figure 3.7: Velocity Vectors for Case (B) of Two Co-Rotating Oblique Savonius Rotors

As a result of the asymmetry in the wake of the single rotor, the power coefficients for the downstream rotors for cases (A) and (B) are different. Figure 3.8 shows the power coefficients of the two rotors in case (A) at different gap distances compared to isolated turbines. At small gap distances, the existence of rotor (2) behind and above rotor (1) retards the rotation of the advancing blade of rotor (1) causing a decrease in its power coefficient below the value of an isolated rotor. However power coefficient enhancement appears in rotor (2) as a result of the

Magnus effect of rotor (1). Figure 3.9 shows a comparison between the average power coefficient of both rotors (case A) and the isolated turbine power coefficient, the maximum average power coefficient is found to be 0.26 at a gap distance equal to 1.0 D.

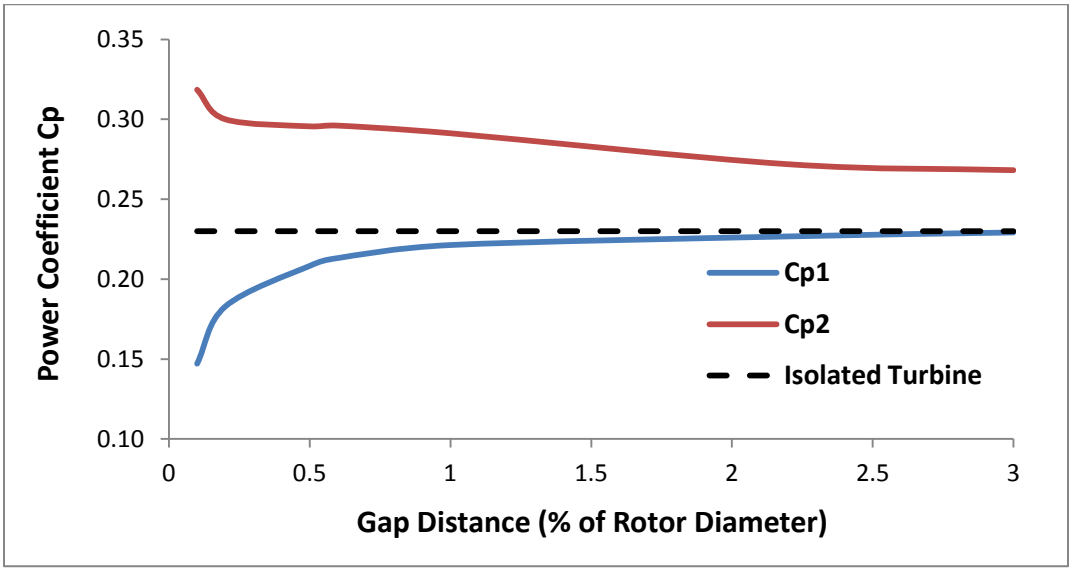

Figure 3.8: Cp for Two Oblique Co-Rotating Savonius Turbines Case (A), Different Gap Distances and $\alpha=60^{o}$

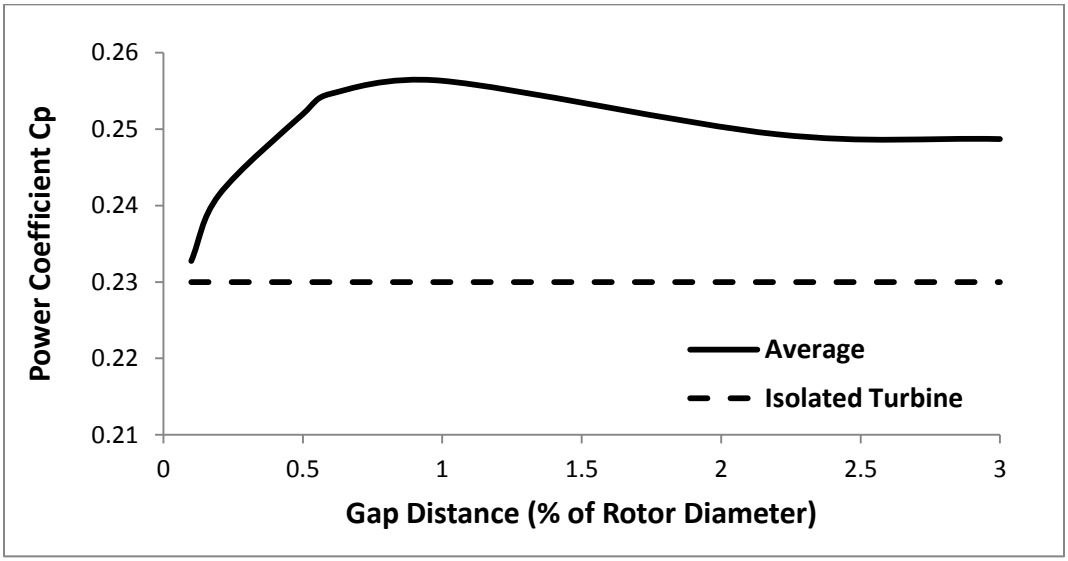

Figure 3.9: C_p^- for Two Oblique Co-Rotating Savonius Turbines Case (A), Different Gap Distances and $\alpha=60^{o}$

Figure 3.10 shows the results of the power coefficients of the two oblique rotors of case (B) at different gap distances compared to isolated turbines. At small gap distances, setting rotor (3) downstream rotor (1) results in a high enhancement in rotor (3) as a result of the combination of the tip vortices generated by the returning blade of rotor (1) and the advancing blade of rotor (3). The velocity increases on the convex surface of the advancing blade of rotor (3), this generates low pressure in this region which pulls the blade in the positive torque direction. Figure 3.11 shows a comparison between the average power coefficient of both rotors and the isolated rotor power coefficient, the maximum average power coefficient is found to be 0.32 exists at a gap distance equal to 0.2D.

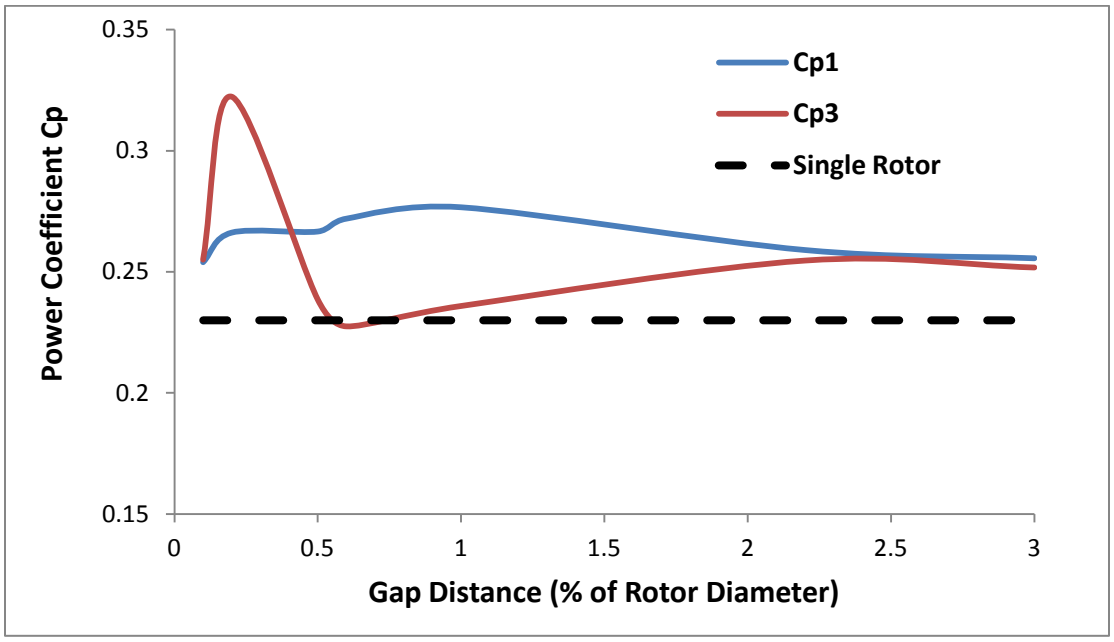

Figure 3.10 *Cp* for Two Co-Rotating Oblique Savonius Rotors Case (B), Different Gap Distances, α= - 60^{o}

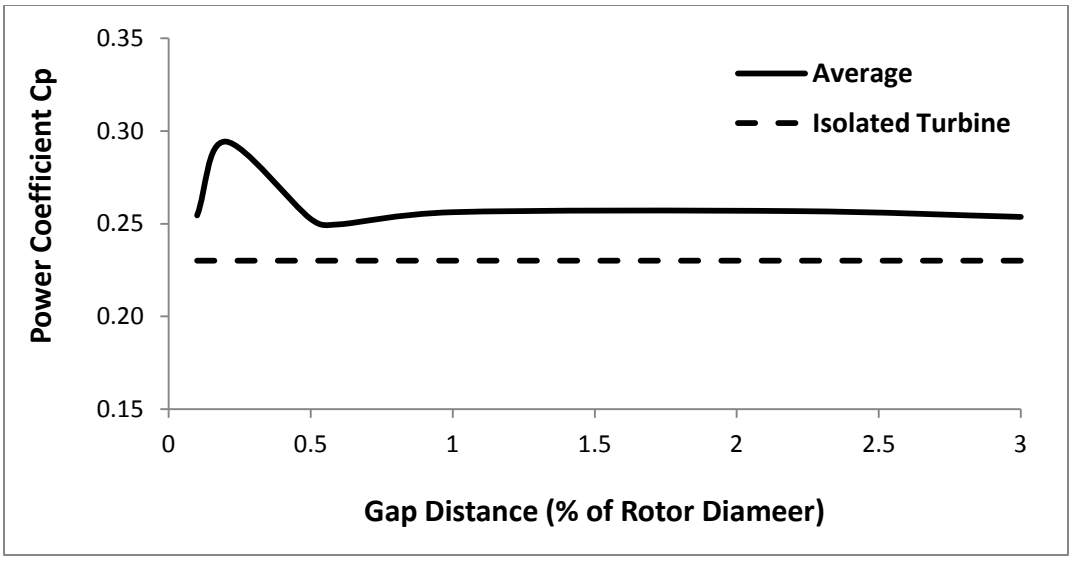

Figure 3.11: C_p^- for Two Co-Rotating Oblique Savonius Rotor Case (B), Different Gap Distances, α= - 60°

The study for both cases (A) and (B) at different angles show that the highest values for the average power coefficient of both rotors are achieved at an angle α equal to 60° as shown in figure 3.12, this show a consistency with the results in reference [11].

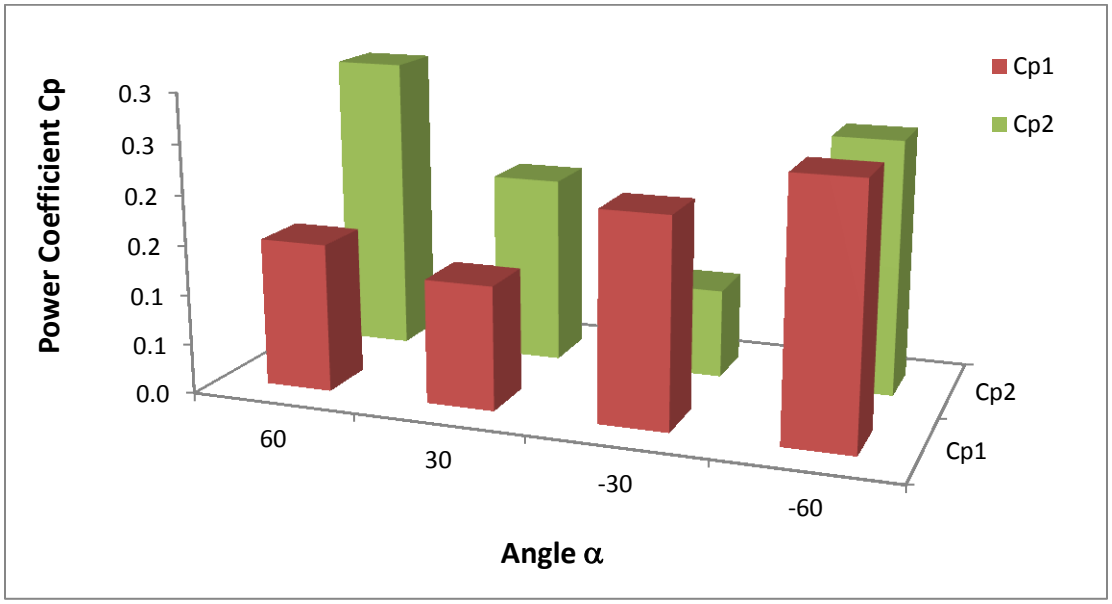

Figure 3.12: C_p for Two Oblique Rotors with Gap Distance 1.0 D at Different Angles α

The comparison between the average power coefficient for both cases (A) and (B) at different gap distances in figure 3.13 show that at small gap distances case (B) is more efficient than case (A) and that they both have approximately similar performance at gap distances more than 0.5D. The two co-rotating oblique turbines (one meter diameter and one meter height) case (B) placed at 0.2D gap distance produce an average power of 67 watt each, this is equivalent to a power density of 61 watt/m^2. The performance at this gap distance is 39% higher than isolated turbines.

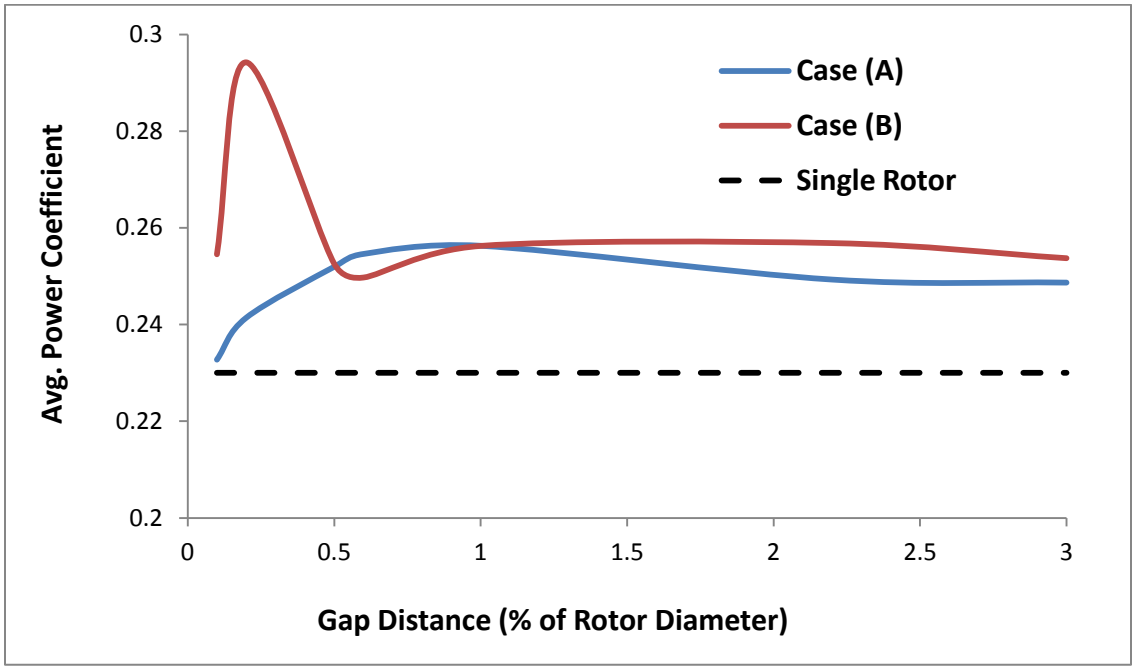

Figure 3.13: C_p^- for Two Oblique Co-Rotating Savonius Turbines Case (A) and Case (B) Vs Single Rotor at Different Gap Distances

3.2. Numerical Simulation of Three Co-Rotating Turbines

The numerical results of the two parallel and oblique Savonius turbines simulation show that mutual enhancement occurs in the power coefficients when the turbines are placed in close proximity. The results for two oblique rotors show that the highest power coefficients are achieved at an oblique angle $\alpha = 60^{o}$ for the downstream rotors. In this section triangular three co-rotating Savonius turbine clusters are simulated at different gap distances. Two triangular three turbine clusters are studied, case (I) is set up with one rotor (1) upstream and two rotors (2) and (3) set symmetrically downstream at the same gap distance and the same oblique angles as shown in figure 3.14, case (II) is set one rotor (1) downstream with two parallel rotors (2) and (3) set symmetrically upstream at the same gap distance and the same oblique angles as shown in figure 3.15. Both cases are numerically simulated and the power coefficients are calculated at different gap distances and oblique angles.

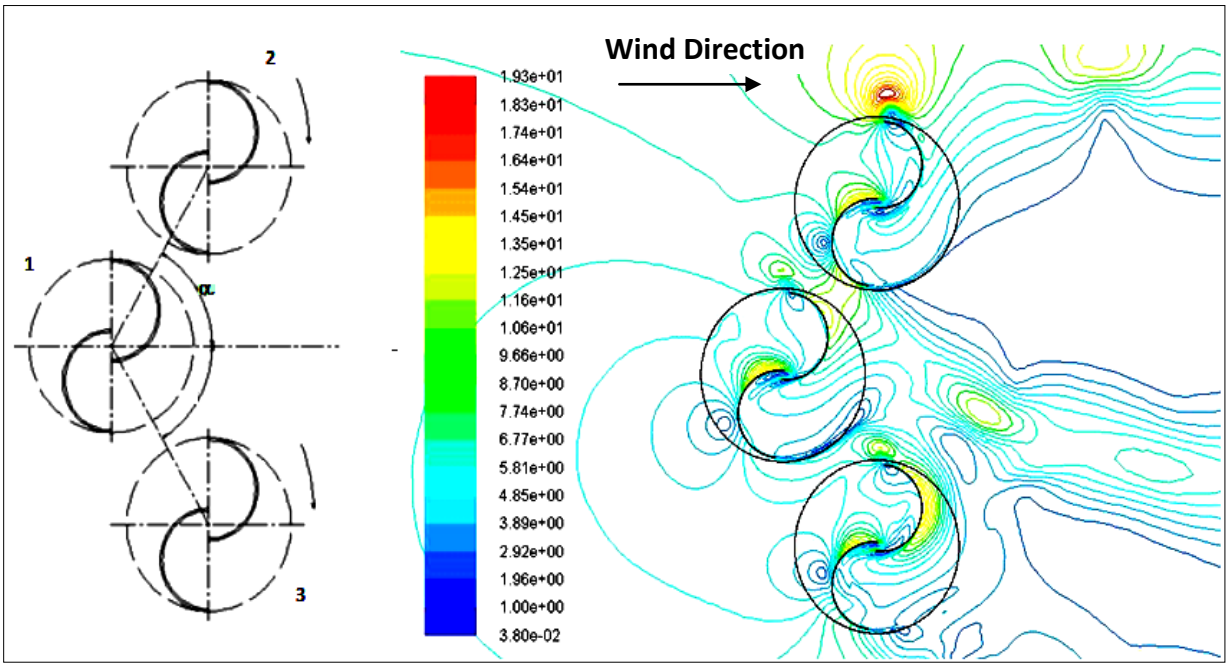

Figure 3.14: Velocity Contours around Three Savonius Turbines Cluster (Case: I)

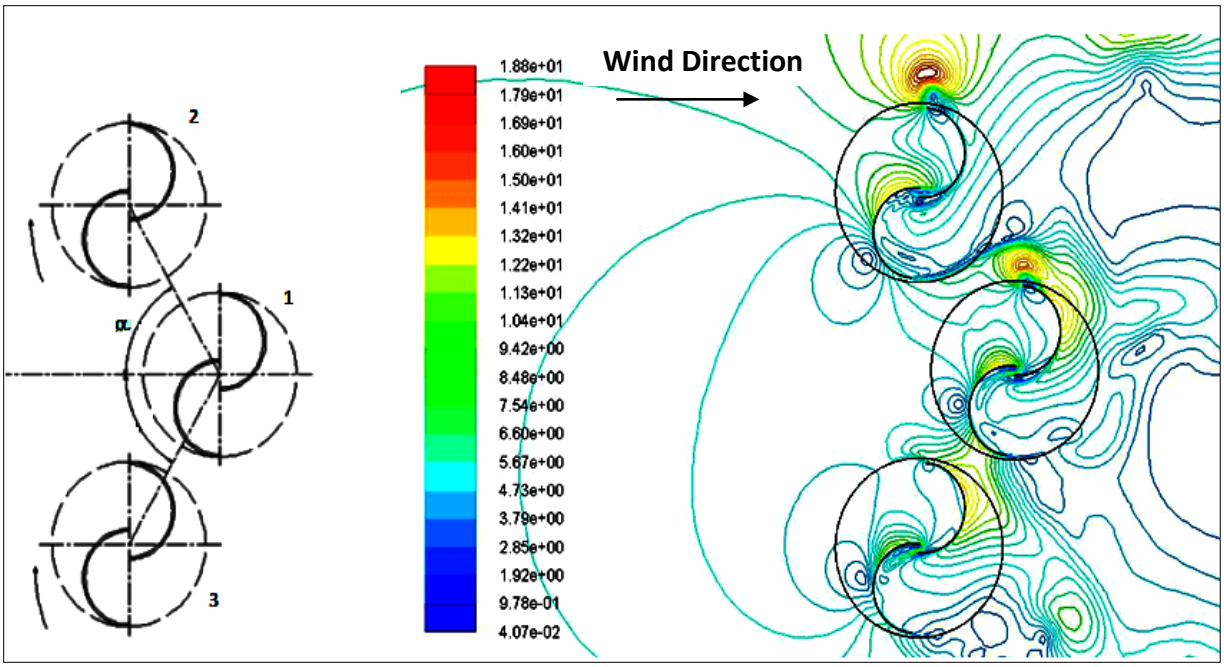

Figure 3.15: Velocity Contours around Three Savonius Turbines Cluster (Case: II)

To confirm that the oblique angle obtained from the results of the two oblique turbines is the same for the three turbine cluster, the three turbine cluster is studied setting the downstream turbines at different oblique angles for different gap distances. The results are found to be consistent with the two oblique rotors, figure 3.16 shown that at small gap distances the highest power coefficients are achieved at oblique angle $\alpha = 60^{o}$, however, at gap distances > 0.5D the power coefficients are very close at oblique angles $>50^{o}$.

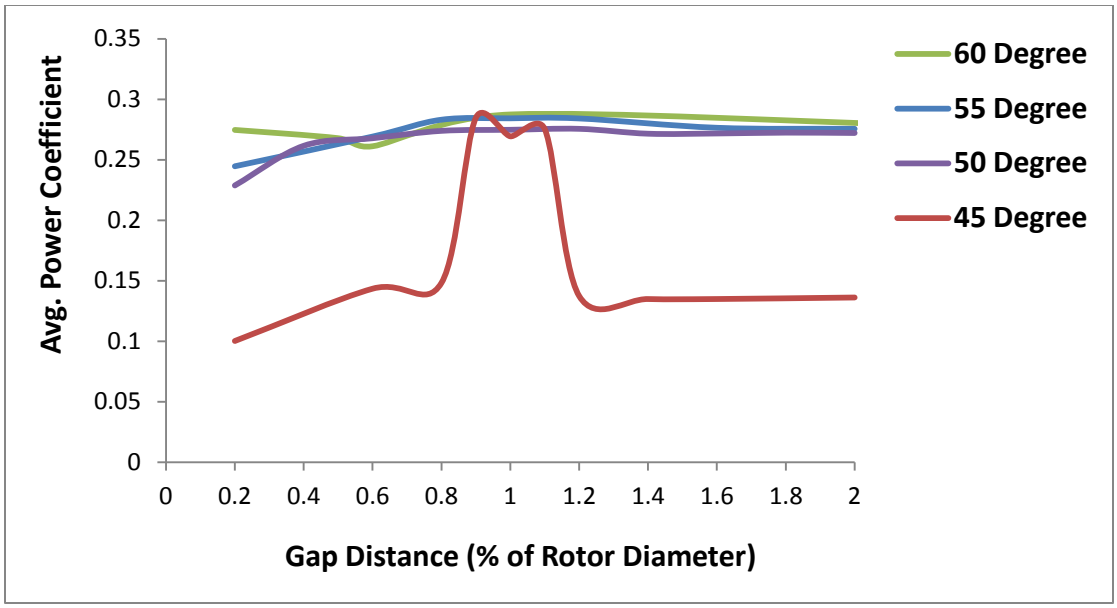

Figure 3.16: C_p^- for Three Savonius Rotors at Different Angles and Gap Distances

3.2.1. Case (I): One Rotor Upstream and Two Rotors Downstream

Figure 3.17 shows the power coefficient for the three turbine cluster case (I) at different gap distances, the power coefficient of rotor (1) is low at small gap distance, the existence of two rotors (2) and (3) downstream of rotor (1) blocks the rotation of the upstream rotor (1). The coupling effect between rotor (1) and the downstream rotor (3) does not appear at small gap distances, the tip vortex on the advancing blade of rotor (3) is weak and its power coefficient is low. However the Magnus effect of rotor (1) accelerates the inflow towards the tip of the advancing blade of rotor (2), this strengthens the tip vortex of the advancing blade of rotor (2) as shown in figure 3.14 and enhances its performance as shown in figure 3.17. Increasing the gap distance reduces the adverse effect of the downstream rotors (2) and (3) on the performance of rotor (1). At large gap distances, the coupling effect occurs between rotors (1) and (3) due to the combination of their tip vortices, this enhances their power coefficients as shown in figure 3.17.

Figure 3.18 shows the average power coefficient of the three rotors compared with a single rotor, the highest average power coefficient of the three rotors is found to be 0.278 exist at a gap distance equal to 2.2D. This value shows an enhancement in the performance for the cluster by approximately 25% compared to that of isolated turbines.

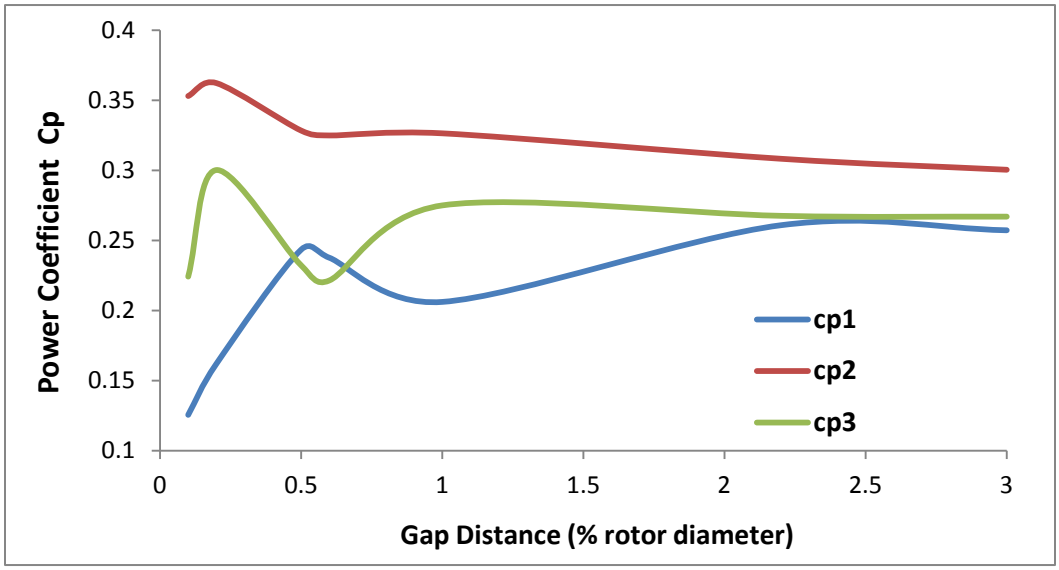

Figure 3.17: C_p for three Rotors (Case I), Angle $\alpha = 60^o$ and Different Gap Distances

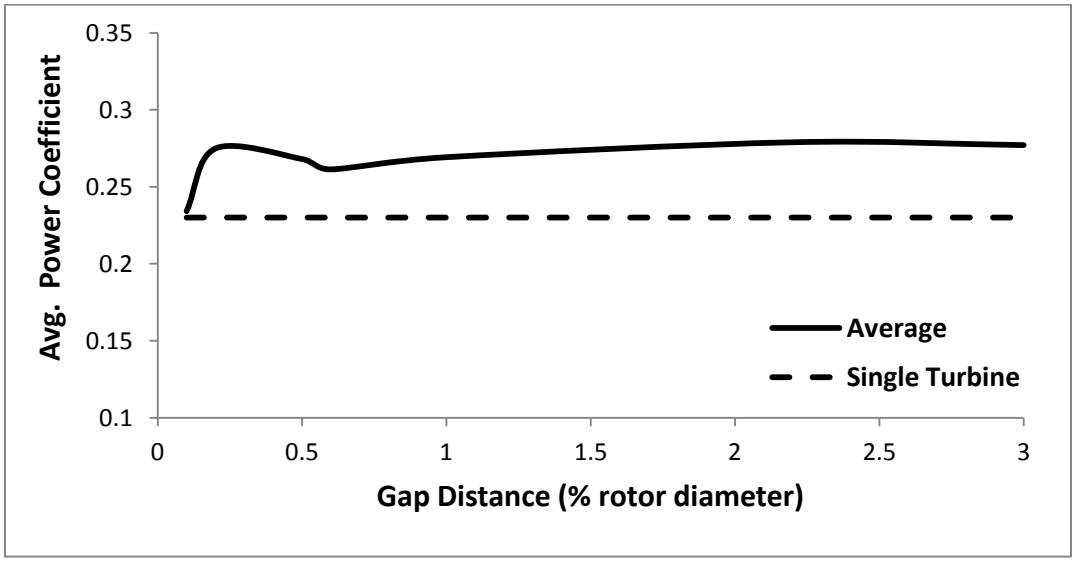

Figure 3.18: C_p^- for Three Rotors (Case I), Angle $\alpha = 60^o$ and Different Gap Distances

At the same gap distances, comparing performance of rotors (2) and (3) in the three turbines cluster case (I) with their corresponding rotors in the two oblique rotor clusters cases (A) and (B) shows a difference in the value of the power coefficients. Rotor (2) has higher power coefficient in the three rotor cluster case (I) than that when it is in case (A) of two oblique rotors ($\alpha=60^{o}$) as shown in figure 3.19. Also, rotor (3) in the three rotors cluster case (I) has a higher power coefficient than its corresponding rotor (3) in case (B) of the two oblique rotors configuration ($\alpha= -60^{o}$) as shown in figure 3.20, this is due to the benefit it takes from the tip vortex of the retarding blade of rotor (1). The results confirms that the enhancement in the three turbine cluster more than for the two turbine clusters.

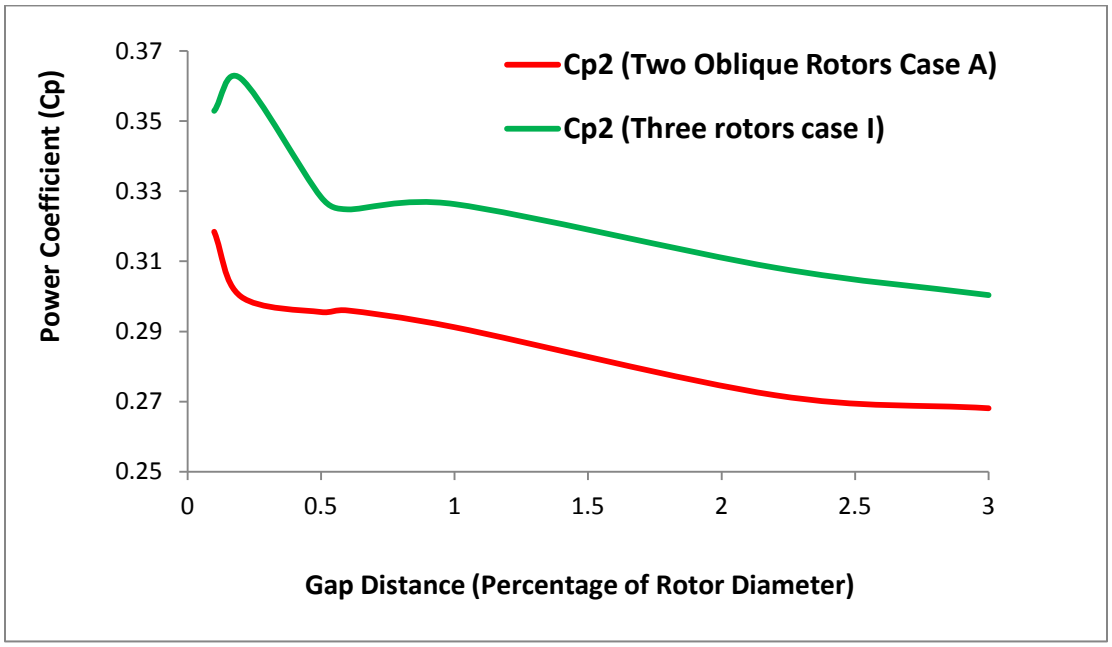

Figure 3.19: C_p for Rotor (2) in Two Oblique Rotors Case (B) Compared to its Values in Three Rotors Cluster Case (I) at Different Gap Distances

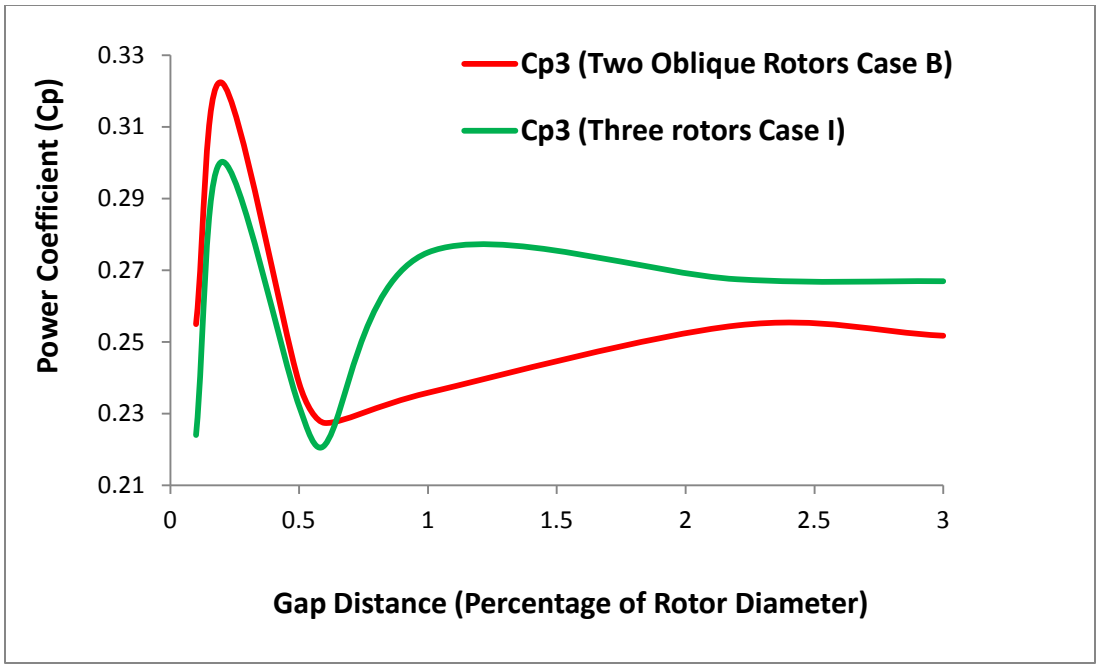

Figure 3.20: C_p for Rotor (3) in Two Oblique Rotors Case (B) Compared to its Values in Three Rotors Cluster Case (I) at Different Gap Distances

3.2.2. Case (II): Two Rotor Upstream and One Rotor Downstream

Figure 3.15 shows that the tip vortices on the advancing blades of rotors (1) and (2) are stronger than that of rotors (3). The performance of the advancing blade of rotor (1) is enhanced by the combination of its tip vortex with that generated by the tip vortex of the retarding blade of rotor (2). Figure 3.21 shows the power coefficients for the three rotors of cluster case II. Rotor (3) shows lower values for its power coefficient due to the blockage of its rotation caused by the returning blade of rotor (1) at small gap distances, this effect vanishes at larger gap distances. Figure 3.22 shows that the highest average power coefficient is 0.31 which exists at a gap distance of 0.2D, this peak result is due to the high improvement in the performance of rotor (1) due to the tip vortices combination explained above, which decreases by the increase of the gap distance. This value shows an enhancement in the performance for the cluster by approximately

34% compared to that of isolated turbines. This cluster case (II) has higher values for the power coefficients of rotors (1) and (2) compared to case (I) at small gap distances.

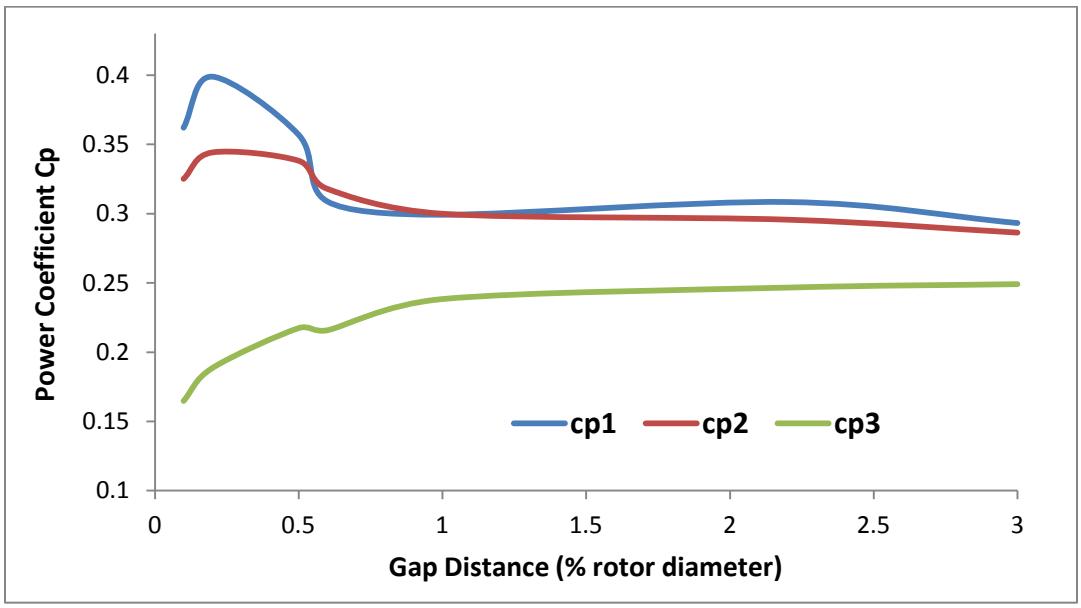

Figure 3.21: C_p for Three Rotors (Case II), Angle $\alpha = 60^o$ and Different Gap Distances

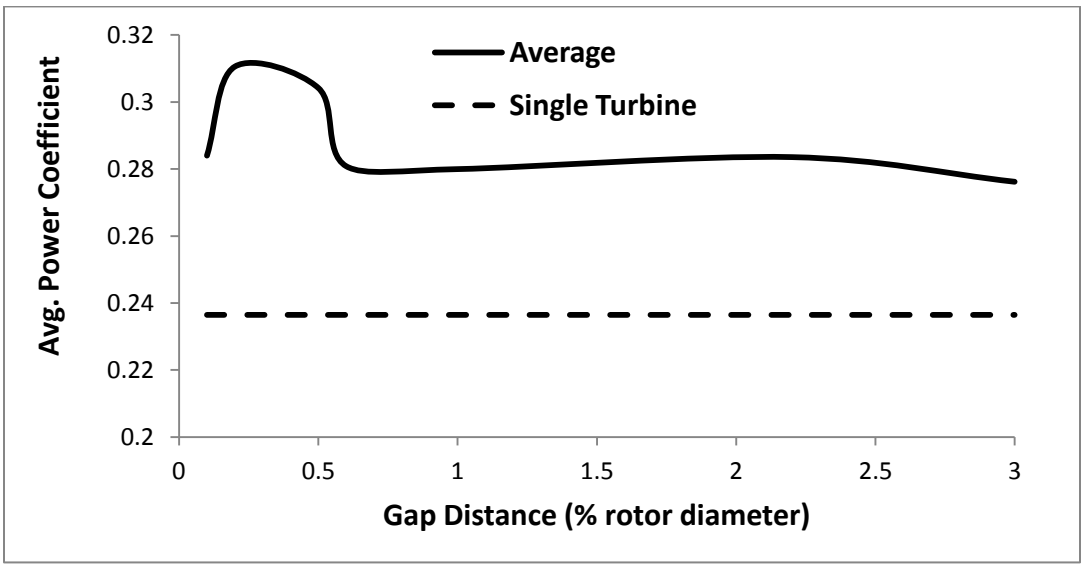

Figure 3.22: C_p^- for Three Rotors (Case II), Angle $\alpha = -60^o$ and Different Gap Distances

At the same gap distances, comparing the results of the power coefficients of the three rotor cluster Case (II) with that of two oblique rotors clusters cases (A) and (B) set at angles 60^o and -60^o shows differences in the values of the power coefficients. Figure 3.23 shows that rotor (1) now is not retarded by any adverse effect since it became the downstream rotor. Its performance is enhanced by the combination of its advancing blade tip with that of the retarding blade of rotor (2). Rotor (2) in the three rotor cluster case (II) has higher power coefficient than its corresponding rotor (1) in the two oblique rotor cluster case (B) (α= -ve 60^o) as shown in figure 3.23 due to the Magnus effect done by rotor (3). Rotor (3) in the three rotors cluster case (II) shows very close results to the corresponding rotor (1) in the two oblique rotor cluster case (A) ($\alpha=60^o$) as shown in figure 3.24, this is because they are subjected to similar circumstances in both layouts. Figure 3.25 shows a comparison between the two case (I) and (II) for the three turbine clusters. The results show that the average power coefficient in case (II) is higher at small gap distances in the unstable region where there is a fluctuation in the values of the power coefficients of the three rotors in both cases, however the average power coefficient values are close at other gap distances for both cases. The choice of the best cluster needs a stability and confirmation of the output for a quite reasonable margin of safety for the orientation.

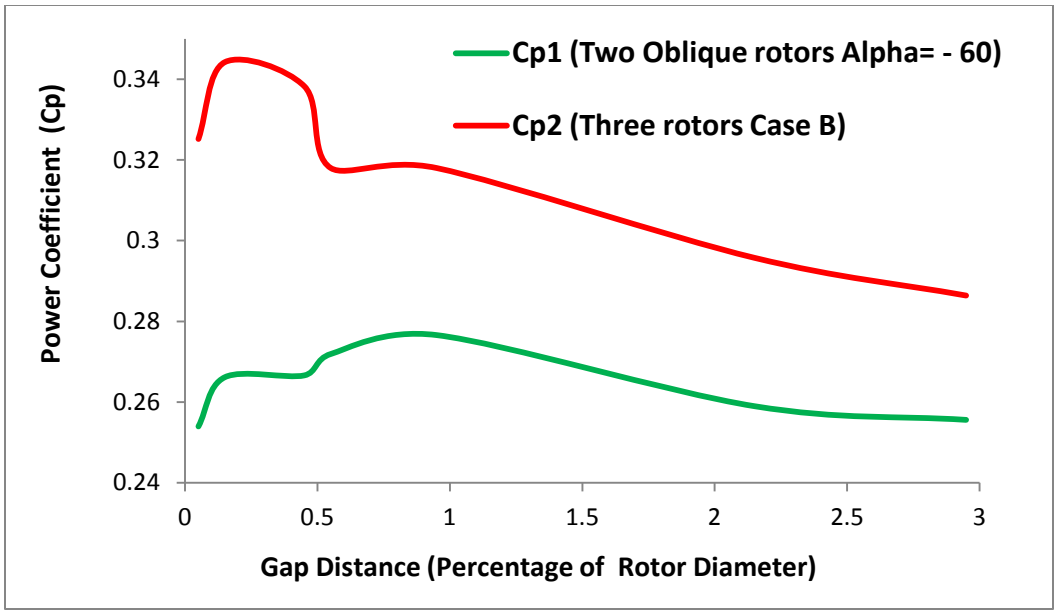

Figure 3.23: C_p for Rotor (1) in Two Oblique Rotors (Angle α= - 60^o) Compared to Rotor (2) in Three Rotors Configuration (Case: B) at Different Gap Distances

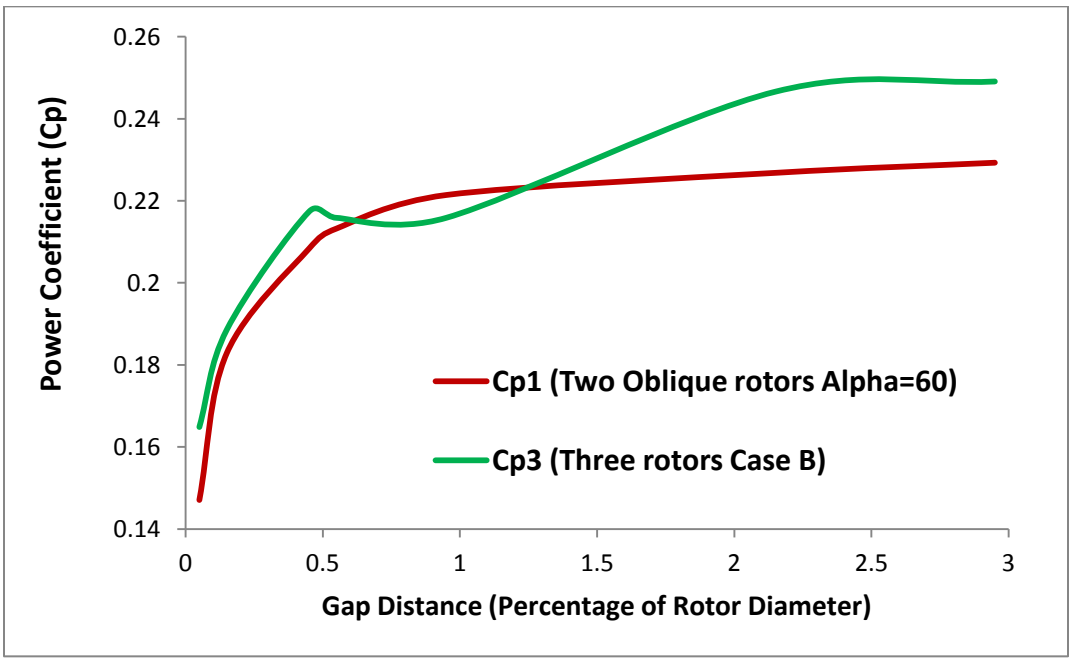

Figure 3.24: C_p for Rotor (1) in Two Oblique Rotors (Angle α = 60) Compared to Rotor (3) in Three Rotors Configuration (Case: B) at Different Gap Distances

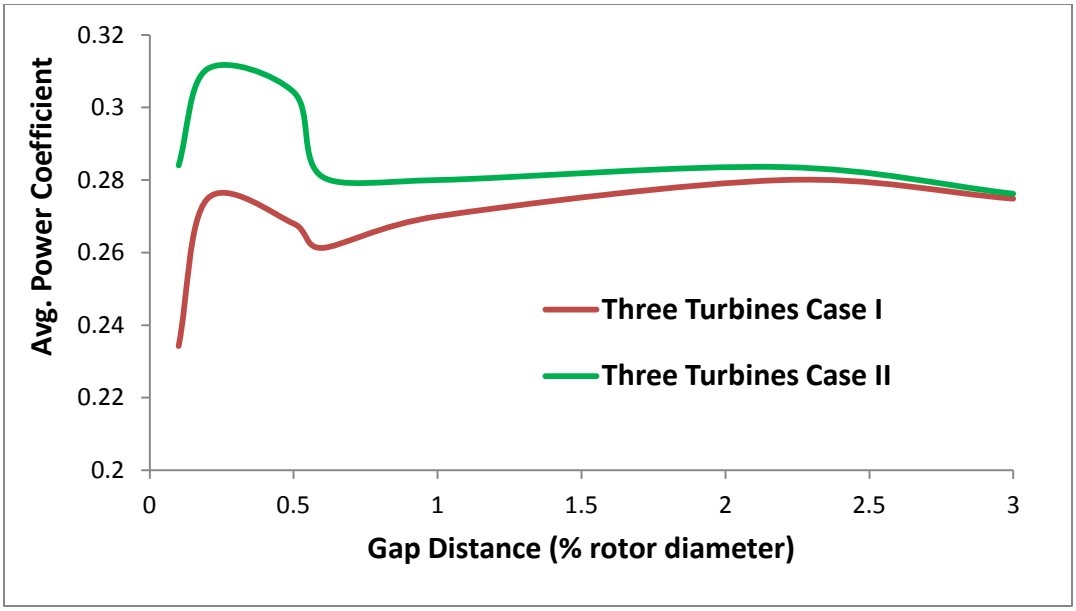

Figure 3.25: Avg. C_p for Three Turbine Clusters Case I and Case II

3.3. Summary

In this chapter, the performance of two and three turbines are studied numerically. The aim is to investigate the enhancement in Savonius VAWTs performance in multiple turbine configurations. This is used to develop an efficient cluster of Savonius turbines to be used as a building unit for efficient VAWT farms. Two and three turbine configurations simulation showed enhanced power coefficients compared to isolated turbines. For two parallel turbines, the optimum gap distance is found to be 0.2 times the rotor diameter. For oblique rotors, an angle of 60^o is found to be the best angle to avoid the wake of the upstream rotor and benefit from the coupling action. The optimum gap distance when the downstream turbine is placed at + 60^o is found to be 1D and 0.2 D when the downstream turbine is positioned at -60^o. The oblique configuration results are used for the construction of a three turbine cluster arranged in a triangular shape and confirmed by the results of the three turbines numerical simulations. At

small gap distances which is a region of unstable performance, three rotor cluster case (II) is found to have better performance compared to the cluster of case (I). However at gap distances higher than one rotor diameter the two cases have the same performance. The best performance for both cases is at a gap distance 2.2D with an average power coefficient up to 25% higher than that of an isolated turbine. The three turbine cluster case (I) will be used for construction of efficient vertical axis co-rotating wind turbine farms having the cluster as a building unit.

Chapter 4

Numerical Study of Counter-Rotating Savonius Wind Turbine Clusters

In chapter 3, we showed that interactions between two co-rotating Savonius turbines in parallel and oblique clusters enhance the output power of individual rotors compared their isolated counter-parts. The results are used to develop an efficient triangular co-rotating three turbine cluster. In this chapter similar studies for two counter-rotating Savonius turbines in parallel and in oblique clusters and three turbines in triangular clusters are performed. The computational results are compared with the co-rotating clusters to determine the most efficient cluster. The same numerical model including: the computational domain, grid structure, turbulence model and solver setting discussed in chapter (1) is implemented.

4.1 Numerical Simulation of Two Parallel Counter-Rotating Turbines

Solution of two counter-rotating Savonius turbines in parallel and oblique clusters are performed. The enhancement in the power coefficients of the two turbines is studied at different gap distances (S) between the rotors' blade tips. The turbines are also set at different relative phase angles (φ), where: $\varphi = \theta_1 - \theta_2$ as shown in figure 4.1 in order to study the effect of relative phase angle on the enhanced performance of the two turbines. The computational results for the counter rotating clusters are compared with their corresponding co-rotating clusters in order to determine the most efficient triangular three turbine cluster for developing efficient VAWT farms.

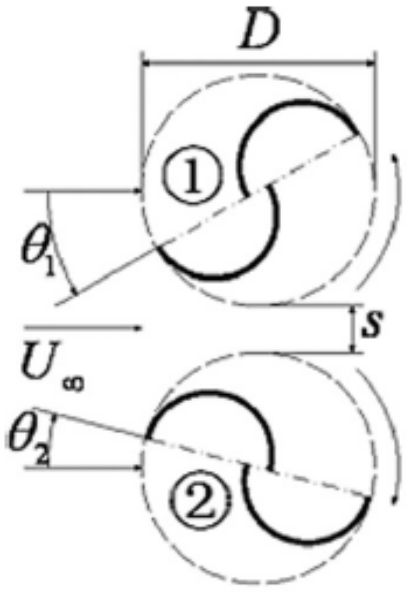

Figure 4.1: Relative Phase Angle between the Turbines

4.1.1 Two Parallel Counter-Rotating Turbines

Two cases (A) and (B) of two parallel counter rotating Savonius turbines are numerically simulated. In case (A): the inward buckets of the two turbines are both returning buckets (they move opposite to the wind direction). In case (B): the inward buckets of the two turbines are both advancing buckets (they rotate with the wind direction). The average power coefficient is calculated for all cases as the two counter rotating rotors are symmetric.

i. Case (A): Inward Buckets are Returning Buckets

Two parallel turbines with case (A) are solved numerically, four different cases with different phase angles are studied (0^0, 30^0, 60^0 and 90^0) as shown in figure 4.2, turbine (1) rotates in the clockwise direction and turbine (2) rotates in the counter clock wise direction. The velocity contours around the two rotors for show the symmetry in the flow field in case of $\phi=0^o$ and shows the effect of the phase shift on the flow field for other values of ϕ. The figure show regions of high velocity are generated by the Magnus effects of the two turbines and the contraction of the stream lines appear at both sides downstream and between the turbines.

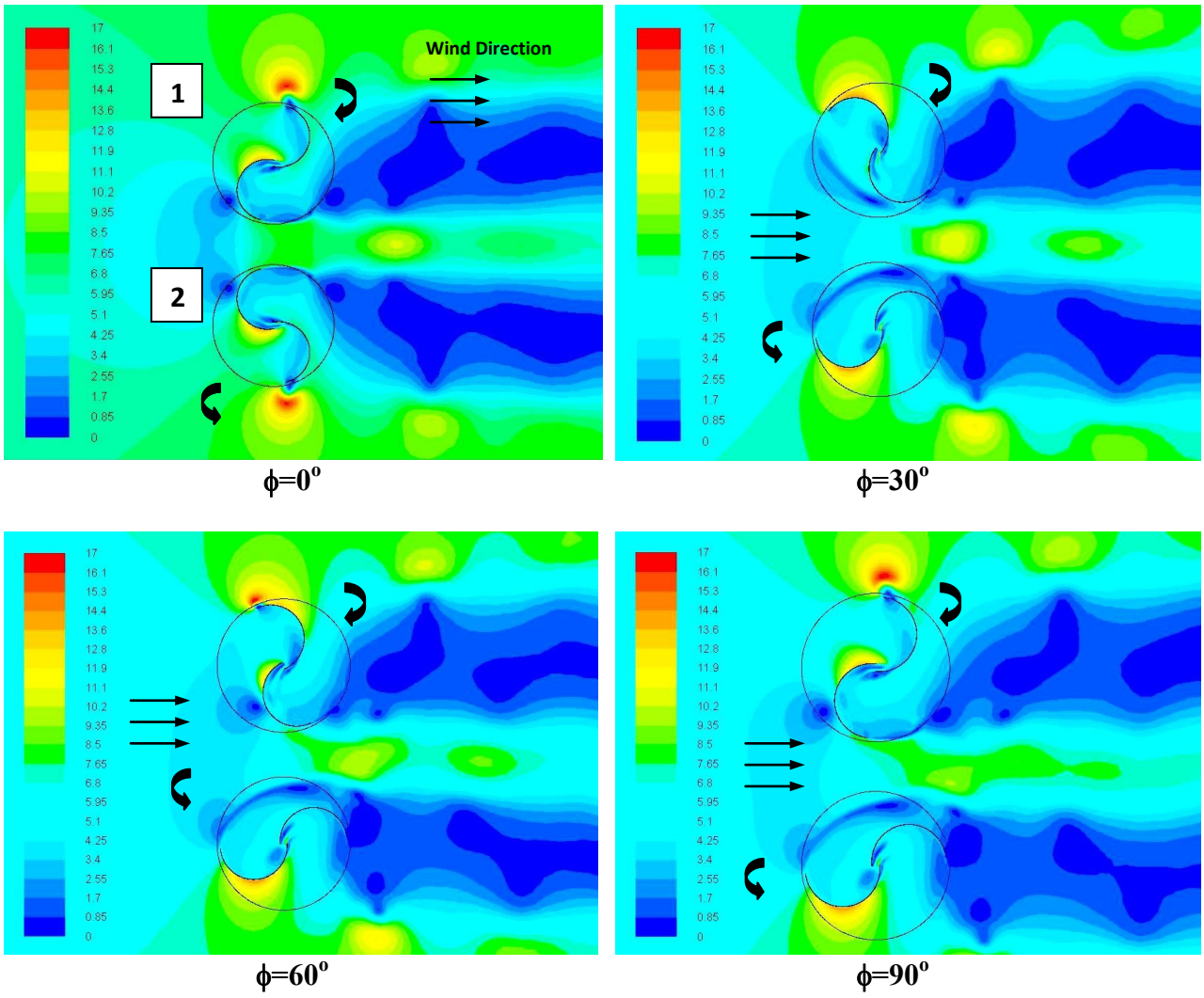

Figure 4.2: Velocity Contours around Two Parallel Counter Rotating Savonius Turbines Case (A) at Different Relative Phase Angles and Gap Distance 0.4D

The results for the power coefficient at different gap distances and relative phase angles are shown in figure 4.3, at small gap distances for all relative phase angles no significant enhancement occurs in the power coefficient, the inflow alters the rotation of the retarding blades of the rotors and increases the negative torque on the two turbines. The performance enhances occurs at higher gap distances specially at relative phase angles 30^{o} and 60^{o}, these phase shift angles allow the enhancement in the tip vortices at the advancing and returning blades of both

turbines to occur. The maximum average power coefficient is found to be 0.263 at a gap distances of 0.8D with $\phi=30^{o}$.

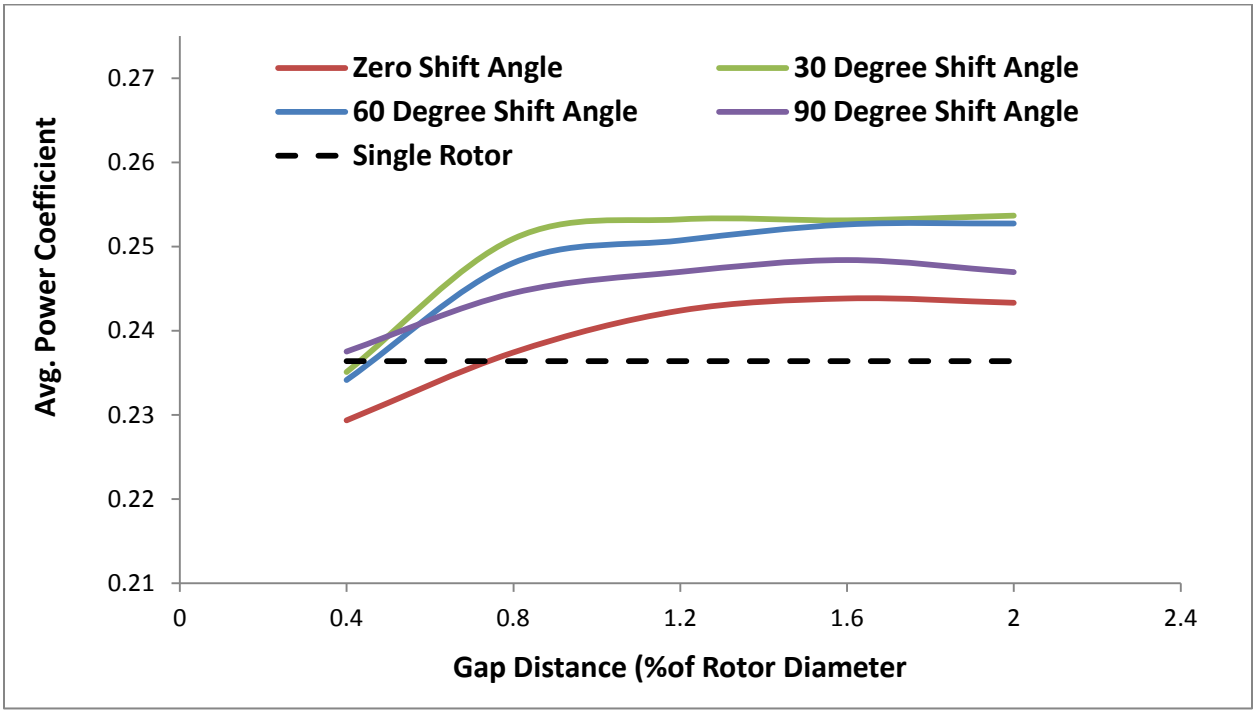

Figure 4.3: Average Cp of Two Parallel Counter Rotating Turbines Case (A) at Different Gap Distances and Relative Phase Angles Vs Single Rotor

ii. Case (B): Inward Buckets are Advancing Buckets

Two parallel turbines with case (B) are solved numerically, four different phase angles are set (0^0, 30^0, 60^0 and 90^0) as shown in figure 4.4. The velocity contours around the two rotors for case (B) in figure 4.4 show that the incoming velocity contours experience a Magnus effect due to the rotation of the two rotors strengthening the tip vortices of the inward advancing buckets. The velocity increases on the convex surface of the advancing buckets, this decreases the pressure and increases the positive torque contribution of the bucket.

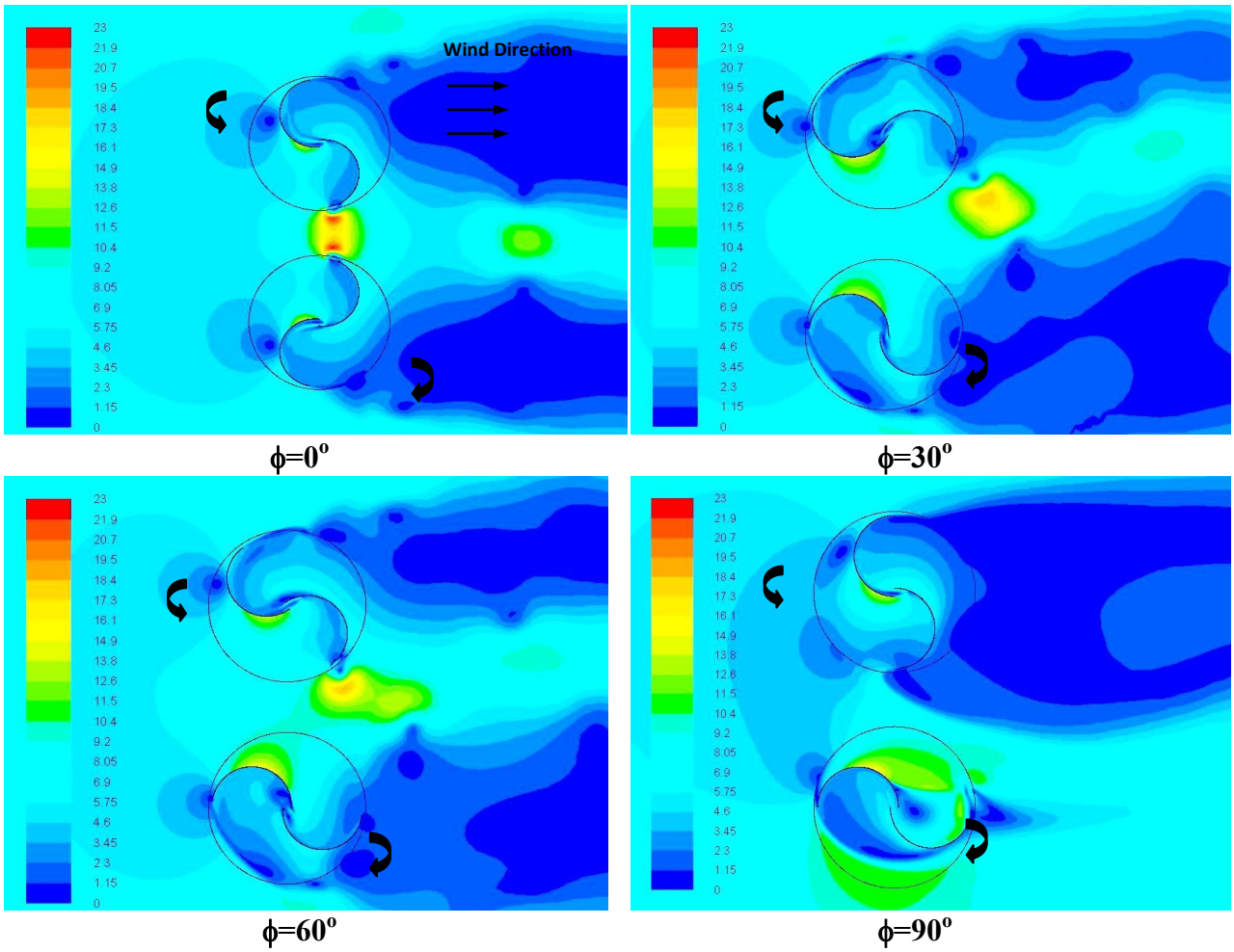

Figure 4.4: Velocity Contours around Two Parallel Counter Rotating Savonius Rotors Case (B) at Different Relative Phase Angles

Figure 4.5 shows the average power coefficients at different gap distances and different relative phase angles compared to the isolated turbines, at small gap distances, significant enhancement in the average power coefficient of the two for all relative phase angles except at $\phi = 0^o$ due to the altering effect of the inward blades on each other as the gap between the advancing blades is the smallest at the nearest approach instants. At gap distances between 0.8 and 2.0 of the rotor diameter, the enhancement is dependent on the relative phase angle between the rotors. The relative phase angle $\phi = 30^o$ is the most efficient for the counter rotating rotors.

The highest average power coefficient is 0.306 achieved at a relative phase $\phi=30^{o}$ and a gap distance 0.8D, this value is higher than that achieved in case (A) at the same gap distance.

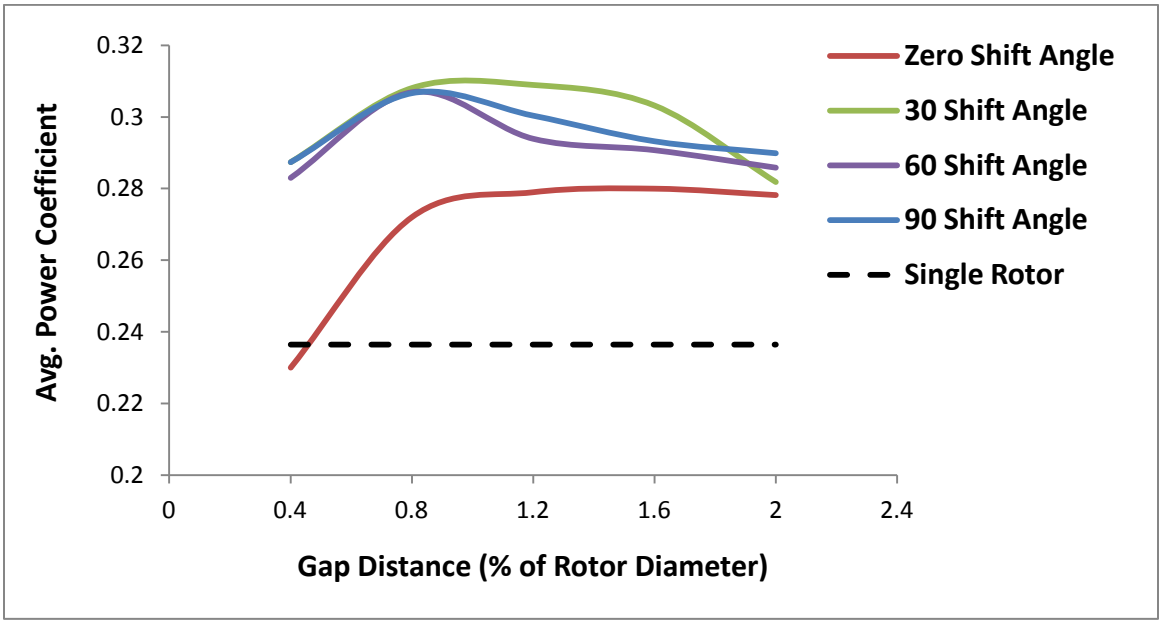

Figure 4.5: Average Cp of Two Parallel Counter Rotating Rotors Case (B) at Different Gap Distances and Relative Phase Angles Vs Single Rotor

iii. Comparison Between Co- and Counter-Rotating Two Parallel Turbines

The average power coefficient for two parallel counter rotating rotors cases (A) and (B) at relative phase angle 30^{o} are compared to that of the two parallel co-rotating rotors obtained in chapter (2). The comparison in figure 4.6 shows that case (B) for counter-rotating rotors at a relative phase angle equal to 30^{o} is the most efficient for two parallel counter-rotating Savonius rotors, where the inward buckets are advancing buckets (rotating in the same direction of the wind). The lowest values of the average power coefficient are that of case (A) of counter rotating turbines where the inward buckets are returning.

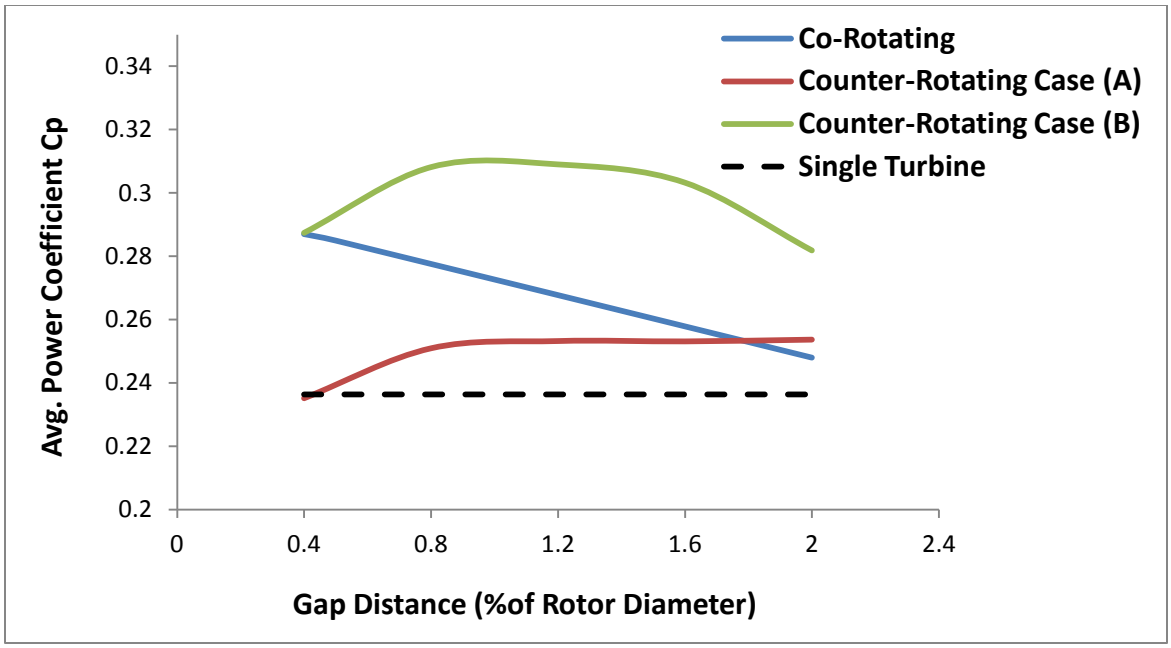

Figure 4.6: Comparison of Avg. Cp for Two Parallel Co-Rotating Turbines Vs Two Parallel Counter-Rotating Turbines Cases (A) and (B) (with 30^{o} Relative Phase Angles) at Different Gap Distances and Vs Single Rotor

4.1.2. Two Oblique Counter-Rotating Turbines

Two cases (C) and (D) of two oblique counter rotating oblique Savonius rotors are numerically simulated. In case (C): the inward buckets of the two turbines are advancing buckets and they rotate with the wind direction. In case (D) the inward bucket of the two turbines are returning buckets and they rotate opposite to the wind direction. The enhancement in the power coefficients of the two oblique rotors is studied at different gap distances between the rotors' blade tips and different relative phase angles.

i. Case (C): Inward Buckets are Advancing

Four different phase angles are set (0^0, 30^0, 60^0 and 90^0) as shown in figure 4.7 and the two oblique turbines are solved numerically. The velocity contours around the two oblique rotors Case (C) at different phase shift angles in figure 4.6 show the combination of the tip vortices of the advancing buckets of the two turbines. The downstream rotor's advancing bucket tip vortex is highly strengthened, where the velocity increases on the convex surface creating a region of low pressure and increasing its positive torque contribution and consequently enhancing the efficiency of the rotor. The same effect is observed on the tip of the advancing blade of the upstream rotor due to the Magnus effect of the down-stream rotor and the contraction of the incoming stream-lines.

The results of the power coefficient at different gap distances and different relative phase angles is show in figure 4.8, a significant enhancement occurs in the power coefficients of the two rotors at very small gap distances starting and decreases to reach an isolated rotor performance at gap distance more than 2D. The average power coefficient achieved at relative phase angles 30^o and 60^o are higher compared to angles 0^o and 90^o. The maximum average power coefficient is found to be 0.35 at a gap distance 0.4D with relative phase angles 30^o and 60^o.

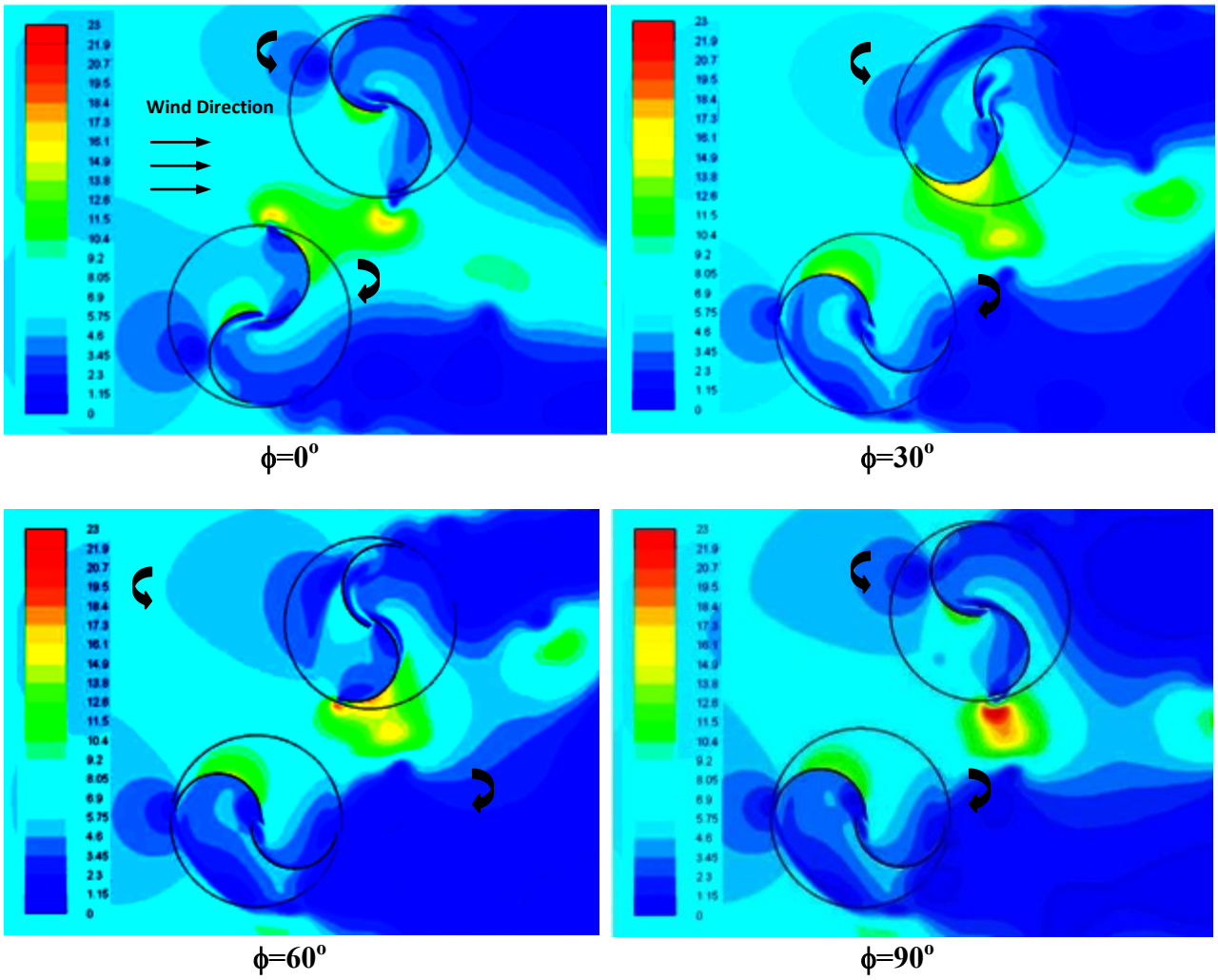

Figure 4.7: Velocity Contours around Two Oblique Counter-Rotating Savonius Rotors Case (C) at Different Relative Phase Angles

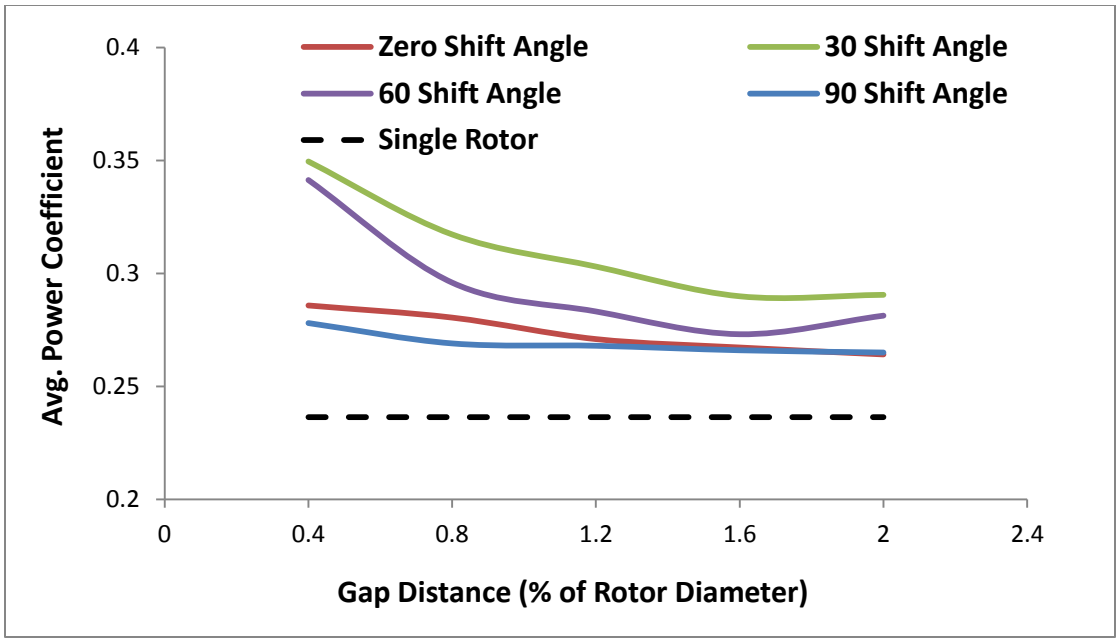

Figure 4.8: Avg. Cp of Two Oblique Counter-Rotating Rotors Case (C) at Different Gap Distances and Relative Phase Angles Vs Single Rotor

ii. Case (D): Inward Buckets are Returning

Four different phase angles are set (0^0, 30^0, 60^0 and 90^0) as shown in figure 4.9 and the two parallel turbines are solved numerically. The velocity contours around the two oblique rotors Case (D) is shown in figure 4.9, the inflow opposes the rotation of the inward returning bucket of the upstream turbine. The returning buckets of the upstream turbine behaves as a barrier to the returning buckets of the downstream turbine which slightly enhances its efficiency. The results of the power coefficient at different gap distances and relative phase angles is show in figure 4.10. No significant enhancement in the average power coefficient of the two turbines is achieved at all relative phase angles, at small gap distances the power coefficient of the two rotors is lower than that of isolated rotors where the inflow alters the rotation of the retarding blades increasing the negative torque on the rotors. This effect vanishes slightly at larger gap distances. The performance of the two turbines is independent on the relative phase angle and the

low average power coefficient in this configuration is mainly due to the low efficiency of the upstream turbine.

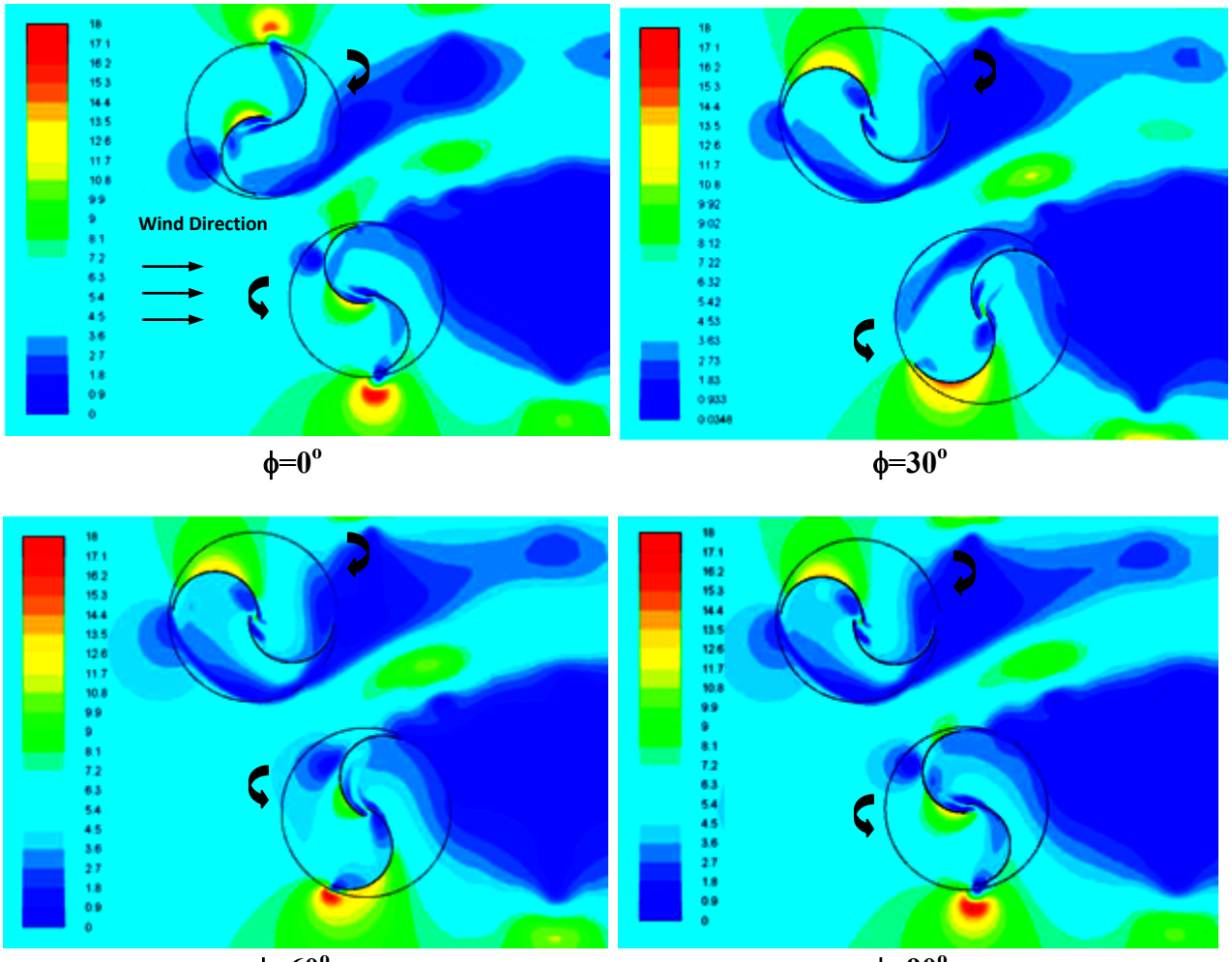

Figure 4.9: Velocity Contours around Two Oblique Counter-Rotating Savonius Rotors Case (D) at Different Relative Phase Angles

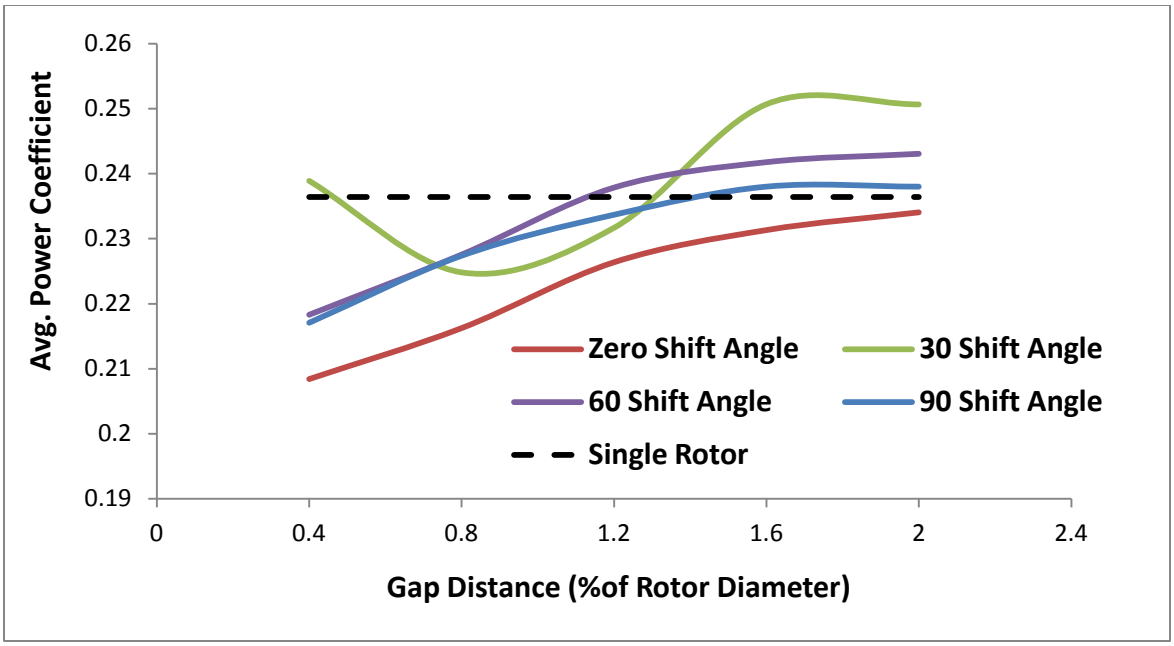

Figure 4.10: Average Cp of Two Oblique Counter Rotating Turbines Case (D) at Different Gap Distances and Relative Phase Angles Vs Single Rotor

iii. Comparison Between Two Co- and Counter-Rotating Oblique Turbines

The numerical results of the two counter rotating oblique rotors cases (C) and (D) at relative phase angle 30^{o} are compared to the results of two co-rotating oblique rotors case (A) and (B) in chapter (3). Figure 4.11 shows that the performance of the two oblique counter-rotating rotors case (C) is higher than its corresponding configuration of two oblique co-rotating rotors case (A) at different gap distances. The most efficient configuration for the downstream rotor place with positive oblique angle (α) is case (C) for the counter-rotating rotors. Figure 4.12 shows that the performance of two oblique co-rotating rotors case (B) is higher than its corresponding configuration of two oblique counter-rotating rotors case (D) at different gap distances. The most efficient configuration for the downstream rotor place with negative oblique angle (α) is case (B) for the co-rotating rotors.

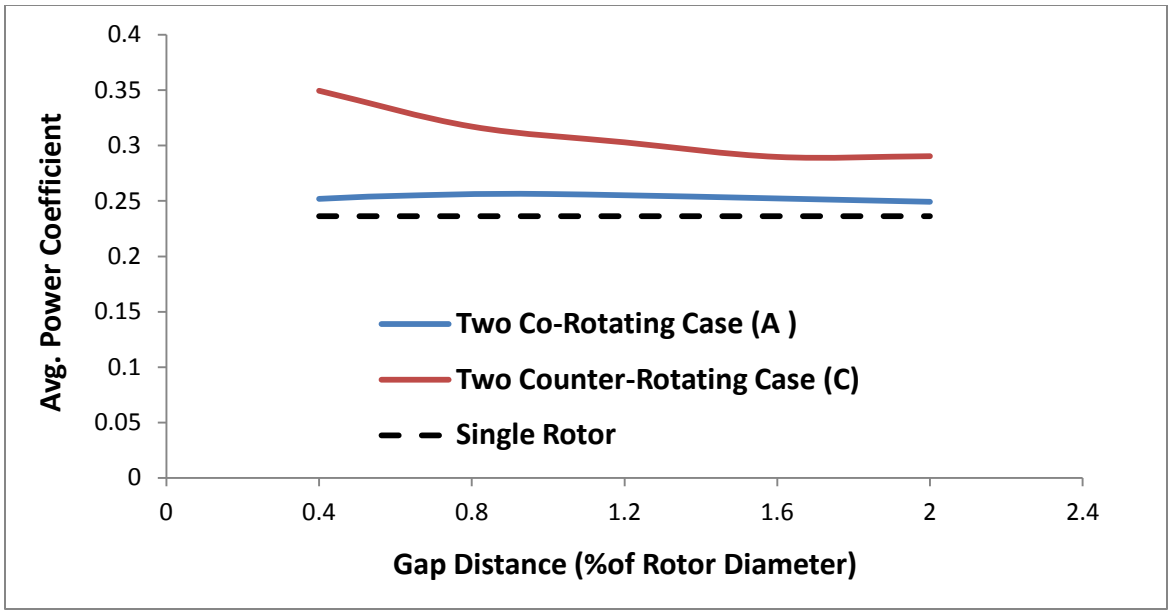

Figure 4.11: Average Cp of Two Counter Rotating Oblique Turbines Case (C) at Different Gap Distances and Relative Phase Angles Vs Single Rotor

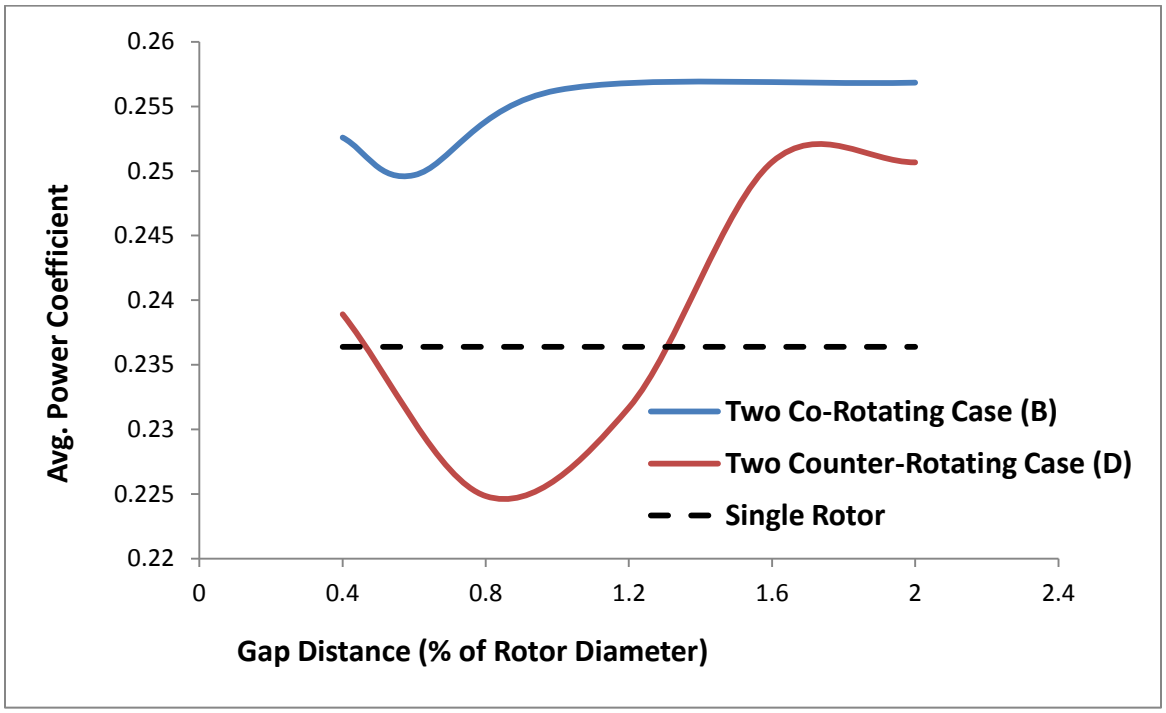

Figure 4.12: Average Cp of Two Counter Rotating Oblique Turbines Case (D) at Different Gap Distances and Relative Phase Angles Vs Single Rotor

4.2 Numerical Simulation of Three Savonius Counter-Rotating Turbines

In this section, the results of the comparison of the parallel and oblique co-and counter-rotating turbines are used to develop a triangular three turbine cluster (III) in order to construct an efficient VAWT farm, the results for cluster (III) is compared to that of clusters (I) and (II) introduced in chapter 3.

4.2.1. Case (III): Counter-Rotating Three Savonius Turbine Cluster

A hybrid Savonius triangular cluster of co- and counter-rotating turbines consisting of three rotors (1), (2) and (3) is developed, where turbine (2) is counter-rotating with turbine (1) with a relative phase angle equal to 30^o, their inward buckets are advancing buckets and they rotate with the wind direction. Turbine (3) is co-rotating with turbine (1). The three turbines are placed on the vertices of an equilateral triangle to keep the two turbines (2) and (3) at symmetric gap distances from turbine (1) at oblique angles +ve 60^o and -ve 60^o as shown in figure 4.13. The cluster is numerically simulated at different gap distances and the power coefficients of the three turbines are computed. The velocity contours around the three turbine cluster (III) in figure 4.13 show the combination between the tip vortices of the returning bucket of rotors (1) and (2). It also shows the strengthening of the tip vortex of the advancing bucket of rotor (3). Figure 4.14 shows the power coefficients of the three turbines at different gap distances, rotor (1) has the highest power coefficient due to the Magnus effect of rotor (3), and the power coefficient of rotor (2) is enhanced by the Magnus effect of rotor (1). Figure 4.15 shows that the average power coefficient of the three rotors compared to the isolated turbines, the average power coefficient is

higher at large gap distances as rotors (2) and (3) enhances more when shifted back, the maximum average power coefficient is 0.3 at gap distance equal to 3D.

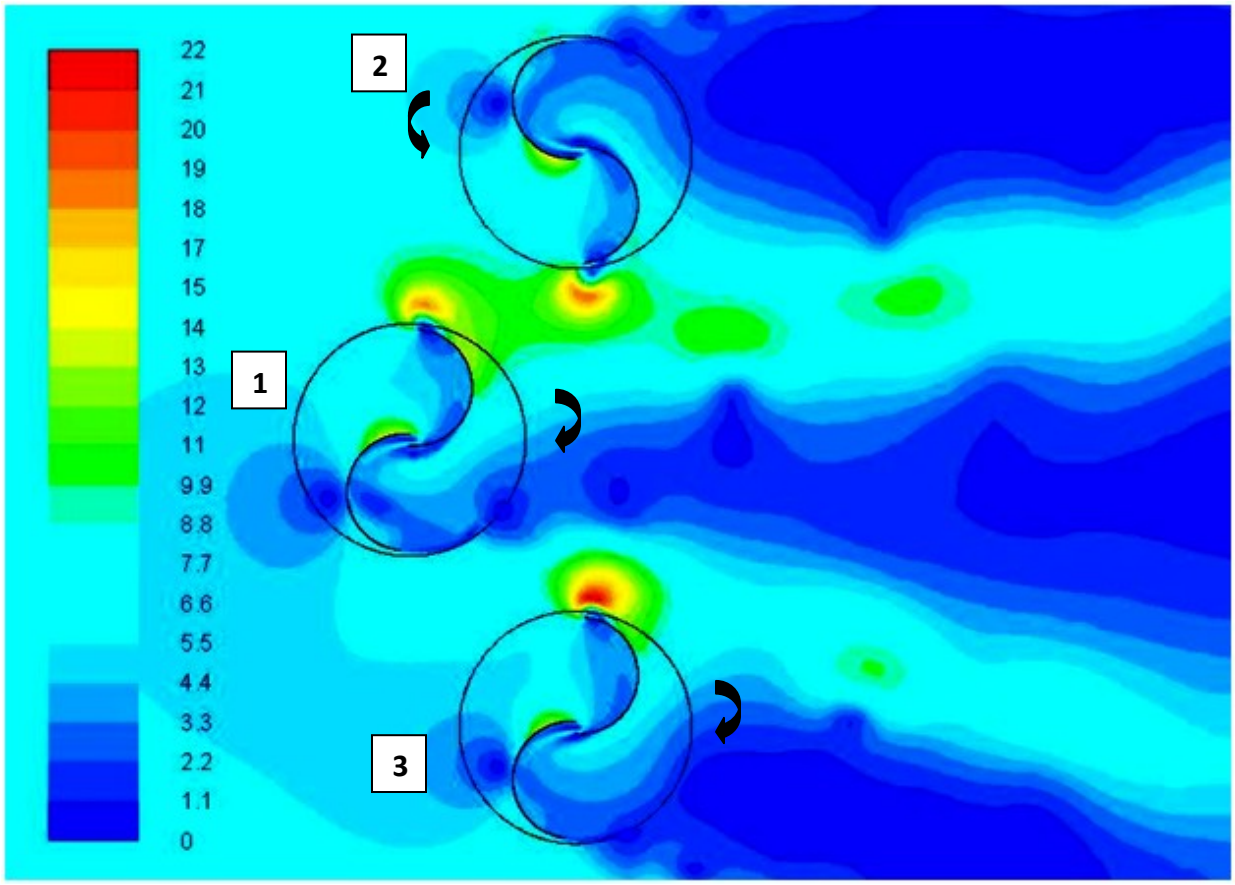

Figure 4.13: Velocity Contours around Three Savonius Turbines Cluster (III)

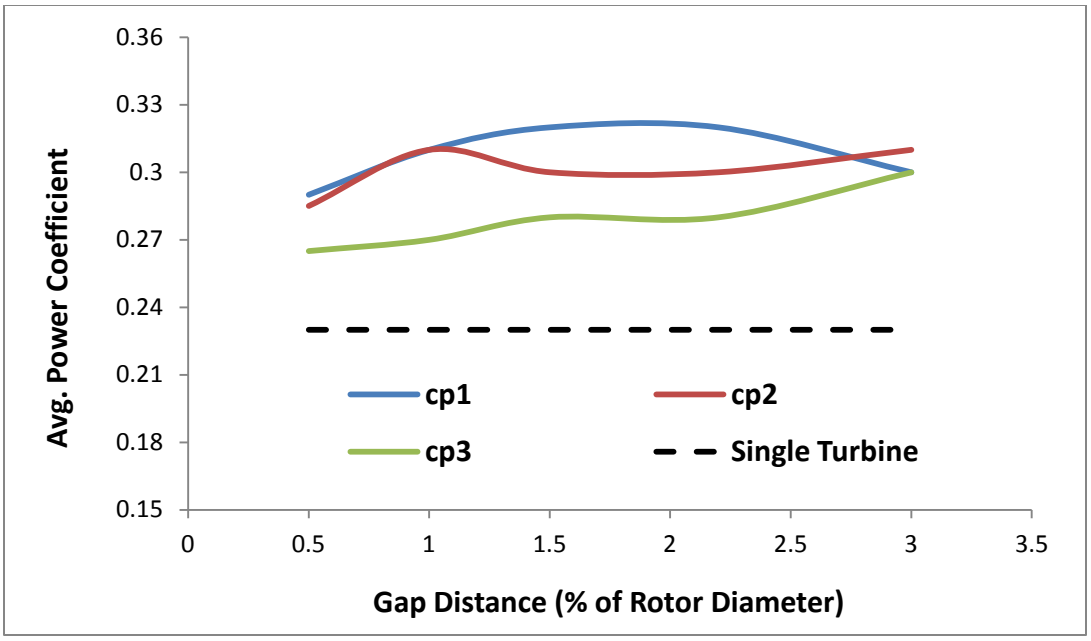

Figure 4.14: Power Coefficients of Three Turbine Cluster Case (III) at Different Gap Distances Vs Single Turbine

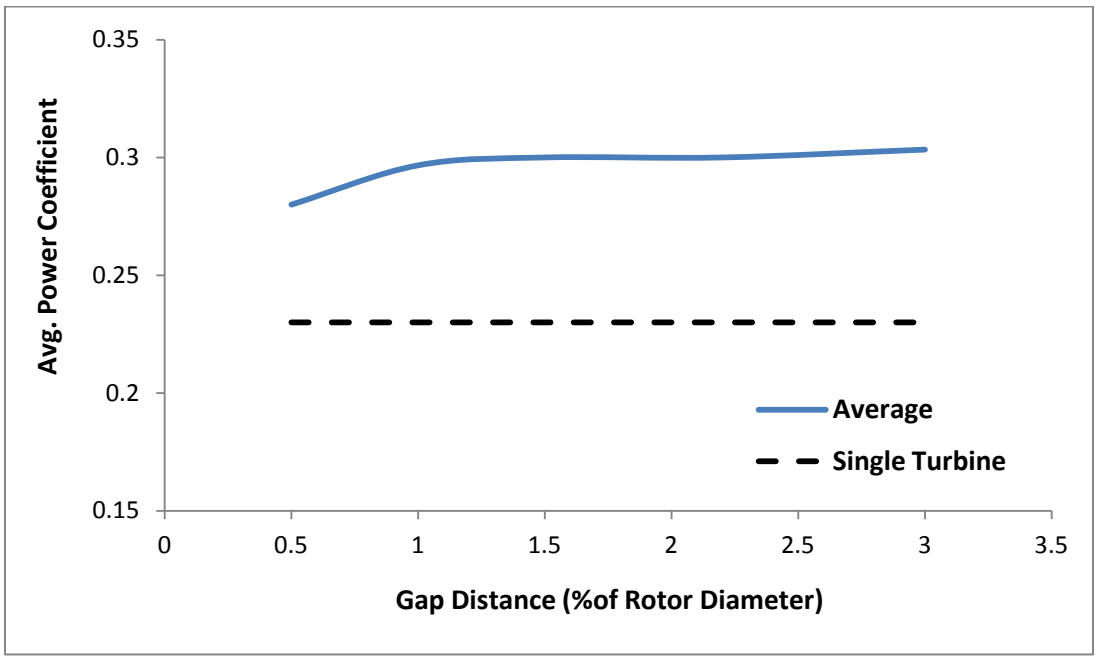

Figure 4.15: Avg. Cp of Three Turbine Cluster Case (III) at Different Gap Distances

At the same gap distances, the performance of rotors (2) and (3) in the three turbines cluster case (III) with their corresponding rotors in the two oblique counter-rotating rotors case (C) and co-rotating case (B) are compared. Rotor (2) has higher power coefficient in the three rotor cluster case (III) than that in case (C) of two counter-rotating oblique rotors ($\alpha=60^{o}$) as shown in figure 4.16. Also, rotor (3) in the three rotors cluster case (III) has higher power coefficient than in case (B) of two co-rotating oblique rotors ($\alpha= -60^{o}$) as shown in figure 4.17. The results confirms that the enhancement in the three turbine cluster more than for the two turbine clusters.

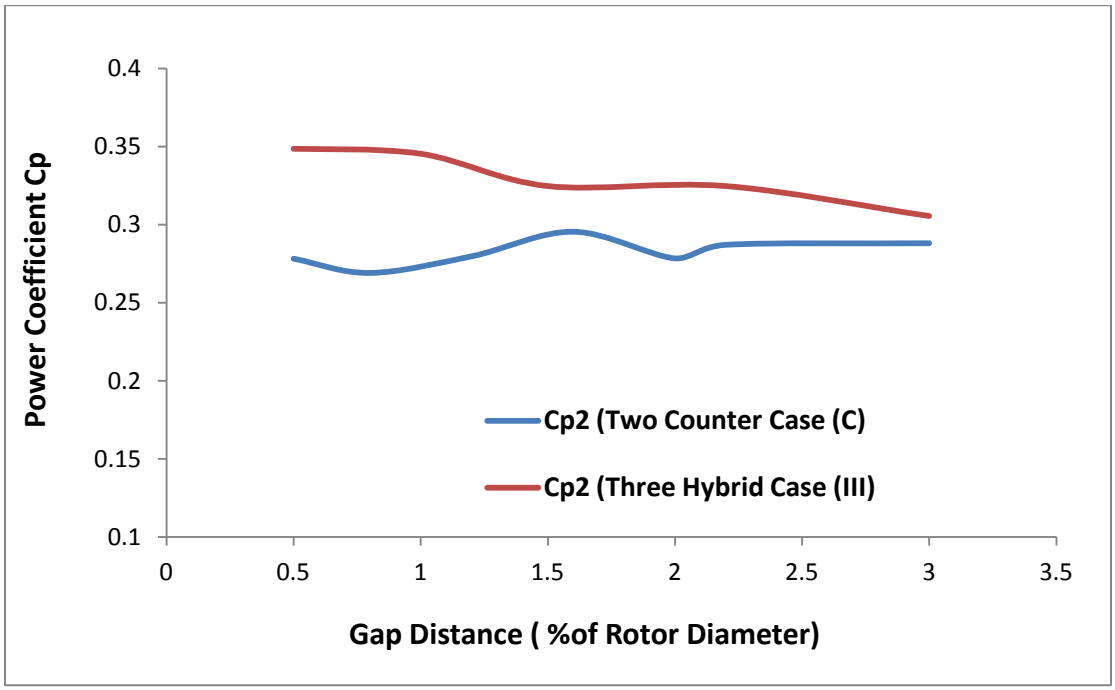

Figure 4.16: C_p for Rotor (2) in Two Oblique Turbines Case (C) Compared to its Values in Three Turbine Cluster Case (III) at Different Gap Distances

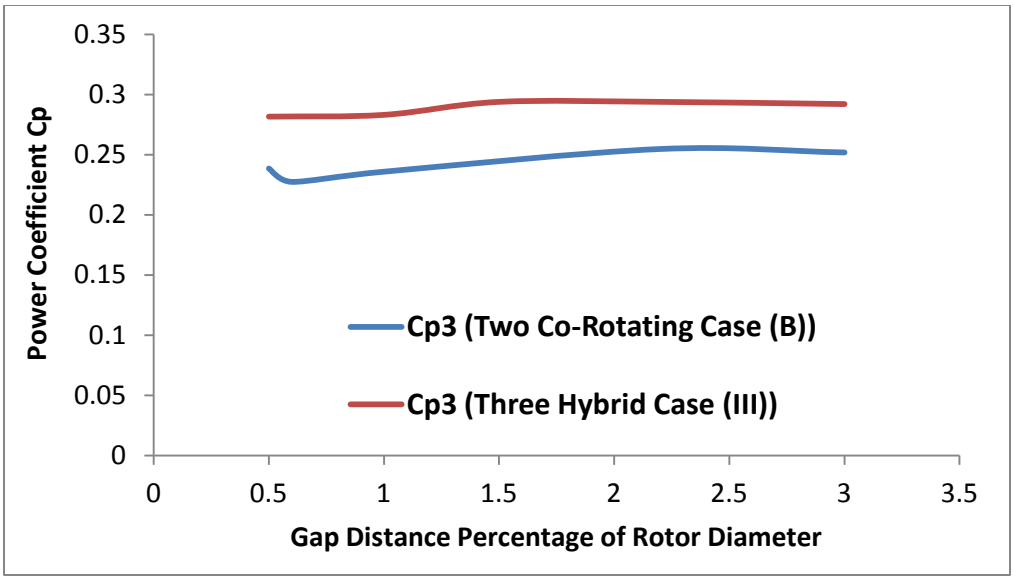

Figure 4.17: C_p for Rotor (3) in Two Oblique Rotors Case (B) Compared to its Values in Three Turbine Cluster Case (III) at Different Gap Distances

4.2.2. Case (IV): Counter-Rotating Three Turbine Cluster

To insure that the results of the comparison of the two oblique co-and counter- rotating clusters applies on the three turbine clusters, another three turbine cluster (IV) is numerically simulated. The cluster (IV) has an opposite layout to cluster (III), rotor (2) is co-rotating with rotor (1), and rotor (3) is counter-rotating with rotor (1) as shown in figure 4.18. The results in figure 4.19 show the power coefficients of the three turbines at different gap distances compared to isolated turbine, an enhancement in the power coefficient occurs for turbines (2) and (3), turbine (2) has the highest power coefficient due to the Magnus effect created by turbine (1). However the rotation of turbine (1) is altered by the downstream turbines rotation causing a decrease in its power coefficient at small gap distances. Figure 4.20 shows the average power coefficient of the three turbines compared to the isolated turbine, at small gap distance the performance is lower than that of the isolated turbines and increases gradually with increasing the gap distance.

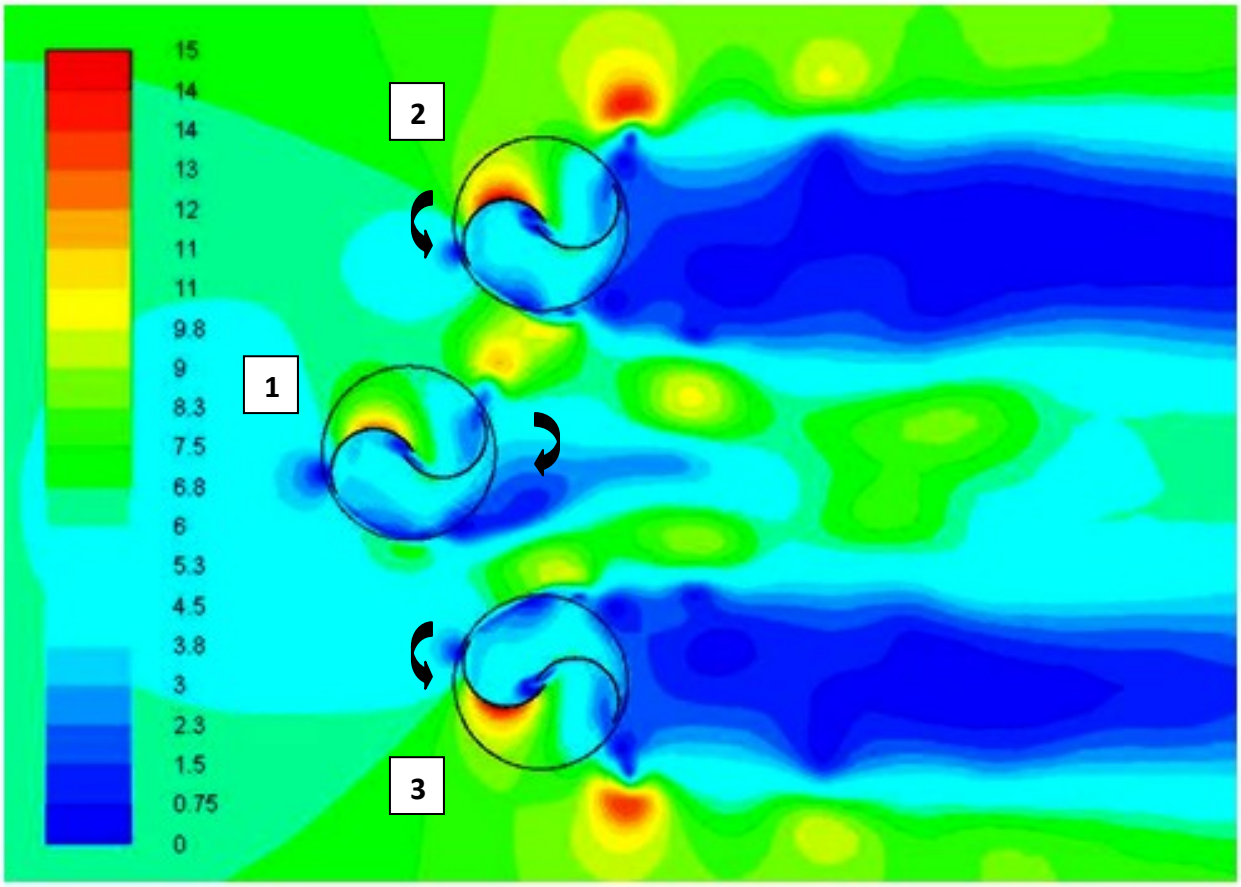

Figure 4.18: Velocity Contours around Three Savonius Turbines Cluster (IV)

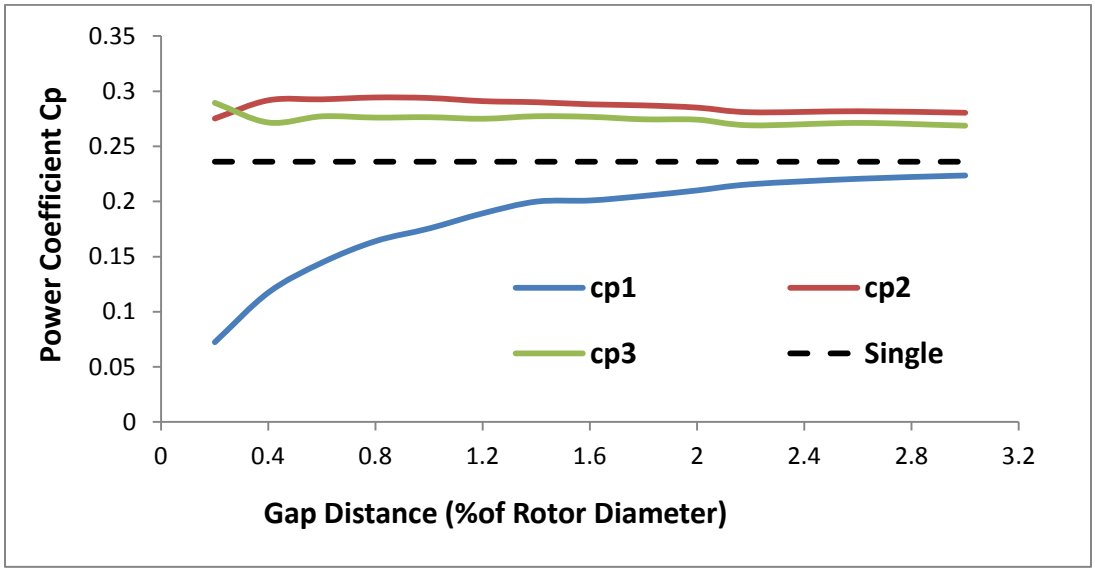

Figure 4.19: Power Coefficients of Three Turbine Cluster Case (IV) at Different Gap Distances Vs Single Rotor

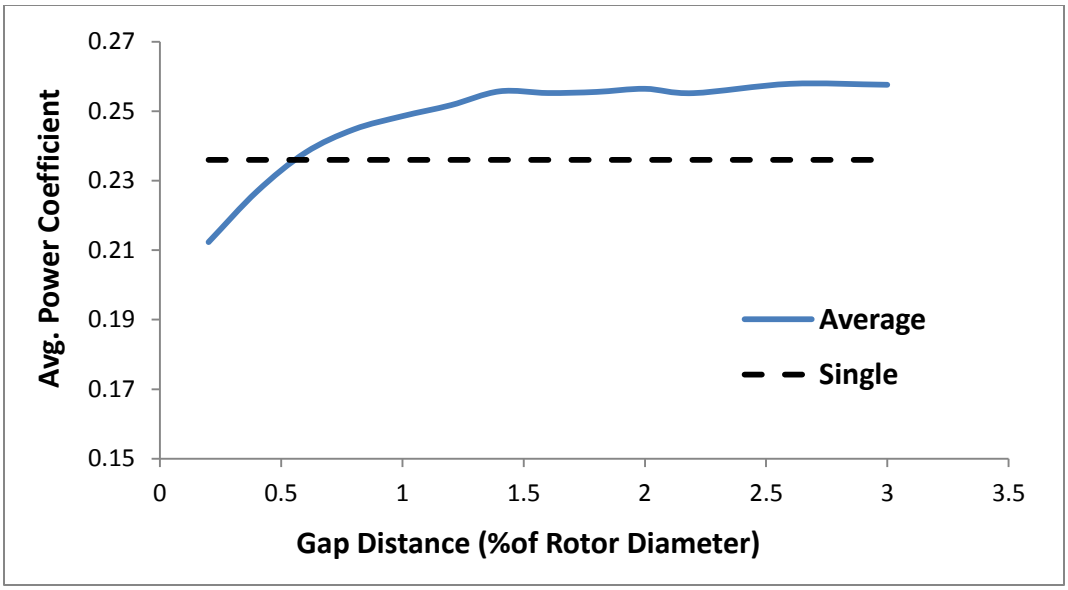

Figure 4.20: Average Cp of Three Turbine Cluster Case (IV) at Different Gap Distances

4.2.3. Comparison between Counter- and Co-Rotating Triangular Three Turbine Clusters (I), (III) and (IV)

In chapter 3, the comparison between the two co-rotating three turbine clusters (I) and (II) showed that they have similar performance at large gap distances. In this section, the results for the three turbine clusters (III) and (IV) are compared to the co-rotating three turbine cluster (I) results introduced in chapter 3 as shown in figure 4.21. The comparison shows that the efficiency of the triangular three turbine cluster case (III) is the highest at different gap distances, however the difference in the average power coefficient between case (III) and the co-rotating cluster case (I) is less than 3%. Taking into consideration that using cluster (III) requires more investment in adding control systems for keeping the phase shift angle (α) between the turbines, then the co-rotating cluster (I) can be adopted to construct efficient Savonius wind turbine farms. At a gap distance 2.2D and triangular cluster height 1.6D the co-rotating cluster (I) has its maximum

average power coefficient, the performance at this geometry is 26% higher than that of isolated turbines.

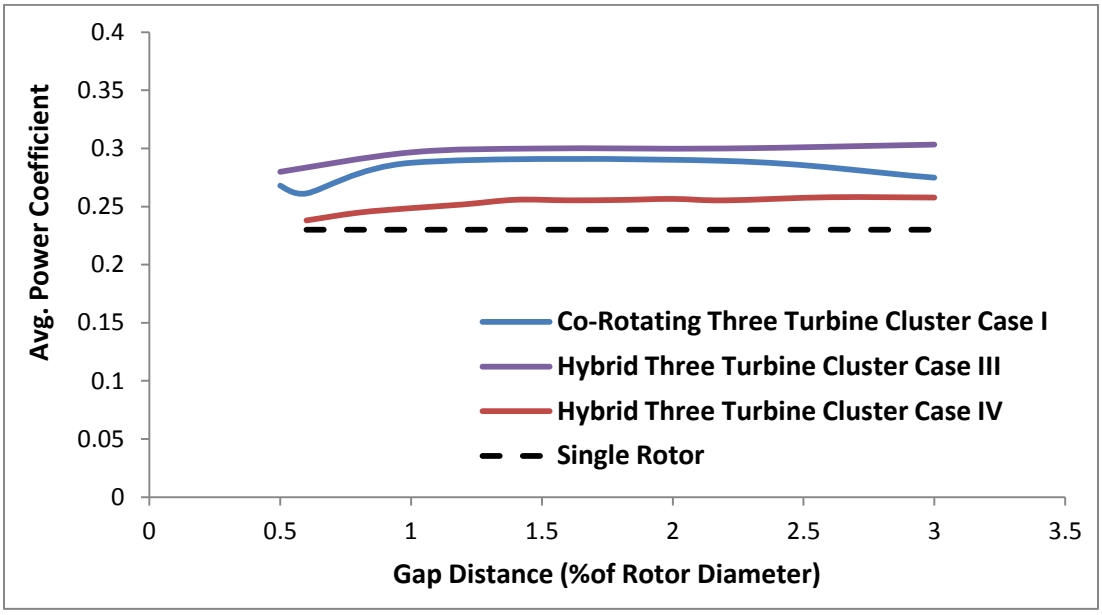

Figure 4.21: Average Cp of Different Three Co-Rotating Turbine Clusters

4.3. Summary

Numerical solutions are performed for clusters of two counter-rotating parallel and oblique Savonius turbines, and counter rotating three turbine clusters. The results show an enhancement in the power coefficient of the closely positioned rotors compared to isolated rotors. This enhancement is found to be dependent on: the relative phase angle between the adjacent counter rotating turbines and the gap distances between the rotor's tips. The results are compared to corresponding co-rotating configuration simulated in chapter 3. The conclusion of the calculated data and the comparison can Summarized as follows:

- Counter-Rotating parallel turbines case (B) is the most efficient configuration for two parallel Savonius rotors, where the inward buckets of the two turbines are advancing buckets and they rotate in the same direction of the wind. The highest values for the average power coefficient for this case is 0.306 achieved at a relative phase angle of 30^o and a gap distance 0.8D.
- In case (C) of two oblique counter-rotating turbines, where the inward buckets of the two turbines are advancing: the highest values for the average power coefficient is 0.34 achieved at a relative phase angle of 30^o and a gap distance 0.4D. In case (D) of two oblique counter-rotating turbines, where the inward buckets of the two turbines are returning: no significant enhancement occurs compared to isolated turbines.
- The comparison between results of two oblique Savonius co- and counter-rotating turbines shows that the most efficient configuration for two oblique turbines at an angle +ve 60^o is the counter-rotating configuration case (C). And the most efficient configuration for two oblique turbines at an angle -ve 60^o is the co-rotating configuration case (B).
- A triangular three turbine cluster (III) is developed based on the above the comparisons, the simulation is performed at different gap distances and the results are compared to the co-rotating three turbine cluster results introduced in chapter (3). The comparison shows that the efficiency of the three turbine triangular cluster case (III) is higher than that of the co-rotating cluster case (I) introduced in chapter (3) by approximately 3%. However, cluster (III) needs more expensive control systems for implementation.
- The co-rotating triangular cluster of three Savonius turbines has an enhanced power of 26% compared to the isolated turbines at gap distance 2.2D, this cluster is the best

configuration for a triangular three turbine cluster that can be used as a building unit for efficient Savonius VAWT farms.

Chapter 5

Patterned Savonius Vertical Axis Wind Turbine Farms

In chapter 3, an efficient triangular three co-rotating turbine cluster is developed. The downstream turbines are in an oblique position to the upstream turbine, the gap distance between the oblique turbines is S=2.2D, the oblique angle is 60^{o} and the triangle height is S_1=1.6D. The cluster has an enhancement of 26% in the average power coefficient higher than the isolated turbine with a ratio of approximately 1:1.2:1 between the power coefficients of its three rotors. In this chapter, the enhancement in the three turbine cluster and the power ratio is confirmed at different tip speed ratios. Keeping the same topology of the cluster, farms that consist of multiple clusters are developed with scaled geometrical ratios of the three turbine cluster. This resulted in patterned farms that have the same power enhancement ratio of the three turbine cluster. Numerical simulations of farms that consist of nine and twenty-seven turbines confirm the enhancement and the pattern progression for larger farms.

5.1. Farm Direction Choice

A wind farm is defined as a group of wind turbines installed in close locations to produce electric energy from wind energy. The number of turbines in a wind farm may reach several hundreds of individual wind turbines and extends to cover an area of hundreds of square miles, where the land between the turbines may be used for agricultural or other purposes or the wind farm can also be located offshore. An economic wind farm require wind speed of 16 km/h (4.4 m/sec) or greater. An ideal for a wind farm is a near constant flow of non-turbulent wind throughout the year. Local wind direction and speed are monitored for a year or more, and detailed wind maps are constructed before wind turbines are installed [11]. The direction for the orientation of a wind farm is chosen according to the distribution of energy across the directions calculated by multiplying the percentage of the mean wind duration by the cube of the mean wind speed as shown in figure 5.1. In this study it is assumed that the main direction that represents the highest wind energy is the west direction.

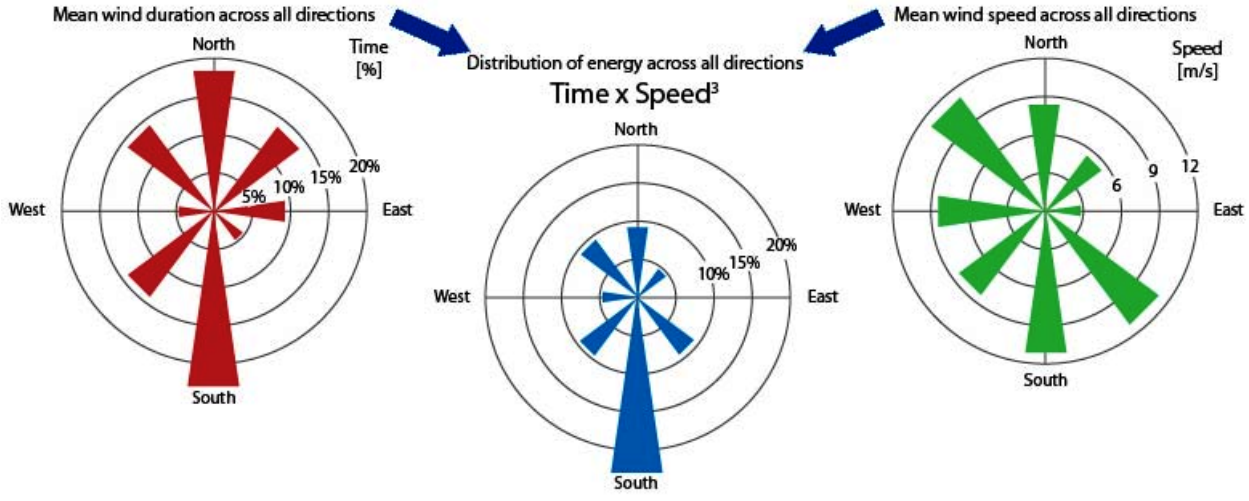

Figure 5.1: Wind Farm Wind Directions, Speeds and Energy Distribution

5.2. Numerical Simulation Model

5.2.1. Computational Domain

The computational domain shown in figure 5.2 is similar to the domain used in the previous chapters, the upstream boundary (semi circle), the upper and lower boundaries are at a distance of 15D from the rotors, and the downstream boundary is 30D from the downstream rotors. The sliding mesh method is used, so the computational domain consists of rotating sub-domains (circles) that contain the rotors, and a fixed zone that extends from the interface of the rotating regions to the boundaries of the domain. The diameter of the circular interface around each rotor is taken as 1.2D. Boundary conditions (BCs) are also defined, a wall type BC is used for the Savonius turbine buckets. The downstream, upper and lower boundaries are defined with velocity inlet BC (x-component = 7 m/sec). The downstream boundary is defined with pressure outlet boundary condition.

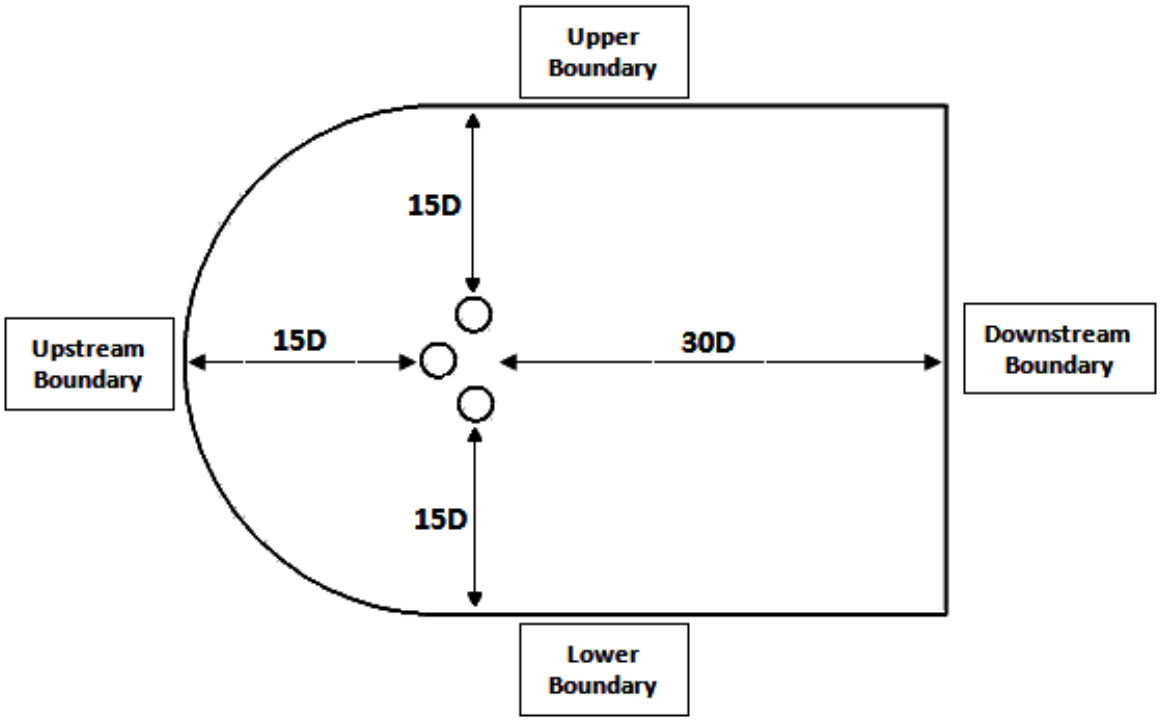

Figure 5.2: Computational Domain

5.2.2. Mesh Generation and Grid Independence Study

For the three turbine cluster, the same grid structure and topology introduced in chapter 2 is used. A grid sensitivity study is also done for the three turbine cluster, the mesh is refined five times until there is no significant change observed in the torque coefficient (C_m) as shown in figure 5.3. The levels of mesh refinement are shown in table 5.1, level 3 with 255,751 elements is found to be adequate. A y+ < 1 is achieved as required by the transition SST turbulence model.

Table 5.1: Grid Refinement Levels for Savonius Three Co-Rotating Turbine Cluster

Grid Level	No. of Cells	Cm1	Cm2	Cm3
1	80,517	0.355	0.344	0.324
2	176,425	0.298	0.340	0.299
3	255,751	0.260	0.327	0.289
4	311,066	0.262	0.326	0.289
5	450,156	0.263	0.328	0.288

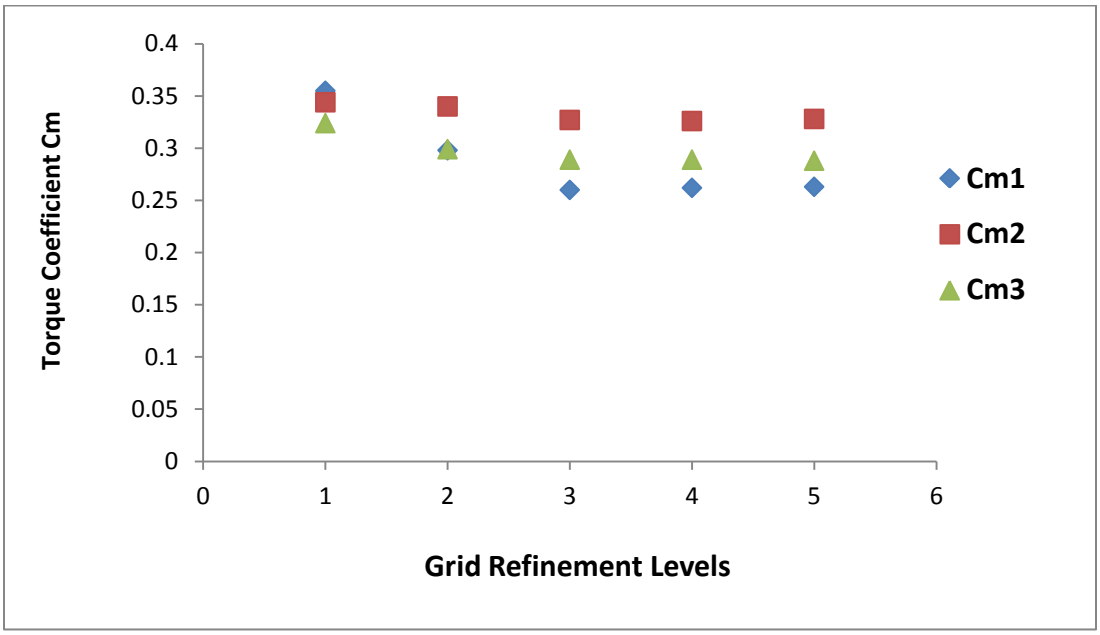

Figure 5.3: C_m of Three Rotors for Different Grid Refinement Levels

The unsteady Reynolds averaged Navier-Stokes equations are solved using SIMPLE algorithm (Semi-Implicit Method) with a second order spatial discretization for all pressure, momentum, and turbulence equations and a Least Squares Cell Based algorithm is used for gradients. The transition SST turbulence model is used as its results were the closest to experimental data in the validation process. Steady flow simulations are obtained initially to set up the flow domain to reasonable parametric values, then unsteady flow simulations are obtained using the sliding mesh model (SMM). A time step size corresponding to a turbine rotation of 1.0 degree is used for the time dependent solution. A drop of at least 3 orders of magnitude in each time step as well as a minimum of 20 iterations per time step is considered as convergence criteria for the time dependent solution.

5.3. Confirmation of the Three Turbine Cluster Performance at Different Tip Speed Ratios

Chapter (3) shows an enhancement in the average power coefficient of Savonius turbines in a three co-rotating three turbine triangular cluster at different gap distances. From the results, a cluster with a gap distance S=2.2D corresponding to a triangle height S1=1.6D shown in figure 5.4 achieves an enhancement of 26% in the average power coefficient compared to isolated turbines.

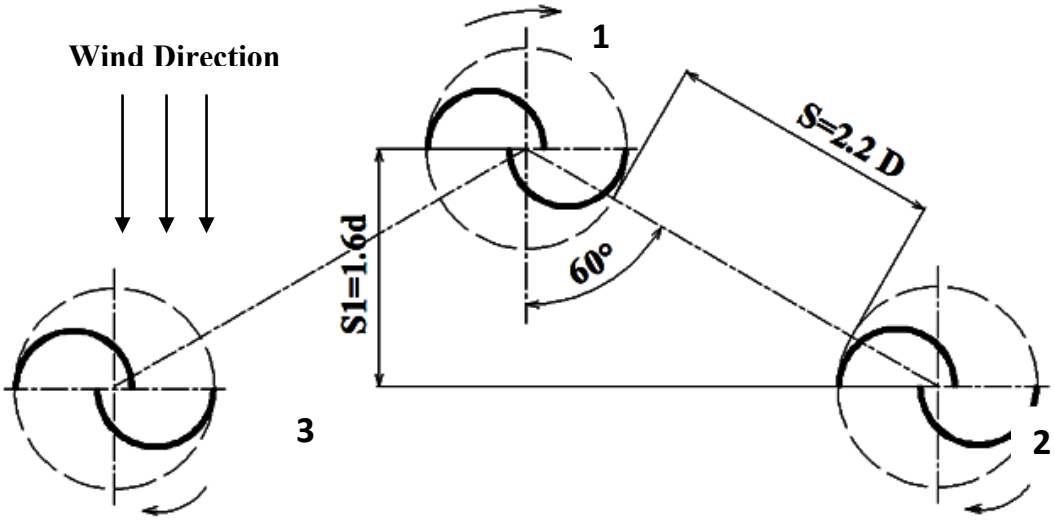

Figure 5.4: A Cluster of Three Co-Rotating Savonius Wind Turbines

The ratio between the power coefficients of the three rotors (1), (2) and (3) in the triangular co-rotating cluster shown in table 5.2 is approximately 1:1.2:1 respectively. Three isolated Savonius turbines (one meter diameter and one meter height) placed at 5D gap distance generate 144 watt and occupy an area of 13 square meters, resulting in a power density of 11 watt/m^2. The developed three turbine cluster has an average power coefficient of 0.29, this generates about 183 watt and occupies an area of 11 square meters, resulting in a power density of approximately 17 watt/m^2. This efficient cluster chosen to be used as a building unit for efficient triangular Savonius wind turbine farms.

Table 5.2: Results of Three Turbines Cluster (S=2.2D, S1=1.6D and angle $\alpha=60^o$) at $\lambda=1$

	Isolated Rotor	Rotor (1)	Rotor (2)	Rotor (3)
Power Coefficient (Cp)	0.23	0.26	0.32	0.28
Enhancement % Compared to Isolated Rotor		13%	42%	25%
Ratio Compared to Rotor (1)		1.0	1.23	1.1

In order to confirm that the enhancement occurring for the power coefficients of the three rotors of the three co-rotating turbine cluster is independent on the speed, the cluster is simulated at different tip speed ratios. The summery of the results in table 5.4 show that the ratio 1:1.2:1 between the power coefficients of the three rotors is consistent for $\lambda>0.6$. Figure 5.5 show the calculate power coefficients for the three turbines at different tip speed ratios, turbine (2) has the highest power coefficient with a maximum power coefficient of 0.32 and turbine (1) and (2) have close performance to each other with a maximum of 0.28 achieved at $\lambda=1$. Figure 5.6 shows the average power coefficient of the three turbines at different tip speed ratios compared to the isolated turbine, the maximum average power coefficient is found to be 0.29 at $\lambda=1$, this represents an enhancement of 26% higher than isolated turbines.

Table 5.3: Results of Three Savonius Turbines Triangular Cluster at Different Tip Speed Ratios

λ	Cp1	Cp2	Cp3	Average	Ratios of Power Coefficients		
					Rotor (1)	Rotor (2)	Rotor (3)
0.2	0.089	0.099	0.090	0.093	1.0	1.12	1.01
0.4	0.174	0.192	0.178	0.181	1.0	1.11	1.02
0.6	0.226	0.265	0.234	0.242	1.0	1.15	1.04
0.8	0.247	0.290	0.259	0.266	1.0	1.18	1.05
1.0	0.260	0.327	0.280	0.289	1.0	1.18	1.02
1.2	0.255	0.302	0.256	0.271	1.0	1.19	1.01
1.4	0.224	0.276	0.224	0.242	1.0	1.23	1.01

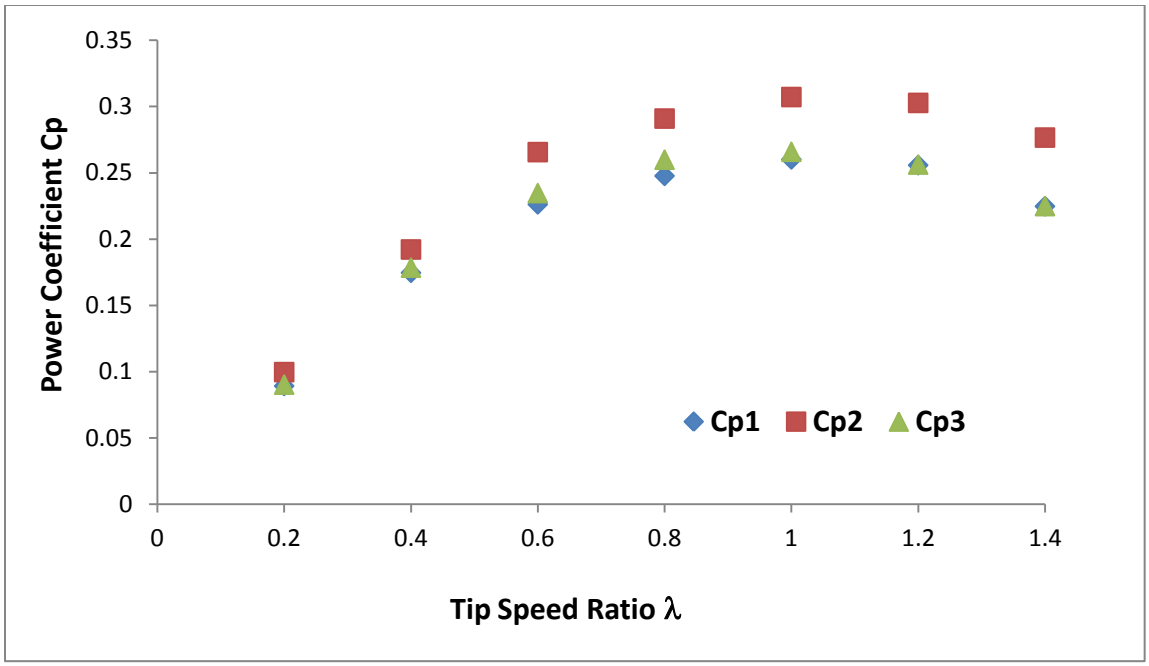

Figure 5.5: Power Coefficients of Three Rotors in the Co-Rotating Turbine Cluster at Different Tip Speed Ratios

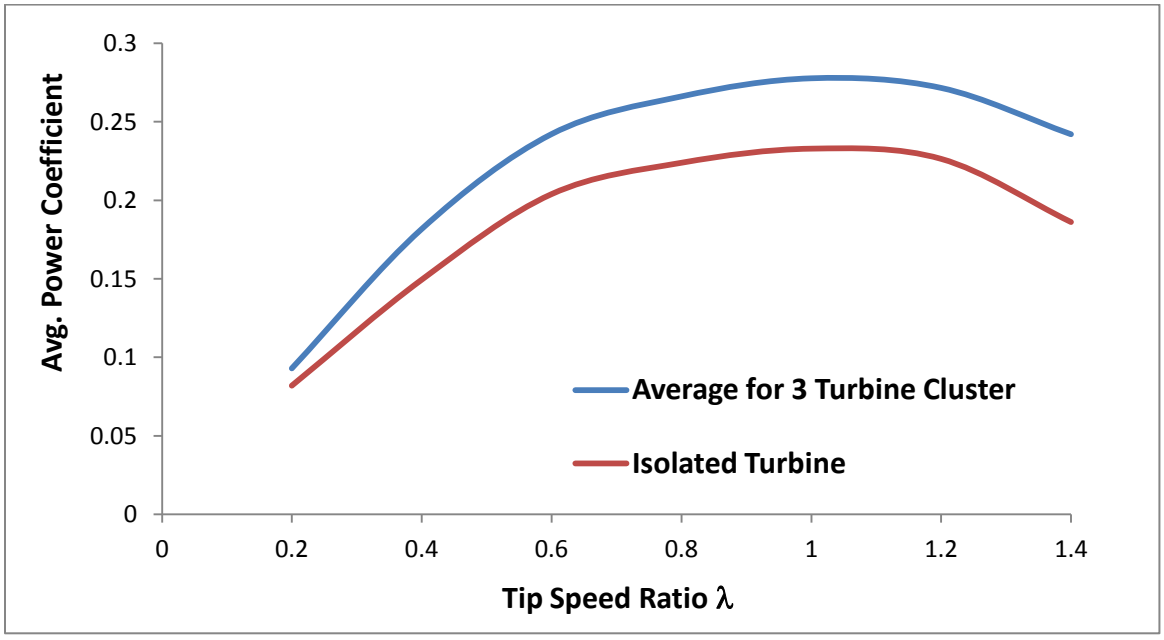

Figure 5.6: Avg. Cp of Three Co-Rotating Turbine Cluster at Different Tip Speed Ratios Vs Isolated Rotor

5.4. Patterned Savonius Wind Turbine Farms

The three turbine cluster is used as a building unit to construct efficient VAWT farms having the same topology of the cluster. The triangular farm has identical geometrical ratios of the three turbine cluster. Numerical simulations of farms that consist of nine and twenty-seven turbines are performed to confirm the same enhancement ratio of the three turbine cluster and the geometric progression.

5.4.1. Simulation of Nine Turbine Farm

A nine turbine triangular farm is developed using one three turbine cluster in the first row and two similar clusters in the second row as shown in figure 5.7. The farm has the same cluster geometric topology, rotors (1), (2) and (3) represent cluster (A), rotors (3), (4) and (5) represent cluster (B) and rotors (6), (7) and (8) represent cluster (C). The farm is numerically simulated at different tip speed ratios and the velocity contours around the nine turbines in figure 5.8 show the interference of the downstream turbines with the high velocity regions created as a result of the Magnus effect of the upstream turbines. Figure 5.9 show the average power coefficient of the nine turbine farm at different tip speed ratios compared to the three turbine cluster and the isolated farms, the same average power enhancement of the three turbine cluster is approximately achieved by the nine turbine farm, the average power coefficient of the developed nine turbine farm is 0.29 which is 26% higher than that of the isolated nine turbine farm. The results of the power coefficient of the nine rotors at $\lambda=1$ summarized in table 5.4 show the same enhancement ratio and confirms the pattern of the three turbine cluster. Within each three turbine cluster (A, B and C) the ratio between the power coefficients of individual turbines is similar to

the ratio achieved for the individual turbines in a single cluster. The results in table 5.5 show that the ratio between the total power generated by clusters (A), (B) and (C) is approximately 1:1.2:1. The enhancement in the performance of the patterned nine turbine farm is in consistency with that of a single three turbine cluster. A (3x3) array of nine aligned and isolated Savonius turbines (one meter height) generates 432 watt and occupies an area of 299 square meters has a power density of 1.5 watt/m^2. The developed Savonius nine wind turbines farm generates 560 watt and occupies an area of 55 square meters, this results in a power density of 10 watt/m^2.

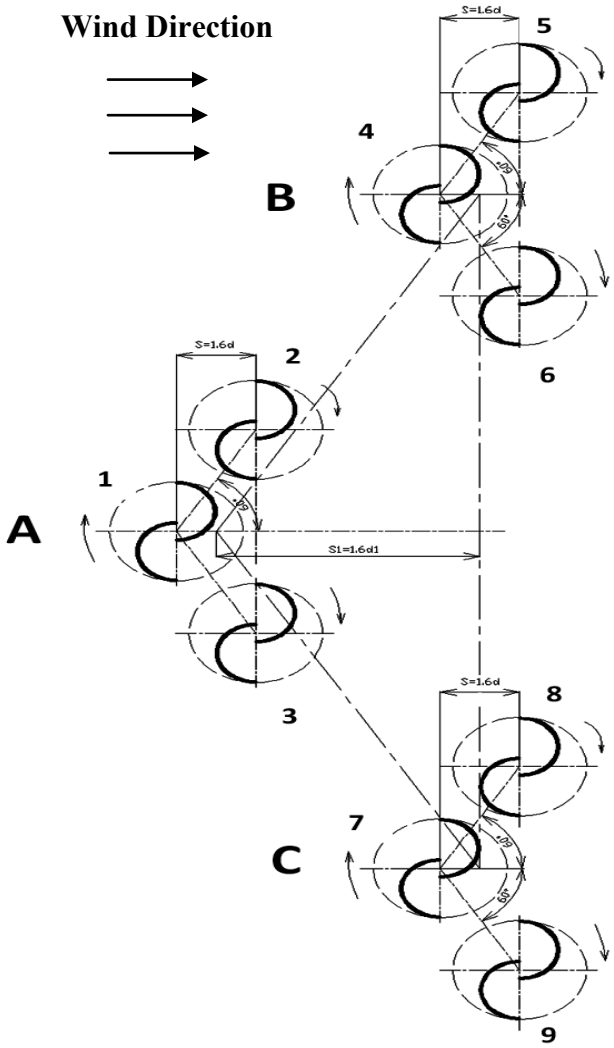

Figure 5.7: Nine Turbines Savonius Wind Farm

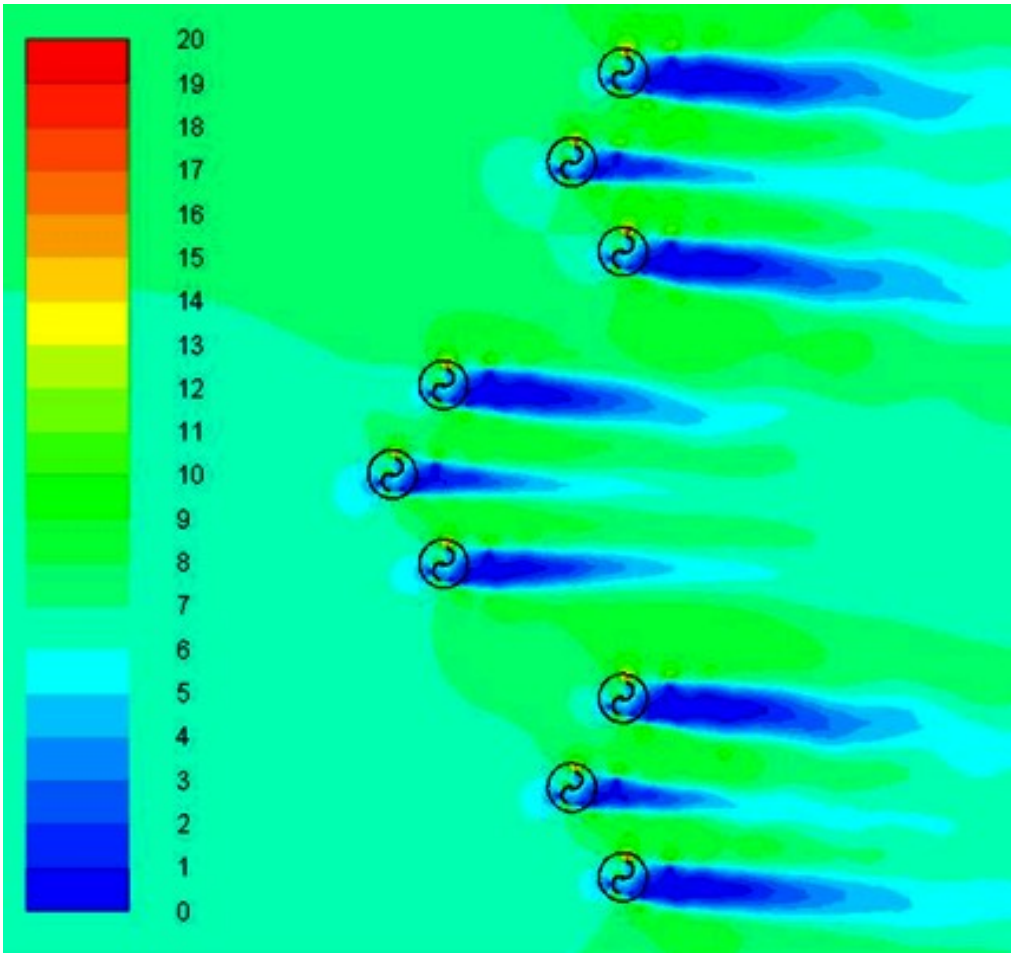

Figure 5.8: Velocity Contours around Nine Savonius Wind Turbine Farm

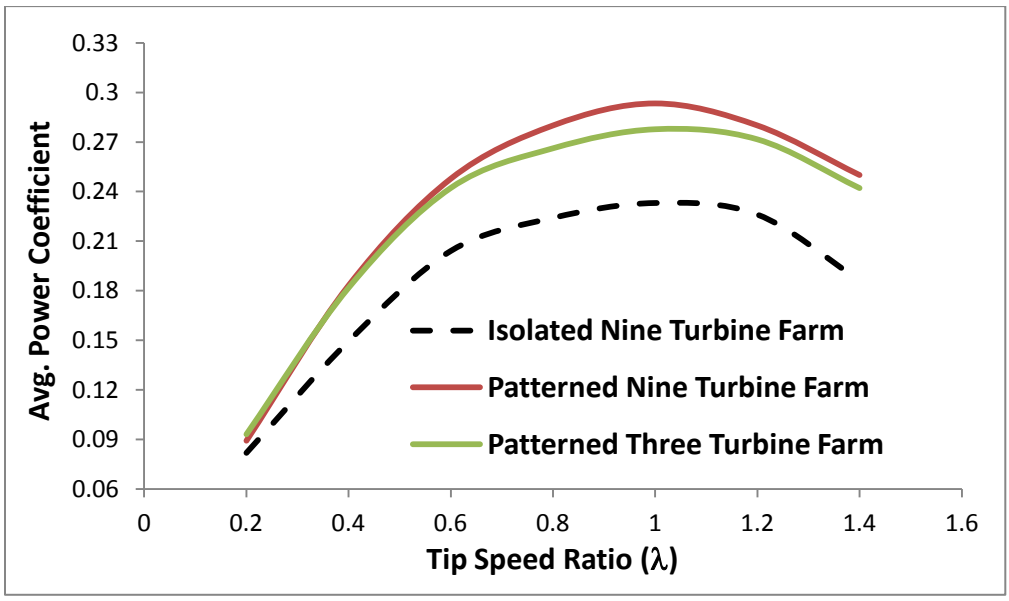

Figure 5.9: Avg. Cp of Nine Turbine Farm at Different Tip Speed Ratios Vs Isolated Farm

Table 5.4: Results of the Nine Savonius Wind Turbine Farm

Cluster A	Isolated Rotor	Rotor (1)	Rotor (2)	Rotor (3)
Power Coefficient (Cp)	0.23	0.24	0.3	0.26
Enhancement % Compared to Isolated Rotor		4%	30%	13%
Ratio Compared to Rotor (1)		1	1.25	1.08
Cluster B	**Isolated Rotor**	**Rotor (4)**	**Rotor (5)**	**Rotor (6)**
Power Coefficient (Cp)	0.23	0.31	0.36	0.32
Enhancement % Compared to Isolated Rotor		34%	56%	39%
Ratio Compared to Rotor (4)		1	1.16	1.03
Cluster C	**Isolated Rotor**	**Rotor (7)**	**Rotor (8)**	**Rotor (9)**
Power Coefficient (Cp)	0.23	0.26	0.32	0.27
Enhancement % Compared to Isolated Rotor		13%	39%	17%
Ratio Compared to Rotor (7)		1	1.23	1.03

Table 5.5: Total Power Generated by the three clusters in Nine Turbines Wind Farm

	Cluster (A)	Cluster (B)	Cluster (C)
Power Coefficient	0.267	0.33	0.28
Total Power (watt)	170	210	180
Ratio Compared to Cluster (A)	1	1.23	1.04

The nine turbine farm is patterned, this means that the performance of the farm can be predicted by simulation of only three turbines. Using the ratio 1:1.2:1 and the results of the simulation of the three turbine cluster, the nine turbine farm efficiency is predicted and compared to the calculated results in table 5.4 as shown in figure 5.10. The results show that error in the predicted average power coefficient of the farm compared to the calculated value is less than 2%.

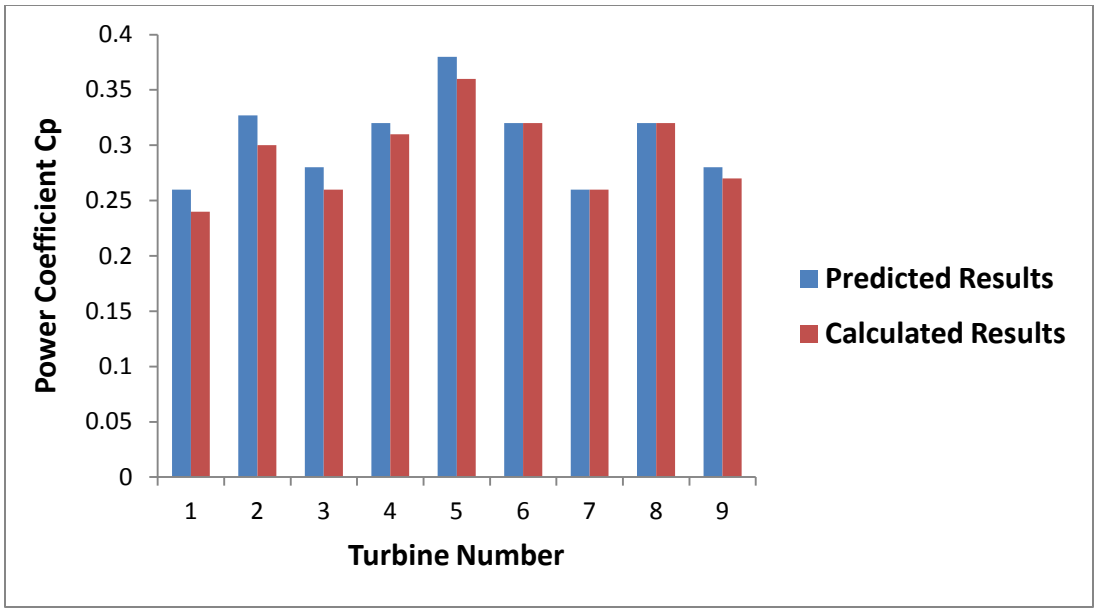

Figure 5.10: Comparison between Predicted and Calculated Results for the Nine Savonius Turbine Farm at λ=1

5.4.2. Simulation of Twenty-Seven Turbine Farm

Using nine three turbine clusters (A-I) a twenty seven turbine triangular farm is developed by setting one nine turbine farm in the first row and two similar farms in the second row as shown in figure 5.11. The velocity contours in figure 5.12 show that the farm has the same topology of the single three turbines cluster. Rotors from (1) to (27) represent the clusters from (A) to (I). Clusters (A), (B) and (C) represent farm I, Clusters (D), (E) and (F) represent farm (II) and Clusters (G), (H) and (I) represent farm (III). The simulation results of the power coefficient of the twenty-seven rotors are summarized in table 5.6 and the total power generated by the nine clusters in table 5.7. Also the total power of the three large clusters (nine turbine cluster) I, II and III is shown in table 5.8. The numerical results in table 5.7 show that the ratio between the power outputs of clusters in each nine turbine farm is about 1:1.2:1, comparing the total power generated by farms I, II and III we get the same ratio as shown in table 5.8. The enhancement in

the twenty-seven turbine farm is in consistency with that of the single three turbine cluster and the nine turbine farm. A (3x9) array of nine aligned and isolated Savonius turbines (one meter height) generates 1296 watt and occupies an area of 1127 square meters has a power density of 1.1 watt/m^2. The developed twenty seven Savonius turbine farm generates 1851 watt and occupies an area of 415 square meters, this results in a power density of 4.4 watt/m^2. The average power coefficient efficiency of the developed twenty-seven turbine farm is 0.32.

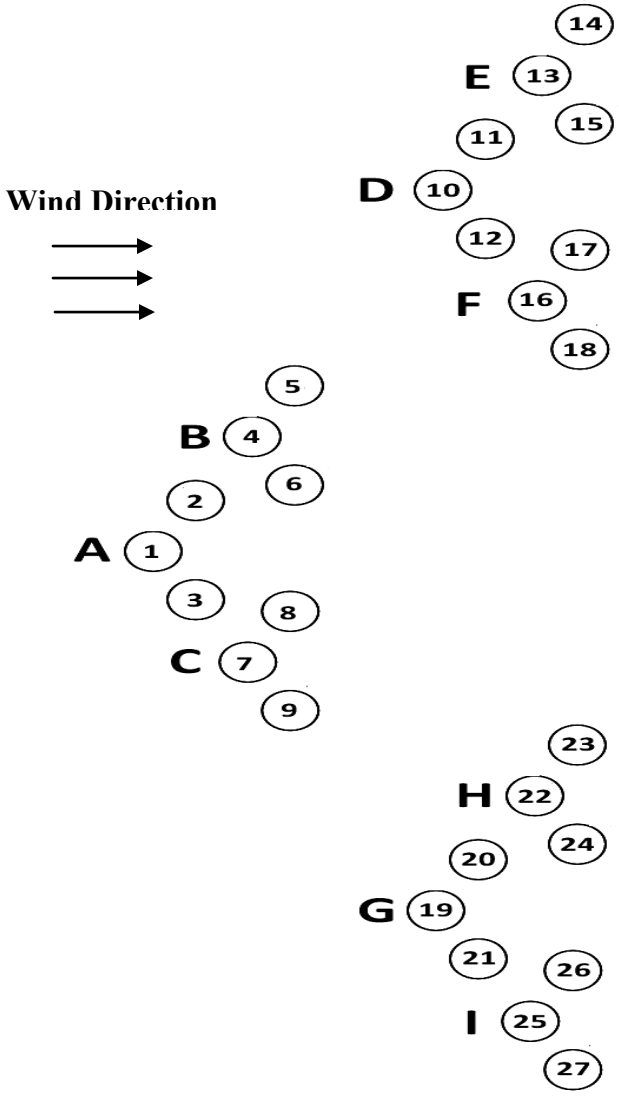

Figure 5.11: A Farm of Twenty Seven Savonius Wind Turbines

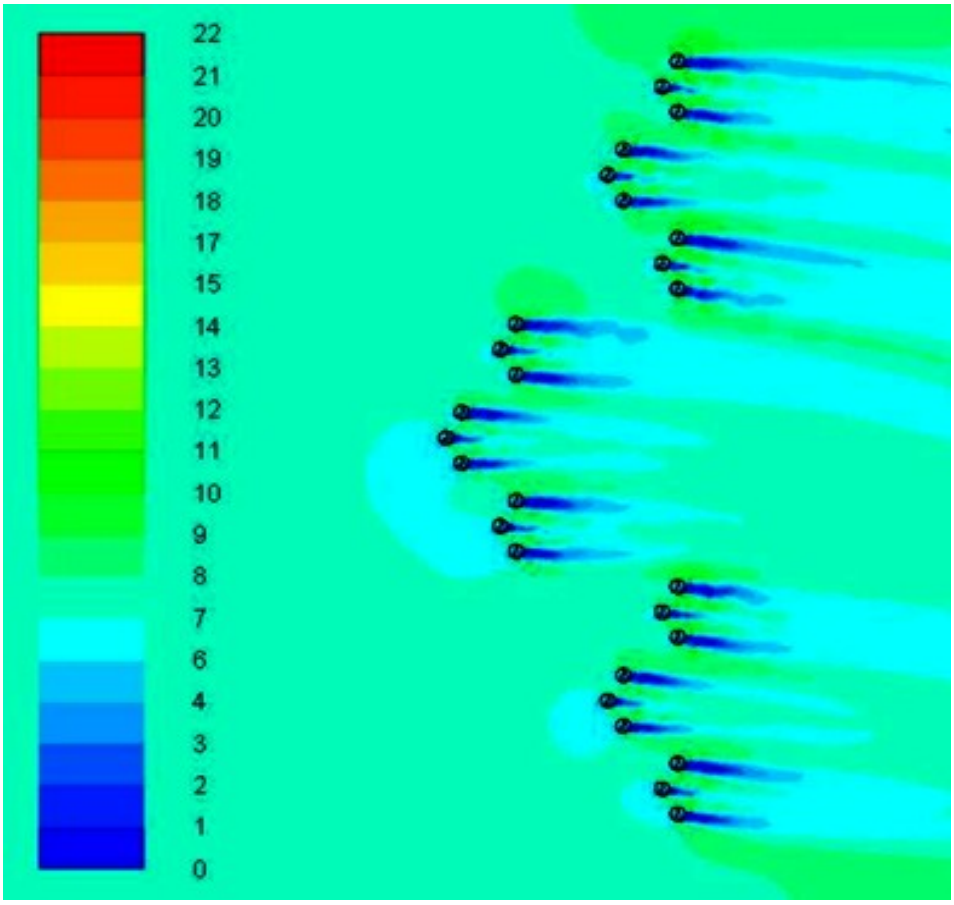

Figure 5.12: Velocity Contours around Twenty-Seven Savonius Wind Turbine Farm

The twenty-seven turbine farm is patterned, this means that the performance of the farm can be predicted by simulation of only three turbines. Using the ratio 1:1.2:1 and the results of the simulation of the three turbine cluster, the twenty-seven turbine farm efficiency is predicted and compared to the calculated results in table 5.6 as shown in figure 5.13. The results show that error in the predicted average power coefficient of the farm compared to the calculated value is less than 0.4%.

Table 5.6: Results of the Twenty-Seven Savonius Wind Turbine Farm

Cluster A	**Isolated Rotor**	**Rotor (1)**	**Rotor (2)**	**Rotor (3)**
Power Coefficient (Cp)	0.23	0.25	0.29	0.26
Enhancement % Compared to Isolated Rotor		8.5%	26%	13%
Ratio Compared to Rotor (1)		1	1.16	1.04
Cluster B	**Isolated Rotor**	**Rotor (4)**	**Rotor (5)**	**Rotor (6)**
Power Coefficient (Cp)	0.23	0.31	0.36	0.32
Enhancement % Compared to Isolated Rotor		34%	52%	39%
Ratio Compared to Rotor (4)		1	1.16	1.03
Cluster C	**Isolated Rotor**	**Rotor (7)**	**Rotor (8)**	**Rotor (9)**
Power Coefficient (Cp)	0.23	0.28	0.32	0.27
Enhancement % Compared to Isolated Rotor		22%	39%	17%
Ratio Compared to Rotor (7)		1	1.14	0.96
Cluster D	**Isolated Rotor**	**Rotor (10)**	**Rotor (11)**	**Rotor (12)**
Power Coefficient (Cp)	0.23	0.32	0.36	0.33
Enhancement % Compared to Isolated Rotor		39%	56%	43%
Ratio Compared to Rotor (1)		1	1.13	1.03
Cluster E	**Isolated Rotor**	**Rotor (13)**	**Rotor (14)**	**Rotor (15)**
Power Coefficient (Cp)	0.23	0.35	0.42	0.35
Enhancement % Compared to Isolated Rotor		52%	78%	52%
Ratio Compared to Rotor (4)		1	1.2	1
Cluster F	**Isolated Rotor**	**Rotor (16)**	**Rotor (17)**	**Rotor (18)**
Power Coefficient (Cp)	0.23	0.34	0.39	0.35
Enhancement % Compared to Isolated Rotor		48%	69%	52%
Ratio Compared to Rotor (7)		1	1.18	1
Cluster G	**Isolated Rotor**	**Rotor (19)**	**Rotor (20)**	**Rotor (21)**
Power Coefficient (Cp)	0.23	0.28	0.32	0.28
Enhancement % Compared to Isolated Rotor		22%	39%	22%
Ratio Compared to Rotor (1)		1	1.18	1
Cluster H	**Isolated Rotor**	**Rotor (22)**	**Rotor (23)**	**Rotor (24)**
Power Coefficient (Cp)	0.23	0.35	0.40	0.36
Enhancement % Compared to Isolated Rotor		52%	74%	56%
Ratio Compared to Rotor (4)		1	1.19	1.02
Cluster I	**Isolated Rotor**	**Rotor (25)**	**Rotor (26)**	**Rotor (27)**
Power Coefficient (Cp)	0.23	0.29	0.34	0.30
Enhancement % Compared to Isolated Rotor		26%	48%	30%
Ratio Compared to Rotor (7)		1	1.17	1.03

Table 5.7: Total Power Generated by the nine clusters in the Twenty-Seven Turbine Farm

	Power Coefficient	Total Power (watt)	Ratio Compared to Cluster (A)
Cluster (A)	0.27	170	1.0
Cluster (B)	0.33	208	1.22
Cluster (C)	0.29	182	1.07
		Total Power (watt)	**Ratio Compared to Cluster (D)**
Cluster (D)	0.34	214	1.0
Cluster (E)	0.37	233	1.09
Cluster (F)	0.36	226	1.05
		Total Power (watt)	**Ratio Compared to Cluster (A)**
Cluster (G)	0.29	182	1.0
Cluster (H)	0.37	233	1.27
Cluster (I)	0.31	195	1.06

Table 5.8: Total Power Generated by the three clusters I, II and III

	Cluster (I)	Cluster (II)	Cluster (II)
Power Coefficient	0.3	0.36	0.32
Total Power (watt)	567	680	604
Ratio Compared to Cluster (I)	1.0	1.2	1.06

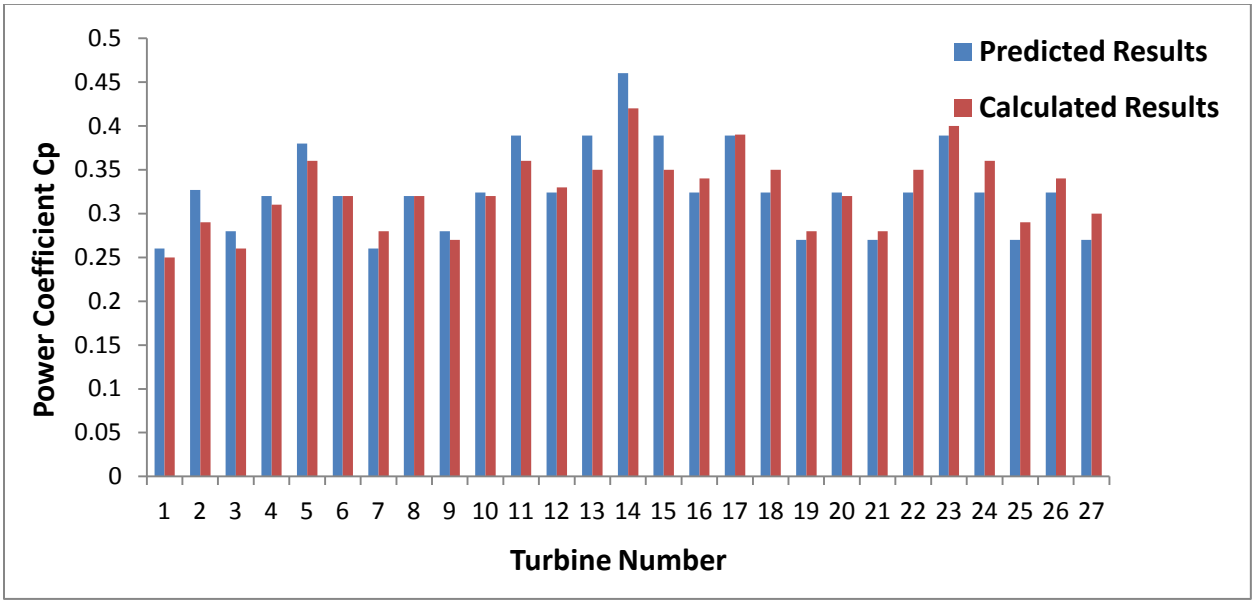

Figure 5.13: Comparison of between Predicted and Calculated Results for the Twenty-Seven Savonius Turbine Farm at λ=1

Figure 5.14 shows the total power achieved by the developed cluster and farms compared to the output from the same number of isolated turbines, the total power achieved by the developed twenty-seven turbine farm is 39% higher than the isolated twenty-seven turbine farm. Figure 5.15 shows the power density of the developed farms compared to the power density of the same number of isolated turbines (5 rotor diameters apart cross field and 10 rotor diameters apart downstream). A power scaling is achieved going from an isolated single turbine to the three turbine cluster to the nine turbine farm to the twenty seven turbine farm as shown in figure 5.16.

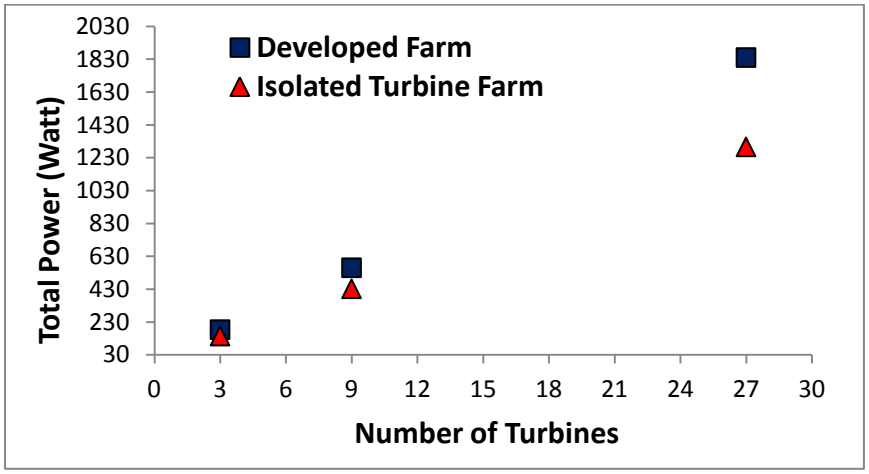

Figure 5.14: Total Power Generated by the developed farms Vs Isolated Turbines

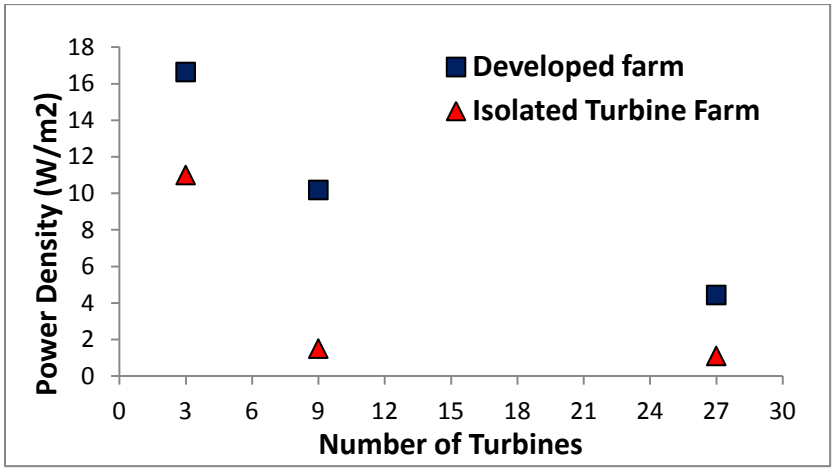

Figure 5.15: Power Density Vs the Number of Turbines in a Farm

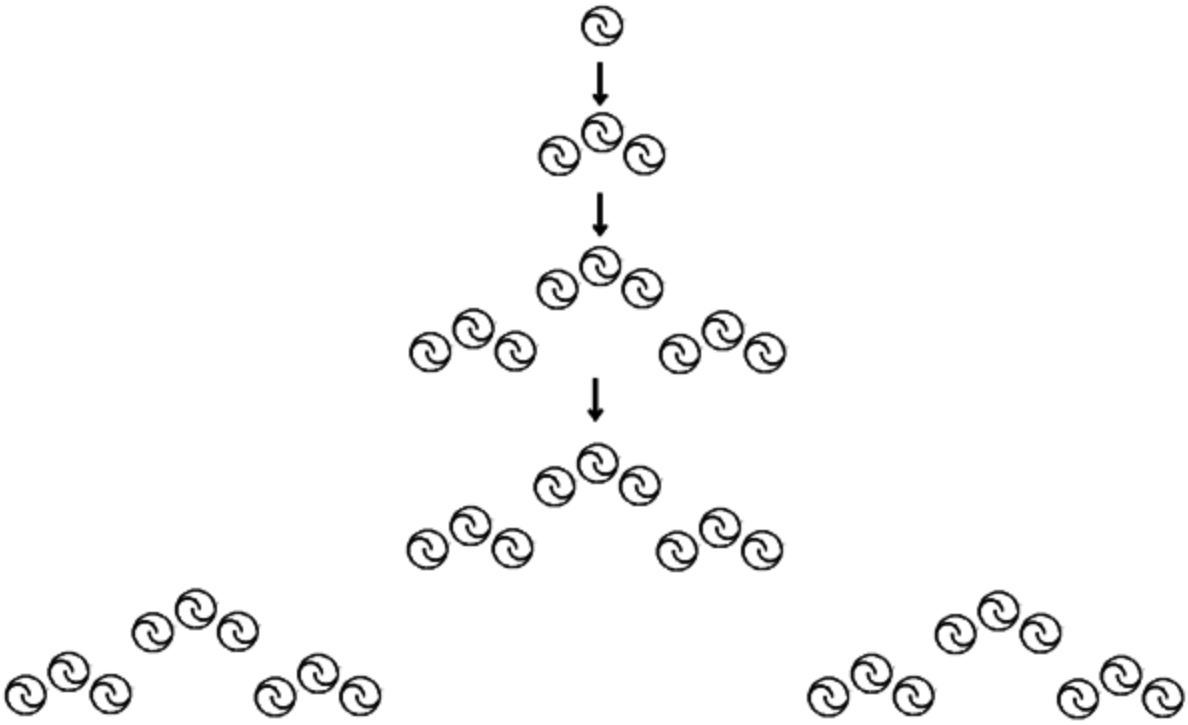

Figure 5.16: Power Scaling

5.5 Non-Patterned Six Co-Rotating Turbine Farms

For a clarification of the advantages of the patterned farms, a non-patterned six turbine farm is simulated. The farm consists of two rows of the co-rotating three turbine cluster, two cases are simulated case (NP-1) and case (NP-2). In order to avoid being in the wake of the first row, the second row is placed staggered to the first row such that in case (NP-1) the two turbines (2) and (4) are the same as case (B) for two oblique turbines as shown in figure 5.17. For case (NP-2) the two turbines (3) and (4) are the same as case (A) for two oblique turbines as shown in figure 5.18. The power coefficients of the six turbines are calculated for each case at different center distances between the up-stream turbines of each row. Figures 5.19 and figure 5.20 show the

power coefficients for the two cases (NP-1) and (NP-2). In case (NP-1), the power coefficient of rotor (1) is the lowest of all rotors, the rotation of the advancing blade of rotor (1) was affected by the reverse rotation of the returning blade of rotor (4). Noticing the strength of the advanced bucket tip vortices for rotors (4) and (5) from the velocity contours explains their high efficiency compared to other rotors as shown in figure 5.19. In case (NP-2), the power coefficient of rotor (3) is the lowest of all rotors, the rotation of the advancing blade of rotor (1) was affected by the reverse rotation of the returning blade of rotor (4). Noticing the strength of the advanced bucket tip vortices for rotors (2), (4) and (5) from the velocity contours explains their high efficiency compared to other rotors as shown in figure 5.20.

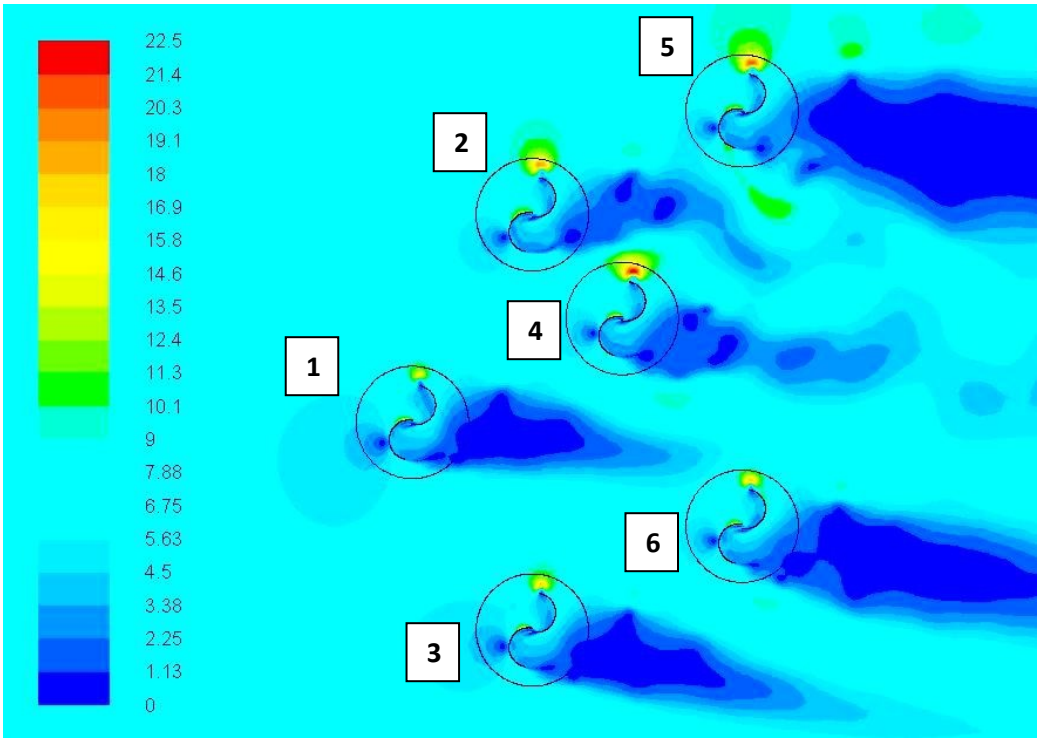

Figure 5.17: Velocity Contours for Non-Patterned six Turbine Farm Case (NP-1)

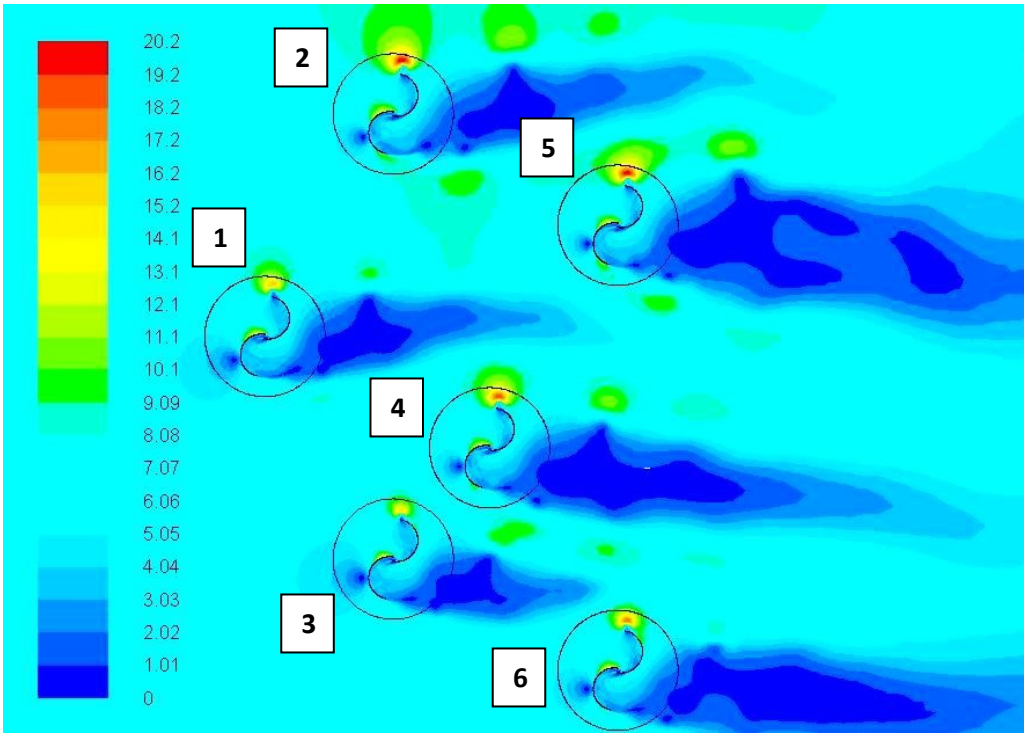

Figure 5.18: Velocity Contours for Non-Patterned six Turbine Farm Case (NP-2)

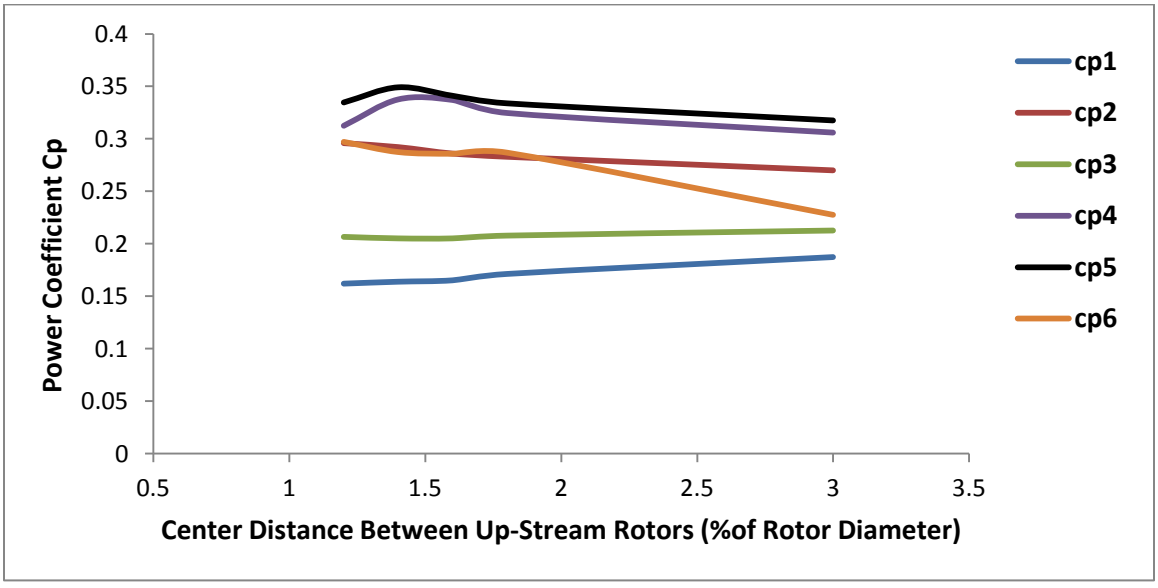

Figure 5.19: Power Coefficient of Six Non-Patterned Savonius Turbines Case (NP-1)

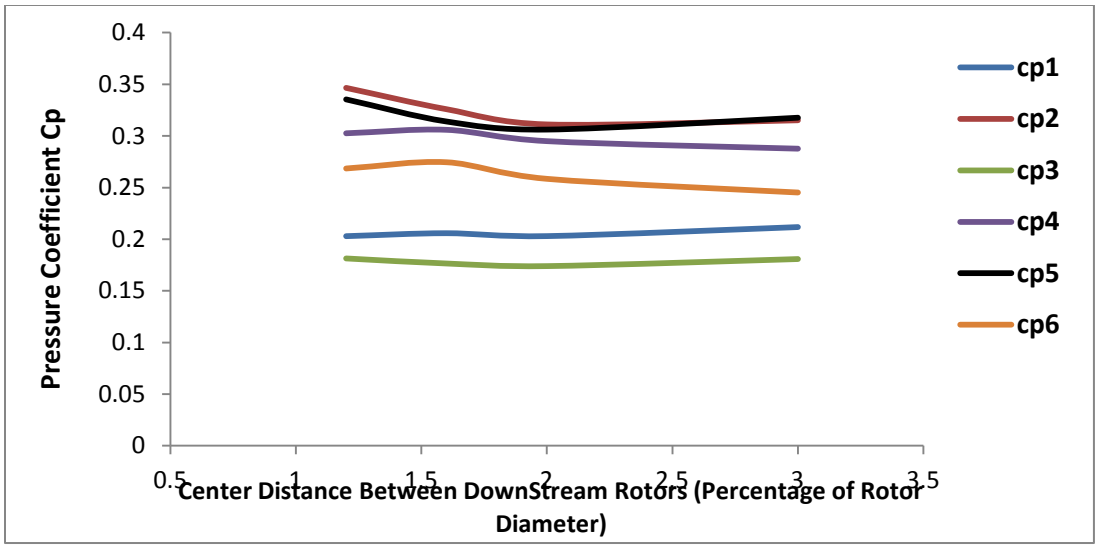

Figure 5.20: Power Coefficient of Six Non-Patterned Savonius Turbines Case (NP-2)

Figure 5.21 shows a comparison between the average power coefficients for the six turbines farms in both case against the power coefficient of a single turbine, the results show that the efficiency of case almost close at different distances. The performance of the upstream cluster is completely different from that of the upstream cluster. Using such farms of no-patterned performance needs a solution of the whole farm for predating its performance. This clarifies how a patterned farm will save calculation hours and man power.

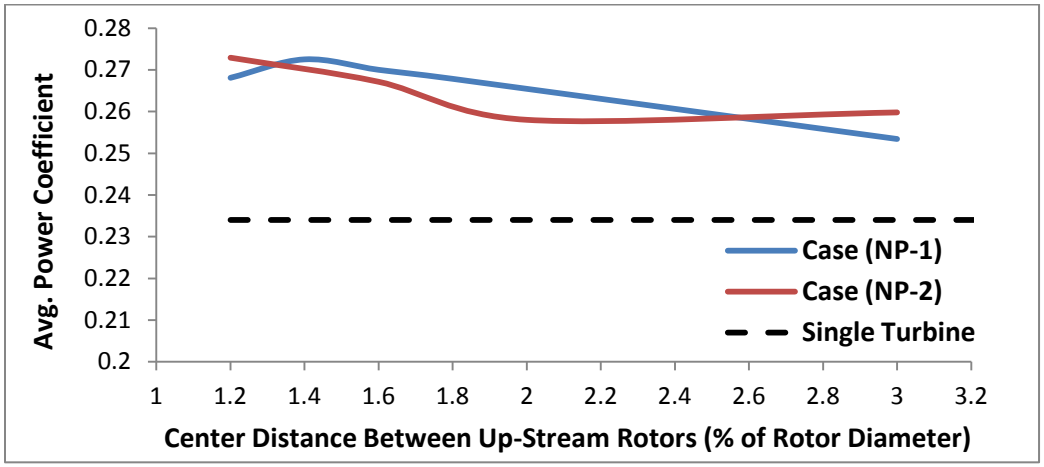

Figure 5.21: Average Power Coefficient of Six Non-Patterned Savonius Turbines for Case (NP-1) and Case (NP-2

5.6 Summary

Savonius wind turbine farms are developed using an efficient three co-rotating triangular turbine cluster as the building unit, the farm topology is a geometric progression of the three turbine cluster by factor 3. The developed farms are patterned and have the same power coefficient enhancement ratios of the three turbine cluster. The pattern and enhanced power coefficient are confirmed by numerical solutions of farms that consist of nine and twenty-seven turbines. The power ratio between individual turbines is 1:1.2:1. The same power ratio is achieved by the nine and twenty seven turbine farms. This power ratio is used to predict the performance of larger farms with the same topology to save processing time and man power. The power density of the developed farms at $\lambda=1$ are higher than that of farms having the same number of isolated turbines. The power density of the nine turbine farm is about 7 times a nine isolated turbine farm, and the power density of the twenty-seven turbine farm is 4 times a twenty-seven isolated turbine farm.

Chapter 6

Numerical Model Validation for Single Darrieus Wind Turbine

In chapter (5), we developed a novel efficient and patterned Savonius (VAWT) farm that consists of multiples of an efficient triangular three Savonius co-rotating turbine clusters. Researches has showed that Darrieus vertical axis wind turbines are also subjected to enhancement in their efficiencies when placed at close distances. In order to confirm the improved performance for other types of VAWTs and develop similar patterned wind farms, clusters of Darrieus VAWTs are numerically studied. In this chapter, the performance of a single Savonius VAWT is numerically investigated, two and three dimensional simulation models are performed and the numerical results are compared with the available experimental data in reference [50] in order to validate the numerical model.

6.1. Two Dimensional Numerical Simulation

The two dimensional CFD model is created using ANSYS 14.5 workbench. The CAD model is drawn using ANSYS design modeler and the mesh is generated using ANSYS meshing. The finite volume Fluent code is used to solve the unsteady Reynolds averaged Navier-Stokes equations using finite volume method [50, 51]. The geometry used in this study is a three blade Darrieus VAWT with Straight-blades founded in scientific literature [50]. The geometric features are listed in the table 6.1. The spokes that connect the turbine blades with the rotating shaft are connected to each blade at the center of pressure of the airfoil (0.25C). Figure 6.1 shows the velocity triangles at different azimuth positions of the turbine rotor blade and the force analysis on the blade, the Darrieus turbine blade is subjected to different relative velocity vectors at different azimuth positions as it rotates, this results in a fluctuation in the values of the generated lift and drag forces and subsequently a fluctuation in the generated torque. Figure 6.2 shows that on its rotation each turbine blade produces, and interferes with a vortex system that it generates or other blades do, two counter rotating vortices are generated from both the leading and the trailing edges of the blades and shed during rotation, this is why the blade aerodynamics involves highly unsteady flow fields [52]. In order to figure out how the unsteadiness in the flow field around the Darrieus turbine blade affects its performance a two dimensional quasi-steady study is done for a single blade and the numerical results are compared to the unsteady performance of a single blade.

Table 6.1: Turbine Geometrical Features

Blade Airfoil	NACA 0021
Number of Blades	3
Turbine Rotor Diameter (mm)	1030
Turbine Height (mm)	1414
Blade Chord Length (mm)	85.8

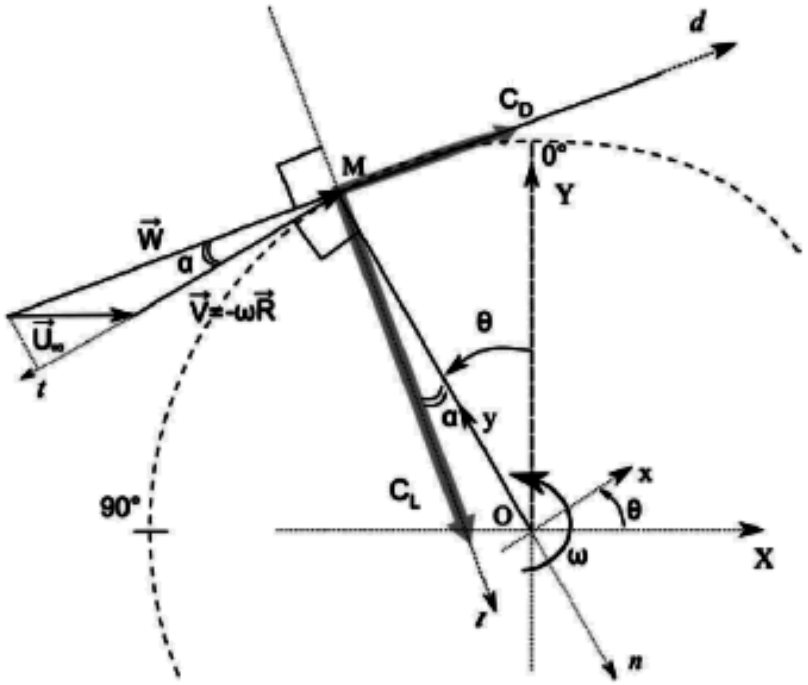

Figure 6.1: Darrieus VAWT Rotor Blades, Velocity Triangles and Force Analysis

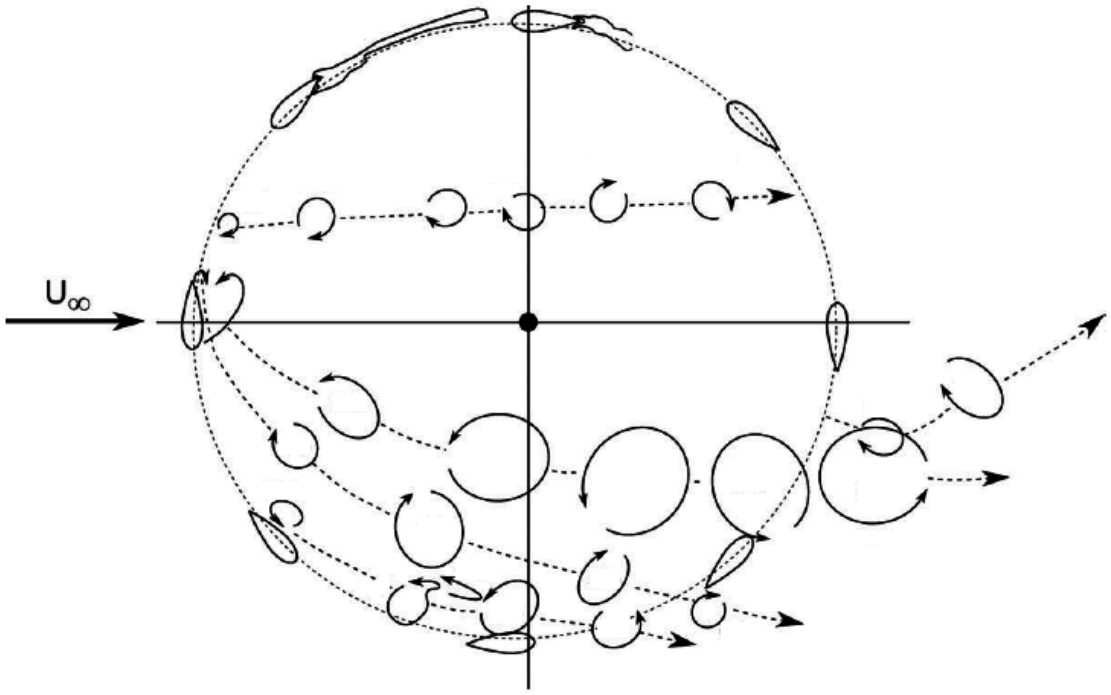

Figure 6.2: Vortex System of a Darrieus VAWT Rotor Blades [52]

6.1.1. Quasi - steady Simulation

A two dimensional quasi-steady study is done for a single blade. The relative velocity and angle of attack of are calculated graphically at different azimuth angles, similar angles of attack are observed at the corresponding positions in the first and second half of the turbine rotation but with opposite signs as shown in figure 6.3. Plots of the lift and drag curves for the blade airfoil are shown in figure 6.4 and figure 6.5, due to the change in the relative velocity magnitude at different azimuth angles, the lift and drag coefficients are computed at different Reynolds numbers at different and angles of attack using the two solvers Fluent 14.5 and Xfoil, a close agreement is observed between the two results. The lift and drag forces are calculated at different positions and the torque generated from both forces is calculated. The torque of the turbine is a resultant of the positive torque generated by the lift forces and the negative torque generated by the drag force. Figure 6.6 shows the quasi-unsteady torque generated by a single turbine blade in one complete cycle, the results are symmetric for the first and second half cycle. The blade has two peak values for the torque along the azimuth, and the average torque generated by a single blade is about 2 N.m.

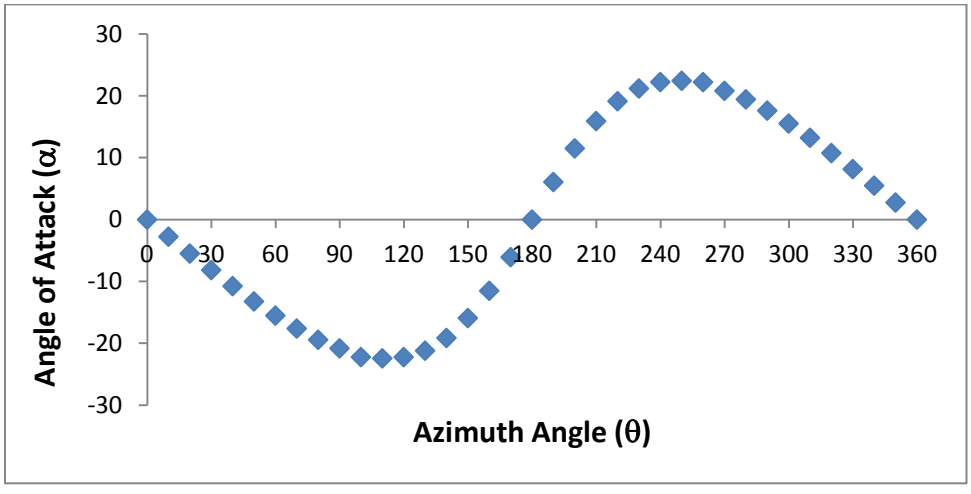

Figure 6.3: Angle of Attack of the Turbine Blade Airfoil at Different Azimuth Angles

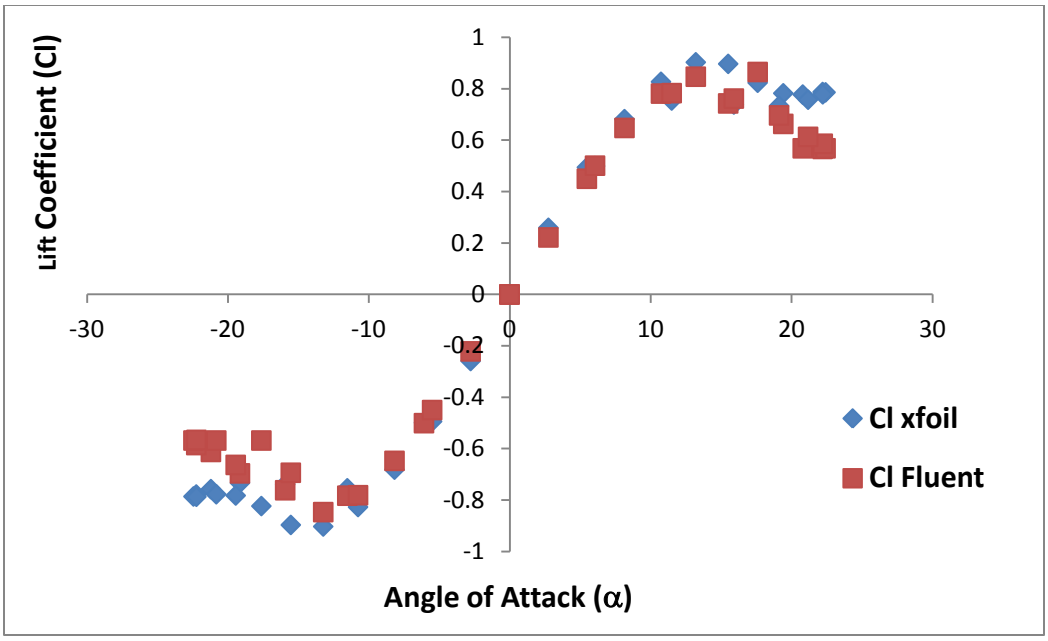

Figure 6.4: Lift Curve, Numerical Results of Fluent Vs Xfoil

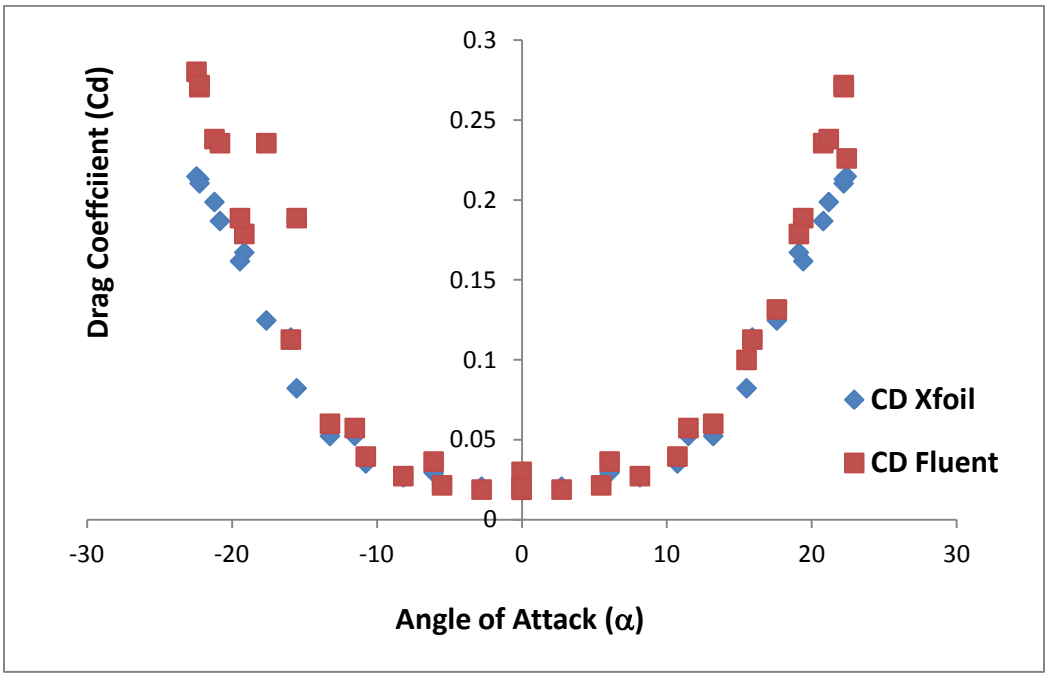

Figure 6.5: Drag Curve, Numerical Results of Fluent Vs Xfoil

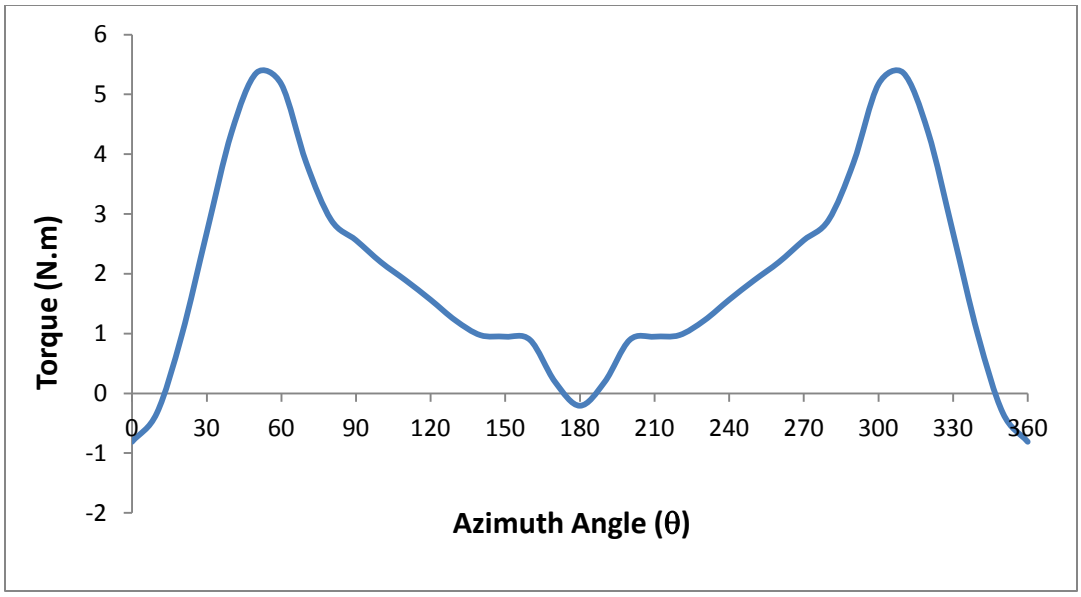

Figure 6.6: Torque at Different Azimuth Angles (Quasi-steady Simulation)

6.1.2. Unsteady Simulation

(i) Computational Domain

Different domains are tested for different speeds in order to obtain the appropriate size of the computational domain shown in figure 6.7, the best compromise is found where the upstream, upper and lower boundaries are at a distance of 15D from the turbine center, while the downstream boundary is at 30D from it avoiding b this way the wall effects [50]. The sliding mesh method is used, the domain is divided into 3 sub-domains: A rotating region that has a torus shape including the turbine blades, a fixed zone that extends from the outer interface of the rotating region to the boundaries of the domain and another fixed zone that extends from the inner interface of the rotating region to the shaft of the turbine. The outer diameter of the rotating region is 1.2D and its inner diameter is 0.8D. The downstream, upper and lower boundaries are

defined with velocity inlet boundary condition (BC) (x-component=9m/sec), and the upstream boundary is defines as pressure outlet BC.

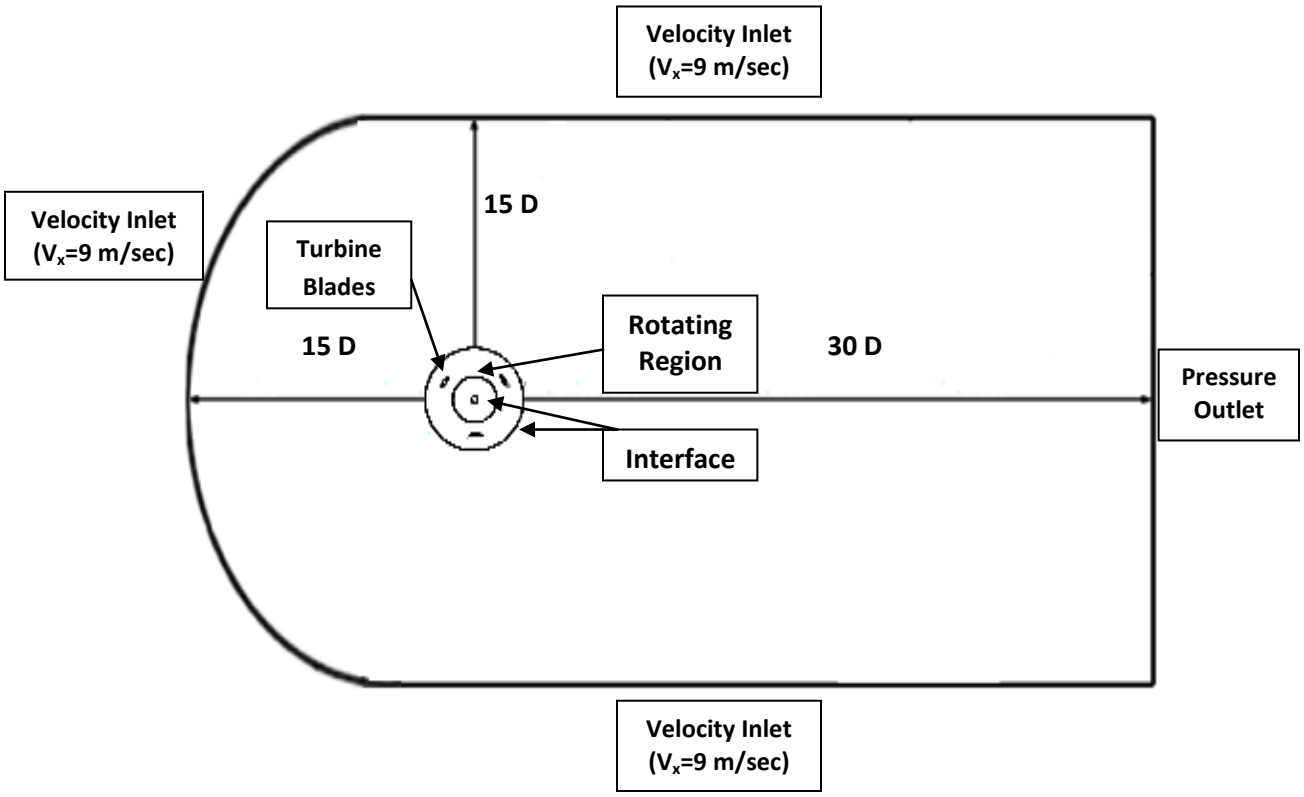

Figure 6.7: Computational Domain for Single Darrieus Turbine

(ii) Grid Generation

The sliding mesh model is used to capture the unsteady flow parameters generated due to the rotation of the turbine blades. A non conformal mesh with unstructured triangular cells is created using ANSYS meshing. The grid structure is shown in figure 6.8 (a) and a close view of the grid in the vicinity of the leading edge of the rotor blade is shown in figure 6.8 (b). An inflation tool with 10 levels of quadrilateral cells is imposed on the airfoils surfaces to account for the

boundary layer with a maximum thickness of 1 mm and growth rate of 1.1. Five grid refinements levels with mesh size ranging from 47,591 up to 450,705 cells are tested, the tests are performed at maximum wind speed and maximum rotational speed [53] in order to obtain y+ < 1 as required by the transition SST turbulence model [37,54]. A mesh of 173,768 cells is found to be adequate as the relative variation in the output quantities are below $1x10^{-3}$ above this grid level as shown in table 6.2.

Table 6.2: Grid Refinement Levels for Single Darrieus Turbine Simulation

Grid level	Number of cells	Cm	Cp
1	47,591	0.059	0.166
2	81,034	0.093	0.259
3	173,768	0.129	0.362
4	235,451	0.131	0.367
5	492,605	0.129	0.361

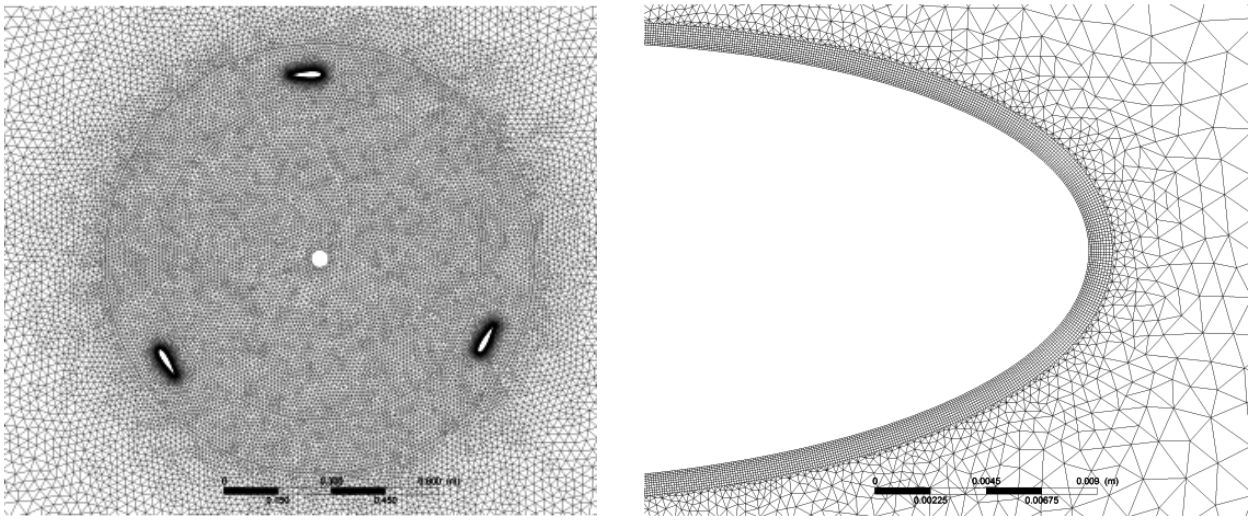

a **b**

Figure 6.8: Grid Structure near the Rotor

(iii) Solver Settings and Turbulence Model

The unsteady Reynolds averaged Navier-Stokes equations are solved using SIMPLE algorithm (Semi-Implicit Method) with a second order spatial discretization for all pressure, momentum, and turbulence equations and a Least Squares Cell Based algorithm is used for gradients [13]. In order to capture the laminar and transitional boundary layers correctly, the transition SST turbulence model used in chapter 2 [40] is adopted. Steady flow simulations are obtained initially to set up the flow domain to reasonable parametric values, then unsteady flow simulations are obtained using the sliding mesh model (SMM) [54]. A time step size corresponding to a turbine rotation of 1.0 degree is used for the time dependent solution [34, 41, and 42]. A drop of at least 3 orders of magnitude in each time step as well as a minimum of 20 iterations per time step is considered as convergence criteria for the time dependent solution. The torque (T) is calculated about the turbine center from the pressure and viscous forces on the turbine blades. The torque coefficient (Cm) is calculated at each time step and averaged after periodic convergence [34], then the power coefficient (Cp).

(iv) Single Darrieus Turbine Unsteady Simulation Results and Validation

Single Blade Results:

The torque of a single blade is plotted at different azimuth angles as shown in figure 6.9, the results shows a great discrepancy between the unsteady and the quasi-unsteady results shown above. The discrepancy in the first half of rotation can be explained as the result of the change in the axial velocity due to stream lines expansion and the discrepancy in the second half is due to the same reason in addition to the interference with the vortex shed from the upstream blades.

Also the quasi-steady solution assumes that the flow velocities normal to the free-stream direction are zero which is not true. The average torque generated by a single blade is found to be 3 N.m which is higher than the value of the quasi-steady solution.

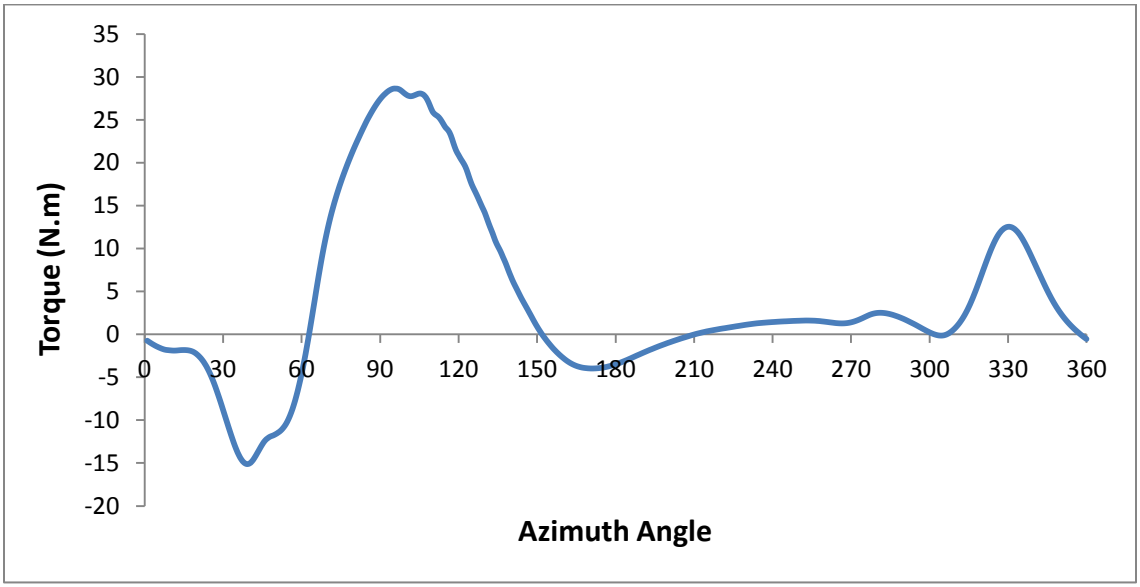

Figure 6.9: Unsteady Torque Generated by a Single Blade of the Darrieus Turbine

Turbine Results:

The power coefficient of the single Darrieus turbine calculated at different tip speed ratios (λ) using time dependent solution for the rotating turbine is plotted in figure 6.10, the results show that the fully turbulent k-omega SST model under predicts the values of the power coefficient and that the transition SST turbulence model has the closest results to the experimental data [50], similar findings are reported in reference [51]. The maximum power coefficient for the single turbine is found to be 0.36 corresponding to λ equal to 2.8. Figure 6.11 shows the vorticity vector at different azimuth angles from 0^o to 120^o, the same structure is repeated every 120^o of the turbine rotation. Each turbine blade generates and interferes with a vortex system generated

by itself and by other blades. The blades in the second half of the turbine rotation interact with the shedding of the turbine shaft. The vorticity vector plots show close results to that introduced in reference [52]. Figure 6.12 shows the mean velocity contours around the Darrieus turbine blades, two regions of high velocity magnitudes are induced on both sides downstream the turbine. The rotating region could not be averaged due to the rotation of the blades which occupies different space in the rotating domain at each time step.

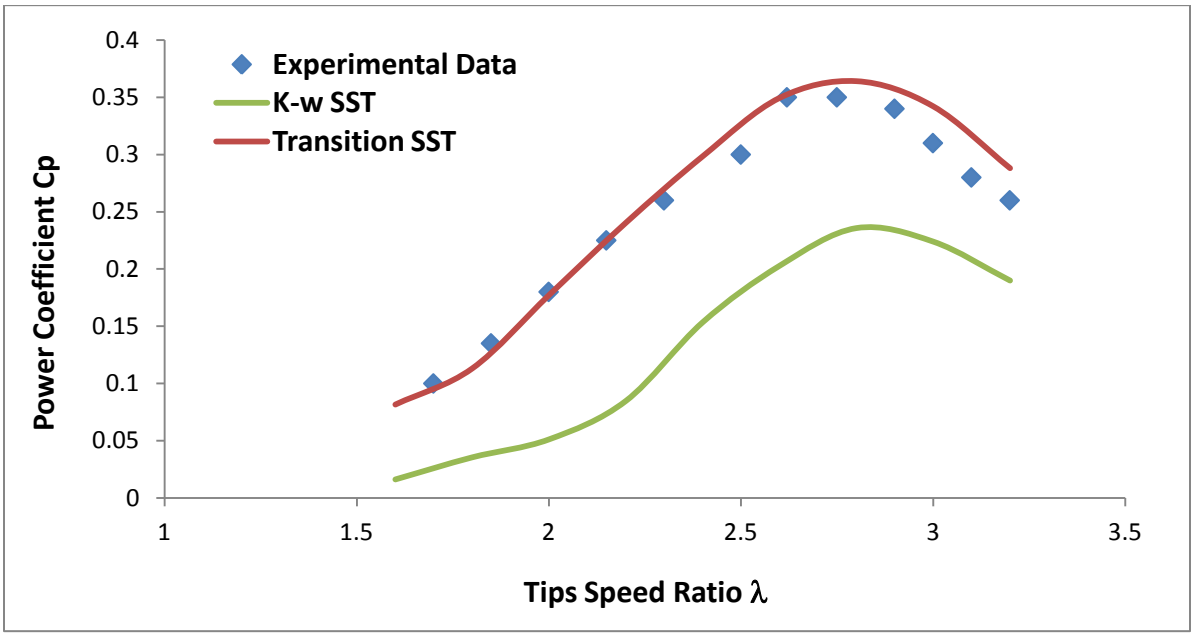

Figure 6.10: Cp at Different Tip Speed Ratios, Numerical Results Vs Experimental data [50]

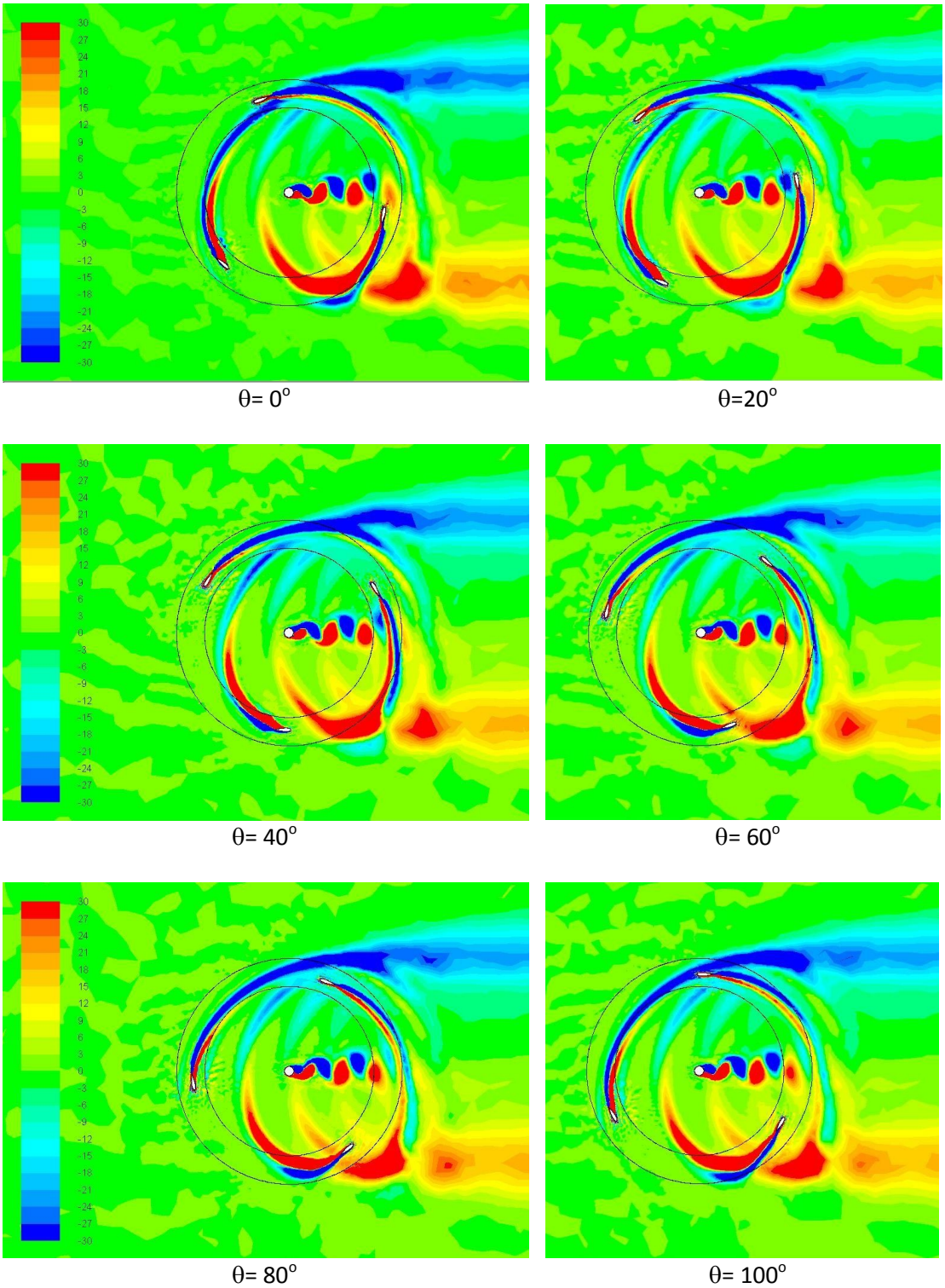

Figure 6.11: Vorticity Magnitude at Different Azimuth Angles

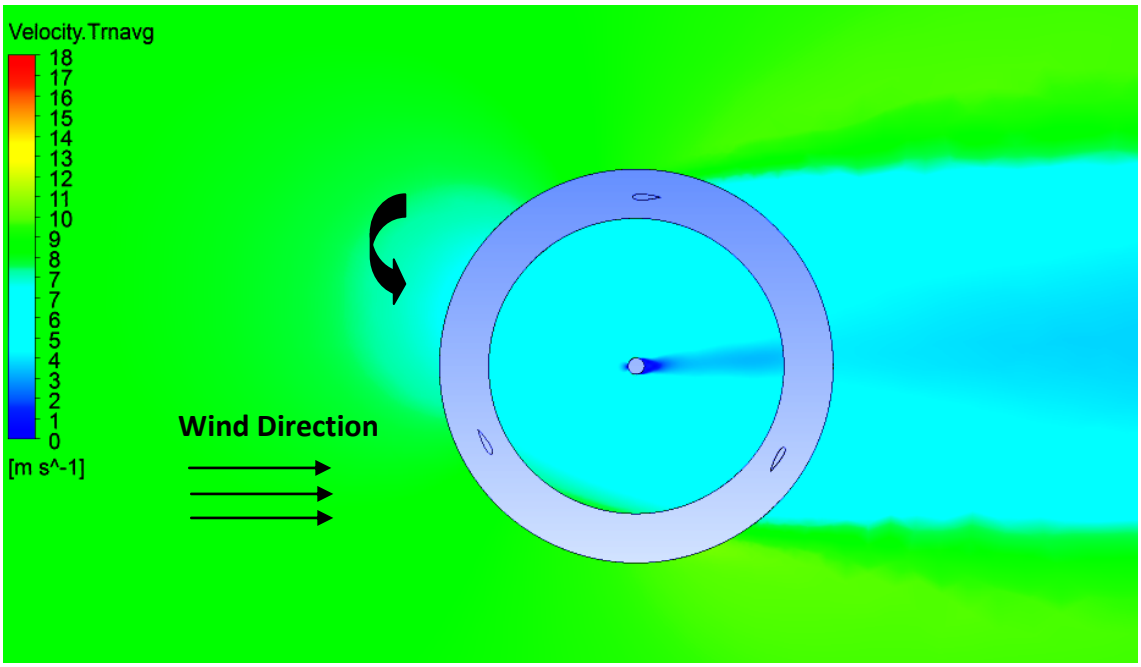

Figure 6.12: Velocity Contours around the Darrieus Turbine Blades

Figure 6.13 shows the instantaneous stream function contours around the Darrieus turbine, the streamlines expand as they pass through the turbine disk due to the reduction in the wind speed . Figure 6.14 shows the mean static pressure around the Darrieus turbine, the large low pressure spot indicates how the flow passing across the rotor plane experiences a pressure drop. The flow slows down downstream of the rotor and causes the pressure to recover back to atmospheric pressure.

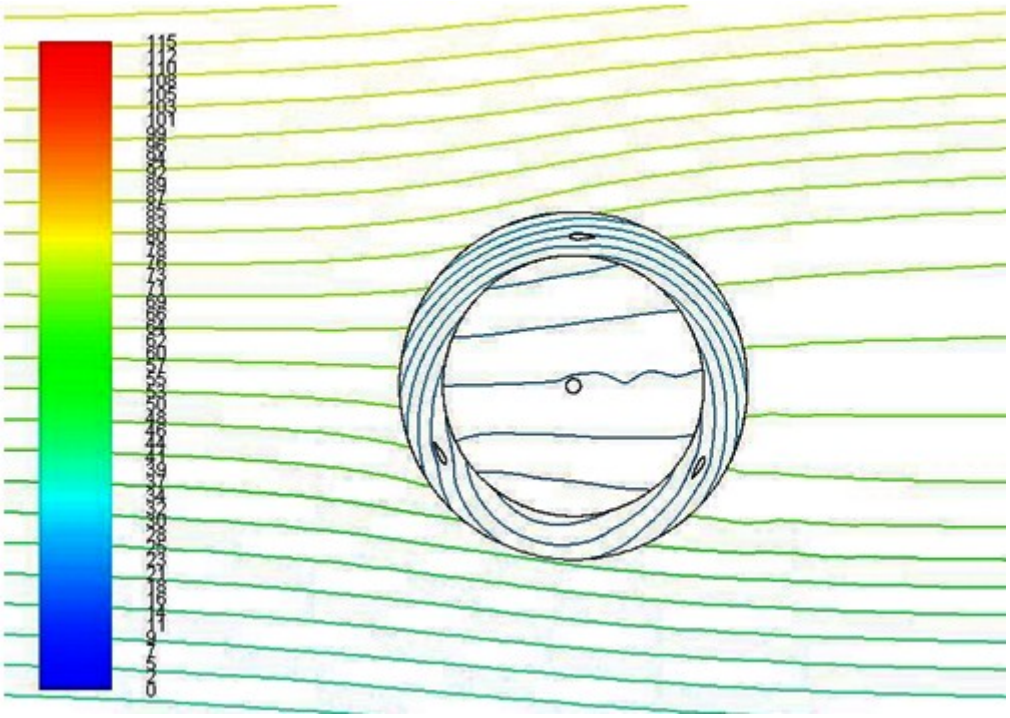

Figure 6.13: Stream Function at zero Azimuth Angle for the Darrieus Turbine

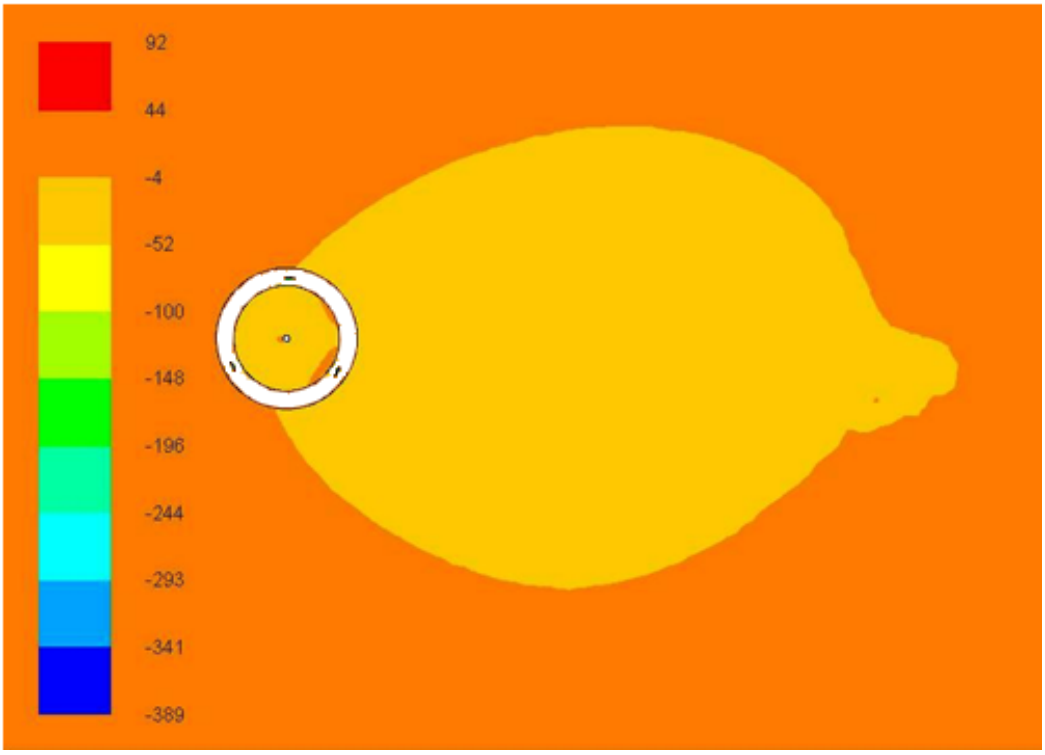

Figure 6.14: Mean Static Pressure Contours around the Darrieus Turbine

6.2. Three Dimensional Numerical Simulation

In this section, a 3D simulation of the single rotor is performed at different tip speed ratios, the results are compared to 2D simulation results and to the experimental data [50]. The 3D CAD model of the Savonius rotor shown in figure 6.15 is built using SOLIDWORKS CAD modeler. The shaft and spokes are removed for simplicity and reduction of the number of cells in the grid.

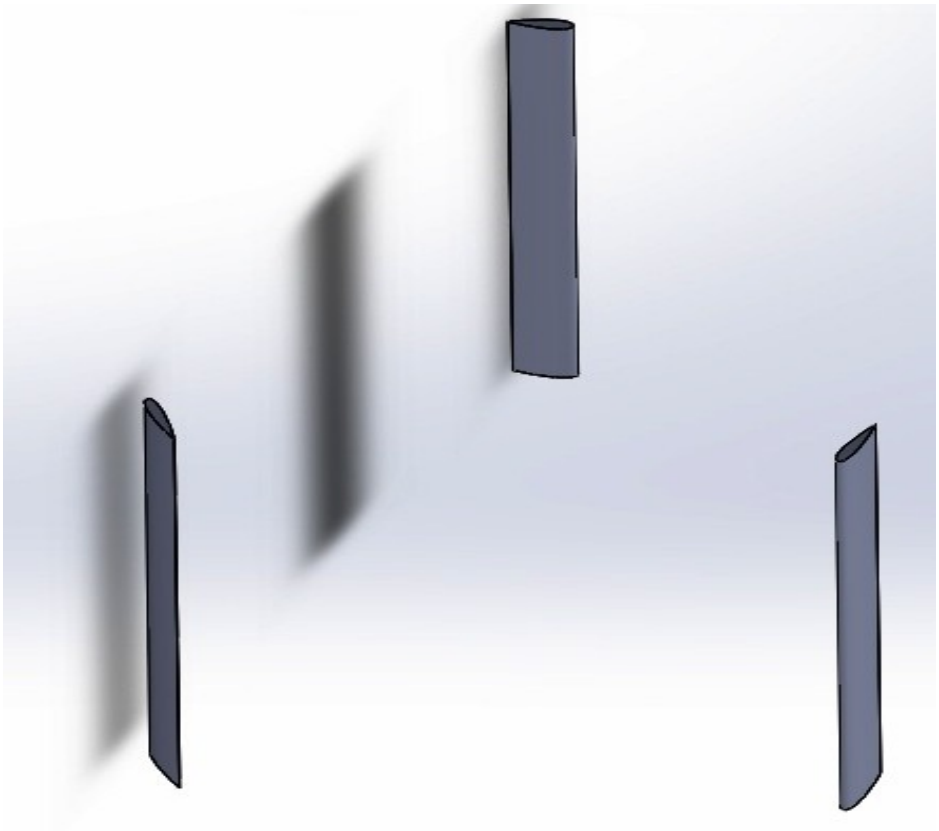

Figure 6.15: Three Blade Darrieus Wind Turbine 3D CAD Model

6.2.1 Three Dimensional Computational Domain

The 3D computational domain is shown in figure 6.16, the same domain used with the single Savonius turbine is repeated in this section. The sliding mesh method is used and the

computational domain consists a rotating and stationary sub-domains. The surface between the two sub-domains is defined as an interface. Velocity inlet boundary condition of 9 m/sec with the x-velocity component is defined at the upstream and side boundaries. The downstream boundary is defined as a pressure outlet.

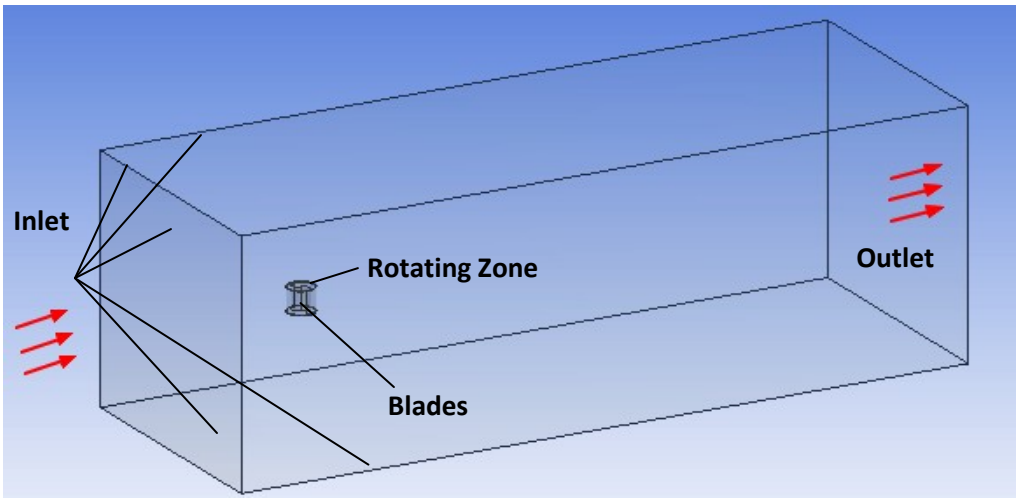

Figure 6.16: Three dimensional Computational Domain

6.2.2 Three Dimensional Grid Generation

The unsteady three dimensional flow is solved using the sliding mesh model, the computational domain is discretized using tetrahedral elements and is created from a rotating zone around the blade and a fixed zones. The grid structure is shown in figure 6.17 (a) and a magnified view of the grid near the rotor is shown in figure 6.17 (b), a refined grid with inflation is imposed in the boundary layer of the blades airfoils with 20 levels of hexahedral cells so that $y+ < 1$ as required by turbulence models [13,14]. A grid independence study is performed using three grid levels shown in table 6.3. Figure 6.18 shows the torque coefficient of the Darrieus rotor calculated at different azimuth angles using the three grid levels, close values are observed for levels 2 and 3. Level 2 with 2,588,998 cells is found to be adequate after periodic convergence.

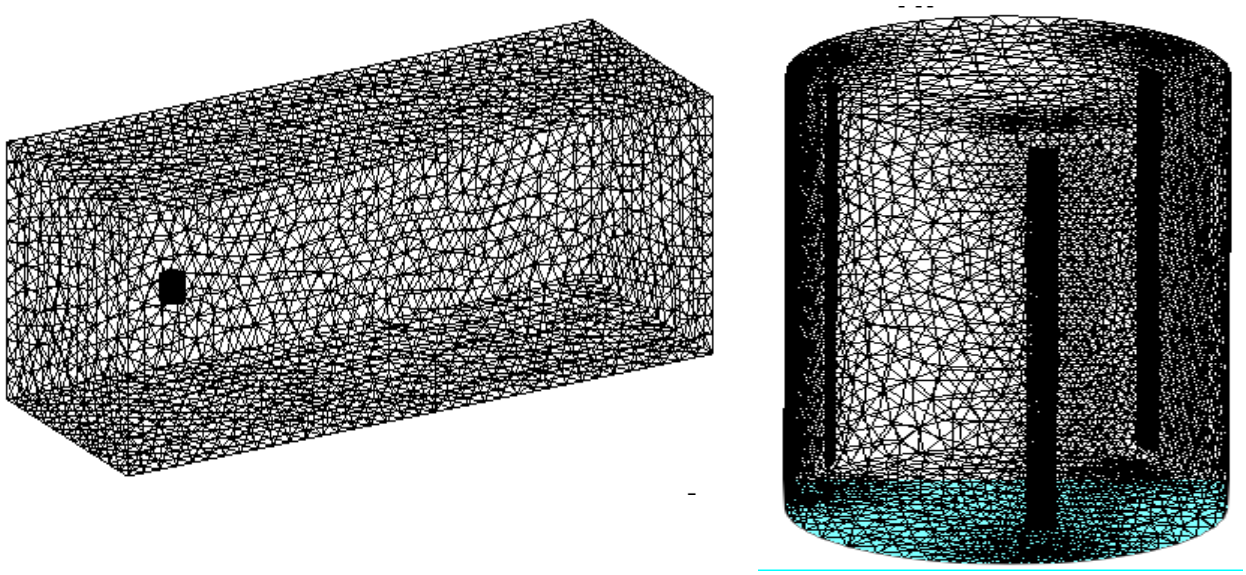

(a) (b)

Figure 6.17: Three Dimensional Grid Structure

Table 6.3: Grid Refinement Levels for Single Darrieus Turbine 3D Simulation

Grid Level	No. of Cells	Cm	Cp
1	1,968,927	0.1807	0.506
2	2,588,998	0.1125	0.315
3	5,362,450	0.1121	0.314

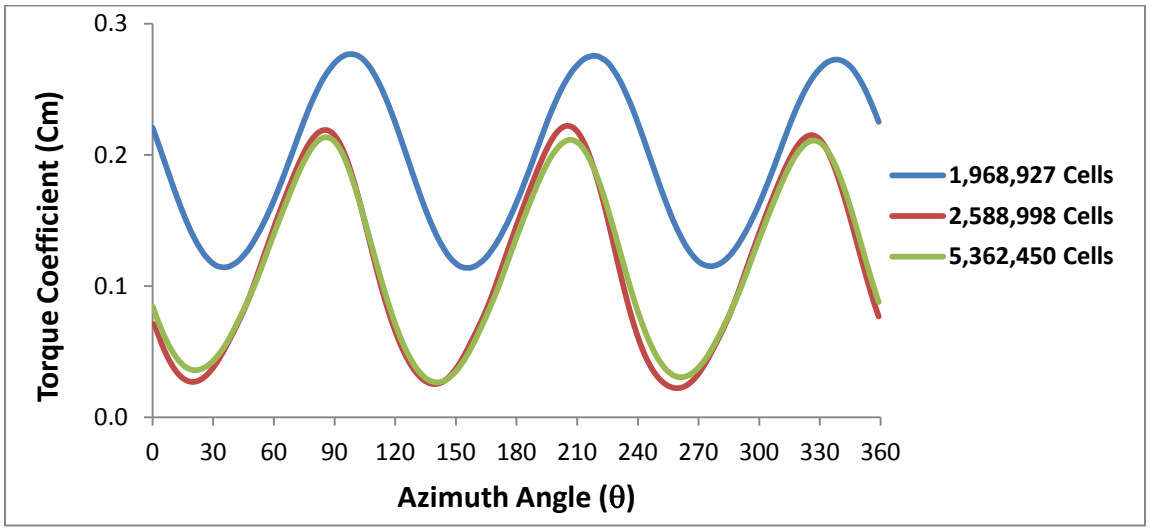

Figure 6.18: Torque coefficient at Different Azimuth Angles for Three Grid Levels

6.2.3 Three Dimensional Solver Settings and Turbulence Model

The same boundary conditions and turbulence parameters used in the 2D solution are used in the 3D solution. The unsteady three-dimensional calculations are performed using ANSYS Fluent 14.5 solver. The SST transition turbulence model is used to solve a dynamic simulation, A time step corresponding to one degree rotation of the rotor is used and the average power coefficient is calculated at different tip speed ratios (λ). Figure 6.19 shows the power coefficient of the single Darrieus turbine calculated at different tip speed ratios, the numerical results obtained using the Transition SST turbulence model are close to the experimental data in both two and three dimensional cases. The results also shows that the 2D solution is closer to the experimental data than the 3D solution The discrepancy between the 3D solution and experimental data for high tip speed ratios are explained by the removal of the shaft from the CAD model for simplicity and reduction of the number of cells in the grid.

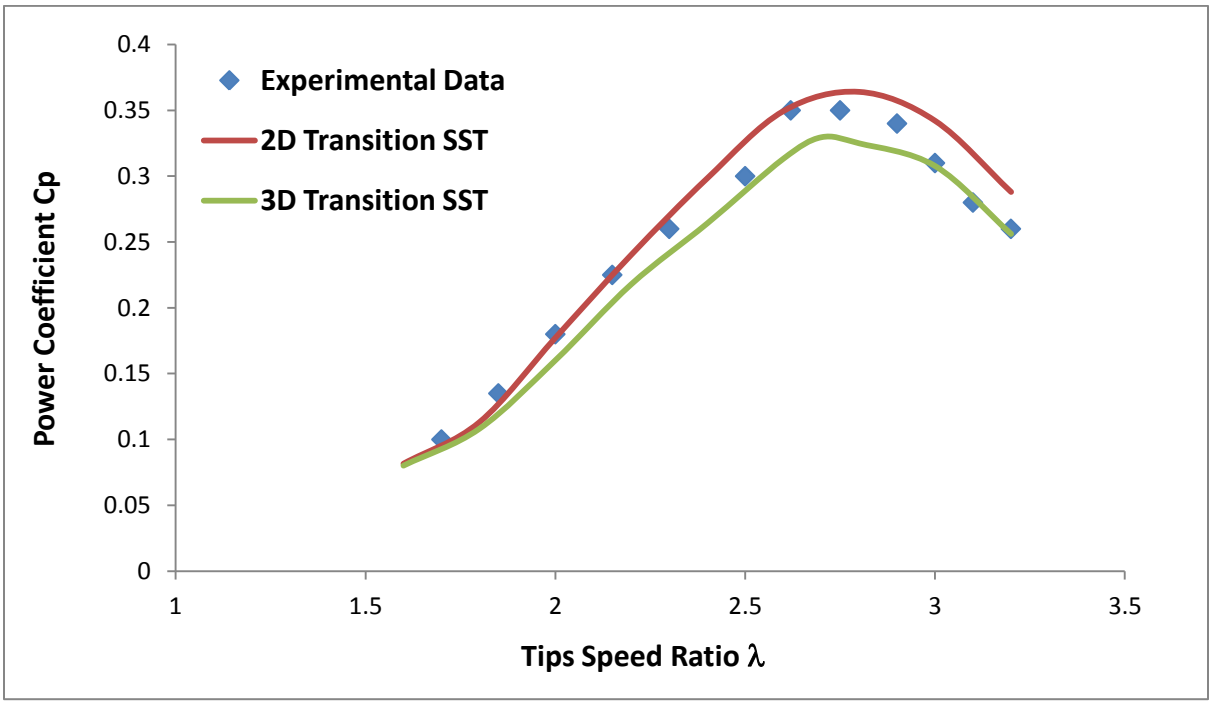

Figure 6.19: Power Coefficient Results for 3D Single Savonius Rotor

The vorticity magnitude contours around the three dimensional Darrieus rotor is shown in figure 6.20, the interactions between blades motion and wake are shown in a mid plane intersection. Each turbine blades generates, and interferes with a vortex system generated by itself and by other blades. This is why the blade aerodynamics involves highly unsteady flow field.

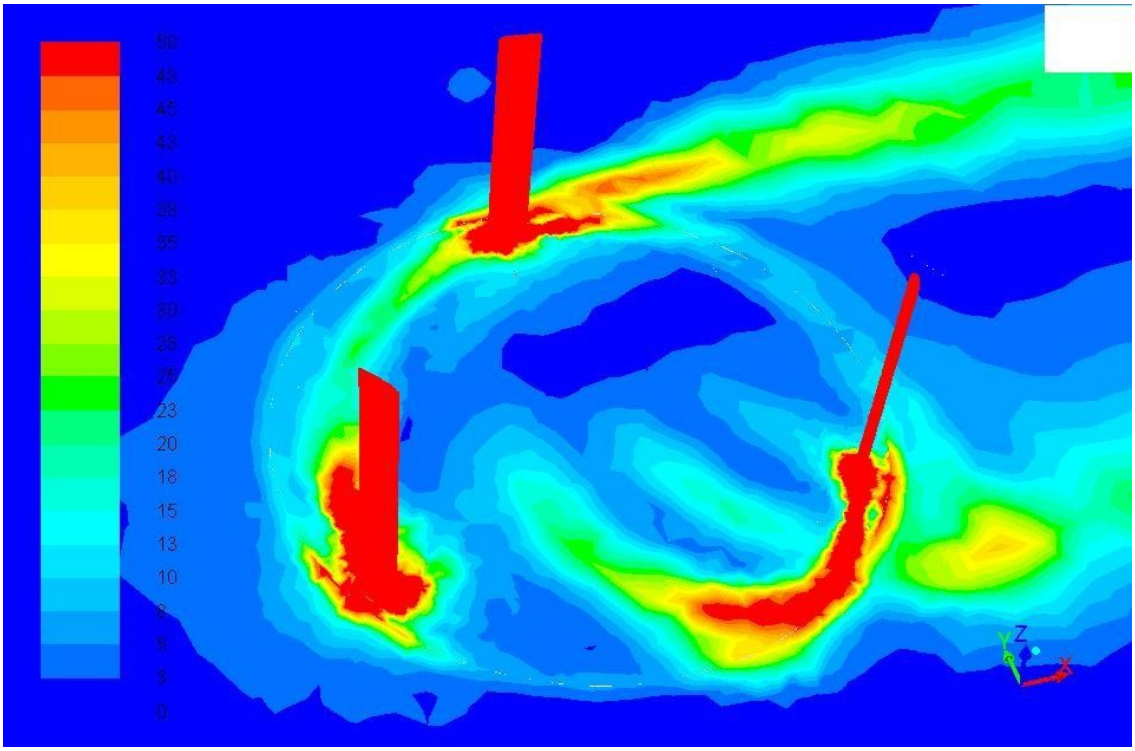

Figure 6.20: Vorticity Magnitude Contours around Three Dimensional Darrieus Turbine

6.3. Physical Insight of the Darrieus Turbine

Different aerodynamic models have been used to predict the performance of Darrieus wind turbines. The vortex models are based on the vorticity equation, the blade element is represented by a lifting line which depend on the azimuth position as shown in figure 6.21, the advantage of this method is that the pressure does not appear in the vorticity equation [55].

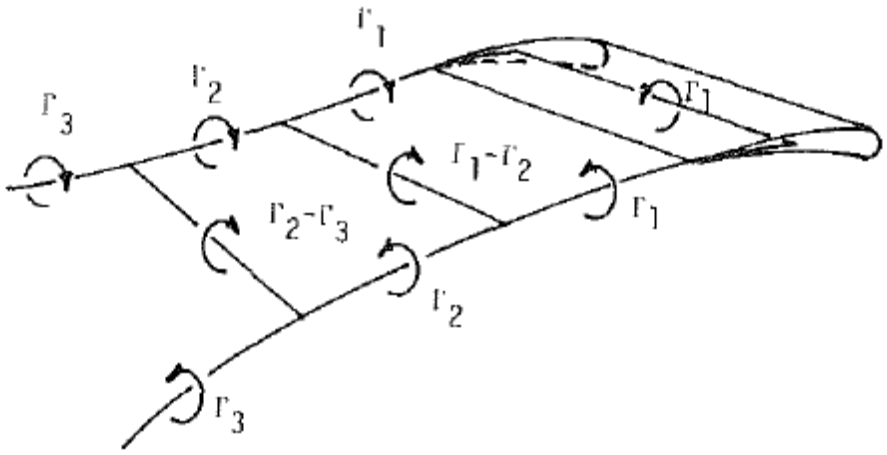

Figure 6.21: Vortex System for a Single Blade Element [56]

In this study the performance of the Darrieus turbine is calculated numerically by solving the unsteady Reynolds averaged Navier-Stokes equations. A preliminary analysis of the mean velocity field around the turbine blades at different tip speed ratios is obtained. This study was not performed on the Savonius turbine as it is a drag device, where there is no lifting airfoils and the vortices are only generated at the two tips of the buckets where they shed downstream without interference with the buckets. For the Darrieus turbine, the mean tangential velocity distribution in the flow field around the turbine rotor is investigated. Data sampling has been performed for a complete cycle and the mean x-velocity component on the positive and negative Y-axis is calculated and plotted as shown in figure 6.22. Also the mean y-velocity component on the positive and negative X-axis is calculated and plotted as shown in figure 6.23, where the turbine center is placed at the origin of the reference co-ordinate system and the blade rotates counter-clockwise.

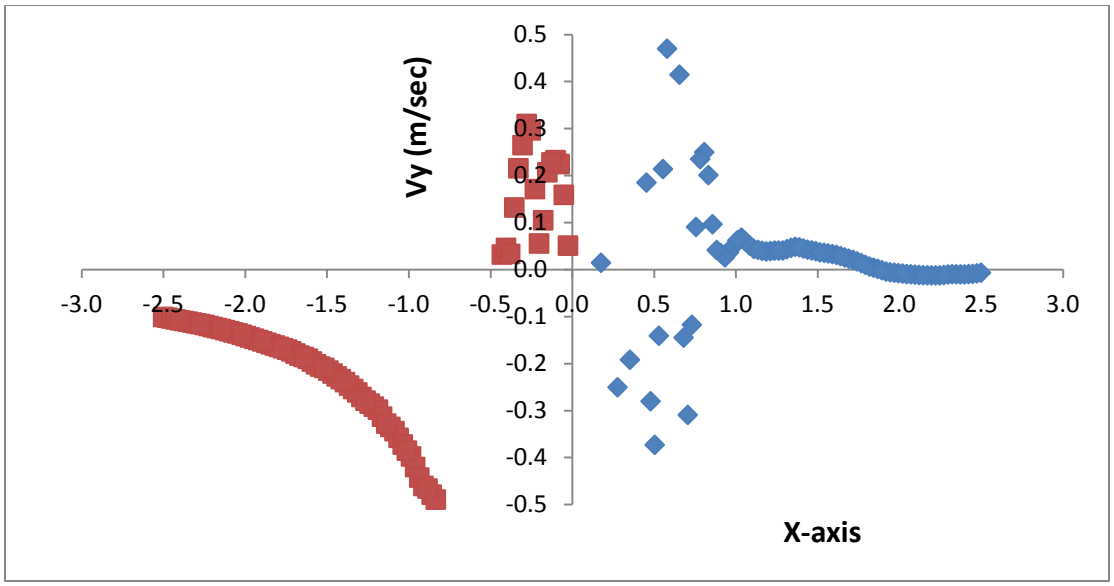

Figure 6.22: Mean y-velocity Component on the X-axis

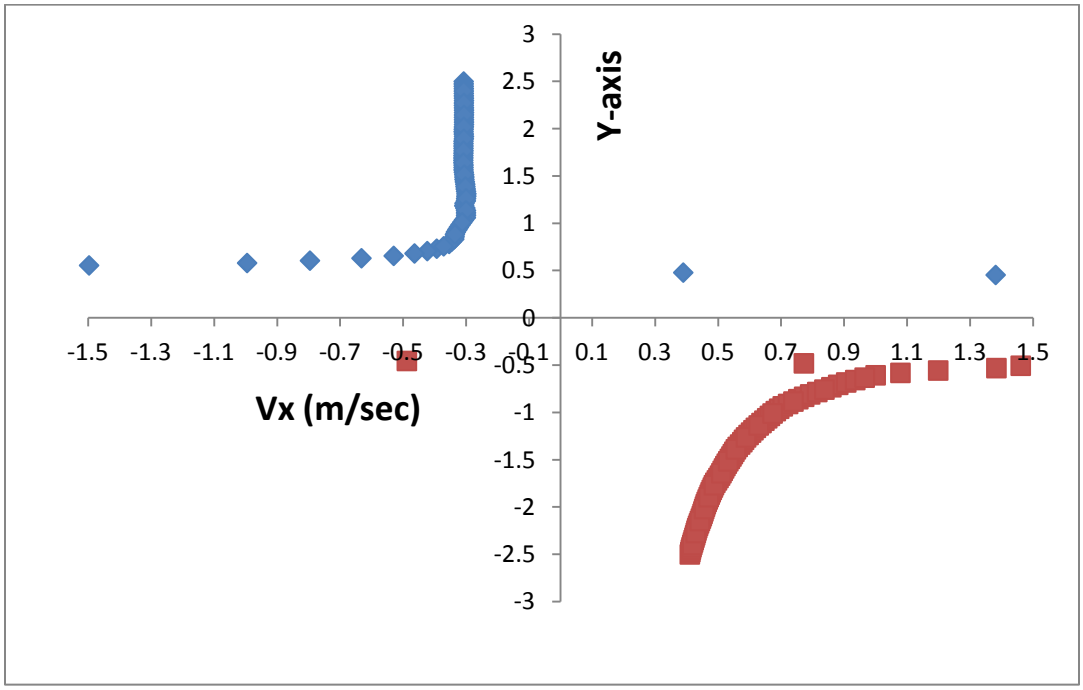

Figure 6.23: Mean x-velocity Component on the Y-axis

The mean x-velocity is a combination of the undisturbed free stream velocity, the velocity induced due to the expansion of the streamlines shown in figure 6.13 and an additional component due to the rotational flow which is generated due to a vortex similar to a non-perfect Rankine vortex, the undisturbed flow component is taken out of the x-velocity plot in figure 6.23.

$$Vx = V_{x-undisturbed} + V_{x-induced} + V_{x-vortex}$$

Figure 6.24 shows the velocity structure of a Rankine vortex, the tangential velocity generated by the vortex is linear inside the vortex core and parabolic outside it computed by:

$$u_\theta(r) = \begin{cases} \Gamma r/(2\pi R^2) & r \leq R, \\ \Gamma/(2\pi r) & r > R. \end{cases}$$

Combining the mean x-velocity on both the positive and negative Y-axes on one plot, they are found to approximately fit a perfect Rankine vortex core having a circulation (Γ) equal to 4.3 for r>0.5 which is the radius of the turbine as shown in figure 6.25. The mean Y-velocity component on the negative x-axis also show a close structure to that of the Rankine vortex core. The mean Y-velocity component on the positive x-axis is disturbed due to the shedding of the turbine shaft. Consistent results have been found at different tip speed ratios. This provides a preliminary description of the Darrieus turbine as a Rankine vortex combined with the free stream. A further analysis will be done in a future work in order to give a detailed and more accurate vortex modeling for the Darrieus turbine avoiding any discrepancy from the perfect vortex which may happen due to the existence of the turbine shaft and its shedding vorticity.

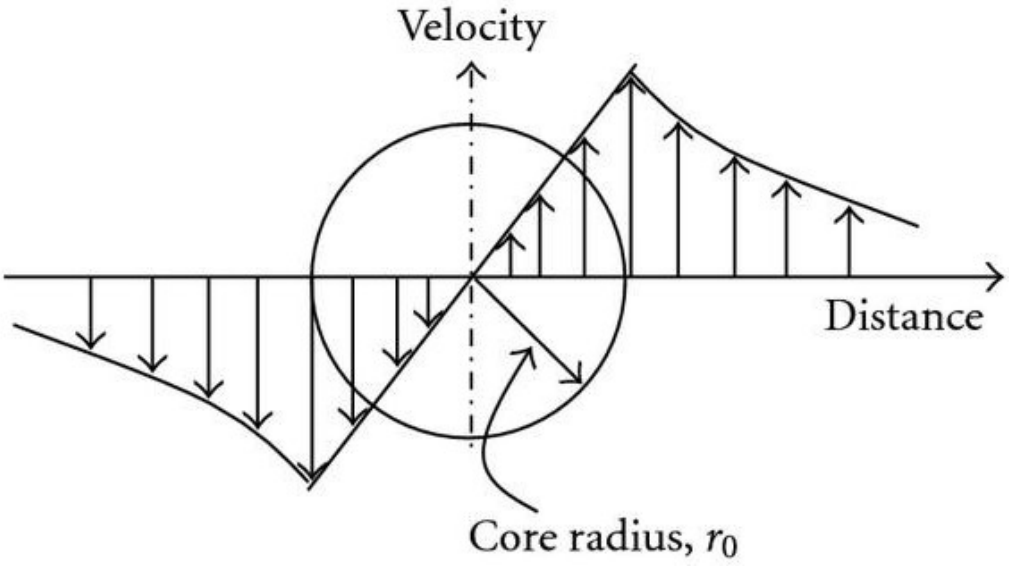

Figure 6.24: Velocity Structure of a Rankine Vortex

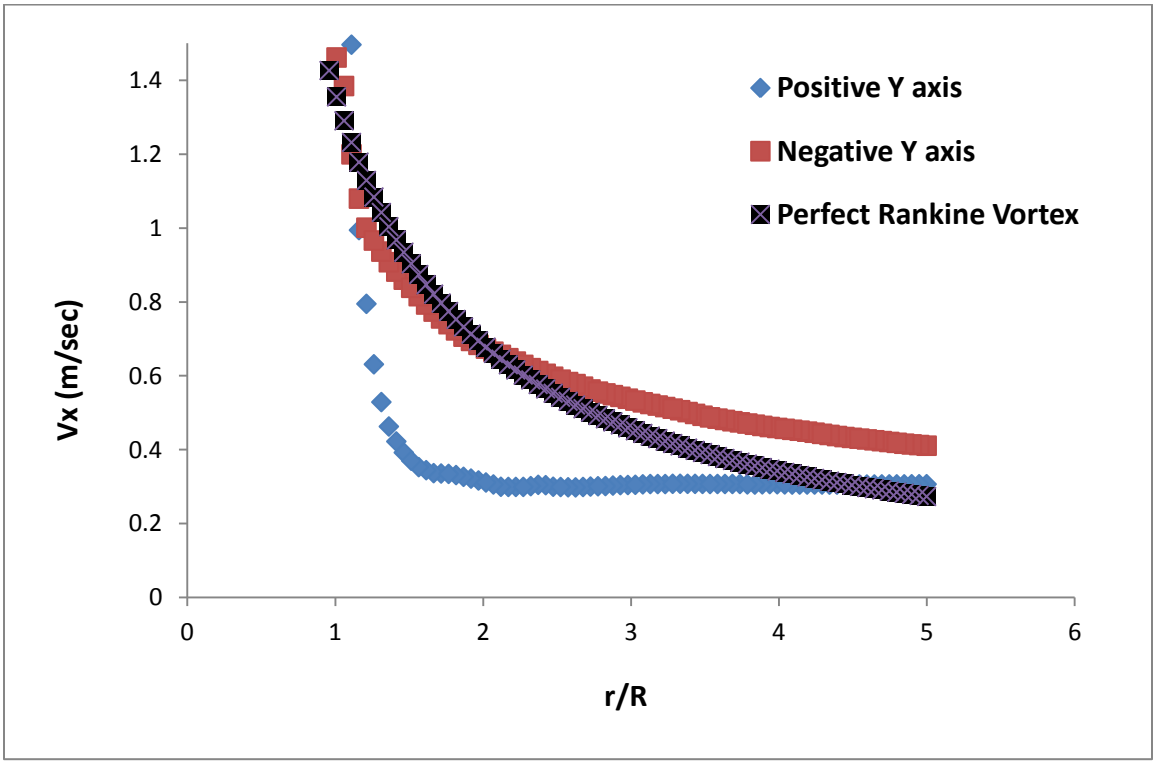

Figure 6.25: Combined Mean x-velocity Distribution on the Y-axis Compared to a Perfect Rankine Vortex Core

6.4. Summery

Numerical solution is performed for a single Darrieus turbine in order to validate the numerical simulation model. Two dimensional and three dimensional simulations are performed. In both cases the computational results shows that the transition SST turbulence model has very close results to the experimental data, the maximum average power coefficient for a single rotor is found to be 0.36 corresponding to λ equal 2.8. A preliminary analysis of the mean velocity field around the turbine blades at different tip speed ratios shows a structure close to that of a Rankine vortex combined with the free stream.

Chapter 7

Numerical Study of Co-Rotating Darrieus Wind Turbine Clusters

In this chapter, the performance of multi-turbine co-rotating Darrieus turbine clusters are numerically studied. Cluster of two co-rotating Darrieus turbine in parallel and oblique configurations are simulated. The results of the two turbine clusters are used to develop an efficient triangular three turbine cluster. The simulation of a single Darrieus turbine shows that the maximum power coefficient is 0.36 achieved at tip speed ratio 2.8. The numerical simulations of the clusters are performed at tip speed ratio 2.8 in order to capture the maximum performance. The numerical model used for the single turbine simulation is used to solve the different clusters.

7.1. Numerical Simulation of Two Co-Rotating Turbine

Clusters of two Darrieus turbines in parallel and in oblique configurations are numerically studied. The study is done at different gap distances and oblique angle 60^o. The numerical simulation is performed at a tip speed ratio equal to 2.8 and the calculated power coefficients of the turbines are compared to the peak performance of the single turbine.

7.1.1. Two Parallel Co-Rotating Turbines

Two parallel Darrieus co-rotating turbines are simulated at different gap distances at λ=2.8. The power coefficients of the two turbines is calculated at different gap distances between the rotors' blade tips. The two turbines (1) and (2) are rotating counter clockwise, the velocity contours in figure 7.1 shows the generation of a high velocity stream tube in the area between the two turbines in addition to two high velocity area on the outward sides downstream the turbines. The results of the power coefficients of the two turbines in figure 7.2 show an enhancement in the efficiency of the two turbines compared to an isolated turbine. The efficiency of turbine (2) is higher than that of turbine (1) due to the direction of rotation of the two turbines and the effect of turbine (1) on turbine (2). The maximum values for power coefficient for turbine (2) is 0.41 and occurs at a gap distance 0.5D, the power coefficients decreases at larger gap distances.

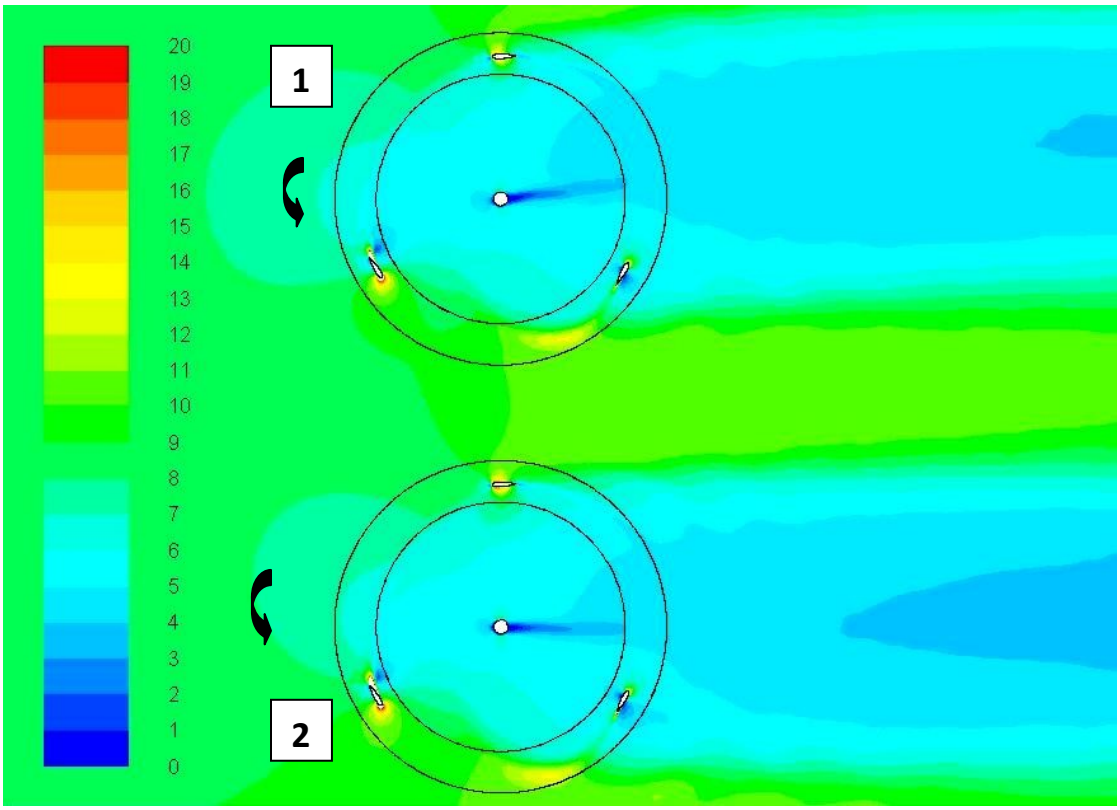

Figure 7.1: Velocity Contours around Two Parallel Co-Rotating Darrieus Turbines

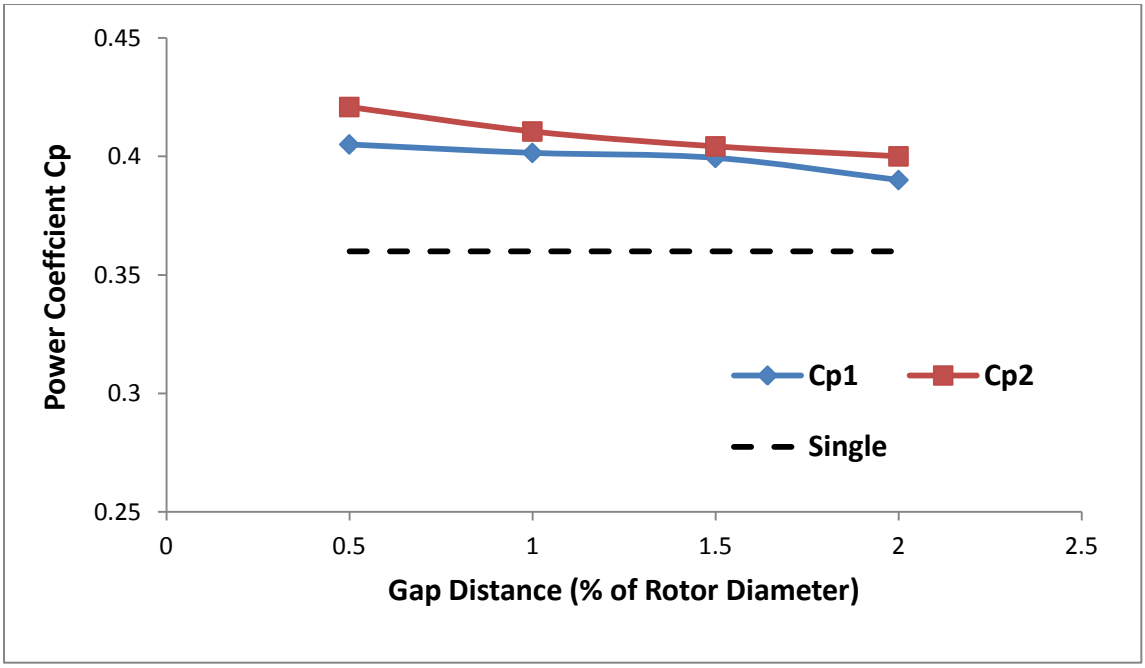

Figure 7.2: C_p of Two Parallel Co-Rotating Turbines at Different Gap Distances Vs Single Rotor

7.1.2. Two Oblique Co-Rotating Turbines

Two oblique co-rotating Darrieus turbines are simulated using the same numerical model used for the single rotor simulation at a tip speed ratio equal to 2.8. Two cases (A) and (B) of oblique configurations are studied. Turbine (1) is upstream and turbine (2) is downstream. In case (A): turbine (2) set at an oblique angle 60^o as shown in figure 7.3 and in case (B): turbine (2) set at an oblique angle -ve 60^o as shown in figure 7.4 [57]. The performance of the two turbines are studied at different rotor gap distances (S). The power coefficient for turbines (1) and (2) for cases (A) and (B) are shown in figure 7.5 and figure 7.6, in case (A) an enhancement occurs in the power coefficients of turbine (2) at small gap distances due to the Magnus effect of turbine (1), however turbine (1) inward blade runs in the wake of the inward blade of turbine (2) and this causes a decreases in turbine (1) efficiency. In case (B) the performance of both turbines is slightly enhanced at small gap distances. Turbine (1) has higher efficiency due to the Magnus effect of turbine (2), and the inward blade of turbine (2) faces a high velocity region behind turbine (1). Figures 7.7 show the average power coefficients for both cases (A) and (B) compared to the isolated turbine power coefficient, case (B) has an average power coefficient higher than in case (A) at different gap distances, the maximum average power coefficient is found to be 0.37 at 0.5D gap distance, the enhancement in the average power coefficient decreases as the gap distance increases. The average power coefficient for Case (B) is lower than that of the isolated turbines at different gap distances.

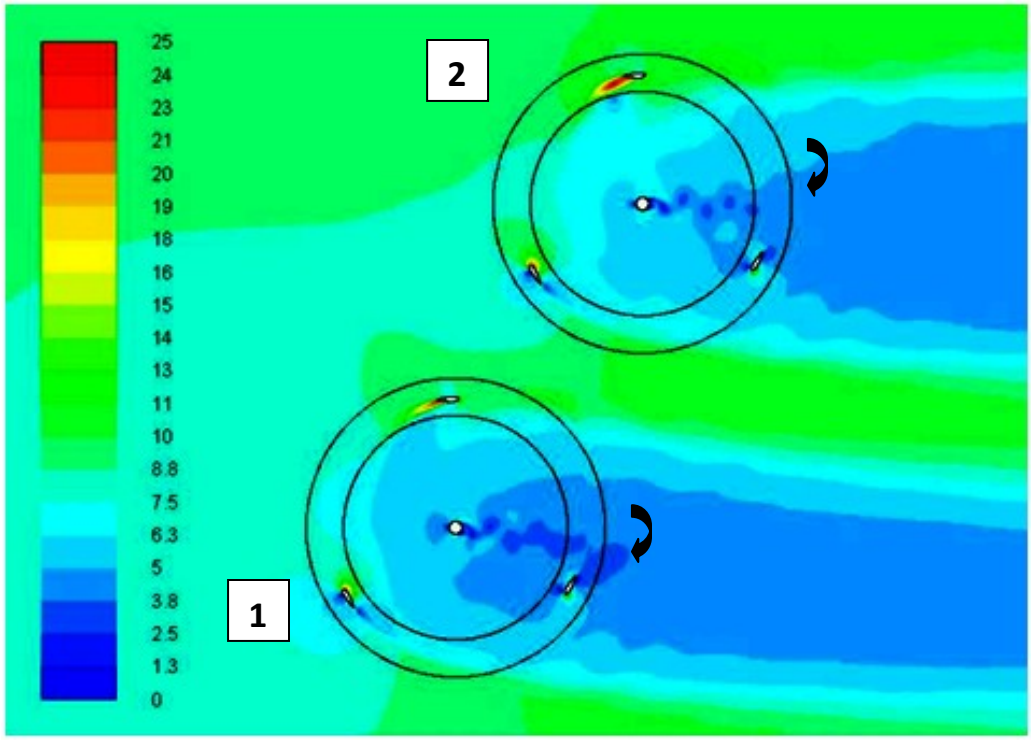

Figure 7.3: Velocity Contours around Two Oblique Co-Rotating Darrieus Turbines Case (A)

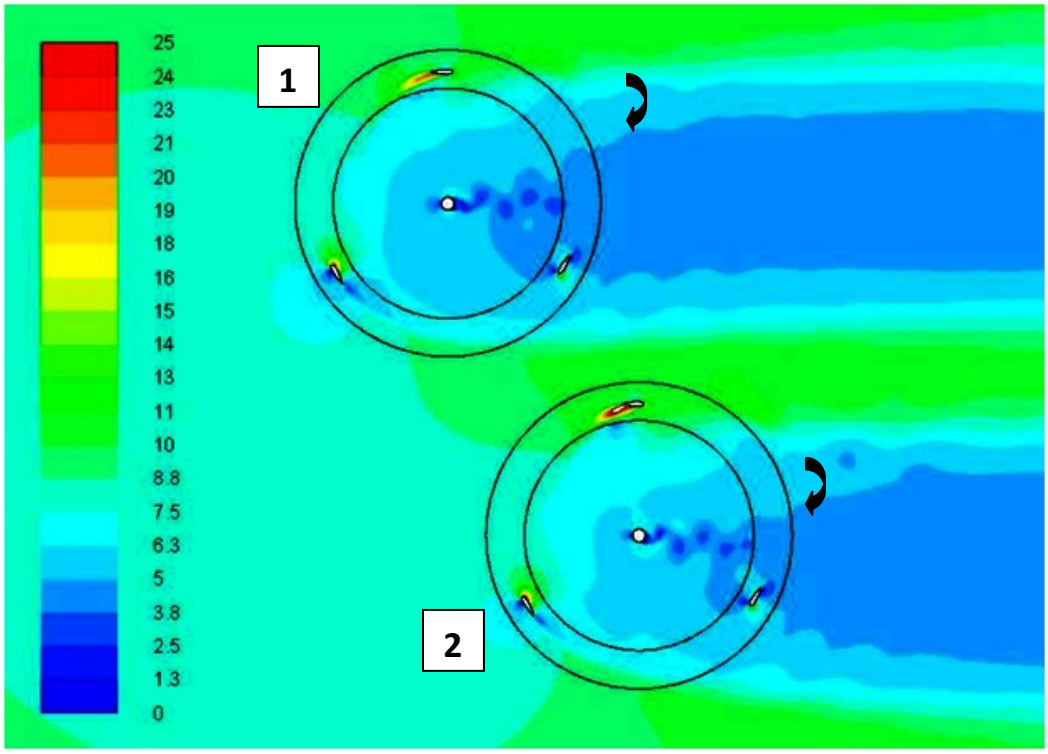

Figure 7.4: Velocity Contours around Two Oblique Co-Rotating Darrieus Turbines Case (B)

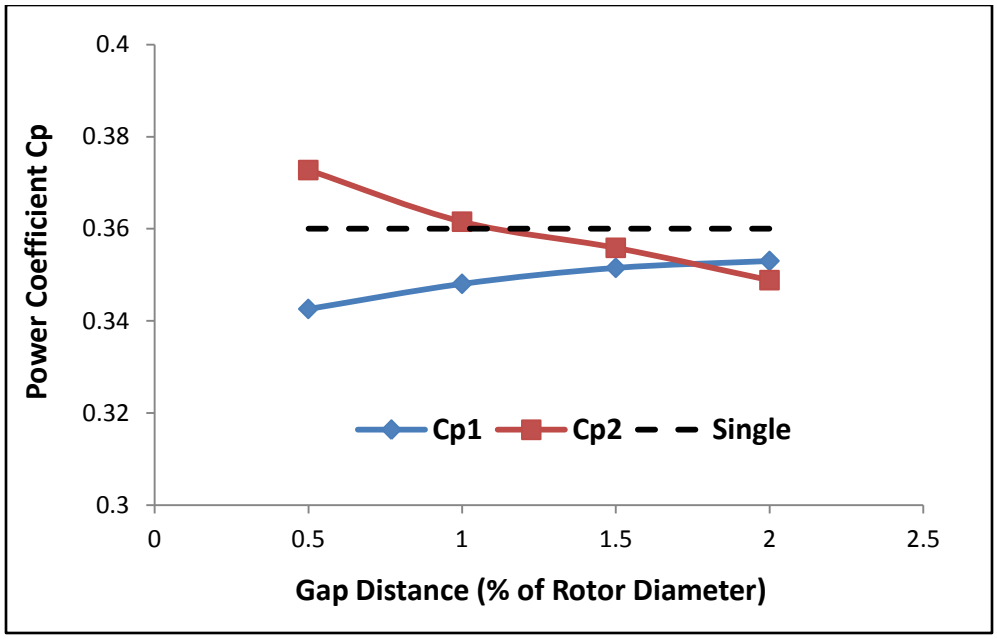

Figure 7.5: C_p of Two Oblique Co-Rotating Darrieus Turbines at Different Gap Distances Vs Single Rotor Case (A)

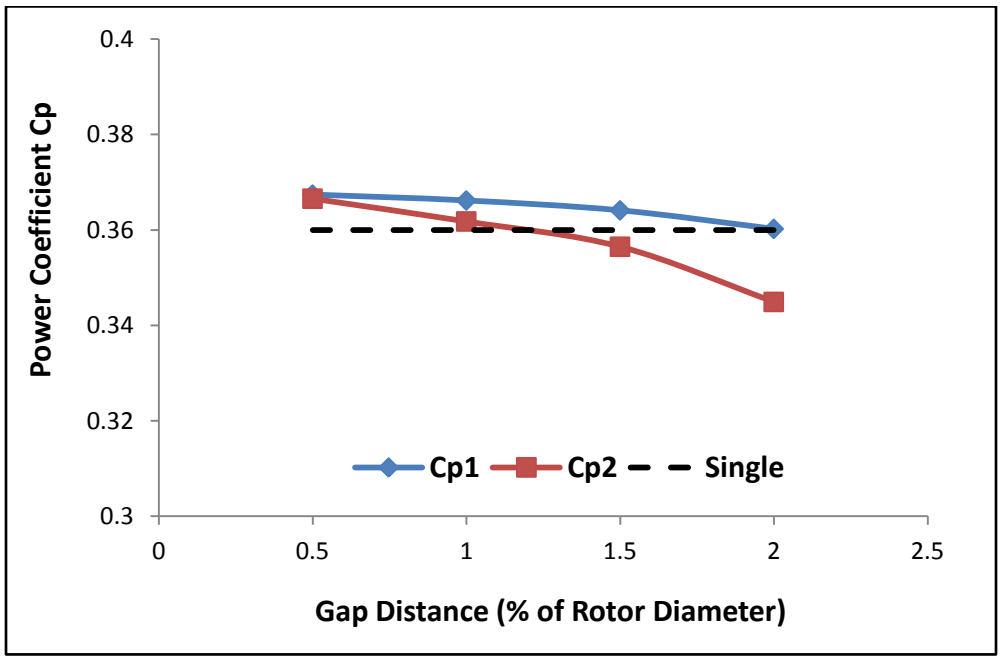

Figure 7.6: C_p of Two Oblique Co-Rotating Darrieus Turbines at Different Gap Distances Vs Single Rotor Case (B)

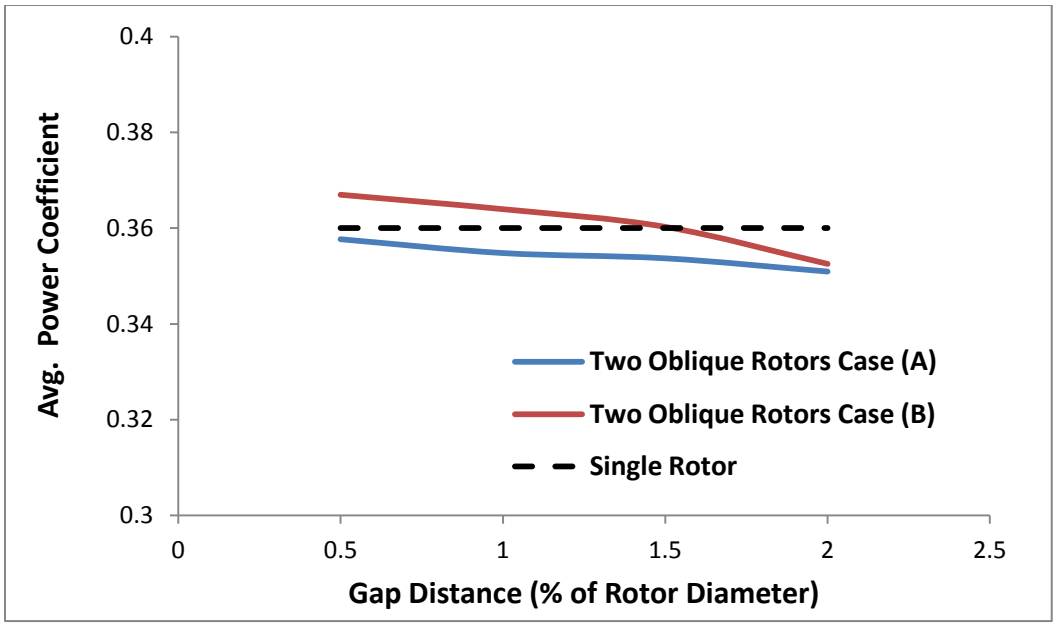

Figure 7.7: C_p^- for Two Oblique Darrieus Turbines Cases (A) and (B) Vs Single Rotor at Different Gap Distances

7.2. Numerical Simulation of Three Co-Rotating Darrieus Turbine Cluster (I)

In order to construct an efficient VAWT farm, a triangular three Darrieus turbine cluster (I) is developed and numerically simulated at different gap distances. The clusters consists of three turbines (1), (2) and (3), turbine (1) is upstream and turbines (2), (3) are downstream. The downstream turbines are oblique to the upstream turbines at an oblique angle 60^o as shown in figure 7.8, the velocity contours around the three turbines in cluster (I) show an increase in the velocity magnitude in the areas between the turbines. The power coefficients of the three turbines are computed as shown in figure 7.9, the results show that performance enhancement occurs to the three turbines at small gap distances and decreases as the gap distance increases. The results for the power coefficients for turbines (2) and (3) shows consistency with the results

of their corresponding turbines in oblique cases (A) and (B). Turbine (2) has the highest performance due to the direction of rotation and the stream lines contraction upwards. Figure 7.10 shows the average power coefficients of the three turbines compared to isolated turbines, the maximum average power coefficient for cluster (I) is 0.38 at 0.5D gap distance which represents 5% higher than an isolated turbine power coefficient. The efficiency of the cluster reduced as the gap distances between the turbines increases, an isolated turbine performance appears for gap distances higher than 2D.

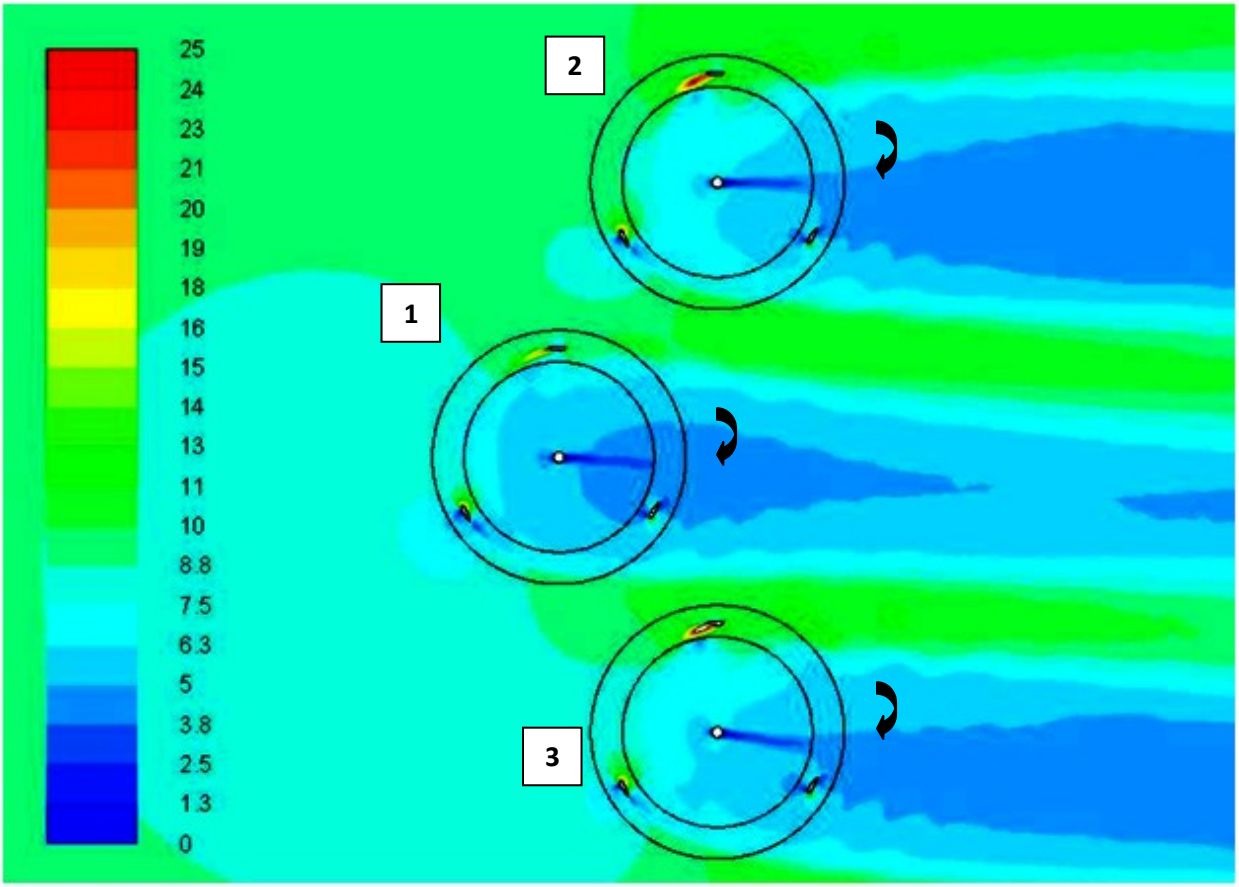

Figure 7.8: Velocity Contours around Three Co-Rotating Darrieus Turbine Cluster (I)

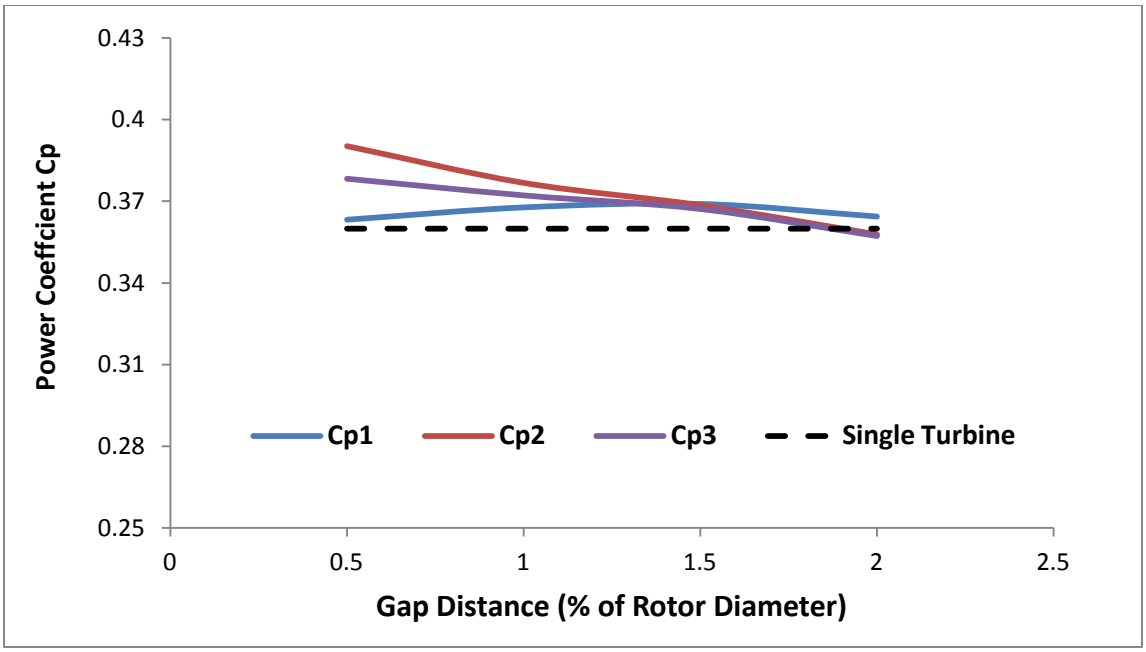

Figure 7.9: Cp for Three Co-Rotating Darrieus Turbine Cluster (I) at Different Gap Distances

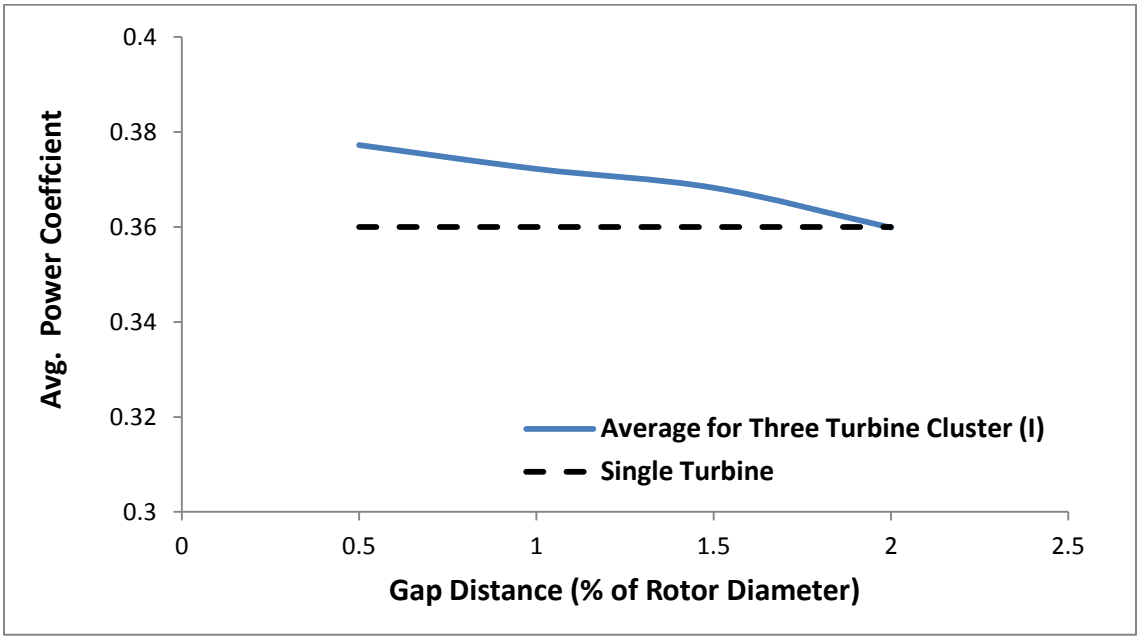

Figure 7.10: C_p^- for Three Co-Rotating Darrieus Turbine Cluster (I) at Different Gap Distances

7.3. Summary

Numerical solutions are performed for clusters of two co-rotating Darrieus turbines in parallel and in oblique configurations, and triangular three turbines clusters at different gap distances. The results show enhancement in the average power coefficients of the clusters compared to the performance of an isolated turbine. For two parallel co-rotating turbines the maximum value for power coefficient is 0.41 and occurs at a gap distance 0.5D. The solution of two oblique turbines shows that the enhancement in case (A) is higher than in case (B) as a result of the Magnus effect due to the direction of rotation of the upstream turbine. The maximum value for power coefficient in case (A) for two co-rotating oblique turbines is 0.37 and occurs at a gap distance 0.5D. A triangular three co-rotating Darrieus turbine cluster (I) is developed, the highest performance of the cluster exists at a gap distance of 0.5D with an average power coefficient of 0.38, this represents an enhancement of 5% compared to a single turbine.

Chapter 8

Numerical Study of Counter-Rotating Darrieus Wind Turbine Clusters

In chapter 7, numerical solutions are performed for clusters of two co-rotating Darrieus turbines in parallel and in oblique configurations, and triangular three co-rotating turbine clusters at different gap distances. In this chapter, the performance of multi-turbine counter-rotating Darrieus turbine clusters are numerically studied. Two counter-rotating Darrieus turbines in parallel and in oblique configurations, and triangular three counter-rotating turbine clusters. The results are used to develop an efficient triangular three turbine cluster. The cluster is used as a building unit for construction of efficient and patterned Darrieus VAWT farms. The numerical simulations of the clusters are performed at tip speed ratio 2.8 in order to capture the maximum performance. The numerical model used for the single turbine simulation is used to solve the different clusters.

8.1. Two Parallel Counter-Rotating Darrieus Turbine Clusters

Two parallel counter-rotating Darrieus turbines are simulated using the same numerical model used for the single rotor simulation at a tip speed ratio equal to 2.8. Two cases (C) and (D) of oblique configurations are studied, and the performance of the two turbines are studied at different rotor gap distances (S). In case (C): Turbine (1) rotates counter clockwise and turbine (2) rotates clockwise and their inward blades moves in the same direction of the wind as shown in figure 8.1, In case (D): Turbine (1) rotates clockwise and turbine (2) rotates counter clockwise and their inward blades moves opposite to the wind direction as shown in figure 8.2. The velocity contours in both figures show that the high velocity area induced between the two turbines is thicker and higher in magnitude for case (c) than in case (D). Figure 8.3 shows a comparison between the average power coefficients of both cases (C) and (D) and the isolated turbines average power coefficient, the results show that the counter-rotating turbines enhance the performance of each other, this enhancement vanishes as the gap distances increases between the turbines. The comparison shows that case (C) where the inward blades moves with the wind direction is more efficient than case (D), an average power coefficient of 0.42 is achieved at a gap distance 0.5D in case (C), this represents 16% higher than the isolated turbines.

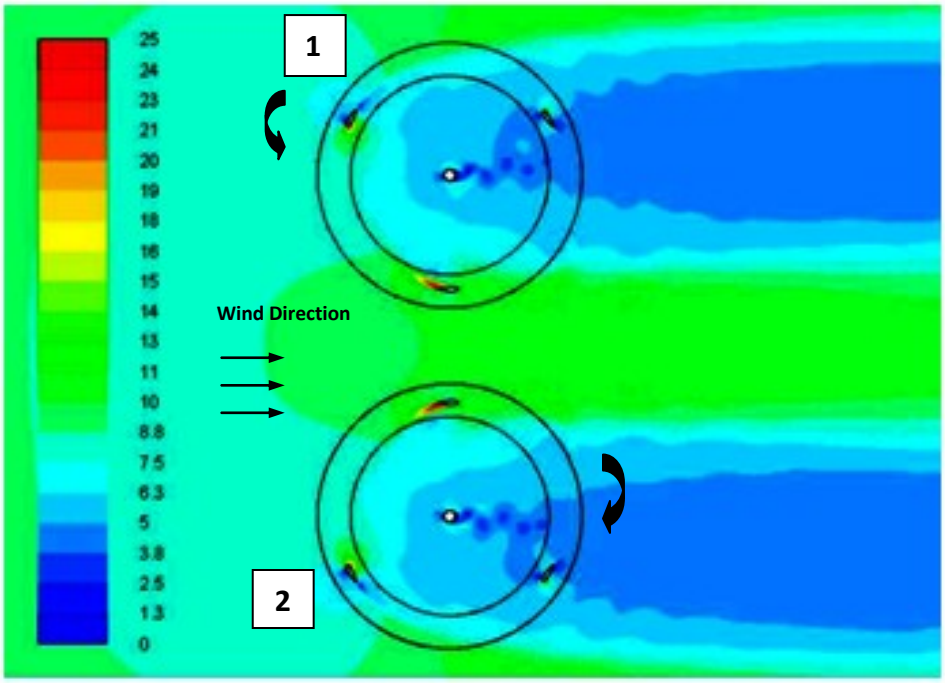

Figure 8.1: Velocity Contours around Two Parallel Counter-Rotating Darrieus Turbines Case (C)

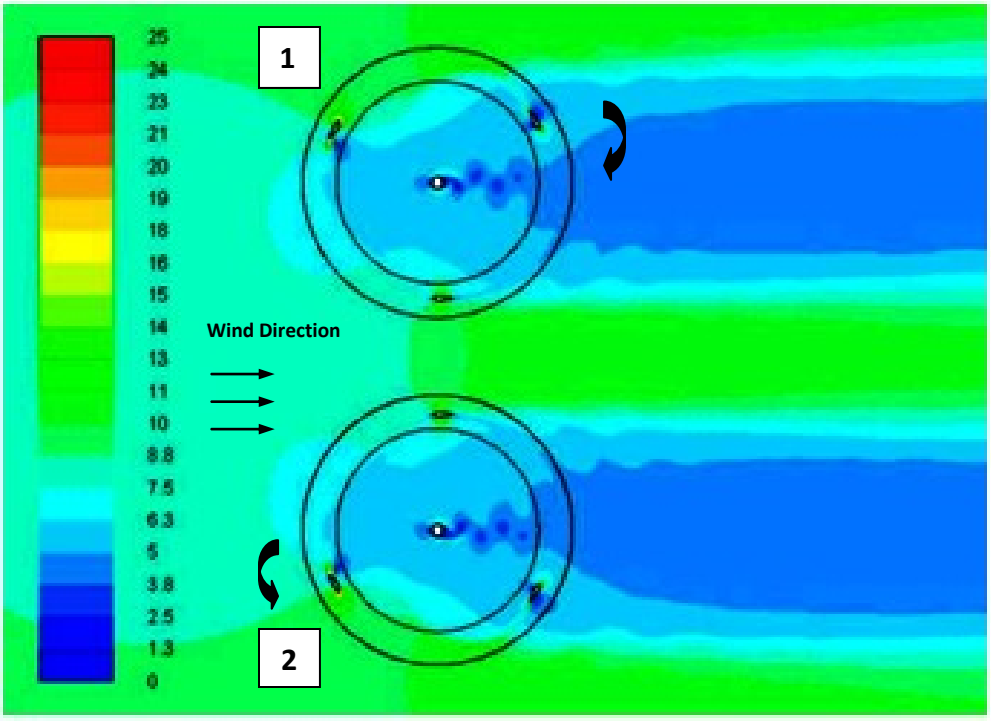

Figure 8.2: Velocity Contours around Two Parallel Counter-Rotating Darrieus Turbines Case (D)

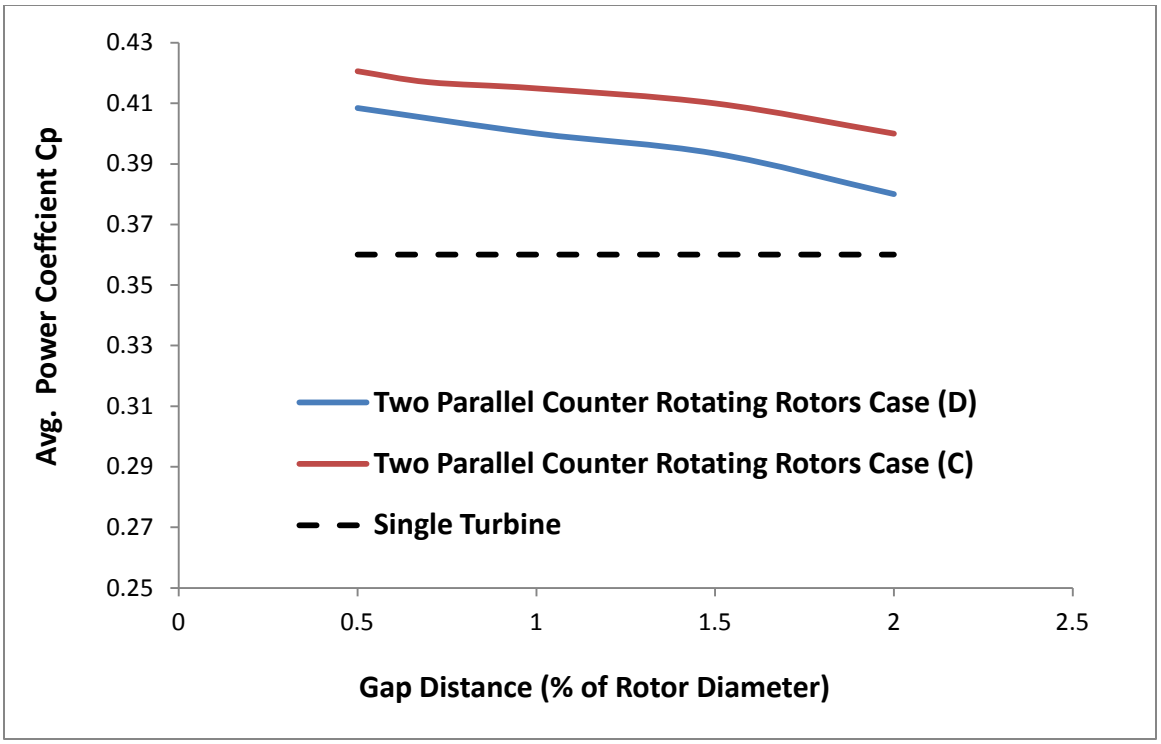

Figure 8.3: C_p^- for Two Parallel Counter-Rotating Darrieus Turbines Vs Single Rotor

8.2. Two Oblique Counter-Rotating Darrieus Clusters

In this section, two oblique counter-rotating Darrieus turbine clusters are studied, two oblique cases (E) and (F) are simulated and the performance of the two oblique turbines in both cases are studied at different rotor gap distances (S). Turbine (1) is upstream and turbine (2) is downstream, in case (E): turbine (2) set at an oblique angle 60^o to turbine (1) and their inward blades moves in the same direction of the wind as shown in figure 8.4 and in case (F): turbine (2) set at an oblique angle -ve 60^o to turbine (1) and their inward blades moves opposite to the wind direction as shown in figure 8.5. The velocity contours in both figures show that the high velocity area induced between the two turbines is thicker and higher in magnitude for case (E) than in case (F).

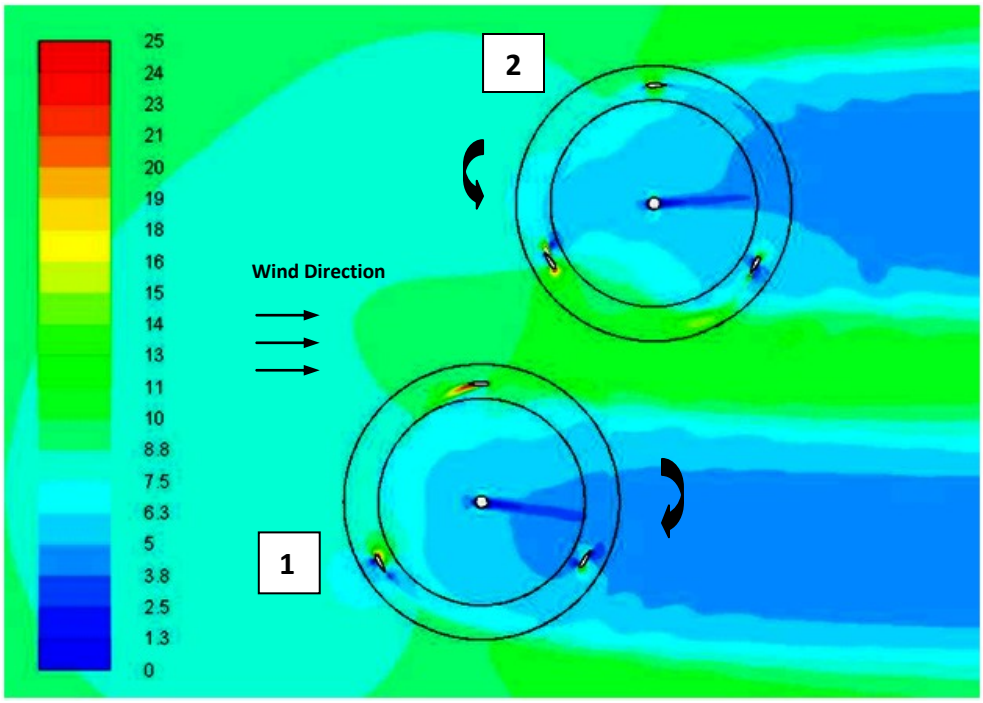

Figure 8.4: Velocity Contours around Two Oblique Counter-Rotating Darrieus Turbines Case (E)

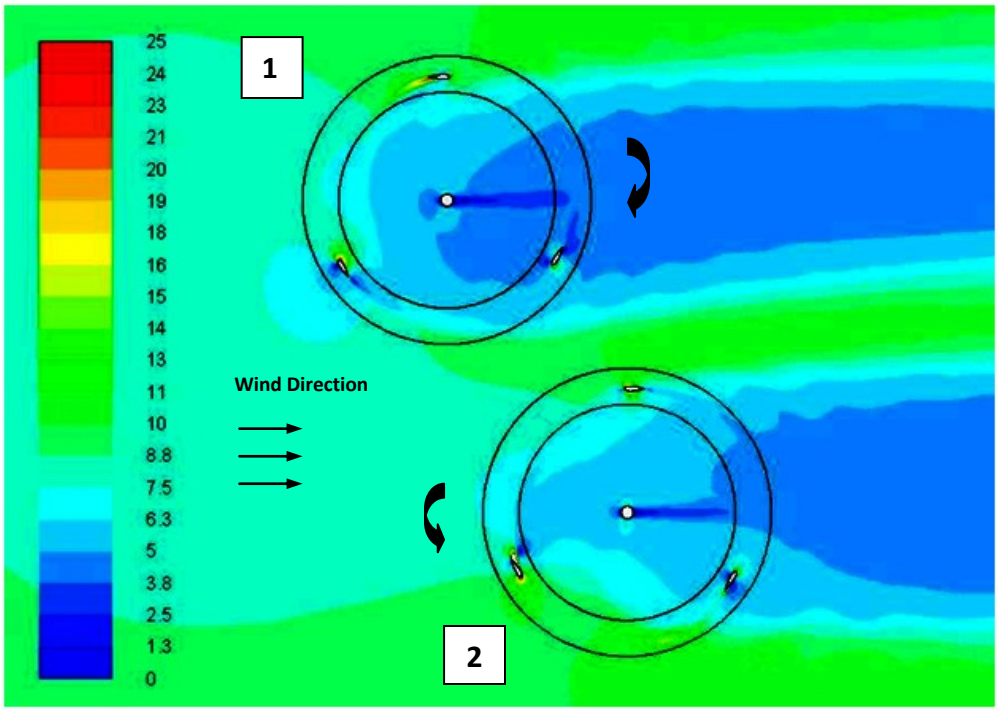

Figure 8.5: Velocity Contours around Two Oblique Counter-Rotating Darrieus Turbines Case (F)

Figure 8.6 shows a comparison between the average power coefficients of both cases (E) and (F) and the isolated turbines average power coefficient, the results show that the counter-rotating turbines enhance the performance of each other, this enhancement decreases as the gap distances increases between the turbines. The comparison shows that case (E) where the inward blades moves with the wind direction is more efficient than case (F) especially at small gap distances. an average power coefficient of 0.41 is achieved at a gap distance 0.5D in case (C), this represents 14% higher than the isolated turbines.

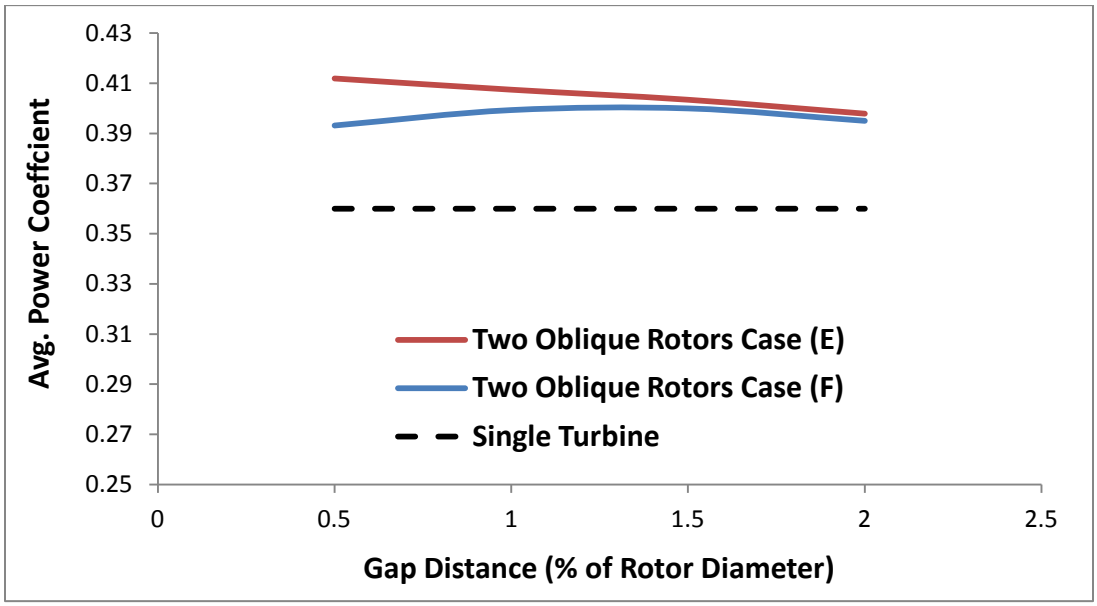

Figure 8.6: C_p^- for Two Oblique Counter-Rotating Darrieus Rotors Vs Single Rotor

8.3. Three Counter-Rotating Darrieus Turbine Cluster (II)

The numerical results for the performance of two co- and counter-rotating parallel and oblique turbines show that case (C) is the most efficient configuration for two parallel turbines, and that case (E) is the most efficient configuration for two oblique turbines. This finding is used to develop an efficient triangular three turbine cluster (II). The base of the triangle is perpendicular

to the wind direction and consists of two counter rotating upstream turbines (1) and (2) as in case (C). The gap distance between the two turbines (1) and (2) are set at different distances from each other and Turbine (3) is set downstream in an oblique position at the smallest possible gap distance, turbine (3) is rotating counter to turbine (1) as in case (E) as shown in figure 8.7. The simulation of the triangular three turbine cluster is performed for gap distances between the two upstream turbines (1) and (3) starting from 0.2D to 1.2 D, and this changed the oblique angles between the upstream and downstream turbines from 30^{o} to 60^{o} in order to keep turbine (2) at the smallest possible gap distance. The average power coefficient for each case is shown in figure 8.8, the results show that the cluster with a gap distance of 1.2D between the turbine (1) and (3) is the most efficient with the highest average power coefficient and the highest power density.

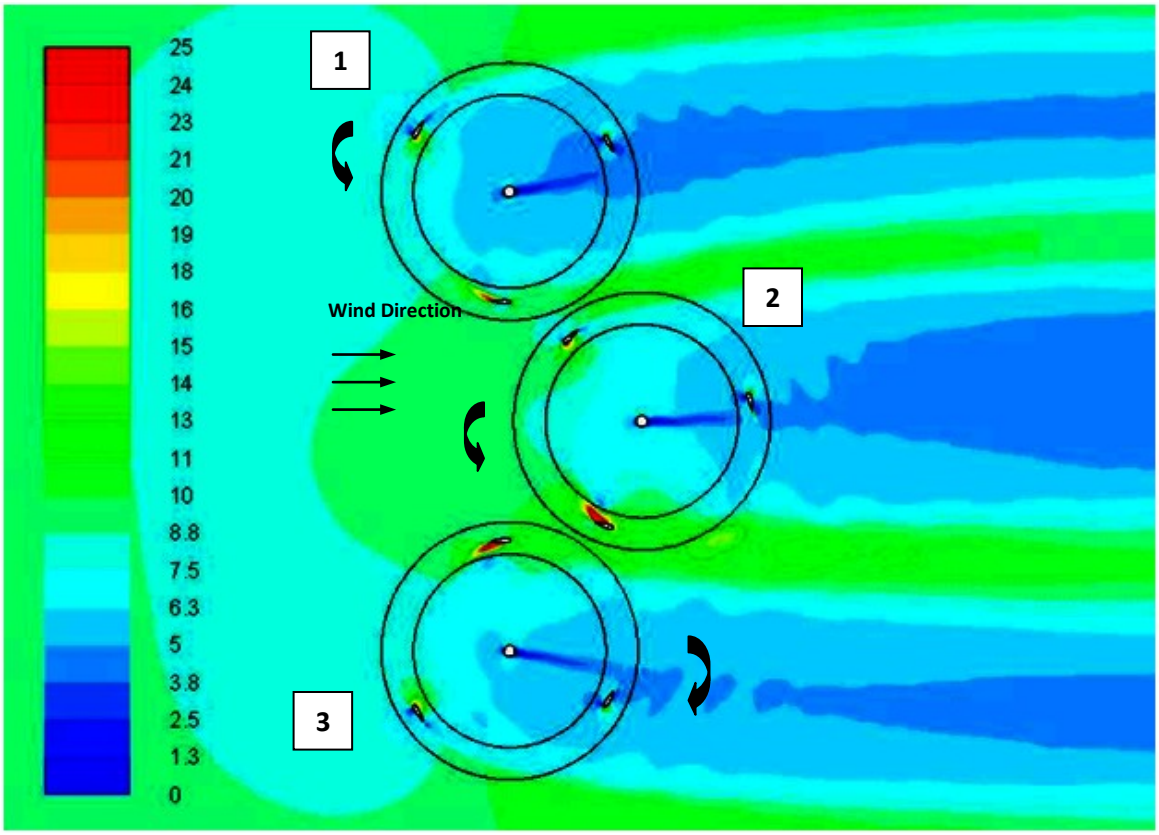

Figure 8.7: Velocity Contours around Three Darrieus Turbine Cluster (II)

In this cluster, the distances from the line joining the centers of the two upstream turbines (1) and (2) to the center of turbine (3) is 0.6D and the oblique angle between the turbines is 60°. The value of the most efficient oblique angle is in consistence with the results in reference [11].

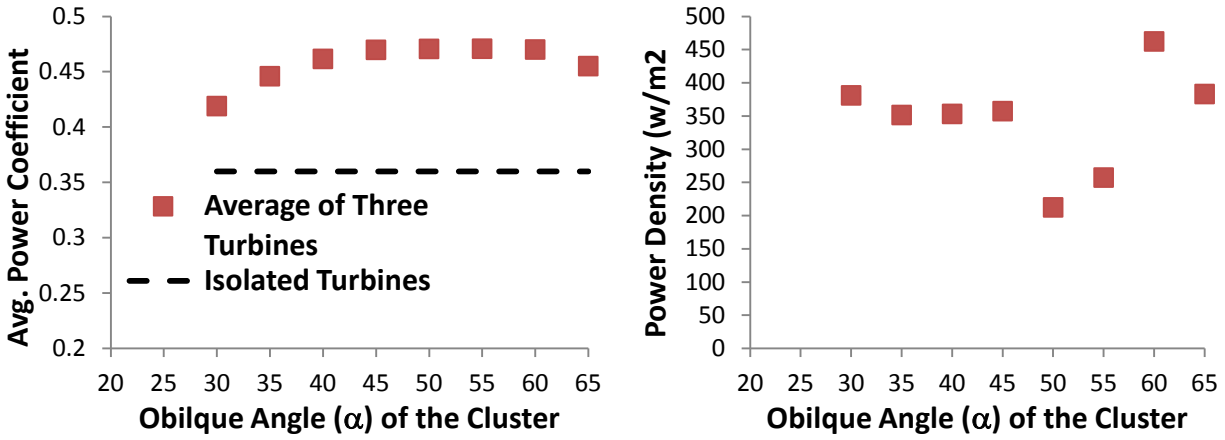

Figure 8.8: C_p^- and Power Density for Three Counter-Rotating Cluster Case (II) at different Oblique Angles

In order to confirm that the separation distance for turbine (3) is the most efficient, the cluster is tested at different distances. Figure 8.9 shows that the power coefficient of the three turbines is enhanced compared to a single isolated turbine at different distances for turbine (3) defined as cluster height. Turbine (3) has the highest power coefficient due to the incoming higher velocity it is subjected to coming out of the stream tube created by the two downstream turbines (1) and (3). Figure 8.10 shows the average power coefficient of the three turbines of the cluster compared to isolated turbines, the maximum average power coefficient for the three turbines is 0.47 at 0.6D cluster height, this represents an enhancement of 30% higher than that of the isolated turbines and the enhancement decreases at smaller cluster heights.

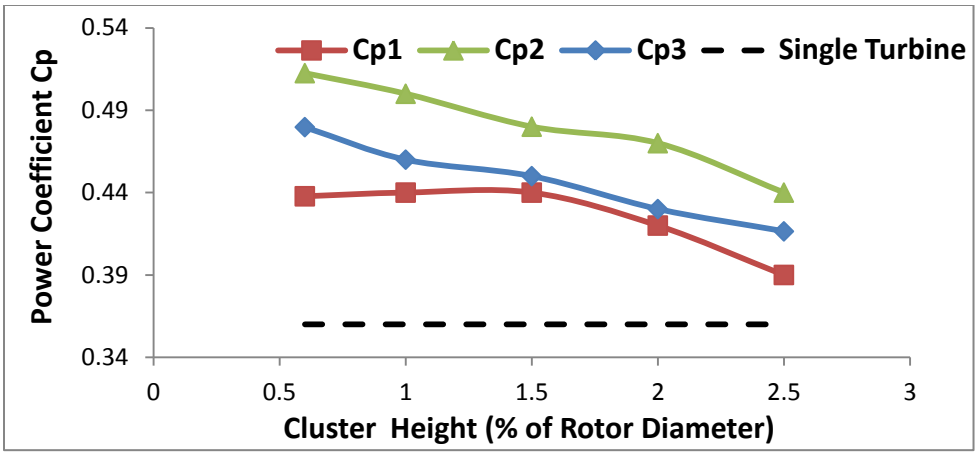

Figure 8.9: Cp for 3 Counter-Rotating Darrieus Rotors Case (II) at Different Distances

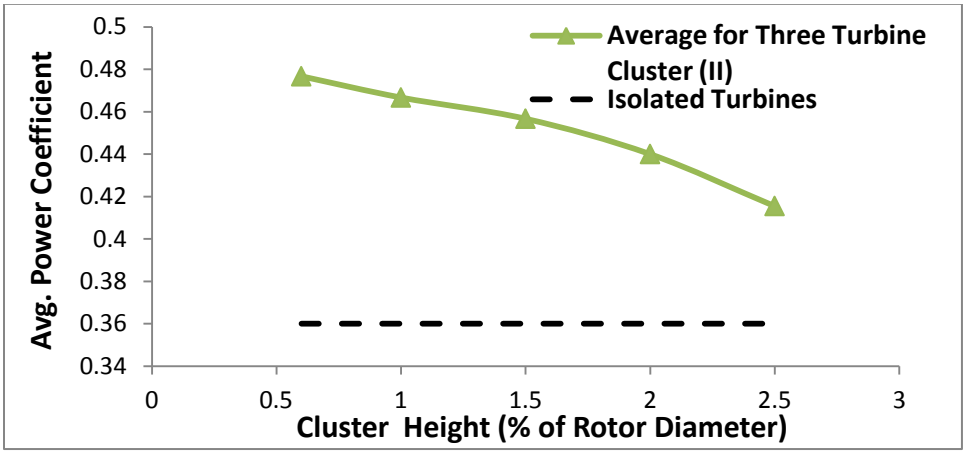

Figure 8.10: C_p^- Three Counter-Rotating Darrieus Cluster Case (II) Vs Isolated Turbines

8.4. Comparison between Clusters (I) and (II)

The results for the three counter-rotating turbine clusters (II) are compared to the co-rotating three turbine cluster (I). The comparison in figure 8.11 shows that the efficiency of the triangular three turbine cluster case (II) is higher at different cluster heights than that of cluster (I), an enhancement of 30% higher than that of the isolated turbines is achieved by cluster (II) at a cluster height 0.6D, however in of cluster (I) the enhancement is less than 5%. Cluster (II) will be used as a building unit for the construction of efficient triangular Darrieus wind turbine farms.

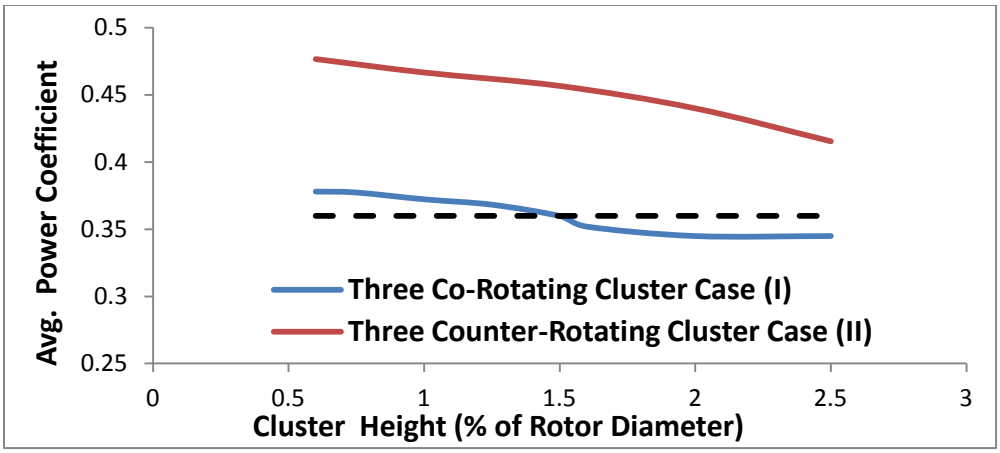

Figure 8.11: C_p^- for Three Turbine Darrieus Clusters Case (I) and (II) Vs Single Turbine

8.5. Summary

Numerical solutions are performed for clusters of two counter-rotating Darrieus turbines in parallel and in oblique configurations, and triangular clusters of three turbines. The enhancement in the power coefficients in the clusters is compared to the performance of an isolated turbine. For two parallel turbines case (C) has better performance than case (D) the maximum power coefficient in case (C) is 0.42 and occurs at a gap distance 0.5D. For two oblique turbines the enhancement in case (E) is higher than in case (F), a maximum average power coefficient of 0.41 is achieved at a gap distance 0.5D in case (E). Based on the previous results, a triangular three Darrieus turbine cluster (II) is developed, the most efficient performance of the cluster exists at a cluster height of 0.6D with an average power coefficient of 0.47, this represents an enhancement of 30% compared to isolated turbines. The results for the three counter-rotating turbine clusters (II) are compared to the co-rotating three turbine cluster (I). The efficient counter rotating three turbine cluster (II) will be used as a building unit for efficient triangular Darrieus wind turbine farms.

Chapter 9

Patterned Darrieus Vertical Axis Wind Turbine Farms

We showed in chapter 8 that a triangular three Darrieus turbine cluster (II) consisting of counter-rotating turbines has an enhancement of 30% in the average power coefficient compared to the isolated turbines. The cluster has a gap distance of 1.2D between the two upstream parallel and counter-rotating turbines. The cluster height from the line joining the two upstream turbines to the center of the downstream turbine is 0.6D and the oblique angle between the turbines is 60^{o}. In this chapter, the performance of the three turbine cluster (II) is confirmed at different tip speed ratios. Keeping the same geometric topology of the cluster, a patterned farm that consist of multiple clusters with scaled geometrical ratios of the three turbine cluster is developed. Numerical simulations of a farm that consists of nine turbines confirm the enhancement and the pattern progression for larger farms. The numerical simulation model is similar to that used in the previous chapters.

9.1. Numerical Simulation Model

The computational domain for the three turbine cluster simulation shown in figure 9.1 is the similar to the domain used in the single turbine simulation. A grid sensitivity study is performed, the mesh is refined five times from 133,175 to 2,257,340 cells until there is no significant change observed in the torque coefficient of the three turbines as shown in table 9.1. A grid with 400,487elements is found to be adequate.

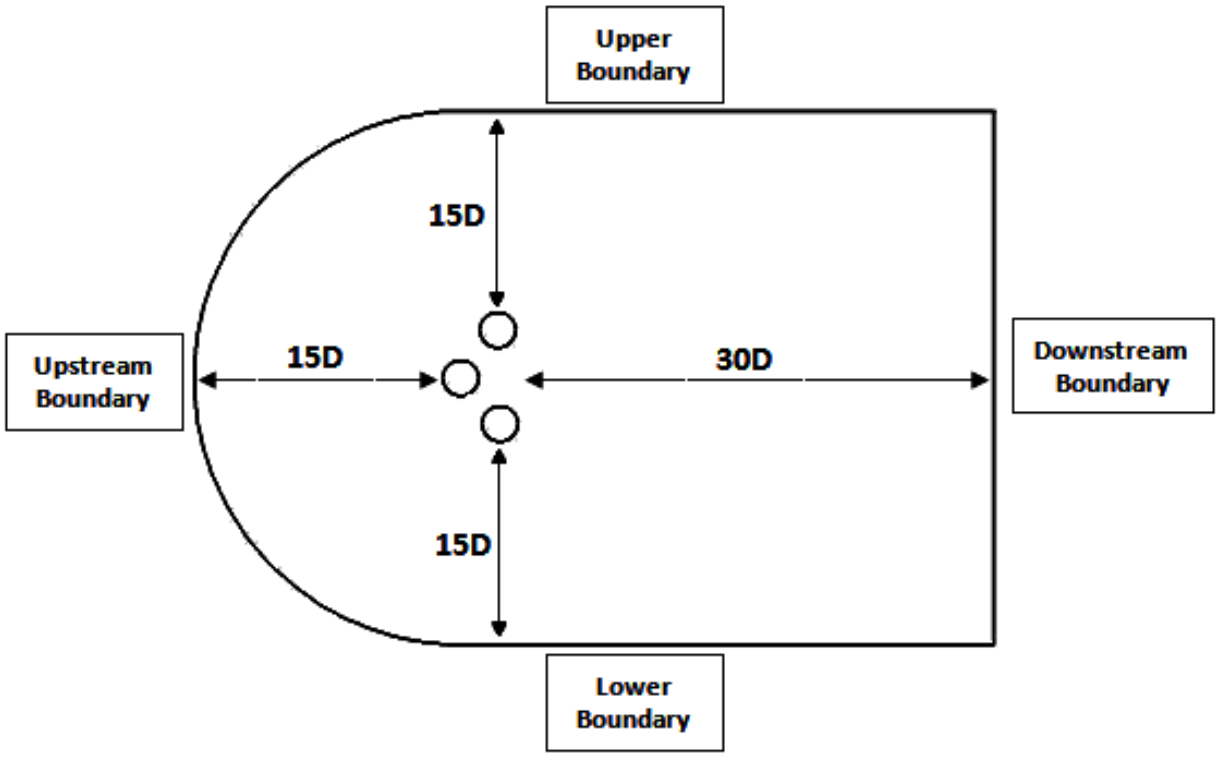

Figure 9.1: Computational Domain for Three Turbine Darrieus Cluster Simulation

Table 9.1: Mesh Refinement Levels for Three Darrieus Turbine Cluster (II)

Grid Level	No. of Elements	Cm1	Cm2	Cm3
1	133,175	0.465	0.500	0.493
2	219,245	0.453	0.495	0.485
3	400,487	0.442	0.513	0.473
4	993,007	0.442	0.512	0.472
5	2,257,340	0.441	0.514	0.472

The unsteady Reynolds averaged Navier-Stokes equations are solved using SIMPLE algorithm (Semi-Implicit Method) with a second order spatial discretization for momentum, and turbulence equations and a Least Squares Cell Based algorithm for gradients. The transition SST turbulence model is used and the sliding mesh model (SMM) is performed. A time step size corresponding to a turbine rotation of 1.0 degree is used for the time dependent solution. A drop of at least 3 orders of magnitude in each time step as well as a minimum of 20 iterations per time step is considered as convergence criteria for the time dependent solution.

9.2. Results and Discussion

9.2.1. Three Turbine Cluster (II)

The results in Chapter 8 show that a three Darrieus counter-rotating turbine cluster with a height of 0.6D achieves an enhancement of 30% in the average power coefficient compared to isolated turbines at λ=2.8. To confirm that the mutual enhancement occurring between the rotors of the three turbine cluster, the cluster is simulated at different tip speed ratios. The results in table 9.2 and figure 9.2 show the power coefficients of the three turbines at different tip speed ratios, the downstream turbine (2) has the highest power coefficient due to the high velocity stream tube generated by the upstream counter rotating turbines. A maximum power coefficient of 0.51 is achieved by turbine (2) at λ=2.8, this enhancement in the power coefficient make the VAWT efficiency reach the values of HAWTs, the ratio between the power coefficients of the three rotors is approximately 1.0:1.1:1.0 for λ>2.4. Figure 9.3 shows the average power coefficient of the three turbines at different tip speed ratios compared to the isolated turbine, the maximum average power coefficient of the cluster is 0.47 at λ=2.8. The enhancement in the average power coefficient of the three turbines compared to a single turbine is observed for λ>2.4. At λ=2.8 an

aligned array of three isolated turbines generates 702 watt and occupies an area of 11 square meters, resulting in a power density of 63 watt/m^2. The developed three turbines cluster (one meter diameter turbines) generates 917 watt and occupies an area of 3.7 square meters, resulting in a power density of 248 watt/m^2. The efficiency of the developed three turbine cluster is 30% higher than the isolated three turbines, also the power density of the developed three turbine cluster is 4 times the isolated three turbines.

Table 9.2: Results of Three Darrieus Turbines Triangular Cluster

λ	Cp1	Cp2	Cp3	Average Cp	Ratios of Power Coefficients		
					Rotor (1)	Rotor (2)	Rotor (3)
1.6	0.05	0.07	0.06	0.06	1.0	1.27	1.08
1.8	0.11	0.11	0.12	0.11	1.0	0.93	1.0
2.0	0.18	0.15	0.16	0.16	1.0	0.83	0.88
2.2	0.26	0.23	0.25	0.25	1.0	0.90	0.96
2.4	0.33	0.34	0.32	0.33	1.0	1.04	0.98
2.6	0.40	0.43	0.41	0.42	1.0	1.08	1.04
2.8	0.44	0.51	0.47	0.47	1.0	1.16	1.06
3.0	0.42	0.48	0.45	0.45	1.0	1.14	1.07
3.2	0.38	0.44	0.39	0.41	1.0	1.15	1.02

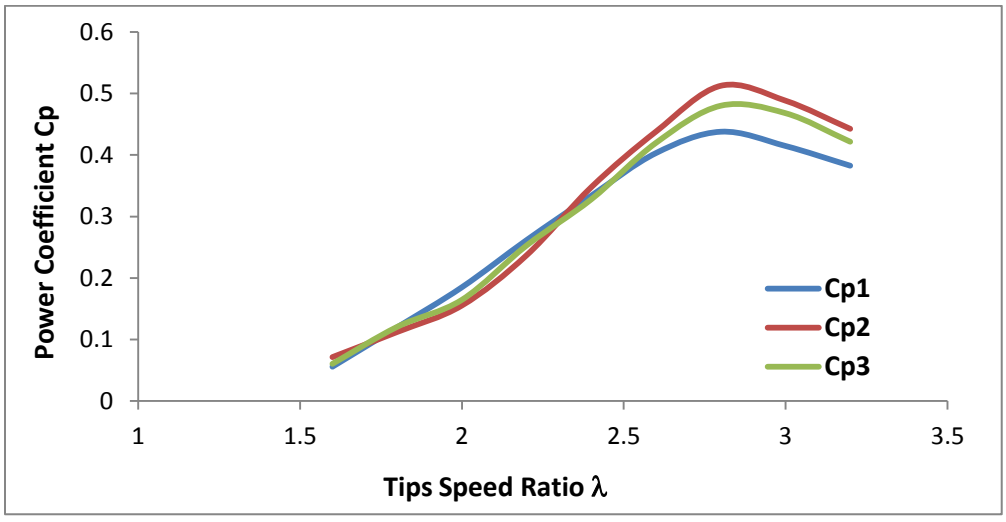

Figure 9.2: Cp of Three Counter-Rotating Turbines Cluster (II) at Different Tip Speed Ratios

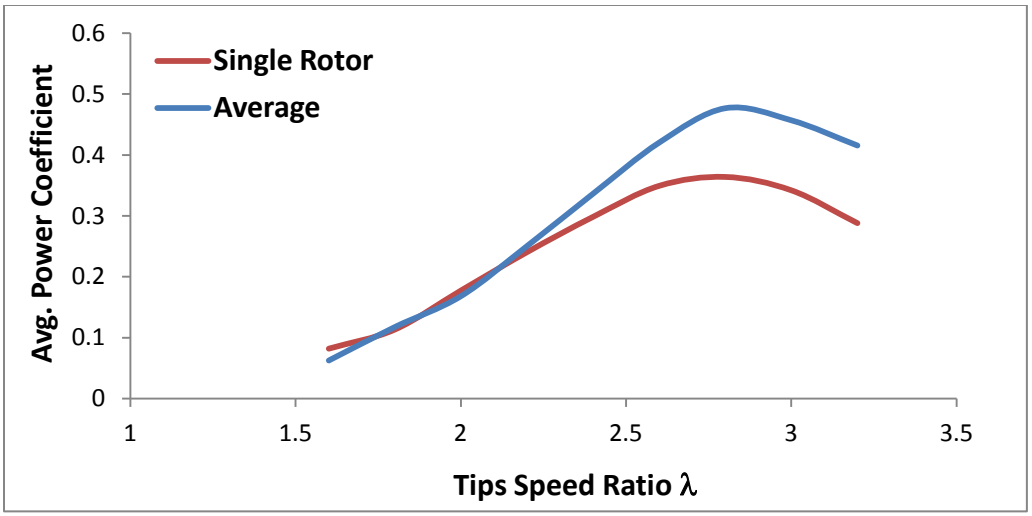

Figure 9.3: Avg. Cp of Three Counter-Rotating Turbines Cluster (II) at Different Tip Speed Ratios Vs Single Turbine

9.2.2. Patterned Nine Darrieus Wind Turbine Farms

The three turbine cluster (II) is used as a building unit to construct efficient VAWT farms having the same topology of the cluster. The triangular farm has identical geometrical ratios of the three turbine cluster, Numerical simulation of a farm that consist of nine turbines is performed to confirm approximately the same enhancement ratio of the three turbine cluster and the geometric progression. The nine turbine triangular farm shown in figure 9.4 is developed using two three turbine cluster in the first row and one similar clusters in the second row, this is consistent with the topology of cluster (II), rotors (1), (2) and (3) represent cluster (A), rotors (3), (4) and (5) represent cluster (B) and rotors (6), (7) and (8) represent cluster (C). Figure 9.5 shows the average power coefficient of the nine turbine farm at different tip speed ratios compared to the three turbine cluster and the isolated turbines, the maximum average power coefficient of the cluster is 0.46 at λ=2.8. The results of the power coefficient of the nine rotors summarized in table 9.3 confirm the pattern. Within each three turbine cluster (A, B and C) the ratio between the

power coefficients of individual turbines is similar to the ratio achieved for the individual turbines in a single cluster. The numerical results in table 9.4 show that the ratio between the total power generated by clusters (A), (B) and (C) is about 1:1.1:1.0. The enhancement in the performance of the patterned nine turbine farm is similar to that of a single three turbine cluster. An aligned array consisting of nine isolated Darrieus turbines generates 2017 watt/m and occupies an area of 245 square meters, resulting in a power density of 8 watt/m^2. On the other hand, this developed nine Darrieus wind turbines farm generates 2711 watt/m and occupies an area of 25 square meters, resulting in a power density of 108 watt/m2. The efficiency of the developed three turbine cluster is 28% higher than the isolated three turbines, also the power density of the developed three turbine cluster is 13 times the isolated three turbines.

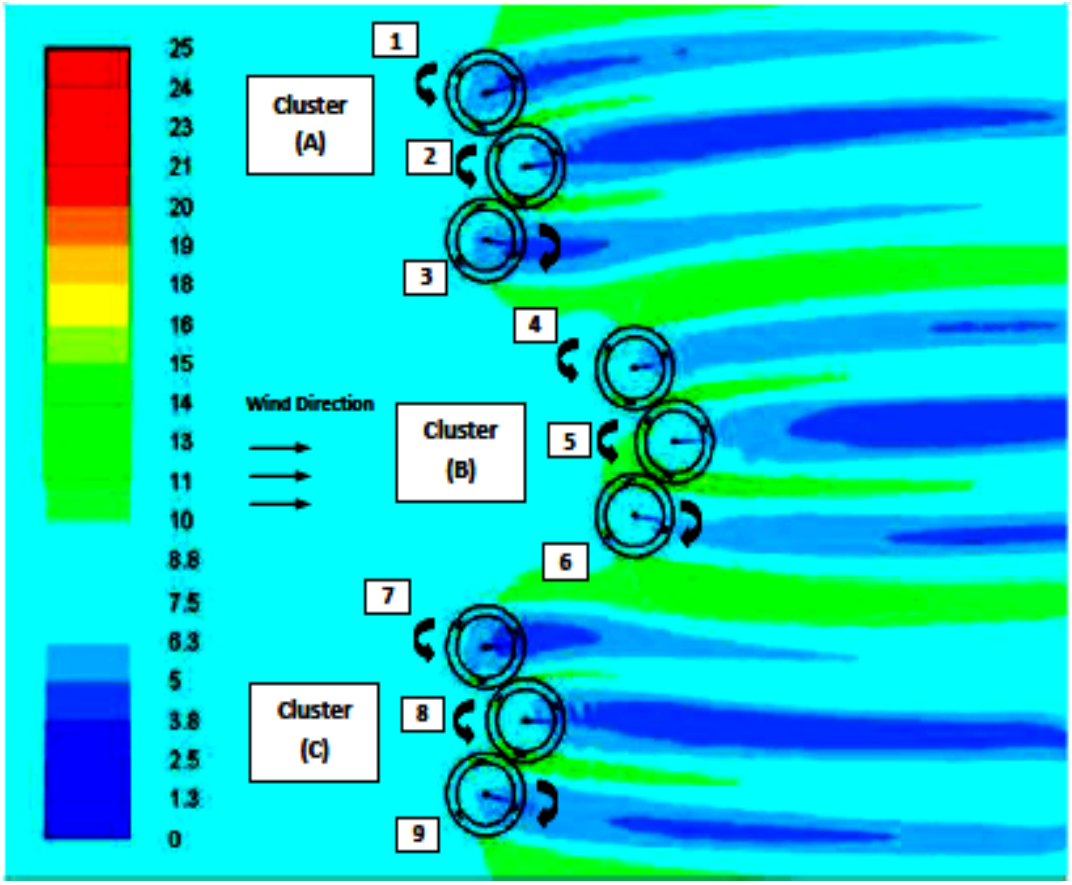

Figure 9.4: Velocity Contours around Nine Savonius Wind Turbine Farm

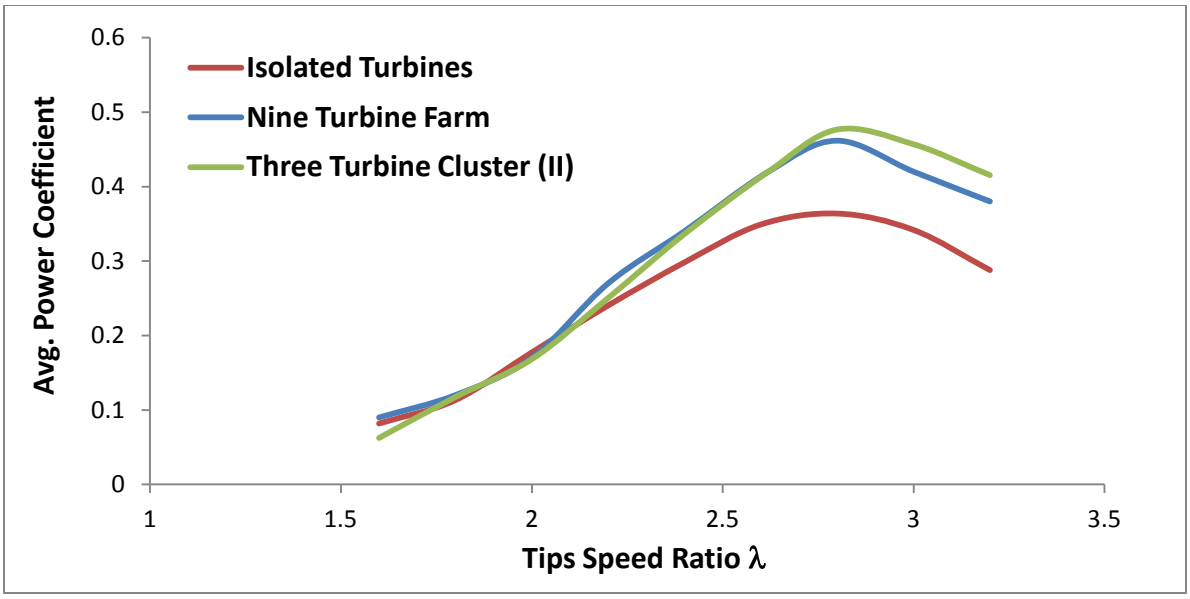

Figure 9.5: Avg. Cp of Nine Turbine Farm and three Turbine Cluster at Different Tip Speed Ratios Vs Isolated Turbines

Table 9.3: Results of the Nine Darrieus Wind Turbine Farm

Cluster A	**Isolated Rotor**	**Rotor (1)**	**Rotor (2)**	**Rotor (3)**
Power Coefficient (Cp)	0.36	0.39	0.45	0.41
Enhancement % Compared to Isolated Rotor		8%	25%	13%
Ratio Compared to Rotor (1)		1.0	1.15	1.05
Cluster B	**Isolated Rotor**	**Rotor (4)**	**Rotor (5)**	**Rotor (6)**
Power Coefficient (Cp)	0.36	0.50	0.55	0.51
Enhancement % Compared to Isolated Rotor		38%	52%	41%
Ratio Compared to Rotor (4)		1.0	1.1	1.02
Cluster C	**Isolated Rotor**	**Rotor (7)**	**Rotor (8)**	**Rotor (9)**
Power Coefficient (Cp)	0.36	0.39	0.46	0.42
Enhancement % Compared to Isolated Rotor		8%	28%	17%
Ratio Compared to Rotor (7)		1.0	1.18	1.07

Table 9.4: Total Power Generated by the three clusters in Nine Turbines Wind Farm

	Cluster (A)	**Cluster (B)**	**Cluster (C)**	**Average**
Power Coefficient	0.42	0.52	0.42	0.453
Total Power (watt)	858	1014	839	
Ratio Compared to Cluster (A)	1.0	1.18	1	

The nine turbine farm is patterned, this means that the performance of the farm can be predicted by simulation of only three turbines. Using the ratio 1:1.1:1 and the results of the simulation of the three turbine cluster, the nine turbine farm efficiency is predicted and compared to the calculated results in table 9.3 as shown in figure 9.6, the results show that error in the predicted average power coefficient of the farm compared to the calculated value is less than 2%.

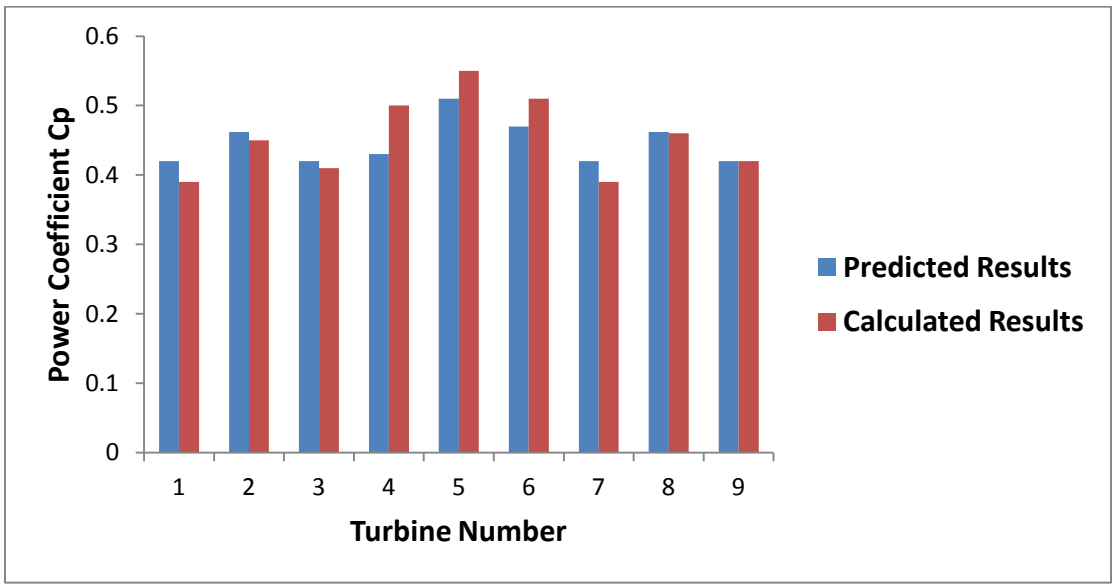

Figure 9.6: Comparison of between Predicted and Calculated Results for Nine Darrieus Turbine Farm at λ=2.8

Figure 9.7 shows the total power achieved by the developed cluster and farms compared to the output from the same number of isolated turbines, the total power generated by the nine turbine farm 28% higher than that of the isolated turbines. Figure 9.8 shows the power density of the developed farms compared to the power density of the same number of isolated turbines (5 rotor diameters apart cross field and 10 rotor diameters apart downstream), the power density achieved by the developed nine turbine farm is 13 times than the isolated nine turbine farm. A power scaling is achieved going from an isolated single turbine to the three turbine cluster to the nine turbine farm to the twenty seven turbine farm as shown in figure 9.9.

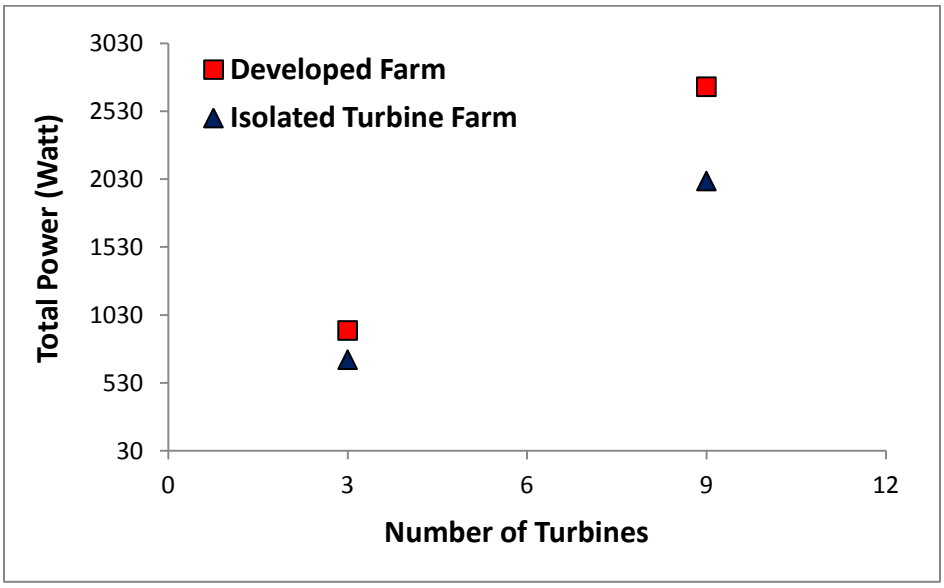

Figure 9.7: Total Power Generated by the developed farms Vs the Power Generated by the Same Number of Isolated Turbines

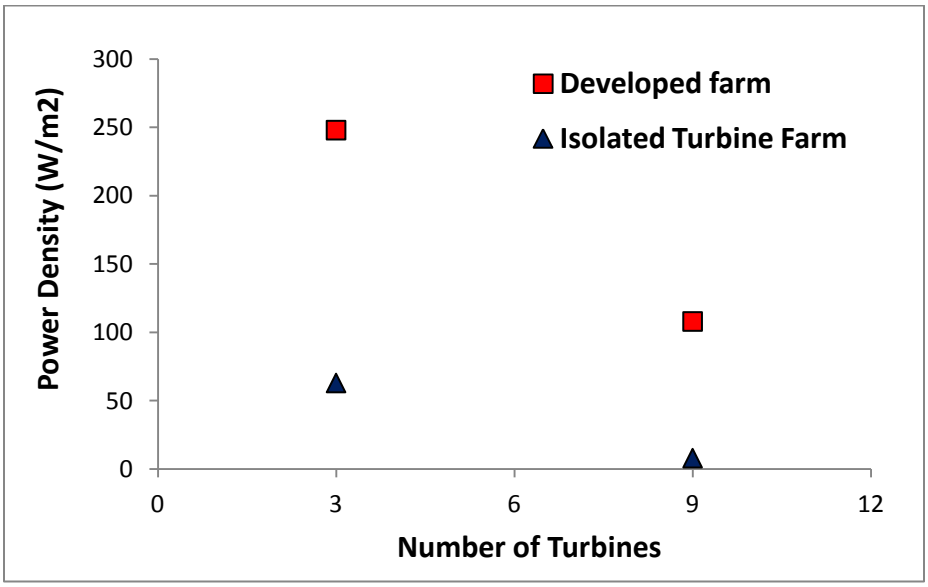

Figure 9.8: Power Density Vs the Number of Turbines in a Farm

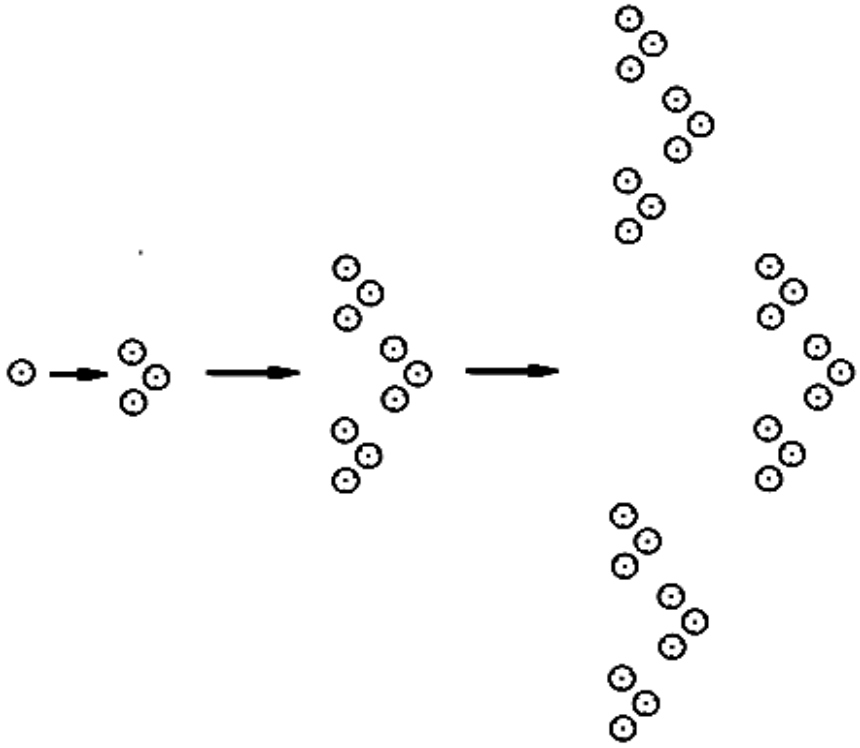

Figure 9.9: Power Scaling

9.3 Summary

An efficient Darrieus wind turbine farm is developed using the efficient three counter-rotating triangular turbine cluster (II) as a building unit. The farm topology is a geometric progression of the three turbine cluster by factor 3. The developed farms are patterned and have the same power coefficient enhancement ratios of the three turbine cluster. The pattern and enhanced power coefficient are confirmed by numerical solutions of farms that consist of nine and is expected to perform the same in twenty-seven turbines as it has occurred in Savonius turbine farms. The power ratio between individual turbines is 1.0:1.1:1.0. The same power ratio is achieved by the nine turbines. The power density of the developed nine turbine farm is more than 13 times a nine isolated turbine farm. The power ratio can be used to predict the performance of larger farms with the same topology to save processing time and man power.

Conclusion

We developed Patterned Savonius and Darrieus Vertical Axis Wind Turbine farms for renewable energy generation. The farms consists of multiples of triangular efficient three turbine clusters. The three turbine cluster has a triangular shape and the turbines inside the cluster are arranged in a close proximity to enhance their average output power. The cluster geometry is optimized using numerical solutions of two co-rotating and counter-rotating turbines in parallel and oblique configurations. The developed VAWT farms performance parameters are assessed numerically by solving RANS equations using Fluent code. The assessment parameters are moment and power coefficients. The following conclusions are drawn:

- Numerical method is validated by comparing the results of single Savonius and Darrieus turbines with the available the experimental data, the maximum power coefficient for a single Savonius turbine is found to be 0.23 at λ= 1, and for a single Darrieus turbine is 0.36 at λ= 2.8. The two dimensional computational results shows that the transition SST turbulence model has the closest results to the experimental data.
- The numerical study of the performance of two co-rotating and counter-rotating turbine clusters show an enhancement in the power coefficient of individual turbines.
- For two co-rotating multiple Savonius turbines, two parallel turbine cluster has a maximum power coefficient of 0.3 at a gap distance of 0.2D. Two oblique turbine cluster at an oblique angle 60^o has a maximum power coefficient of 0.26 at a gap distance of 1.0D, and for an oblique angle -60^o the maximum power coefficient is 0.32 at a gap distance 0.2D. The results of the two co-rotating parallel and oblique turbines are used to develop a three co-rotating turbine cluster (I).

- For two counter-rotating multiple Savonius turbines, the enhancement in the power coefficient is found to be dependent on: the relative phase angle between the adjacent counter rotating turbines and the gap distances between the rotor's tips. Two parallel turbine cluster case (A) has a maximum power coefficient of 0.26 at a gap distance of 0.8D and case (B) has a maximum power coefficient of 0.3 at a gap distance of 0.8D. Two oblique turbine cluster case (C) has a maximum power coefficient of 0.35 at a gap distance of 0.4D and case (D) has a maximum power coefficient of 0.25 at a gap distance of 1.6D achieved at a relative phase angle of 30^{o}. The results of the two co-rotating and counter-rotating oblique turbines are compared to develop a three counter-rotating turbine cluster (II) and the results are compared to the co-rotating three turbine cluster (I).
- The co-rotating three turbine Savonius cluster (I) has an average power coefficient of 26% higher than isolated turbines at gap distance 2.2D and a height of 1.6D. The power ratio between the three turbines of the cluster is 1:1.2:1. This cluster is chosen to be a building unit for constructing efficient Savonius VAWT farms.
- The developed Savonius farms topology is a geometric progression of the three turbine cluster by factor 3. The developed farms are patterned and have the same power coefficient enhancement ratios of the three turbine cluster. The pattern and enhanced power coefficient are confirmed by numerical solutions of farms that consist of nine and twenty-seven turbines. The same power ratio of the cluster is achieved by the nine and twenty seven turbine farms. The power density of the nine turbine farm is about 7 times a nine isolated turbine farm, and the power density of the twenty-seven turbine farm is 4 times a twenty-seven isolated turbine farm.

- For co-rotating multiple Darrieus turbines, two parallel turbine cluster has a maximum power coefficient of 0.41 at a gap distance of 0.5D. Two oblique turbine cluster at an oblique angle 60^{o} has a maximum power coefficient of 0.35 at a gap distance of 0.5D, and for an oblique angle -60^{o} the maximum power coefficient is 0.37 at a gap distance of 0.5D. The results of the two co-rotating parallel and oblique turbines are used to develop a three co-rotating Darrieus turbine cluster (I). The maximum power coefficient of the cluster (I) exists at a gap distance of 0.5D with an average power coefficient of 0.377, this represents an enhancement of 5% compared to isolated turbines.
- For counter-rotating Darrieus turbines in parallel and oblique configurations, two parallel turbines case (C) with the inward blades moving with the wind direction has better performance than case (D) the maximum values for power coefficient in case (C) is 0.42 and occurs at a gap distance 0.5D. The solution of two oblique turbines shows that the enhancement in case (E) is higher than in case (F) at small gap distances and the same performance as the gap distance increases, a maximum average power coefficient of 0.41 is achieved at a gap distance 0.5D in case (E). Based on these results, a triangular three counter-rotating Darrieus turbine cluster (II) is developed, the most efficient performance of the cluster exists at a cluster height of 0.6D with an average power coefficient of 0.47, this represents an enhancement of 30% compared to isolated turbines. The ratio between the power coefficients of the three turbines (1), (2) and (3) is 1:1.1:1. The results for the three counter-rotating turbine clusters (II) are compared to the co-rotating three turbine cluster (I). The counter rotating cluster (II) is found to be the most efficient triangular cluster to be used as a building unit for an efficient Darrieus wind turbine farm.

- An efficient Darrieus wind turbine farm is developed using the efficient three counter-rotating triangular turbine cluster (II) as a building unit. The farm topology is a geometric progression of the three turbine cluster by factor 3. The developed farms are patterned and have the same power coefficient enhancement ratios of the three turbine cluster. The pattern and enhanced power coefficient are confirmed by numerical solutions of a farm that consist of nine turbines. The same power ratio between the individual turbines in the cluster is achieved in the nine turbine farm. The power density of the nine turbine farm is more than 13 times a nine isolated turbine farm. These patterned efficient farm designs will make the VAWT farms competitive with the existing HAWT farms which have a power density of 2-3 watt/m^2.
- The advantage of the patterned farm appears in the power ratio achieved by the clusters and confirmed by the farms which is used to predict the performance of larger farms with the same topology to save processing time and man power.
- A preliminary analysis of the mean velocity field around the turbine blades at different tip speed ratios shows a velocity distribution close to the structure of a Rankine vortex. A future work will be considered for numerical modeling of the Darrieus turbine as a combination of the free stream with a Rankine vortex. The solution of adjacent vortices can be used to determine the performance of closely oriented Darrieus turbines. A Darrieus VAWT farm can be represented by a group of vortices.

Summary of Savonius Turbine Clusters

	Co-Rotating				Counter-Rotating					Farms	
	Two Turbines			Three Turbines	Two Turbines				Three Turbines	Nine Turbines	27 Turbines
	Parallel	Oblique			Parallel		Oblique				
		Case A	Case B		Case A	Case B	Case C	Case D			
Cp	0.3	0.26	0.32	0.29	0.26	0.3	0.35	0.25	0.3	0.292	0.32
Gap Distance	0.2D	1.0D	0.2D	2.2D	0.8D	0.8D	0.4D	1.6D	2.2D		

Summary of Darrieus Turbine Clusters

	Co-Rotating				Counter-Rotating					
	Two Turbines			Three Turbines	Two Turbines				Three Turbines	Nine Turbines
	Parallel	Oblique			Parallel		Oblique			
		Case A	Case B		Case C	Case D	Case E	Case F		
Cp	0.41	0.35	0.37	0.37	0.42	0.4	0.4	0.39	0.47	0.46
Gap Distance	0.5D	0.5D	0.5D	0.5D	0.5D	0.5D	0.5D	0.5D	0.5D	

Bibliography

[1] Renewables 2014 Global Status Report "REN21".

[2] http://iipdigital.usembassy.gov/st/english/article/2013/08/20130807280196.html#ixzz3DgpapHHh

[3] World Wind Energy Association. 2014 half year report. August 2014.

[4] U.S. Department of Energy. 20% Wind Energy by 2030 - Increasing Wing Energy's Contribution to U.S. Electricity Supply. July 2008.

[5] U.S. Department of Energy. 2013 Market report on wind technologies in distributed applications energy. *Efficiency and Renewable Energy*, 2014.

[6] Betz A. Introduction to the theory of flow machines. (D. G. Randall, Trans.). *Oxford: Pergamon Press,* 1966.

[7] MacKay D.J.C. Sustainable Energy—Without the Hot Air. *UIT Cambridge Ltd., Cambridge, UK,* 2009.

[8] John O. Dabiri. Potential order-of-magnitude enhancement of wind farm power density via counter-rotating vertical-axis wind turbine arrays. *Journal Of Renewable And Sustainable Energy,* 3: 043104, 2011.

[9] Robert W Whittlesey, Sebastian Liska and John O Dabiri. Fish schooling as a basis for vertical axis wind turbine farm design. *Bioinspiration & biomimetics,* 5: 035005, 2010.

[10] Lih-Shyng Shyu. A pilot study of vertical-axis turbine wind farm layout planning. Advanced Materials Research, 953-954: 395-399, 2014.

[11] R. Ganesh Rajagopalan, Ted L. Ricke. Aerodynamic interference of two vertical axis wind turbines. AIAA Applied Aerodynamics Conference; 6: 174-184, 1988.

[12] P.R. Schatzle, P.C. Klimas, and H.R. Spahr. Aerodynamic interference between two darrieus wind turbines. *Journal of Energy*, 5: 84-88, 1981.

[13] Zhou, T., Rempfer, D. Numerical study of detailed flow field and performance of Savonius wind turbines. *Renewable Energy,* 51: 373-381, 2013.

[14] Xiaojing, S., Daihai, L., Diangui, H., Guoqing, W. Numerical study on coupling effects among multiple Savonius turbines. *Journal of Renewable and Sustainable Energy* 4: 053107, 2012.

[15] The inside of a wind turbine. *US Department of Energy, Office of Energy Efficiency & Renewable Energy*, http://energy.gov/eere/wind/inside-wind-turbine-0

[16] Sandra Eriksson, Hans Bernhoff and Mats Leijon. Evaluation of different concepts for wind power, *Renewable and Sustainable Energy*, 12: 1419-1434, 2008.

[17] Windspire 1.2. Windspire Energy. *Ark Alloy, LLC*.

[18] Wikipedia the free encyclopedia. Savonius wind turbine, http://en.wikipedia.org/wiki/Savonius_wind_turbine

[19] R. Howell, N. Qin, J. Edwards, N. Durrani. Wind tunnel and numerical study of a small vertical axis wind turbine, Renewable Energy 35: 412–422, 2010.

[20] A. Shigetomi, Y. Murai, Y. Tasaka, Y. Takeda. Interactive flow field around two Savonius turbines, *Renewable Energy,* 36: 536-545, 2011.

[21] R. E. Sheldahl, B. F. Blackwell, and L. V. Feltz. Wind tunnel performance data for two- and three-bucket Savonius rotors, *Sandia Report*, SAND 77-0131, 1977.

[22] B. D. Altan, M. Atilgan, and A. Ozdamar. An experimental study on improvement of a Savonius rotor performance with curtaining, *Exp. Therm. Fluid Sci.* 32(8): 1673–1678, 2008.

[23] B. Kirke. Development in ducted water current turbines, www.Cyberiad.net.

[24] N. Fujisawa. On the torque mechanism of Savonius rotors, *J. Wind Eng. Ind. Aerodyn.* 40(2): 277–292, 1992.

[25] Dixon, K. R. The Near Wake Structure of a Vertical Axis Wind Turbine. *Thesis. Delft University of Technology*, 2008.

[26] Tong, Wei. Wind Power Generation and Wind Turbine Design. Southampton: WIT, 2010.

[27] http://www.windturbine-analysis.netfirms.com

[28] D'Ambrosio M., Medaglia M. Vertical Axis Wind Turbines: History, Technology and Applications: Master thesis, (2010).

[29] Ajedegba J.O. Effect of Blade Configuration on Flow Distribution and Power Output of a Zephir Vertical Axis Wind Turbine, *University of Ontario Institute of Technology: Master thesis*, 2008.

[30] Shepherd W., Zhang L., Electricity Generation using Wind Power, *World scientific,* 2011.

[31] K. Pope, G.F. Naterer, I. Dincer and E. Tsang. Power correlation for vertical axis wind turbines with varying geometries, *International Journal Of Energy Research*, 35: 423–435, 2011.

[32] H. Riegler. HAWT Versus VAST Small VAWTs Find a Clear Niche. *Refocus* 4: 44–46, 2003.

[33] Yaoa. J, Wanga J., Yuanb W., Wanga H. & Caoa L. Analysis on the influence of Turbulence model changes to aerodynamic performance of vertical axis wind turbine, *International Conference on Advances in Computational Modeling and Simulation*, 31: 213-219, 2011

[34] K. N. Morshed, M. Rahman, G. Molina and M. Ahmed. Wind tunnel testing and numerical simulation on aerodynamic performance of a three-bladed Savonius wind turbine, *International Journal of Energy and Environmental Engineering*, 4-18, 2013.

[35] Uzarraga-Rodriguez N. Cristobal, Gallegos-Muñoz A. and Riesco Ávila J. Manuel. Numerical Analysis of A Rooftop Vertical Axis Wind Turbine, *International Conference on Energy Sustainability*, ES2011-54173, 2011.

[36] K. Kacprzak, G. Liskiewicz, K. Sobczak. Numerical investigation of conventional and modified Savonius wind turbines, *Renewable Energy*, 60: 578-585, 2013.

[37] M.H Mohamed, G. Janiga, E. Pap, D. Thévenin. Optimal Blade Shape of a Modified Savonius Turbine using an Obstacle Shielding the Returning Blade, *Energy Conversion and Management* 52(1): 236-242, 2011.

[38] R. Lanzafame, S. Mauro, M. Messina, " 2D CFD Modeling of H-Darrieus Wind Turbines using a Transition Turbulence Model," Energy Procedia 45 (2014) 131–140

[39] F. R. Menter, "Two Equation Eddy Viscosity Turbulence Models for Engineering Applications," AIAA Journal Vol. 32, No. 8, August 1994.

[40] Langtry R.B., Menter F.R., Likki S.R., Suzen Y.B., Huang P.G., Völker S. A correlation based transition model using local variables part I: model formulation, ASME GT 2004 - 53452, 2006

[41] McLaren KW. A numerical and experimental study of unsteady loading of high solidity vertical axis wind turbines, *McMaster: McMaster University*, 2011. Open Access Dissertations and Theses Paper 6091. http://digitalcommons.mcmaster.ca/opendissertations

[42] J. M. Edwards, L. A. Danao and R. J. Howell. Novel Experimental Power Curve Determination and Computational Methods for the Performance Analysis of Vertical Axis Wind Turbines, *Journal of Solar Energy Engineering*, 134: 031008-1, 2012.

[43] M. Nakajima, S. IIO and T. Ikeda. Performance of Double-step Savonius Rotor for Environmentally Friendly Hydraulic Turbine, Journal of Fluid Science and Technology 3, 2008.

[44] N. Fujisawa and F. Gotoh. Visualization study of the flow in and around a Savonius rotor, *Experiments in Fluids*, 12: 407-412, 1992.

[45] Ivan Dobrev, Fawaz Massouh. CFD and PIV investigation of unsteady flow through Savonius wind turbine, *Energy Procedia*, 6:711–720, 2011.

[46] Zullah M.A, Prasad D, Choi Y.D, Lee Y.H. Study on the performance of helical Savonius rotor for wave energy conversion, *AIP Conf. Proc*,1225: 641-649, 2010.

[47] Kang, C., Zhang, F., Mao, X. Comparison study of a vertical-axis spiral rotor and a conventional Savonius rotor, *APPEEC*, Art. No. 5448791, 2010.

[48] Yaakob O.B, Tawi, K.B, Sunanto, D.T.S. Computer Simulation Studies on the effect overlap ratio for Savonius type vertical axis marine current turbine, " *Int. J. of Eng., Trans. A*: Basics, 23(1): 79-88, 2010.

[49] J. V. Akwaa,H. A. Vielmob, A. P. Petry. A Review on The Performance of Savonius Wind Turbines, *Renewable and Sustainable Energy Reviews*, 16: 3054 – 3064, 2012.

[50] Taher G. Abu-El-Yazied, Hossam N. Doghiem, Ahmad M. Ali, and Islam M. Hassan," Investigation of the Aerodynamic Performance of Darrieus Vertical Axis Wind Turbine," IOSR Journal of Engineering (2014) 4: 18-29

[51] R. Lanzafame, S. Mauro, M. Messina, " 2D CFD Modeling of H-Darrieus Wind Turbines using a Transition Turbulence Model," Energy Procedia (2014) 45: 131 – 140

[52] E. Amet, T. Maitre, C. Pellone, J. L. Achard " 2D Numerical Simulations of Blade-Vortex Interaction in a Darrieus Turbine," Journal of Fluids Engineering (2009) 131: 111103-1

[53] Lanzafame R., Mauro S., Messina M. Wind turbine CFD modeling using a correlation-based transitional model. Renewable Energy 52 (2013) 31 - 39

[54] K. Kacprzak, G. Liskiewicz, K. Sobczak, " Numerical investigation of conventional and modified Savonius wind turbines," Renewable Energy (2013) 60: 578-585

[55] I. Paraschivoiu, " Wind Turbine Design With Emphasis on Darrieus Concept," Polytechnic, Brooklyn, NY, (2002).

[56] J.H. Strickland, B.T. Webster, and T. Nguyen, "A Vortex Model of the Darrieus Turbine: An Analytical and Experimental Study," American Society of Mechanical Engineers (1979) 79- WA/FE-6.

[57] R. Rajagopalan and T. Rickerl, "Aerodynamic Interference of Vertical Axis Wind Turbines," Journal of Propulsion (1990) 6: 645-653